IECM Technical Documentation:

Integrated Gasification Combined Cycle Power Plants

March 2019

IECM Technical Documentation:

Integrated Gasification Combined Cycle Power Plants

Prepared by:

The Integrated Environmental Control Model Team
Department of Engineering and Public Policy
Carnegie Mellon University
Pittsburgh, PA 15213
www.iecm-online.com

For
U.S. Department of Energy
National Energy Technology Laboratory
P.O. Box 880

Compiled in March 2019

Contents

List of Figures

List of Tables

Acknowledgements

This documentation is a compilation of two previously-issued reports:

- Edward S. Rubin, Michael B. Berkenpas, H. Christopher Frey, Chao Chen, Sean McCoy, and Constance J. Zaremsky. Technical Documentation: Integrated Gasification Combined Cycle Systems (IGCC) with Carbon Capture and Storage (CCS). Prepared by Carnegie Mellon University for the National Energy Technology Laboratory. Pittsburgh, PA 15213, May 2007.
- Michael B. Berkenpas, Karen Kietzke, Hari Mantripragada, Sean McCoy, Edward S. Rubin, Peter L. Versteeg, and Haibo Zhai. IECM Technical Documentation Updates, Vol. IV. Prepared by Carnegie Mellon University for the National Energy Technology Laboratory. Pittsburgh, PA 15213, November 2009.

These prior reports were sponsored by the U.S. Department of Energy's National Energy Technology Laboratory under Contract Nos. DE-AC21-92MC29094 and DE-AC26-04NT41917. Any opinions, findings, and conclusions or recommendations expressed in this material are those of the authors alone and do not reflect the views of any government agency.

1. Gasification

This chapter provides a description of the coal-based power generation and integrated environmental control systems selected for case studies in this research. An advanced system was selected on the basis of promising costs, plant performance, and emission reductions. A baseline system, representative of conventional technology, was also selected for the purpose of comparative analysis. The engineering performance, emissions, and cost models of each system are also described. Later updates to this chapter appear in Chapter 10.

1.1 Overview of Gasification Systems

Gasification systems are a promising approach for clean and efficient power generation as well as for polygeneration of a variety of products, such as steam, sulfur, hydrogen, methanol, ammonia, and others (Philcox and Fenner, 1996). As of 1996, there were 354 gasifiers located at 113 facilities worldwide. The gasifiers use solid fuels (petroleum residuals, petroleum coke, refinery wastes, coal, and other fuels) as inputs, and produce a synthesis gas containing carbon monoxide (CO), hydrogen (H_2), and other components. The syngas can be processed to produce liquid and gaseous fuels, chemicals, and electric power. In recent years, gasification has received increasing attention as an option for repowering at oil refineries, where there is currently a lack of markets for low-value liquid residues and coke (Simbeck, 1996).

A general category of gasification-based systems is Integrated Gasification Combined Cycle (IGCC) systems. IGCC is an advanced power generation concept with the flexibility to use coal, heavy oils, petroleum coke, biomass, and waste fuels to produce electric power as a primary product. IGCC systems typically produce sulfur as a byproduct. Systems that produce many co-products are referred to as "polygeneration" systems. IGCC systems are characterized by high thermal efficiencies and lower environmental emissions than conventional pulverized coal fired plants (Bjorge, 1996).

A generic IGCC system is illustrated schematically in Figure 1-1. In an IGCC power plant, the feedstock to the gasifier is converted to a syngas, composed mainly of hydrogen and carbon monoxide, using a gasification process. After passing through a gas cleanup system, in which particles and soluble gases are removed via wet scrubbing and in which sulfur is removed and recovered via a selective removal process, the syngas is utilized in a combined cycle power plant. Different variations of IGCC systems exist based upon the type of coal gasifier technology, oxidant (e.g., oxygen or air), and gas cleanup system employed.

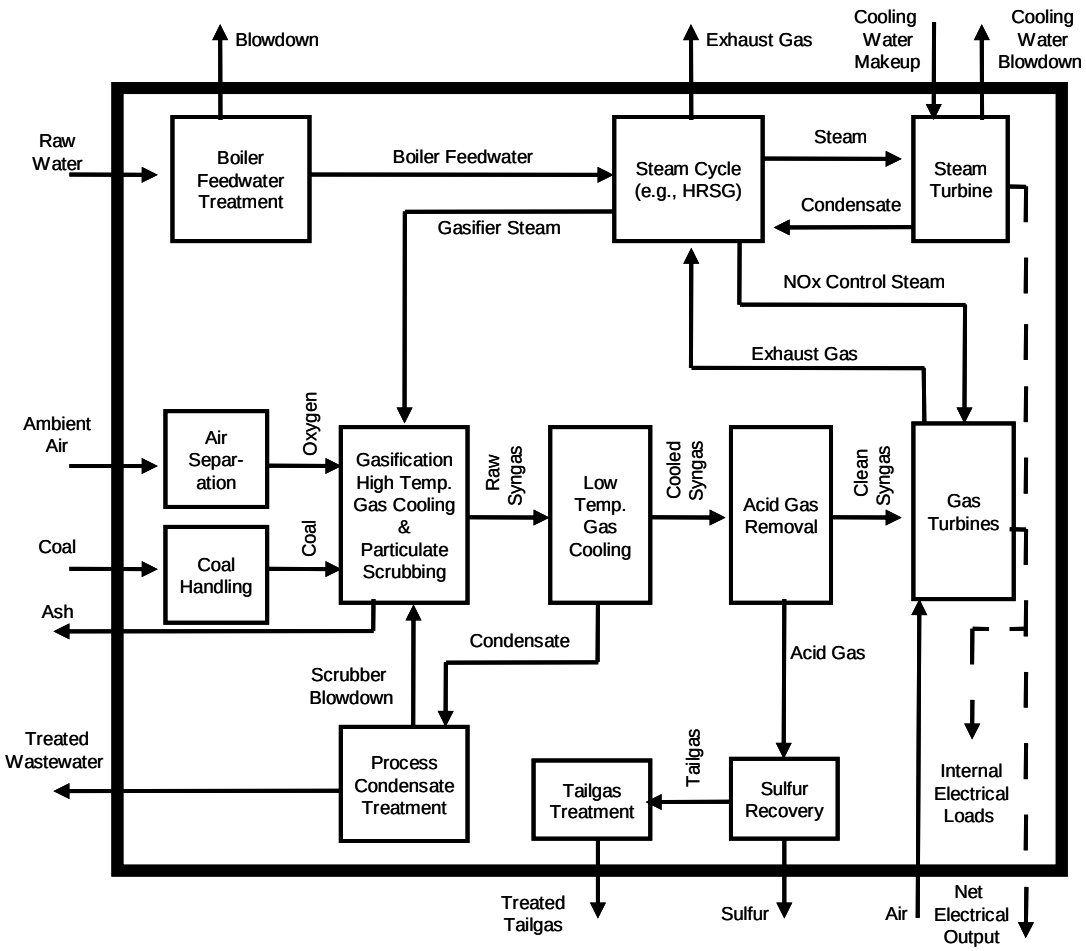

Figure 1-1. IGCC Schematic Diagram

A typical IGCC system includes process sections of

- Fuel Handling
- Gasification
- High-Temperature Gas Cooling
- Low Temperature Gas Cooling and Gas Scrubbing
- Acid Gas Separation
- Fuel Gas Saturation
- Gas Turbine
- Heat Recovery Steam Generator
- Steam Turbine
- Sulfur Byproduct Recovery

The specific design of each of the process sections such as gasification and high-temperature gas cooling varies in different IGCC systems.

1.2 Gasification Types

Three generic designs of gasification are typically employed in IGCC systems, each of which is described below. In all types of reactors, the feedstock fuel is converted to syngas in reactors with an oxidant and either steam or water. The oxidant is required to partially oxidize the fuel. The exothermic oxidation process provides heat for the endothermic gasification reactions. Water or steam is used as a source of hydrolysis in the gasification reactions. The type of reactor used is the primary basis for classifying different types of gasifiers.

1.2.1 Moving-Bed or Counter-Current Reactors

Moving bed reactors feature counter-current flow of fuel with respect to both the oxidant and the steam. For example, in the case of coal gasification, coal particles of approximately 4 mm to 30 mm (Simbeck et al., 1983) in diameter are introduced at the top of the reactor, and move downward. Oxidant is introduced at the bottom of the reactor. A combustion zone at the bottom of the reactor produces thermal energy required for gasification reactions, which occur primarily in the central zone of the reactor. Steam is also introduced near the bottom of the gasifier. As the hot gases from combustion and gasification move upward, they come into contact with the fuel introduced at the top. The heating of the fuel at the top of the reactor results in devolatilization, in which lighter hydrocarbon compounds are driven off and exit as part of the syngas. Because the gases leaving the gasifier contact the relatively cool fuel entering the gasifier, the exit syngas temperature is relatively low compared to other types of reactors. The counter-current flow of fuel with the oxidant and steam can result in efficient utilization of the fuel, as long as the residence time of the fuel is long enough for even the larger particles to be fully consumed. Ash and unconverted fuel exit the bottom of the gasifier via a rotating grate.

A typical syngas exit temperature for a moving bed gasifier is approximately 1,100 ^{o}F. At this temperature, some of the heavier volatilized hydrocarbon compounds, such as tars and oils, will not be cracked and can easily condense in downstream syngas cooling equipment. Because fuel is introduced at the top of the gasifier where the syngas is exiting, this type of gasifier cannot handle fine fuel particles. Such particles would be entrained with the exiting syngas and would not be converted to syngas in the reactor bed. Cyclones are typically used to capture fine particles in the syngas, which are often sent to a briquetting facility to form larger particles and then recycled to the gasifier for another attempt at conversion.

An overall measure of gasifier performance is the cold gas efficiency. The cold gas efficiency is the ratio of the heating value of "cold" syngas, at standard temperature, to the heating value of the amount of fuel consumed/required to produce the syngas. The cold gas efficiency does not take into account recovery of energy in the gasifier such as through steam generation or associated with sensible heat of the syngas at high temperatures. Moving bed gasifiers tend to have very high cold gas efficiencies, with values in the range of 80 to 90 percent.

Typical examples of such reactors are Lurgi dry bottom gasifiers and the British Gas/Lurgi slagging gasifiers.

1.2.2 Fluidized-Bed Gasifiers

Fluidized bed reactors feature rapid mixing of fuel particles in a 0.1 mm to 10 mm size range with both oxidant and steam in a fluidized bed. The feedstock fuel, oxidant and steam are introduced at the bottom of the reactor. In these reactors, backmixing of incoming feedstock fuel, oxidant, steam, and the fuel gas takes place resulting in a uniform distribution of solids and gases in the reactors. The gasification takes place in the central zone of the reactor. The coal bed is fluidized as the fuel gas flow rate increases and becomes turbulent when the minimum fluidizing velocity is exceeded.

The reactors have a narrow temperature range of 1800 ^{o}F to 1900 ^{o}F. The fluidized bed is maintained at a nearly constant temperature, which is well below the initial ash fusion temperature to avoid clinker formation and possible defluidization of the bed. Unconverted coal in the form of char is entrained from the bed and leaves the gasifier with the hot raw gas. This char is separated from the raw gas in the cyclones and is recycled to the hot ash agglomerating zone at the bottom of the gasifier. The temperature in that zone is high enough to gasify the char and reach the softening temperature for some of the eutectics in the ash. The ash particles stick together, grow in size and become dense until they are separated from the char particles, and then fall to the base of the gasifier, where they are removed.

The processes in these reactors are restricted to reactive, non-caking coals to facilitate easy gasification of the unconverted char entering the hot ash zone and for uniform backmixing of coal and fuel gas. The cold gas efficiency is approximately 80 percent (Supp, 1990). These reactors have been used for Winkler gasification process and High-temperature Winkler gasification process. A key example of fluidized gasification design is the KRW gasifier.

1.2.3 Entrained-Flow Reactors

The entrained-flow process features a plug type reactor where the fine feedstock fuel particles (less than 0.1 mm) flow co-currently and react with oxidant and/or steam. The feedstock, oxidant and steam are introduced at the top of the reactor. The gasification takes place rapidly at temperatures in excess of 2300 ^{o}F. The feedstock is converted primarily to H_2, CO, and CO_2 with no liquid hydrocarbons being found in the syngas. The raw gas leaves from the bottom of the reactor at high temperatures of 2300 ^{o}F and greater. The raw gas has low amounts of methane and no other hydrocarbons due to the high syngas exit temperatures.

The entrained flow gasifiers typically use oxygen as the oxidant and operate at high temperatures well above ash slagging conditions in order to assure reasonable carbon conversion and to provide a mechanism for slag removal (Simbeck et al., 1983). Entrained-flow gasification has the advantage over the other gasification designs in that it can gasify almost all types of coals regardless of coal rank, caking characteristics, or the amount of coal fines. This is because of the relatively high temperatures which enable gasification of even relatively unreactive feedstocks that might be unsuitable for the lower temperature moving bed or fluidized bed reactors. However, because of the high temperatures, entrained-flow gasifiers use more oxidant than the other designs. The cold gas efficiency is approximately 80 percent (Supp, 1990). Typical examples of such reactors are GE gasifiers and E-Gas gasifiers.

The advantage of adopting entrained flow gasification over the above-mentioned reactors is the high yield of synthesis gas containing insignificant amounts of methanol and other hydrocarbons as a result of the high temperatures in the entrained-flow reactors.

GE gasification is a specialized form of entrained flow gasification in which coal is fed to the gasifier in a water slurry. Because of the water in the slurry, which acts as heat moderator, the gasifier can be operated at higher pressures than other types of entrained-flow gasifiers. Higher operating pressure leads to increased gas production capability per gasifier of a given size (Simbeck et al., 1983)

In this study, we focus on modeling assessment of entrained flow gasification. Assessments of moving bed and fluidized bed gasifier-based systems have been done in previous work (Frey and Rubin, 1992a, 1992b, Frey et al., 1994, Frey, 1998).

1.3 Gasification Cooling Types

1.3.1 High Temperature Gas Cooling

The design of the high temperature syngas cooling process area depends on the type of gasifier used. The gas cooling requirements for entrained flow gasification systems are more demanding than for other gasification systems as the former produce syngas at higher temperatures. Typically, the gas cooling process for systems employing entrained flow gasification systems either use heat exchangers to recover thermal energy and generate steam or use water quenching. The former design can be radiant and convective or radiant only, while the latter is known as total quench high temperature gas cooling. The former is more efficient as it can produce high temperature and pressure steam, whereas the latter is much less expensive (Doering and Mahagaokar, 1992).

1.3.2 Radiant and Convective Syngas Cooling Design

The design of a radiant and convective gasification system is shown in Figure 1-2. Each gasifier has one radiant cooler and one convective cooler. The hot syngas is initially cooled in a radiant heat transfer type of heat exchanger. High pressure steam is generated in tubes built into the heat transfer surface at the perimeter of the

cylindrical gas flow zone. The molten slag drops into a slag quench chamber at the bottom of the radiant gas cooler where it is cooled and removed for disposal. The gas leaves the radiant cooler at a temperature of approximately 1500 °F.

The syngas from the radiant heat exchanger flows into a convection type of heat exchanger. In the convective heat exchanger, the syngas flows across the boiler tube banks. These tubes help remove the entrained particles in the syngas that are too fine to drop out in the bottom of the radiant cooler. High pressure steam is generated in these tubes. The cooled gas leaves the convective chamber at a temperature of approximately 650 °F.

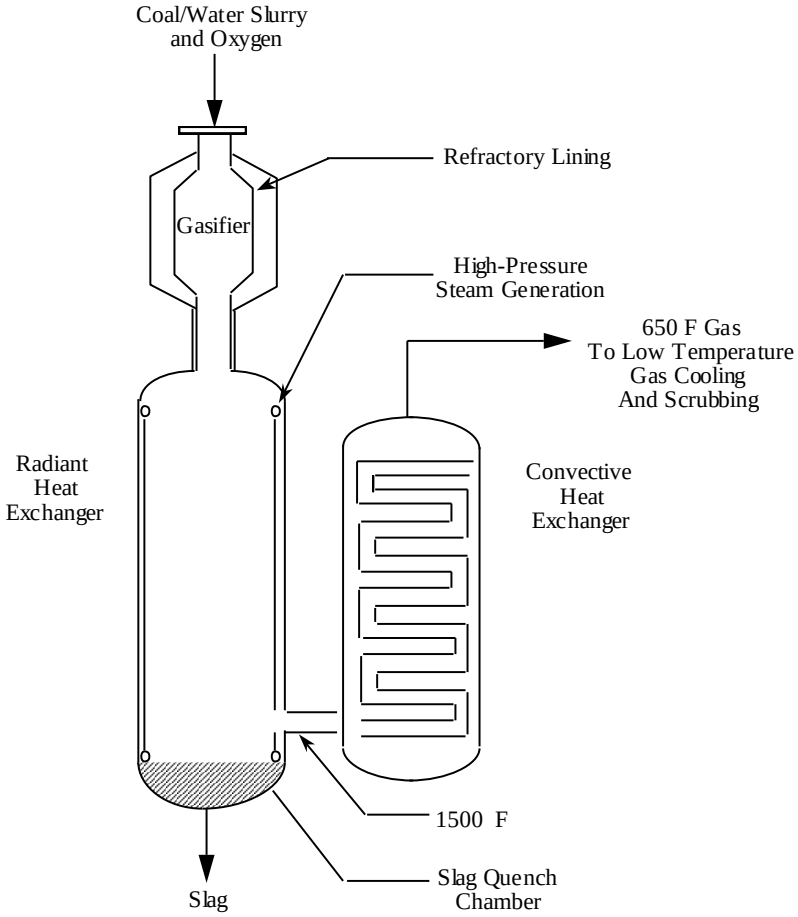

Figure 1-2. Radiant and Convective High Temperature Syngas Cooling Design

1.3.3 Radiant Only Syngas Cooling Design

The hot syngas is cooled initially in the radiant cooler and high-pressure steam is generated as in the radiant and convective design. However, in this case both the molten slag and the raw gas are quenched in the water pool at the bottom of the radiant cooler. The cooled slag is removed from the cooler for disposal. The raw gas, saturated with moisture, flows out of the radiant cooler at a temperature of approximately 400 °F.

1.3.4 Total Quench Design

The total quench design is depicted in Figure 1-3. In this design, the hot syngas and the molten slag particles flow downward through a water spray chamber and a slag quench bath. Water is sprayed just beneath the partial oxidation chamber to cool the hot syngas. The entrained slag is separated from the syngas in the slag quench bath (Nowacki, 1981). There is no high-pressure steam generation in this method as in the previous two designs since there is no heat recovery. The raw gas saturated with moisture flows to the gas scrubbing unit at a temperature of 430 °F.

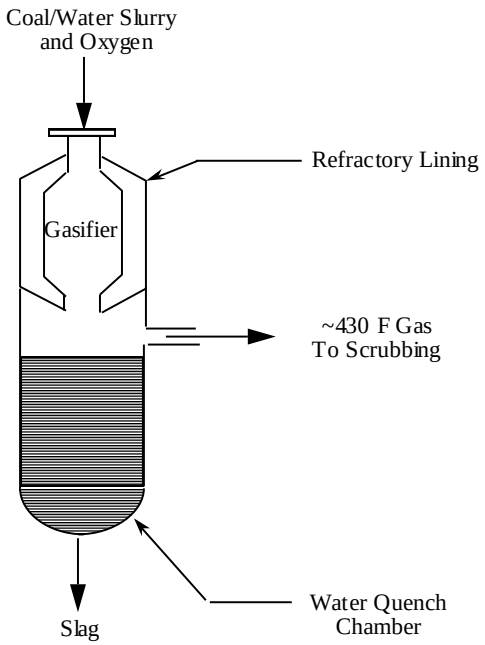

Figure 1-3. Total Quench High Temperature Syngas Cooling Design

In this study, both the radiant and convective and the total quench high temperature syngas cooling designs are evaluated. The radiant and convective design has the advantage over total quench syngas cooling of a higher plant efficiency. However, the cost of the radiant and convective design is higher than that of the total quench design. The total quench design results in increased moisturization of syngas, which can prove effective in terms of preventing NO_X formation in the gas turbine combustor and in terms of augmenting power production from the gas turbine. In a water quench system, large quantities of water are used and thus contaminated by the slag, requiring complex primary and secondary treatment facilities. Hence total quench design has additional operating problems such as those caused due to increased water treating facilities, increased discharge water permitting issues, and added operating and maintenance costs when compared to radiant and convective design (Doering and Mahagaokar, 1992).

1.4 Commercial Status of Gasification Systems

The IGCC concept has been demonstrated commercially. Table 1-1 lists the IGCC plants currently in operation or undergoing construction. The GE coal gasification process has been successfully used in a number of chemical plants since the early 1980s for the production of synthesis gas from coal. A GE-based 95 MW IGCC power plant was operated successfully from 1984 to 1988 in California (Simbeck, 1996). API Energia, a joint venture of Asea Brown Boveri and API, adopted GE gasification to gasify visbreaker residue from an API refinery to produce steam and power. Tampa Electric Company's Polk Power station also utilizes GE gasification, gasifying about 2,000 tons of coal per day to produce 250 MW of power. The El Dorado gasification project demonstrates that hazardous waste streams can be converted by gasification to valuable products. (Farina, 1998).

An E-Gas gasifier-based IGCC power plant at Wabash River Station is currently under operation (Simbeck, 1996). A 335 MW IGCC demonstration plant for European electricity companies is operating at Puertollano, Spain (Mendez-vigo, 1998). The GE gasifier-based El Dorado plant, the Shell-Pernis plant in The Netherlands, and the Sarlux plant in Italy use low pressure (38 barg) GE gasification to produce hydrogen and/or steam along with power (Bjorge, 1996).

Table 1-1. IGCC Projects under Operation or Construction

Project	Location	Start-up Date	Plant Size	Products	Gasifier	Fuel
Cool Water IGCC	Barstow, California	1984	120 MW	Power	GE	Coal
PSI Wabash River	Terre Haute, Indiana	1996	262 MW	Power	E-Gas	Coal
Tampa Electric	Polk, Florida	1996	250 MW	Power	GE	Coal
Pinon Pine Sierra Pacific	Sparks, Nevada	1996	100 MW	Power	KRW	Coal
GE El Dorado	El Dorado, Kansas	1996	40 MW	Co-generation Steam and H_2	GE	Pet Coke
Shell Pernis	Netherlands	1997	120 MW	Co-generation H_2	Shell/ Lurgi	Oil
Sarlux	Sarroch, Italy	1998	550 MW	Co-generation Steam	GE	Oil
API Energia	Falconara Marittima	1999	234 MW	Power	GE	Oil
Puertallano		1997	335 MW	Power	Prenflo	Coal

1.5 Overall Plant Efficiency

1.5.1 Net Power Output and Plant Efficiency

The net plant power output is the total power generated from the gas turbines and steam turbines less the total auxiliary power consumption. The gas and steam turbines have been modeled as a series of compressors and turbines. This unit operation block requires outlet pressure and isentropic efficiencies as parameters. The power consumed by the compressors and the power generated by the turbines are calculated by the performance model. The net power output in MW is given by

$$MW_{net} = MW_{GT} + MW_{ST} - W_{e,\,AUX} \tag{1-1}$$

The net plant efficiency on a higher heating value basis is given by

$$\eta = 3.414\ x\ 10^{6}\ \frac{MW_{net}}{M_{cf,CH,i}\ x\ HHV} \tag{1-2}$$

where,

η = net plant efficiency.

$M_{cf,\,CH,\,i}$ = Coal feed rate, lb/hr.

HHV = Higher heating value of fuel, BTU/lb.

1.6 Economics

1.6.1 Total Plant Costs

The total plant costs of an IGCC power plant include the process facilities capital costs, indirect construction costs, engineering and home office fees, sales tax, allowances for funds used during construction (AFUDC), project contingency, and total process contingencies.

The equations for the plant cost model are the same as those given in Frey and Rubin (1990) and are not repeated here. However, the model is briefly described.

Indirect construction costs include worker benefits, supervision and administrative labor, purchased and rented construction equipment, and construction facilities. Engineering and home office fees include the costs associated with engineering, office expenses, and fees or profit to the engineer. Sales tax cost is specific to the state where the power plant is constructed and is estimated as the tax on material costs. AFUDC is the estimated debt and equity costs of capital funds necessary to finance the construction of new facilities. Startup costs include one month of fixed operating costs and one month of variable costs based on full plant capacity.

Process contingency is used in deterministic cost estimates to quantify the expected increase in the capital cost of an advanced technology due to uncertainty in performance and cost for the specific design application. Project contingency is used in deterministic cost estimates to represent the expected increase in the capital cost estimate that would result from a more detailed estimate for a specific project at a particular site.

1.6.2 Total Capital Requirement

The total capital requirement (TCR) includes the total plant investment, prepaid royalties, spare parts inventory, preproduction (or startup) costs, inventory capital, initial chemicals and catalyst charges, and land costs. The methodology for calculating TCR is given in detail in Frey and Rubin (1990).

1.6.3 Annual Costs

The annual costs of an IGCC plant consists of fixed and variable operating costs. The fixed operating costs are annual costs including operating labor, maintenance labor, maintenance materials, and overhead costs associated with administrative and support labor. The variable operating costs include consumables, fuels, slag and ash disposal, and byproduct credits. For more details on the annual cost models, please refer to Frey and Rubin (1990).

1.6.4 Levelized Costs

The total capital requirement, fixed operating cost, and operating variable cost are used to calculate the cost of producing electricity that is available for sale from the power plant, based on the net electrical output from the power plant. The calculated cost of electricity is also known as total annualized cost and is the levelized annual revenue requirement to cover all of the capital and operating costs for the economic life of the plant.

$$C_{elec} = \frac{[1{,}000\ f_{cr}\ TCR + f_{vclf}\ (FOC + VOC)]\left(\frac{1{,}000\ mills}{dollar}\right)}{MW_{net}\ 8{,}760\ c_f} \qquad (1\text{-}3)$$

where,

C_{elec} = cost of electricity (mills / kWh)

TCR = Total capital requirement in $1,000

FOC = Fixed operating costs in dollars

VOC = Variable operating costs in dollars

MW_{net} = Net power output (MW)

f_{cr} = Fixed charge factor

f_{vclf} = Variable levelization cost factor

C_f = Capacity Factor

2. Oxidant Feed

Nomenclature

η_{ox}= oxygen purity (vol%)

η= isothermal efficiency of the compressor (fraction)

$M_{O,G,i}$ = oxygen flow rate into gasifier (lb-mole/hr)

$N_{O, OF}$ = number of operating trains in oxidant feed system

$N_{T, OF}$ = total number of trains in oxidant feed system (operating and spare)

P_i = input pressure to compressor (kPa)

P_o = product pressure to gasifier (kPa)

T_a = ambient air temperature (˚F)

V = volumetric flow rate (m^3/sec)

2.1 Oxidant Feed Process Description

Cryogenic air separation units (ASU) are used over a wide range of flow rates and purities. Cryogenic plants are capable of producing oxygen at purities exceeding 99.5%. They are used exclusively for large-scale oxygen production, ranging from 600 tons per day to over 8000 tons per day.

Historically, most gasifier systems have used high purity oxygen instead of atmospheric air. Japanese development, however, has concentrated on air blown systems.

The basic advantages of oxygen blown gasification are:

- reduced gasifier size and subsequent lower cost;
- higher syngas heating value;
- smaller gas handling and cleanup equipment due to lower syngas volume and subsequent lower cost;
- smaller heat exchangers to recover sensible heat from the syngas prior to cleanup.

The disadvantage of using high purity oxygen as an oxidant is the higher complexity of plant integration required. Hence, controlling and operating a power plant becomes more closely associated with running a chemical plant. Matching the requirements for availability, reliability and flexibility of operation (for example, to load follow) at a competitive cost over a long period are the major challenges. Auxiliary power consumption in oxygen blown systems is estimated to be 10-15%, twice that of an air-blown system.

The oxidant feed section modeled is applicable to oxygen-blown gasification systems or advanced combustion systems (e.g., oxyfuel). A typical air separation plant consists of two parallel operating trains. There are typically no spare trains because product availability is greater than 99% from large plants (Alstom, 2003). Each train includes an air compression system, air separation unit and an optional oxygen compression system. The oxygen plants produce an oxidant feed to the gasifier containing typically 95 to 98 percent oxygen on a volume basis. It is possible to recover argon as a saleable byproduct from high purity oxygen plants operating at a purity rate of 99.5 percent oxygen or greater; however, the available data are not for the oxygen purity levels and plant designs required to do this. The oxygen plants used to determine costs are commercially available.

This process section typically has an air compression system, an air separation unit, and an oxygen compression system per train. The oxygen compression system is not treated for power plant types that operate at or near

atmospheric pressure. The minimum number of operating trains is two and there are no spare trains. The number of trains depends on the total mass flow rate of oxygen.

2.1.1 Cryogenic Distillation

The heart of the cryogenic distillation process is the distillation column. It is in this column that air is separated into its components. The difference in the boiling points of the components of air is the driving principle behind the operation of the column. This is illustrated by Figure 2-1. This figure shows the temperature versus composition of air, treated as a binary mixture of nitrogen and oxygen. The upper line is the dewpoint line, when liquid drops start to form in gas as air is cooled. The lower line is the bubble line, when gas bubbles first form in liquid as air is warmed. The boiling point of pure oxygen (0% nitrogen) is shown by the top left point on the graph, at -292˚F. The boiling point of pure nitrogen is shown by the bottom right point on the graph, at -316˚F. Atmospheric air contains 0.93% argon by volume, which has a boiling point of 303˚F. As this is much closer to the boiling point of oxygen than nitrogen, most of the argon in air will go with the oxygen through the main distillation column. Thus, air can be treated as 78% Nitrogen and 22% oxygen for the purposes of this discussion.

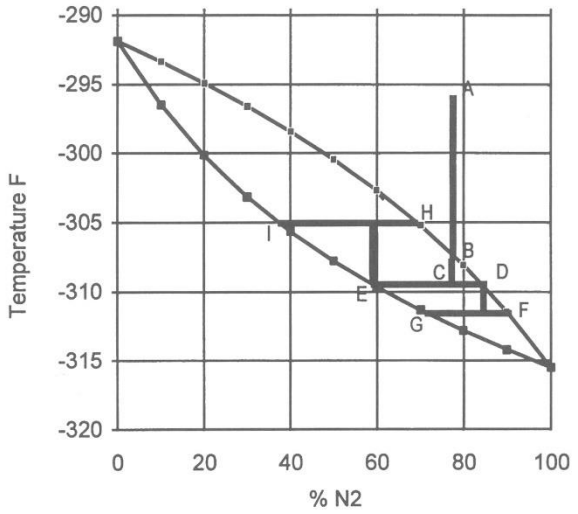

Figure 2-1. Equilibrium diagram with stage separation (Baukal, 1998)

Following the dark, lettered line shows how the separation process occurs. Ambient air (A) is cooled below the dew point (B) to a temperature between the bubble point and the dew point (C). The air is now a mixture of liquid and gas, and is pumped into a column. The mixture is allowed to settle on a tray in the distillation column until it reaches thermal equilibrium and the liquid and vapor phases separated. The liquid phase (E) is now richer in oxygen and the gas phase (D) is richer in nitrogen.

The oxygen-rich liquid is now removed and heated slightly until it is at a temperature between the liquid and bubble lines. As a result of the heating the liquid becomes a froth of vapor and liquid. This mixture is allowed to cool until it reaches thermal equilibrium and the vapor (H) and liquid (I) phases separate. The liquid, which is now richer in oxygen than both points (A) and (E), is removed and heated again. The cycle continues until the desired purity of oxygen is reached. The vapor (H) is mixed with another "batch" of liquid from (E), providing the heat to turn the liquid into foam.

The nitrogen-rich vapor (D) is cooled slightly until is a foam again. It is then allowed to reach equilibrium, where it separates into vapor (F) and liquid (G) phases. The vapor, now richer in nitrogen then both (A) and (D), is removed and cooled again. The cold liquid (G) is recycled back into the vapor (D), providing the cooling for that stream.

In the distillation column, each separation and equilibrium occurs on a sieve tray. These are metal trays with many small holes that allow vapor to bubble through them into liquid on the tray. When the foam on a tray separates into vapor and liquid, the vapor will rise up to the tray above, and bubble through into the liquid. The liquid that forms will overflow a short wall and fall to the next tray downward. In a column, there is a constant

flow of rising vapor and a counter flow of descending liquid. As the vapor moves upwards through the trays it becomes colder and richer in nitrogen. As the liquid flows downward through the trays it becomes warmer and richer in oxygen. The number of trays in the column determines the purity of the products.

2.1.2 ASU Process Areas

The ASU can be separated into several steps, each important in efficiently separating oxygen from the air. Figure 2-2 shows a diagram of the entire cryogenic process. The sections that follow will describe the various sub-sections.

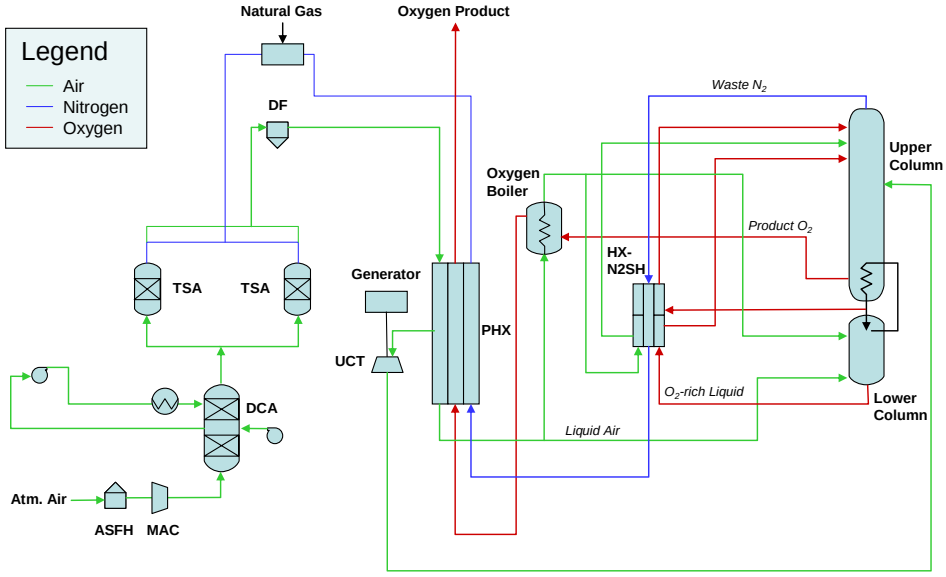

Figure 2-2. Air Separation Unit Process Flow Diagram (Alstom, 2003)

Air Compression

Ambient air is drawn through an air separation filter house (ASFH) for the removal of dust and large airborne particles prior to entering the three-stage main air compressor (MAC). The compressor can be treated as isothermal. The filtered air is compressed in the MAC to approximately 550 kPa (65 psig) and then flows through the two-stage direct contact after-cooler (DCA). Air is cooled by exchanging heat with cooling water in the first stage and with chilled water provided by a mechanical chiller in the second stage.

Pre-purification

The after-cooled air is then passed through the pre-purification system. The pre-purification system uses a two-bed temperature-swing adsorption (TSA) process that allows continuous operation. One bed purifies the feed air while the other bed is being regenerated with first hot then cool waste nitrogen. A natural gas regeneration heater provides regeneration energy. The pre-purifier beds utilize a split adsorbent design (molecular sieve and alumina) to remove water, carbon dioxide, and most of the hydrocarbons from the air stream. Since water and carbon dioxide have boiling points well above that of nitrogen and oxygen, they would freeze in the main heat exchanger and eventually block air flow. The hydrocarbons would be an extremely dangerous impurity in an oxygen stream. After pre-purification, the air stream is passed through a dust filter to remove any solid particles.

Air Feed Streams

The treated air enters a large, heavily insulated building containing the distillation columns and all of the cryogenic equipment. For larger plants this building can be 10 stories tall. This building is called the cold box as the temperature inside is always below -250 F. There are also conventional refrigeration systems to compensate for heat leaks and other non-idealities in the cold box.

The cold box requires one air feed stream. This stream is sent through the Primary Heat Exchanger (PHX) and then split into three streams. One stream is fed to the oxygen boiler. A second air stream (turbine air) is cooled partially in the PHX and fed to the upper column turbine (UCT). Adjusting the turbine airflow can modulate the total amount of refrigeration generated by the cold box. A third air stream is fed to the bottom of the lower column. These three streams are described in the next section.

Cold Box

Early cryogenic designs had a single distillation column and were inefficient and incapable of producing oxygen at very high purities. The two-column design, as shown in Figure 2-2, solved both problems. The two columns are thermally linked by a reboiler, a heat exchanger that prohibits mixing of fluids. The double column design has not changed since its introduction in the 1930s. The upper column is under low pressure and the lower column is under high pressure.

The air stream to the oxygen boiler is cooled and condensed against product oxygen and waste nitrogen streams. The outgoing product oxygen stream and waste nitrogen stream are heated from cryogenic temperatures up to approximately ambient temperature. The cooled air stream is sent to both the upper and lower columns.

The turbine air stream is also cooled against warming nitrogen and oxygen streams. It is drawn from an intermediate location between the warm leg and the cold leg of the PHX. It is then expanded and cooled in the upper column turbine (UCT). The UCT drives a generator that provides power for the plant. The UCT air stream enters two-thirds of the way down the upper (low-pressure) distillation column. Injecting this stream directly into the low-pressure column increases mixing and thus the effectiveness of the column.

The cooled air stream entering the lower column is separated into nitrogen at the top and oxygen-enriched air (kettle liquid) at the bottom. The crude liquid oxygen at the bottom is approximately 45% pure. Argon is removed at this point to allow oxygen product purity of greater than 97% later. The nitrogen at the top of the column is condensed in the main condenser against boiling oxygen from the upper column. A portion of the condensed nitrogen from the main condenser is used as reflux for the lower column. The remainder is sub-cooled in the cross-flow passages in the nitrogen superheater section of the PHX against warming gaseous nitrogen streams from the upper column. This sub-cooled liquid nitrogen stream then enters the top of the upper column as reflux. The kettle liquid is sub-cooled in the cross flow passes of the nitrogen superheater section of the PHX and then enters the upper about 2/3 of the way down the column.

The upper column also produces waste nitrogen from the top. This nitrogen may be further purified in the upper column and sold as a by-product. The gaseous nitrogen stream is the coldest stream in the plant and is often used to subcool other streams within the coldbox, as illustrated in Figure 2-2. The nitrogen is warmed in all sections of the PHX to near-ambient temperatures. The product oxygen is boiled in the oxygen boiler against the condensing air stream and exits as product.

The upper column produces high purity liquid oxygen. The liquid oxygen falls to the bottom of the column. Unlike the high-pressure column, this liquid is high purity product. When LOX product is desired, it can be taken from this pool. However, this results in a loss of plant efficiency and a lower gaseous oxygen output. Since oxygen needed for combustion is usually gaseous, it is assumed that large quantities of LOX are not needed. The liquid at the bottom of the column is sent through the reboiler, where it is boiled by the heat of the condensing nitrogen in the high-pressure column. This high purity gas is piped out of the low-pressure column and sent through the main heat exchanger (PHX), where it cools the incoming air. The product oxygen exits near ambient temperature and 115 kPa (2 psig). If high-pressure product is desired, the oxygen is compressed by oxygen compressors.

2.2 Oxidant Feed Performance Model

2.2.1 Gas Flow – Gasification

IGCC systems operate at high pressures and require a pressurized oxidant feed. The IGCC power plant is modeled to consist of 95 percent pure oxygen at 250 ^{o}F and 734 psia. The mass flow rate of oxidant is set to match the

molar flow rate of oxygen required by the gasifier model. The oxidant is assumed to be combined with the coal slurry. The only impurities in the oxidant are nitrogen and argon.

2.2.2 Gas Flow – Oxyfuel

Advanced combustion systems (e.g., oxyfuel) operate at near-atmospheric pressures and do not require a pressurized oxidant fee. First generation Oxyfuel systems will likely adapt a standard boiler design by mixing recycled flue gas with high-purity oxygen. Future designs will likely avoid externally recycled flue gas and use high-purity oxygen directly in the boiler. This type of system is modeled to consist of 95 percent pure oxygen at 59 ˚F and atmospheric pressure. The mass flow rate of oxidant is set to match the molar flow rate of oxygen required by the boiler model. The only impurities are nitrogen and argon.

2.2.3 Energy Use

The oxygen plant consumes significant amounts of electric power, thereby reducing the saleable electrical output of the power plant. When reporting costs on a normalized basis (e.g., $/kW or mills/kWh), it is important to use an accurate estimate of the net electrical production available for sale. The performance model does not estimate the internal electrical load, hence a simple regression model of power consumption versus key flow rates has been developed for the oxygen plant. This model provides an accurate estimate of the plant electrical requirements. It replaces the previous regression models (Frey, 1990 and Frey, 2001).

There are three main factors that affect the required power input to an ASU:

1. the volume or amount of oxygen product to be produced,
2. the purity of the product, and
3. the delivery pressure of the product.

While there are other factors that affect plant performance, such as the ratio of liquid versus gaseous oxygen produced, they are not considered in this model.

The power required to operate an oxygen plant can be divided into four sections: (1) the main air compressor (MAC), (2) the refrigeration system to compensate for heat losses in the cold box, (3) auxiliary and control systems, and (4) the final oxygen product compressor (if required). The first three sections will be combined together into one component of the energy model and referred to as the MAC power. Since the delivery pressure, and thus the amount of power needed to compress the oxygen product, is independent of the separation process, it will be treated as a separate component of the energy model.

Figure 2-3 shows the power required by an oxygen plant as a function of the oxygen purity of the product stream (McKetta, 1990). This figure shows a characteristic shape that is a result of the interaction of two factors, namely the input air stream compression (not a function of oxygen purity) and power generated from exhaust air expansion (decreasing with oxygen purity).

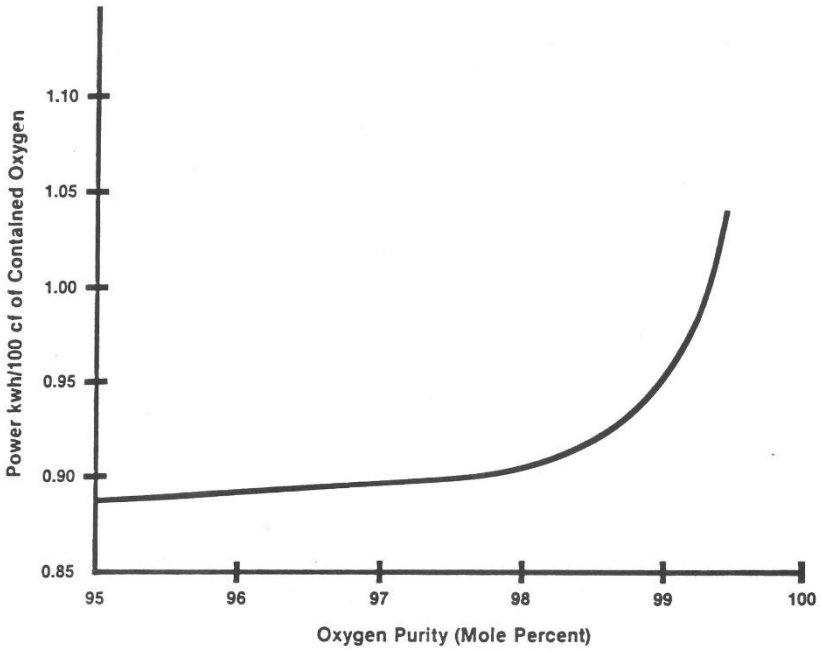

Figure 2-3. Effect of oxygen purity on ASU power (McKetta, 1990)

The input air stream must be compressed to approximately 550 kPa (79.8 psi), regardless of the product purity. This requires around 1.05 kW/100 cubic feet of oxygen product. This assumes a compressor efficiency of 75%, which is a typical value for current commercial applications in large-scale plants. After the air stream is compressed, it is later expanded in the plant to cool the air stream. The process is called a Joule-Thompson expansion.

The air stream is expanded through a turbo expander, which generates power that can be fed back into the oxygen separation plant. This expansion creates a power credit. As the purity requirement increases, the fraction of the air stream that can be expanded in this way decreases exponentially. This is because the air stream is expanded in the low-pressure column rather than going through the high-pressure column first. This air will avoid the numerous distillation stages in the high-pressure column, and therefore will decrease the purity of the product. This dilution effect becomes more pronounced as the desired purity increases. The overall result is a decrease in the power credit from about 0.16 kW/100 cubic feet of oxygen at 95% purity to approximately zero at 99.5%, even though the required power input remains constant at 1.05 kW/ 100 cubic feet of oxygen product.

The MAC power as summarized in Figure 2-3 is given in units of kilowatts per 100 cubic feet of oxygen product as a function of the oxygen purity. The relationship can be divided into two regimes with a purity of 97.5% separating them. Each region is represented by a regression curve to fit the relationship.

$$MAC\ Power = 4.88e^{-3}\eta_{ox} + 0.4238 \qquad \eta_{ox} < 97.5 \qquad (2\text{-}1)$$

$$MAC\ Power = \frac{7.361e^{-2}}{(100 - \eta_{ox})^{1.316}} + 0.8773 \qquad \eta_{ox} > 97.5 \qquad (2\text{-}2)$$

where,

$$0.85 \le MAC\ Power \le 1.05\ \text{kW/100 cf of oxygen}$$

$$95 \le \eta_{ox} \le 99.5$$

In Equations (2-1) and (2-2), MAC Power has a range from 0.85 to 1.05 kW/100 cubic feet of oxygen. The oxygen purity range specified above is typical for a cryogenic ASU.

The oxygen product exits at 115 kPa (16.7 psi). If higher pressure oxygen is desired, the product is fed through inter-cooled oxygen compressors. The model for this process utilizes the ideal gas law and is stated below in Equation (2-3)

$$PC\ Power = P_i \times \dot{V} \ln\left(\frac{P_o}{P_i}\right) \times \frac{1}{\eta} \tag{2-3}$$

PC Power is the required power input to the oxygen product compressor in kW. A typical value for the efficiency is 0.75.

2.3 Oxidant Feed Cost Model

Cost data for 31 cryogenic oxygen plants were taken from 14 studies of oxygen-blown IGCC systems, all prepared for EPRI. These plants all include electric motor-driven compressors. Data from coal-to-syngas systems were not included because many of these use steam-driven, rather than motor-driven, compressors. Electric motor-driven systems offer advantages in terms of plant operation, although steam-driven systems may be more energy efficient. These plants produced between 625 and 11,350 lb mole/hr of oxygen per train. A typical plant consists of two parallel operating trains with no spare trains. Each train includes an air compression system, air-separation unit and an oxygen compression system. For more detail on the oxygen plant design, see Fluor (2003). The oxygen plants represented in the database are considered commercially available.

2.3.1 Direct Capital Cost

This process section typically has an air compression system, an air separation unit, and an oxygen compression system. The direct cost of oxygen plants is expected to depend mostly on the oxygen feed rate to the gasifier, because the size and cost of compressors and the air separation systems are proportional to this flow rate. The oxygen purity of the oxidant feed stream is expected to affect the cost of the air separation system. As oxygen purity increases, it is expected that the cost of the oxygen plant will increase because the size of equipment in the air separation plant (e.g., high pressure column) increases. The ambient temperature determines the volume flow rate of air entering the inlet air compressor; as ambient temperature increases, the volume flow rate increases for a given mass flow, thereby requiring an increased compressor size.

A number of regression models were considered in which alternative combinations of predictive parameters and functional forms were assumed. These regressions were based on nonlinear variable transformations using the natural logarithm. A single variant regression of cost and oxygen flow rate, using an exponential scaling formulation yielded excellent results ($R^2 = 0.9$). The scaling exponent in this case was 0.9. The addition of terms for ambient temperature and oxidant purity yielded a marginal improvement in the summary statistics for the model. From an engineering viewpoint, the inclusion of these additional predictive terms significantly improves the utility of the model, allowing costs to be sensitive to both primary and secondary factors. A multivariate regression is assumed for the oxidant feed process area direct capital cost (Frey, 2001). The direct cost model for the oxidant feed section is given in Equation (2-4):

$$DC_{OF} = 196.2 \frac{N_{T,OF} T_a^{0.067}}{1 - \eta_{ox}^{0.073}} \left(\frac{M_{O,G,i}}{N_{O,OF}}\right)^{0.5618} \qquad \begin{matrix} R^2 = 0.86 \\ n = 7 \end{matrix} \tag{2-4}$$

where,

$$20 \le T_a \le 95$$

$$625 \le \frac{M_{O,G,i}}{N_{O,OF}} \le 17{,}000$$

$$0.95 \le \eta_{ox} \le 0.98$$

The regression form used in Equation (4) is based on the regression form developed by Frey (Frey, 1990). Frey developed the regression equation based on 31 data points, resulting in a variance of 0.94. The Frey regression

form was modified to fit data from recently published reports (Chase and Kehoe, 2003; Foster et al., 2003; IEA, 2003; Brdar and Jones, 2003). Figure 2-4 shows the data points used for this regression. Costs are provided in December 2000 dollars and can be scaled to other years using the Chemical Engineering Plant Cost Index.

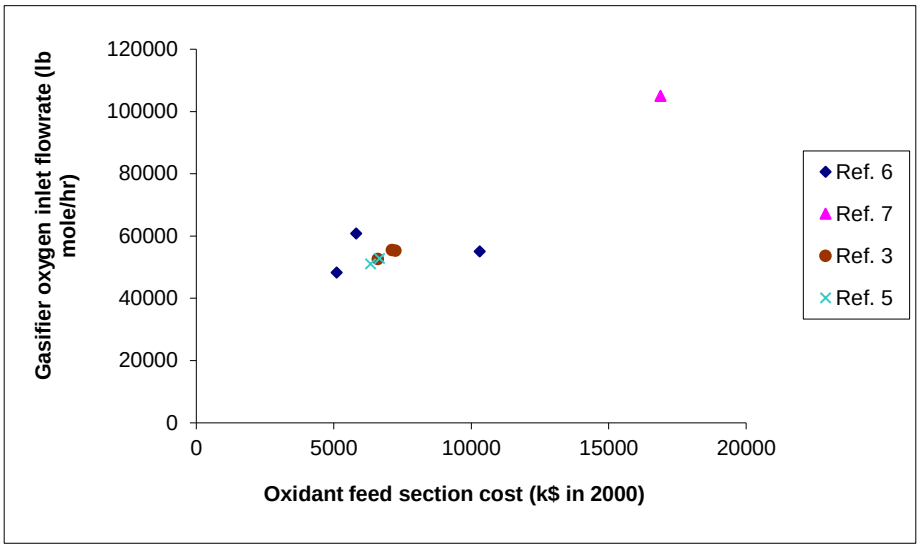

Figure 2-4. Oxygen flow rate vs. oxidant feed section cost

The robustness of the exponential scaling relationship between oxygen flow rate and direct capital cost is indicated by the similarity of the exponent for oxygen flow rate in the single and multi-variable regression models. In the single variable model previously described, the exponent was 0.9, while for the multivariate model above it is 0.86. The limits for each parameter indicated above represent the ranges for which the regression model is valid. While to obtain accurate results, these ranges should not be violated, it is not a severe violation to exceed the range for the oxygen flow rate per train, particularly on the high side, because the model reasonably captures the expected relationship between oxygen flow rate and cost. An alternative to extrapolating the model for oxygen flow rate per train, however, is to alter the number of trains so that the flow rate per train is within the limits given above. The ambient temperature and oxygen purity parameters should not be extrapolated.

2.3.2 Indirect Capital Cost

Indirect capital costs are directly related to direct capital costs (referred here as process facilities capital or PFC) and often expressed as a fraction of the plant facilities capital. There are several categories of indirect costs that are specified in the model.

The general facilities section includes cooling water systems, plant and instrument air, potable and utility water, and electrical systems. Engineering and home office fees include the costs associated with engineering, office expenses, and fees or profit to the engineer. Process contingency is used to determine cost estimates for expected increase in the capital cost of an advanced technology due to uncertainty in performance. Project contingency is used to determine cost estimates for expected increase in the capital cost resulting from a more detailed estimate for a specific project at a particular site. Miscellaneous capital includes equipment needed to bring the system to full capacity. Inventory capital includes raw materials and spare parts available in storage.

Indirect Cost Category	Cost
General Facilities	15% PFC
Engineering & Home Office Fees	10% PFC
Project Contingency	15% PFC
Process Contingency	5% PFC*
Royalty Fees	0.5% PFC
Miscellaneous Capital	2% TPI
Inventory Capital	0.5% TPC

PFC = Plant Facility Cost (direct capital only); TPC = Total Plant Cost (direct and indirect costs ignoring finance and escalation costs); TPI = Total Plant Investment (direct and indirect costs including finance and escalation costs)

2.3.3 O&M Cost

The annual costs of the ASU consist of fixed and variable operating costs. The fixed operating costs are annual costs including operating labor, maintenance costs (2% of the total plant cost) of which a portion is allocated to maintenance labor, and overhead costs associated with administrative and support labor. These are defined by the following equations:

$$Oper.\ Labor = \left(\frac{\$}{hr}\right) \times \left(\frac{jobs}{shift}\right) \times \left(\frac{shifts}{day}\right) \times \left(\frac{40\ hr}{wk}\right) \times \left(\frac{52\ wk}{yr}\right)$$

$$Maint.\ Labor = 0.4 \times Total\ Maint.\ Cost$$

$$Adm.\ \&\ Support\ Labor = 0.3 \times (Oper.\ Labor + Maint.\ Labor)$$

The variable operating costs include consumables, fuels, and byproduct credits. For the ASU process area, these costs are assumed to be negligible.

2.4 Illustrative Example

Suppose an IGCC plant requires a maximum production of 2,500 standard tons per day of 97.5% purity oxygen. The required pressure at the gasifier is 700 kPa. In order to provide this amount of oxidant, the number of ASU production trains, the power requirements, capital cost, and operating costs need to be determined. The following sections detail the calculations to determine these values. The costs are reported in December 2000 dollars, but may be adjusted to other years using the Chemical Engineering Plant Cost Index.

2.4.1 Number of Trains

Equation (4) includes a maximum size limit of 11,375 lbmole/hr of oxygen for one ASU train. Because we wish to compare the required flow rate to the maximum flow rate, we need the actual flow rate of oxygen:

$$2{,}500\ stpd * \left(\frac{1{,}000\ scfh}{1\ stpd}\right) = 2{,}500{,}000\ scfh\ product$$

$$(2{,}500{,}000\ scfh\ product) * 0.975 = 2{,}437{,}500\ scfh\ O_2$$

$$2{,}437{,}500\ scfh\ O_2 * \left(\frac{0.00255\ lbmole}{1\ scf}\right) = 6{,}220\ lbmole/hr\ O_2$$

* This level of contingency is associated with a well-defined plant that has been demonstrated commercially.

This required flow rate is below the maximum flow rate for one ASU train (11,375 lbmole/hr). Hence, only one ASU train is required to transport the 6,220 lbmole/hr of oxygen required by the IGCC plant.

2.4.2 Power Requirement

The IGCC requires oxygen pressure of 700 kPa to be delivered, higher than the 115 kPa threshold of the main air compressor. Additional compression will be required of the product stream, so both Equation (2-1) and Equation (2-3) will be used to determine the total power requirement. The main air compressor power can be calculated from either Equation (2-1) or equation (2-2) (97.5% purity is the cutoff value). Equation (2-1) is used to calculate the main air compressor power requirement below:

$$2500\,stpd * (\frac{1000\,scfh}{1\,stpd}) = 2{,}500{,}000\ scfh$$

$$\begin{aligned} MAC\ Power &= 4.88 * 10^{-3} * (97.5) + 0.4238 \\ &= 0.8996\ kWh/100\,scf \end{aligned}$$

$$\begin{aligned} MAC\ Power &= (0.8996\ kWh/100\ scf) * (2{,}500{,}000\ scfh) \\ &= 22{,}490\,kW = 22.49\ MW \end{aligned}$$

The additional power to compress the product stream from 115 kPa to 700 kPa is calculated from Equation (2-3). Assume the efficiency of the compressor is 75%.

$$2{,}500{,}000\,scfh * (\frac{1\,m^3}{35.31\,ft^3}) * (\frac{1h}{3600\,s}) = 19.66\,m^3/s$$

$$\begin{aligned} PC\ Power &= (115\,kPa) * (19.66\,m^3/s) * \ln(\frac{700\,kPa}{115\,kPa}) * \frac{1}{0.75} \\ &= 5{,}450\ kW = 5.45\ MW \end{aligned}$$

$$Total\ Power = 22.49\ MW + 5.45\ MW = 27.94\ MW$$

The total power required to produce the maximum flow rate of oxygen product is 27.9 MW. This is the power that must be supplied to the air separation unit from an outside source or from the plant directly.

2.4.3 Capital Cost

The average ambient temperature surrounding the plant is 65°F. For this example, only one ASU train is required as shown in the previous sections. We will assume that this train operates continuously (i.e., no spare train).

$$2{,}500\,stpd * (\frac{1{,}000\,scfh}{1\,stpd}) = 2{,}500{,}000\ scfh\ product$$

$$(2{,}500{,}000\ scfh\ product) * 0.975 = 2{,}437{,}500\ scfh\ oxygen$$

$$2{,}437{,}500\ scfh\ O_2 * (\frac{0.00255\,lbmole}{1\,scf}) = 6{,}220\ lbmole/hr\ O_2$$

$$PF\ Cost = \frac{15.91 * (1train) * (65°F)^{0.067}}{(1 - 0.975)^{0.073}} (\frac{6{,}220\,lbmole/hr}{1train})^{0.852}$$

$$PF\ Cost = \$47{,}032\ (\$1{,}000) = 47.0\ M\$$$

$$General\ Facilities = 0.15 \times 47.0 = 7.05\ M\$$$

$$Eng'r\ \&\ Home\ Office = 0.10 \times 47.0 = 4.7\ M\$$$

$$Project\ Contingency = 0.15 \times 47.0 = 7.05\ M\$$$

$$Process\ Contingency = 0.05 \times 47.0 = 2.35\ M\$$$

$$Royalty\ Fees = 0.005 \times 47.0 = 0.24\ M\$$$

$$Total\ Plant\ Cost = 47.0 + 7.05 + 4.7 + 7.05 + 2.35 + 0.24$$
$$= 68.39\ M\$$$

The costs are reported in December 2000 dollars, but may be adjusted to other years using the Chemical Engineering Plant Cost Index.

2.4.4 Operating and Maintenance Cost

There are only fixed variable costs associated with the air separation unit, as mentioned above. The total maintenance cost combines materials and labor costs and is taken to be 2% of the total plant cost calculated in the previous section. The maintenance cost is:

$$Maint.Cost = 0.02 \times \$68.39 = \$1.37\ M\$$$

Maintenance labor is 40% of the total maintenance cost, or 0.55 M$. The operating labor assumes 6.67 jobs/shift and 4.75 shifts/day. With a labor rate of 25 $/hr, the operating labor cost is:

$$Oper.\ Labor = 25 \times 6.67 \times 4.75 \times \left(\frac{40\ hr}{wk}\right) \times \left(\frac{52\ wk}{yr}\right) = 1.65\ M\$$$

$$Maint.\ Labor = 0.4 \times 1.37 = 0.55\ M\$$$

$$Adm.\ \&\ Support\ Labor = 0.3 \times (1.65 + 0.55) = 0.66\ M\$$$

$$Fixed\ O\&M\ Cost = 1.37 + 1.65 + 0.66 = 3.68\ M\$$$

These costs are given in December 2000 dollars (the cost year basis for the total plant cost).

References

Alstom (2003). Volume 1: Evaluation of Advanced Coal Combustion & Gasification Power Plants with Greenhouse Gas Emission Control and Volume 2: Bench-scale Fluidized Bed Combustion Testing**.** Final Report prepared by Alstom Power, Inc. to Department of Energy National Energy Technology Center. Pittsburgh, PA. PPL-03-CT-09. May, 2003.

Baukal, C.E. (1998). Oxygen-Enhanced Combustion, CRC Press, LLC, Boca Raton, FL. 1998.

Brdar R.D., and R.M. Jones (2003): *GE IGCC Technology and Experience with Advanced Gas Turbines*, GE Power Systems, GER-4207, 2003.

Chase, D.L., and P.T. Kehoe (2003). *GE Combined-Cycle Product Line and Performance*. GE Power Systems, GER-3574G, 2003.

Foster A.D., H.E. Doering, and M.B. Hilt M.B. (2003): *Fuel flexibility in heavy-duty gas turbines*, GE Company, Schenectady, New York, 2003.

Frey, H.C. and E.S. Rubin (1990). Stochastic Modeling of Coal Gasification Combined Cycle Systems: Cost Models of Selected Integrated Gasification Combined Cycle (IGCC) Systems**.** Task 2 Topical Report prepared by Carnegie Mellon University for the U.S. Department of Energy, Morgantown Energy Technology Center, Morgantown, WV. DOE/MC/24248-2901, NTIS DE90015345. June 1990.

Frey, H.C., and N. Akunuri (2001). Probabilistic Modeling and Evaluation of the Performance, Emissions, and Cost of Texaco Gasifier-Based Integrated Gasification Combined Cycle Systems Using ASPEN. Prepared by

North Carolina State University for Carnegie Mellon University and U.S. Department of Energy, National Energy Technology Center, Pittsburgh, PA. January 2001.

IEA (2003). *Potential for improvement in gasification combined cycle power generation with CO_2 capture*, IEA Greenhouse Gas R&D Program, report number PH4/19, 2003.

McKetta, J. (1990). Encyclopedia of Chemical Processing and Design, Vol. 31, pg. 214, 1990.

3. GE Entrained-Flow Gasifier

Nomenclature

Technologies

LTGC = Low temperature gas cooling area (gas quench)

CH = Coal handling and slurry preparation

G = Gasifier area

PG = Process condensate treatment

Parameters

$W_{e, CH}$ = Coal handling auxiliary power, kW

$W_{e, G}$ = Gasification auxiliary power, kW

$W_{e, LT}$ = LTGC auxiliary power, MW

$W_{e, PC}$ = Process condensate auxiliary power, kW

$m_{cf, G, i}$ = Coal feed rate to gasifier, tons/day

$m_{syn,LT\ i}$ = Syngas flowrate into LTGC, lbmole/hr

$m_{syn,LT\ o}$ = Syngas flowrate from LTGC, lb/hr

m_{SBD} = Scrubber blowdown flowrate, lb/hr

$N_{O, G}$ =Number of operating gasifier trains

$N_{T, G}$ = Total number of gasifier trains (operating and spare)

$N_{O, LT}$ =Number of operating LTGC trains

$N_{T, LT}$ = Total number of LTGC trains (operating and spare)

DC_{CH} = Direct capital cost of coal handling section, $1000

DC_{G} = Direct capital cost of gasification section, $1000

DC_{LT} = Direct capital cost of LTGC section, $1000

3.1 GE Gasifier Process Description

This report describes a GE entrained-flow gasifier-based IGCC system with total quench high temperature syngas cooling using coal. The GE entrained-flow gasifier (originally developed by Texaco) has been used since 1956 for chemical and power applications. Although primarily used for chemical production in the past, a prototype gasifier was built in 1984 (Clearwater Project) and the first full-scale plant was built in 1995 (Polk Station).

The GE gasifier is an entrained flow gasifier, as are the Shell gasifiers and ConocoPhillips E-Gas gasifiers (originally developed by Dow). Entrained flow gasifiers have high outlet temperatures and operate in the slagging range (the ash is fully liquid with low viscosity). The GE gasifier has the benefit of being able to handle a large variety of coal types, produce a syngas free of oils and tars, exhibit a high carbon conversion, produce low concentrations of methane, and produce a high throughput (due to the high reaction rates at elevated

temperatures). A detraction of the GE gasification system is the higher oxygen requirement to achieve the higher temperature, resulting in higher auxiliary electrical requirements. Also associated with the higher temperature is the increased coal oxidation, resulting in a lower cold gas efficiency.

The GE gasification system uses a coal in water slurry in a single-stage down flow reactor configuration, as shown in Figure 3-1. The dry solids concentration in the slurry is typically around 65%. A pump delivers the slurry to the gasifier at pressures in the range of 500-1,000 psi. The gasifier is refractory lined and typically operates in the range of 2250-2,900 F. Oxygen is used to combust only a portion of the feedstock in order to provide thermal energy needed by endothermic gasification reactions. The hot raw syngas leaves the gasifier and is cooled either by a series of radiant and convective heat exchangers to a temperature of 650 ^{o}F or by contact with water to a temperature of 433 ^{o}F. The syngas passes through a wet scrubbing system to remove particulate matter and water soluble gases such as NH_3.

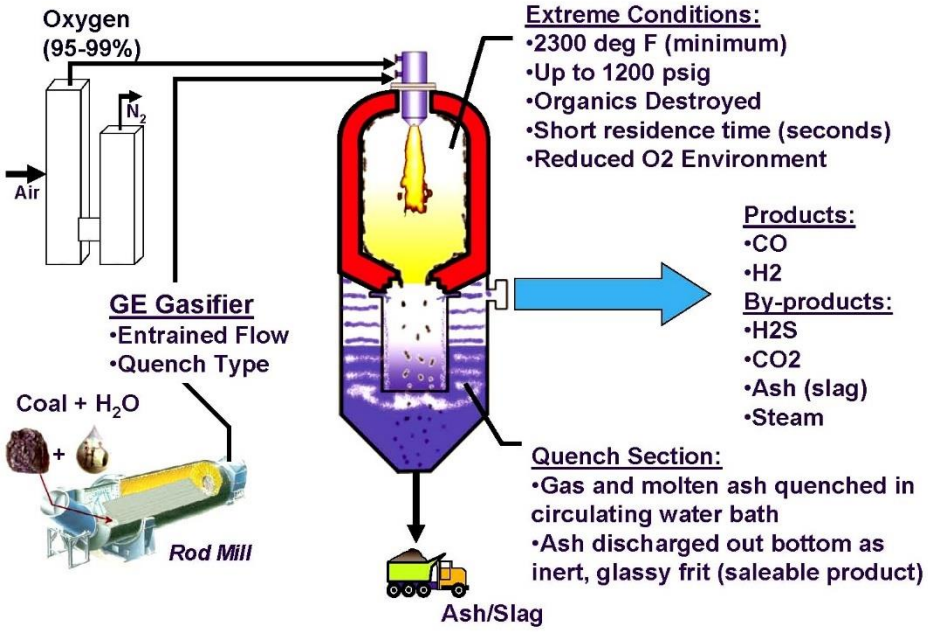

Figure 3-1. GE entrained gasifier schematic (taken from Eastman Gasification Services Company, 2005)

The details of the major process areas are briefly described below.

3.1.1 Coal Handling

Coal handling involves unloading coal from a receiving vessel (train, truck or barge), storing the coal, moving the coal to the grinding mills, and feeding the gasifier with positive displacement pumps. A typical coal handling section contains one operating train and no spare train. A train consists of a bottom dump railroad car unloading hopper, vibrating feeders, conveyors, belt scale, magnetic separator, sampling system, deal coal storage, stacker, reclaimer, as well as some type of dust suppression system.

Slurry preparation trains typically have one to five operating trains with one spare train. The typical train consists of vibrating feeders, conveyors, belt scale, rod mills, storage tanks, and positive displacement pumps to feed the gasifier. All of the equipment for both the coal handling and the slurry feed are commercially available.

The feed coal is crushed and slurried in wet rod mills. The coal slurry containing about 66.5 weight percent solids is fed into the gasifier, which is an open refractory-lined chamber, together with a feed stream of oxidant. The slurry is transferred to the gasifier at high pressure through charge pumps. The water in the coal slurry acts as a temperature moderator and also as a source of hydrogen in gasification (Simbeck et al., 1983).

3.1.2 Gasification

GE entrained-flow gasification can handle a wide variety of feedstocks including coal, heavy oils, and petroleum coke (Preston, 1996). The current study focuses on IGCC systems using coal feed. Oxygen is assumed as the oxidant for the IGCC systems evaluated in this study. The oxidant stream contains 95+ percent pure oxygen. The oxygen is compressed to a pressure sufficient for introduction into the burner of the GE entrained-flow gasifier (Matchak et al., 1984). Operation under high pressure is beneficial to increase the capacity of the gasifier reactor volume and thereby reduce capital cost. It is also beneficial to downstream processes because of increased partial pressures.

The coal slurry and oxidant feed are delivered to the gasifier burners. Gasification takes place rapidly at temperatures exceeding 2,300 °F. Coal is partially oxidized at high temperature and pressure. Figure 3-2demonstrates the temperature variation across the gasifier (Simbeck et al., 1983). The combustion zone is near the top of the reactor, where the temperature in the gasifier changes from approximately 250 to 2500 °F. The operating temperature is sufficiently higher than the ash fusion temperature of 2,300 °F to cause the ash to become molten and separate out easily from the raw gas. A portion of the coal feed burns, providing heat for the endothermic gasification reactions that result in the formation of CO, CO_2, H_2, CH_4, and H_2S.

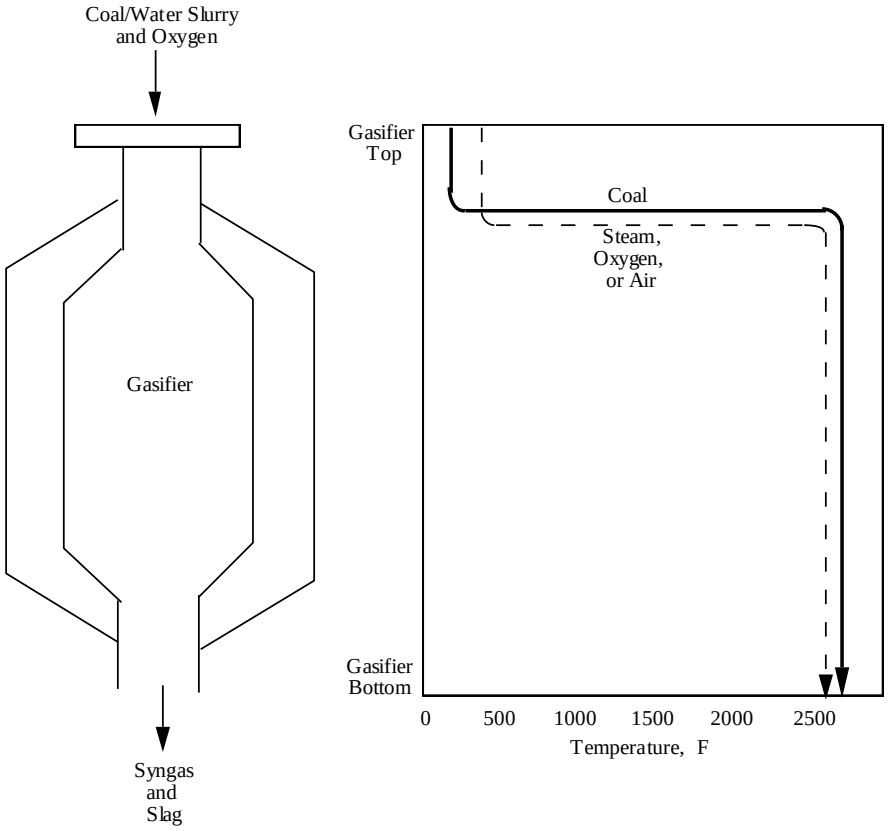

Figure 3-2. Temperature Variation in an Entrained Gasifier (Based on Simbeck et. al., 1983)

The syngas leaves the gasifier at temperatures in the range of 2300 °F to 2700 °F. Because of the high temperatures characteristic of entrained-flow gasifiers, the syngas contains smaller amounts of methane than other types of gasifiers and is free of tars and other hydrocarbons (Simbeck et al., 1983).

Chemical Reactions

The chemical reactions modeled in the equilibrium gasifier reactor model are:

$$C + 2H_2 \rightarrow CH_4 \quad (3\text{-}1)$$

$$C + H_2O \rightarrow CO + H_2 \quad (3\text{-}2)$$

$$CO + H_2O \rightarrow CO_2 + H_2 \quad (3\text{-}3)$$

$$CH_4 + 1.5O_2 \rightarrow CO + 2H_2O \quad (3\text{-}4)$$

$$2CO + O_2 \rightarrow 2CO_2 \quad (3\text{-}5)$$

$$S + H_2 \rightarrow H_2S \quad (3\text{-}6)$$

$$N_2 + 3H_2 \rightarrow 2NH_3 \quad (3\text{-}7)$$

$$CO + H_2S \rightarrow COS + H_2 \quad (3\text{-}8)$$

$$Ar \rightarrow Ar \quad (3\text{-}9)$$

Equations (3-1), (3-2), and (3-3), are the primary gasification reactions. Equation (3-1) is an exothermic reaction and is known as methanation. The formation of methane increases the heating value of the product gas. Equation (3-2) is an endothermic reaction, more generally known as the "water gas reaction". Equation (3-3) is an exothermic reaction, more generally known as the "water gas shift reaction." Equations (3-2) and (3-3) together lead to the formation of hydrogen. Equation (3-4), in series with Equation (3-1), represents the partial combustion of coal and Equation (3-5) in sequence with Equations (3-1) and (3-2), models the complete oxidation of coal.

Sulfur Compounds

Over 90% of the sulfur in the feedstock is converted to hydrogen sulfide (H_2S) and the rest is converted to carbonyl sulfide (COS). Compounds such as SO_2 and SO_3 are absent in the syngas. Because COS is difficult to capture, a hydrolysis unit or shift reactor is required to convert the COS to H_2S prior to acid gas removal.

Nitrogen Compounds

Nitrogen enters the gasifier both as a molecule (an impurity from the air separation unit) and as fuel-bound nitrogen. Gasifiers produce primarily ammonia (NH_3) with negligible amounts of NO or NO_2, because of the reducing conditions in the gasifier.

Chlorine Compounds

Most of the chlorine in the coal is converted to hydrogen chloride gas (HCl). Chlorine compounds from the coal may also react with ammonia to form ammonium chloride (NH_4Cl). Most of the chlorides are removed in a water scrubber.

Solid carbon and ash

Some char (unconverted carbon) and ash will always be entrained in the gas flow exiting the gasifier. The quench removes a majority of the solid particles, preventing fouling occurrences downstream. After capture, the particles may be recycled to the gasifier to increase the carbon conversion efficiency.

3.1.3 Syngas Quenching

The temperature of the syngas exiting the gasifier is typically around 2,300 F and the fly ash or slag exists in liquid form. To protect downstream components from fouling, a quench is needed to solidify the slag.

A water quench uses sensible heat from the syngas to vaporize water. This quench drives the water gas shift reaction to increase the H2/CO ratio, a benefit in the case of CO_2 capture performed downstream.

The scrubbed gas enters various heat exchangers in the low temperature gas cooling section. The heat removed from the syngas is utilized to generate low-pressure steam to heat feed water or as a source of heat for fuel gas saturation.

3.1.4 Particle Capture

Dry solids still entrained in the syngas are removed by a wet scrubbing system. The scrubbers operate at a temperature below the dew point of the gas so that the particles can serve as nuclei for condensation and result in more efficient removal. The particle-laden water is sent to a water treatment plant and the clarified water used again as quench water.

3.2 GE Gasifier Performance Model

The Integrated Environmental Control Model (IECM) is a desktop model developed by Carnegie Mellon University as a tool for assessing the technical performance, cost and environmental effectiveness of different fossil fuel power generation technologies. The broad framework of the model consists of a base power plant, with options to add modules for meeting environmental regulations with respect to emissions of NO_x, SO_x, particulates, mercury and CO_2. The user is thus able to determine the performance and cost of the overall plant equipped with one or several of the above modules. The IECM has recently been expanded to include Integrated Gasification Combined Cycle (IGCC) process in addition to the combustion-based systems.

IGCC is a promising technology for power generation from coal. It offers several advantages as compared to the conventional PC boiler including higher process efficiency, lower emissions of SO_2 and NO_x and easier capture CO_2 for sequestration. Because of the differences between different types of gasifiers, it is important to have a gasifier model that accurately predicts the syngas composition, which in turn determines the power output of the downstream gas turbine and steam cycle blocks. However, there are trade-offs involved because of the complexity associated with modeling the gasification process. Detailed gasifier models that employ computational fluid dynamics (CFD) are time consuming, data intensive and costly to run. A less complex (but still time consuming) approach is to model the gasifier using a commercial process simulator like ASPEN Plus, and then "import" the results into the IECM by developing suitable output data tables (Figure 3-3).

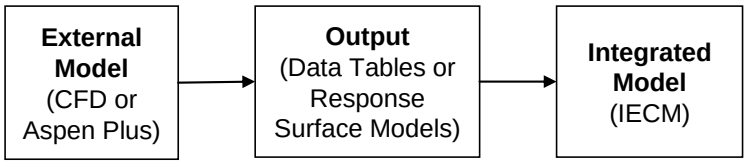

Figure 3-3. Linkage between the gasifier external model and the IECM

We have taken this approach in modeling the gasifier. This report summarizes the development of data tables for performance assessment of a coal gasifier in IGCC power plants. The major objective of this evaluation is to identify the key thermodynamic and process variables in a gasifier and to study the impact on the composition of synthesis gas. Our modeling approach was an extension of the Aspen Plus model previously developed by the National Energy Technology Laboratory (NETL). These models were modified to run as a stochastic simulation. This capacity provides a powerful and efficient way to generate model response to simultaneous changes in several key input variables. The output results are then used to develop an output data table and a response surface model of the gasifier.

3.2.1 Aspen Plus Gasifier Simulation

The next several sections briefly describe the Aspen Plus flowsheet components used to generate the output data tables and response surface models.

Oxidant Feed

The reaction temperature and heat loss in the gasifier, which is assumed to be 1% of the total low heating value of the inlet coal flow, in the gasification reactor is maintained by adjusting the inlet flow rate of oxygen.

The gasifier oxidant feed was fixed at a value of 95% purity. The Aspen Plus gasifier model adjusted the flow of oxidant required such that the heat loss from the gasifier is less than or equal to one percent of the total heat input to the gasifier. Thus, the Aspen Plus model calculates the oxygen flow required obtaining the user specified

gasifier outlet temperature and overcoming this heat loss. The coal slurry and oxidant feed are mixed and sent to the gasification unit model.

Coal Slurry Preparation and Gasification

Coal from the coal grinding system is continuously fed to the grinding mill. Grey water from waste water treatment facility is used for slurrying the coal feed. The coal slurry with a desired slurry concentration is pumped into the gasifier. In this section, the methodology used to model coal preparation is presented.

Coal is a type of non-conventional solid, and its composition has to be input in a form suitable to Aspen Plus. In Aspen Plus, the component attributes of coal are specified in three forms: (1) a proximate analysis, (2) an ultimate analysis, and (3) a sulfur analysis. Table 3-1, as an example, gives the typical compositions of Pittsburgh #8 coal and its input values for the Aspen Plus model. Aspen Plus estimates the heat of coal combustion based on these tables unless the heat of combustion is provided directly.

Table 3-1. Coal composition and its corresponding input in Aspen Plus

Coal composition (wet basis)		**Proximate Analysis**		**Ultimate Analysis**		**Sulfur Analysis**	
Element	Value	Element	Value	Element	Value	Element	Value
Ash	7.24	Moisture	5.05	Ash	7.63	Pyritic	1.23
Carbon	73.81	Fixed Carbon	49.855	Carbon	77.74	Sulfate	0
Hydrogen	4.88	Volatile Matter	42.515	Hydrogen	5.14	Organic	1
Nitrogen	1.42	Ash	7.63	Nitrogen	1.5		
Chlorine	0.06			Chlorine	0.06		
Sulfur	2.13			Sulfur	2.23		
Oxygen	5.41			Oxygen	5.7		

Figure 3-4 illustrates the mass and heat flows in the coal slurry preparation process and gasification units. The coal slurry is compressed through a slurry pump. The gasification simulation calculates the Gibbs free energy of the coal. However, the Gibbs free energy of coal cannot be calculated because it is a non-conventional component with regard to Aspen Plus. Hence, a coal decomposition unit operation, which simulates a reactor with a known yield and does not require the reaction stoichiometry and kinetics, decomposes the coal into its constituent elements based on the ultimate composition analysis of coal.

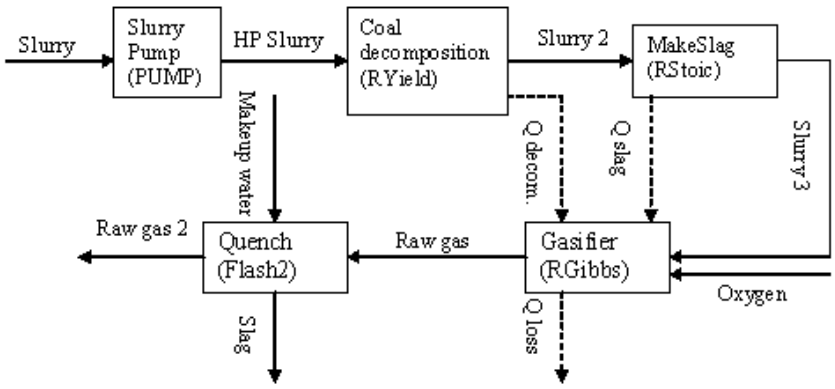

Figure 3-4. Slurry preparation and gasification flowsheet

The gasifier unit converts coal slurry into syngas. The coal slurry and oxygen from the air separation unit react in the gasifier at high temperature (approximately 2450 °F), high pressure (approximately 620 psia in this study) and under the condition of insufficient oxygen to produce syngas. Chemical reactions and their approach

temperatures[†] modeled in this equilibrium gasifier reactor are shown in Table 3-2.The syngas produced consists primarily of hydrogen and carbon monoxide with lesser amounts of water vapor, carbon dioxide, hydrogen sulfide, methane, and nitrogen. Traces of carbonyl sulfide and ammonia are also formed.

Table 3-2. Approach temperatures used in Aspen Plus to characterize non-equilibrium ([Altafini, 2003; Zaimal, 2002, Zhu, 2003)

Chemical Reaction	Approach Temperature
$C+2H_2 \rightarrow CH_4$	300°F
$C+H_2O \rightarrow CO+H_2$	
$C+O_2 \rightarrow CO$	
$2CO+O_2 \rightarrow 2CO_2$	550°F
$CH_4+2O_2 \rightarrow CO_2+2H_2O$	500°F
$S+H_2 \rightarrow H_2S$	500°F
$N_2+3H_2 \rightarrow 2NH_3$	500°F
$CO+H_2S \rightarrow COS+H_2$	500°F
$Cl_2+H_2 \rightarrow 2HCl$	300°F

Ash present in the coal melts into slag. Hot syngas and molten slag from the gasifier flow downward into a quench chamber, which is filled with water, and is cooled into medium temperature (approximately 450 °F). The slag solidifies and flows to the bottom of the quench chamber.

Third, raw syngas and molten slag discharge from the reactor into the quench chamber, which is simulated by the quench unit. This unit performs rigorous vapor-liquid equilibrium calculations to determine the thermal and phase conditions of syngas saturation process. In this quench unit, molten slag is cooled down and separated from the syngas.

Modeling Approaches

Computational Fluid Dynamics

There are two main approaches to modeling a gasifier. A detailed Computational Fluid Dynamics (CFD) based approach involves solving two sets of coupled equations. The first set of equations consists of the gas-phase Eulerian equations of the flow, transport and energy in the gasifier (essentially the turbulent Navier-Stokes equations modified for volatile combustion). The second set of equations consists of the discrete particle equations modeled in a Lagrangian frame. These equations involve particle's heating, devolatilization and char combustion. These two sets of equations are solved simultaneously with an appropriately defined grid. This approach is useful if one is interested in obtaining the temperature profiles in the gasifier, volatile combustion contours, kinetics of pollutant formation and carbon conversion. This approach is extremely time consuming and costly; the setup and run time of a typical simulation can take anywhere from days to weeks. This makes it difficult to identify and explore the critical variables and do sensitivity analysis.

Chemical Equilibrium

A second approach is to use the basic thermodynamics of carbon/char gasification based on a chemical equilibrium approach. This is the approach implemented in ASPEN. It can be accomplished much faster than CFD and hence is more convenient for sensitivity analysis. This approach is appropriate if one is interested only in the syngas composition and heating value, which is the primary need of the Integrated Environment Control Model (IECM). Thus, we have taken this approach in modeling the gasifier.

[†] The approach temperature is a pseudo-temperature used in Aspen Plus to adjust calculated equilibrium concentrations to actual (observed) values under non-equilibrium conditions.

Input Parameters

DOE's National Energy Technologies Laboratory (NETL) previously developed flowsheets for IGCC power plants in ASPEN for four different types of gasifiers: Shell, KRW, GE (previously Texaco) and E-Gas (previously Destec), all fed with nominal Illinois # 6 coal characteristics. These models were used to develop suitable data output tables for seven different types of coals:

4. Appalachian (Low Sulfur),
5. Appalachian (Medium Sulfur),
6. Illinois # 6,
7. North Dakota (Lignite),
8. WPC Utah (Bituminous),
9. Wyoming (PRB), and
10. Wyodak.

For each gasifier, there are several key design variables that are of interest such as temperature, pressure, oxidant flow rate, carbon conversion and the relative amounts of coal, oxidant and steam or water inputs to the gasifier. Perturbations in these quantities have an impact on the resulting syngas composition and heating value. We used NETL's ASPEN models to reflect this functionality by incorporating a stochastic variation of key gasifier variables as explained below.

The overall framework of the IECM for IGCC power plants is carried out as follows:

1. The user selects a gasifier technology from the four options mentioned above.
2. The user chooses a coal variety from several available options.
3. For each gasifier, there are several process variables that the user can vary within a specified range about the nominal (NETL specified) default value as will be discussed in a following section.
4. The model then calculates the composition and heating value of the syngas corresponding to the coal type and the process variables defined above. The syngas may consist of CO, H_2, CO_2, CH_4, H_2O, N_2, NH_3, COS, Ar, and H_2S.
5. The syngas composition along with user-specified plant size and other parameters is then utilized for mass and energy balance calculations for the overall plant.

As shown in Figure 3-3, an external model of the different gasifiers was used in Aspen Plus. A stochastic block developed at Carnegie Mellon University was added to the model to allow the model to vary parameters automatically and produce multiple output tables. Figure 3-5 shows the flow diagram for these simulations.

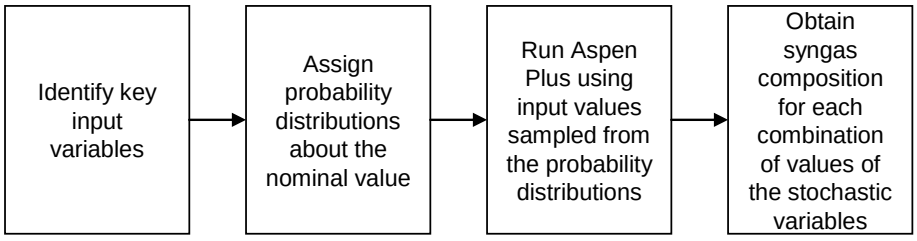

Figure 3-5. Flow diagram to generate data tables from Aspen Plus simulations

Running the Simulation

Running the Aspen Plus simulation involves the following steps:

1. First, a few key input variables are identified, which are critical in modeling the process and whose values are likely to fluctuate within a range, such as gasifier temperature, steam flow rate, carbon lost in slag etc.

2. The user then specifies a probability distribution for each of the above variables. In this case, a uniform distribution was used to reflect a range of values (typically $\pm 10\%$) around the nominal value. The distributions could be uniform, normal, logarithmic or lognormal etc. The user also decides on the number of samples (in this case 100 iterations).
3. Each of the probability distributions is sampled to obtain one set of random variables corresponding to the uncertain variables. The sampling technique used was Latin Hypercube Sampling.
4. The random variables are then propagated through the Aspen Plus flowsheet to obtain the syngas composition or mole fractions of the various constituents.
5. The above process is repeated for the chosen number of samples.
6. The above procedure was then repeated for different coal compositions.

3.2.2 Syngas Composition

In this section we discuss the two main options for modeling a coal gasifier to quantify the syngas being produced and justify the approach taken in our model (IECM).

3.2.3 Response Surface Models

The output of ASPEN is used to obtain the **partition factors**. The partition factor of an element i into a syngas constituent j is defined as the fraction of the total element i which is contained in j. For instance, partition factor of C into CO is obtained as follows: First we consider the total mass of carbon entering the gasifier. (This is obtained from the coal flow rate and the coal composition data). Then we obtain the total mass of carbon contained in the CO exiting the gasifier. The ratio of the latter to the former gives the partition factor of C into CO. Similarly, we define the partition factors of H_2 into H_2O. We obtain the partition factor for each of the possible option as follows: C to CO, C to CO_2, C to CH_4, S to H_2S, S to COS, H to H_2, H to H_2O and H to NH_3. The above set of partition factors completely specifies the composition of the syngas if the inlet flow rates are completely known. We obtain these partition factors for each combination of the random variables, hence for a number of samples. The partition factors are the independent variables and the gasifier process variables are the dependent variables. A linear regression is fitted to obtain each of the partition factors as a function of the uncertain process variables. These regression models can then be implemented in IECM.

NOTE: This method was implemented and found to be numerically unstable. Hence, the data output table approach below was used.

3.2.4 Data Output Tables

In this approach, we take all the outputs generated by the stochastic ASPEN flowsheet and select discrete data points of the syngas composition by the component to build up a table, which is then used in the IECM. The carbon content in the slag and the gasifier temperature were the two variables varied in this approach. We selected 3 discrete values for each variable: two extreme points of the range and the mid point nominal value. Therefore, the data table will have all possible combinations of the discrete values of all these variables.

The data for the four bituminous coals available in the IECM are shown in Table 3-3, Table 3-4, Table 3-5, and Table 3-6. Although sub-bituminous and lignite coals can successfully be gasified in a GE entrained-flow gasifier, the optimal temperature is much different, the efficiency is much lower, and the water content into the gasifier is much harder to control. Due to these issues, non-bituminous coal runs were not included in the IECM.

Table 3-3. Volume fraction of syngas components exiting the gasifier using the Appalachian (Low Sulfur) coal as a function of carbon in slag and gasifier temperature.

Carbon in Slag	1%			3%			5%		
Temp. (F)	2350	2450	2550	2350	2450	2550	2350	2450	2550
H_2	0.35306	0.35503	0.35724	0.35360	0.35488	0.35608	0.34656	0.34722	0.34779
CO	0.39475	0.38761	0.37917	0.40142	0.39328	0.38505	0.40458	0.39659	0.38850
CO_2	0.13889	0.14155	0.14463	0.13191	0.13495	0.13797	0.12824	0.13119	0.13413
H_2O	0.07556	0.07886	0.08289	0.08674	0.09090	0.09525	0.09853	0.10302	0.10770
N_2	0.00883	0.00886	0.00890	0.00883	0.00887	0.00891	0.00889	0.00893	0.00897
CH_4	0.01878	0.01796	0.01703	0.00727	0.00687	0.00648	0.00282	0.00266	0.00250
C_2H_6	-	-	-	-	-	-	-	-	-
C_3H_8	-	-	-	-	-	-	-	-	-
H_2S	0.00178	0.00180	0.00182	0.00174	0.00176	0.00178	0.00172	0.00174	0.00176
NH_3	0.00011	0.00011	0.00012	0.00009	0.00009	0.00009	0.00007	0.00007	0.00007
COS	0.00009	0.00009	0.00009	0.00009	0.00009	0.00009	0.00009	0.00009	0.00009
HCl	0.00018	0.00019	0.00019	0.00018	0.00018	0.00018	0.00018	0.00018	0.00018
Ar	0.00795	0.00794	0.00792	0.00814	0.00813	0.00811	0.00832	0.00831	0.00830
O_2	-	-	-	-	-	-	-	-	-

Table 3-4. Volume fraction of syngas components exiting the gasifier using the Appalachian (Medium Sulfur) coal as a function of carbon in slag and gasifier temperature.

Carbon in Slag	1%			3%			5%		
Temp. (F)	2350	2450	2550	2350	2450	2550	2350	2450	2550
H_2	0.35306	0.35503	0.35724	0.35360	0.35488	0.35608	0.34656	0.34722	0.34779
CO	0.39475	0.38761	0.37917	0.40142	0.39328	0.38505	0.40458	0.39659	0.38850
CO_2	0.13889	0.14155	0.14463	0.13191	0.13495	0.13797	0.12824	0.13119	0.13413
H_2O	0.07556	0.07886	0.08289	0.08674	0.09090	0.09525	0.09853	0.10302	0.10770
N_2	0.00883	0.00886	0.00890	0.00883	0.00887	0.00891	0.00889	0.00893	0.00897
CH_4	0.01878	0.01796	0.01703	0.00727	0.00687	0.00648	0.00282	0.00266	0.00250
C_2H_6	-	-	-	-	-	-	-	-	-
C_3H_8	-	-	-	-	-	-	-	-	-
H_2S	0.00178	0.00180	0.00182	0.00174	0.00176	0.00178	0.00172	0.00174	0.00176
NH_3	0.00011	0.00011	0.00012	0.00009	0.00009	0.00009	0.00007	0.00007	0.00007
COS	0.00009	0.00009	0.00009	0.00009	0.00009	0.00009	0.00009	0.00009	0.00009
HCl	0.00018	0.00019	0.00019	0.00018	0.00018	0.00018	0.00018	0.00018	0.00018
Ar	0.00795	0.00794	0.00792	0.00814	0.00813	0.00811	0.00832	0.00831	0.00830
O_2	-	-	-	-	-	-	-	-	-

Table 3-5. Volume fraction of syngas components exiting the gasifier using the Illinois #6 coal as a function of carbon in slag and gasifier temperature.

Carbon in Slag	1%			3%			5%		
Temp. (F)	2350	2450	2550	2350	2450	2550	2350	2450	2550
H_2	0.33966	0.33996	0.34011	0.32948	0.32915	0.32878	0.31631	0.31558	0.31487
CO	0.30680	0.29917	0.29264	0.31395	0.30638	0.29989	0.31888	0.31137	0.30493
CO_2	0.19004	0.19257	0.19469	0.18268	0.18520	0.18732	0.17757	0.18005	0.18212
H_2O	0.12800	0.13314	0.13767	0.14314	0.14856	0.15334	0.15802	0.16371	0.16871
N_2	0.00854	0.00857	0.00860	0.00861	0.00864	0.00868	0.00870	0.00874	0.00877
CH_4	0.00767	0.00721	0.00683	0.00279	0.00261	0.00247	0.00105	0.00099	0.00093
C_2H_6	-	-	-	-	-	-	-	-	-
C_3H_8	-	-	-	-	-	-	-	-	-
H_2S	0.00976	0.00986	0.00995	0.00965	0.00975	0.00984	0.00959	0.00970	0.00979
NH_3	0.00010	0.00010	0.00011	0.00008	0.00008	0.00008	0.00006	0.00006	0.00006
COS	0.00040	0.00039	0.00039	0.00041	0.00041	0.00040	0.00043	0.00043	0.00042
HCl	0.00048	0.00049	0.00049	0.00048	0.00048	0.00048	0.00047	0.00048	0.00048
Ar	0.00854	0.00853	0.00853	0.00873	0.00872	0.00872	0.00892	0.00891	0.00891
O_2	-	-	-	-	-	-	-	-	-

Table 3-6. Volume fraction of syngas components exiting the gasifier using the WPC Utah coal as a function of carbon in slag and gasifier temperature.

Carbon in Slag	1%			3%			5%		
Temp. (F)	2350	2450	2550	2350	2450	2550	2350	2450	2550
H_2	0.32304	0.32257	0.32195	0.30986	0.30888	0.30777	0.30984	0.29373	0.29228
CO	0.27961	0.27206	0.26446	0.28704	0.27950	0.27191	0.28701	0.28492	0.27736
CO_2	0.21830	0.22077	0.22319	0.21068	0.21317	0.21561	0.21071	0.20759	0.21001
H_2O	0.15346	0.15928	0.16534	0.16983	0.17591	0.18222	0.16985	0.19200	0.19856
N_2	0.00896	0.00900	0.00904	0.00904	0.00909	0.00913	0.00904	0.00918	0.00923
CH_4	0.00502	0.00468	0.00436	0.00179	0.00166	0.00155	0.00179	0.00062	0.00058
C_2H_6	-	-	-	-	-	-	-	-	-
C_3H_8	-	-	-	-	-	-	-	-	-
H_2S	0.00165	0.00167	0.00169	0.00164	0.00166	0.00168	0.00164	0.00165	0.00167
NH_3	0.00010	0.00010	0.00010	0.00008	0.00008	0.00007	0.00008	0.00006	0.00006
COS	0.00006	0.00006	0.00006	0.00007	0.00007	0.00007	0.00007	0.00007	0.00007
HCl	0.00003	0.00003	0.00003	0.00003	0.00003	0.00003	0.00003	0.00003	0.00003
Ar	0.00977	0.00977	0.00978	0.00995	0.00996	0.00997	0.00995	0.01015	0.01017
O_2	-	-	-	-	-	-	-	-	-

3.2.5 Energy Use

Coal Handling

The GE gasifier system uses a coal slurry with typically 66.5 weight percent of solids as feed to the gasifier. Coal handling involves coal unloading, stacking, reclamation, and conveying equipment followed by three operating and one spare train of wet grinding equipment.

To estimate the auxiliary power requirements of the coal handling unit, a predictive model was developed by Rocha and Frey (1997) using 14 data points (one column) obtained from the sources listed in Table 3-7. The coal feed rate was chosen as the independent variable for development of an auxiliary power model. Two models were selected for consideration: power consumed per slurry train vs. coal feed rate per slurry train; and total power consumed by the slurry preparation process area vs. total coal flow to slurry preparation. The power consumed per slurry train vs. coal feed rate per slurry train produced a standard error of 1,183 kW per train and a R^2 of 0.716, whereas the standard error for the other model is 2,949 kW for the entire plant and the R^2 value is 0.807. Because of the higher R^2 value, the latter model was selected.

Table 3-7. Summary of Design Studies used for Coal Handling and Slurry Preparation Auxiliary Power Model Development

Report No.	Company	Authors	Year	Sponsor	Gasifier	Coal
AP-3109	Synthetic Fuels Associates	Simbeck et al.	1983	EPRI	Texaco	Illinois #6
AP-3486	Fluor Engineers	Matchak et al.	1984	EPRI	Texaco	Illinois #6
AP-4509	Energy Conversion Systems	McNamee and White	1986	EPRI	Texaco	Illinois #6 /Texas Lignite
AP-5950	Bechtel Group	Pietruszkiewicz	1988	EPRI	Texaco	Illinois #6
GS-6904	Fluor Daniel	Hager and Heaven	1990	EPRI	Dow	Eastern Bituminous
TR-100319	Fluor Daniel	Smith and Heaven	1991	EPRI	Destec	Illinois #6
MRL Texaco	Montebello Research Lab, Texaco Inc.	Robin et al.	1991	DOE	Texaco	Pittsburgh #8

$$W_{e,\,CH} = 1.04\, m_{cf,\,G.\,i} \quad R^2 = 0.807 \tag{3-40}$$

where,

$$3{,}300 \le m_{cf,G.i} \le 20{,}000 \text{ tons/day (as received)}$$

The model and data are shown in Figure 3-6. The model fit is greatly influenced by the data point that is at 6,500 tons/day gasifier coal feed rate (McNamee and White, 1986). A much better fit could occur if this value was removed from the power consumption model consideration. The data point was not removed because no reason could be found to exclude the value from the development of the power consumption model.

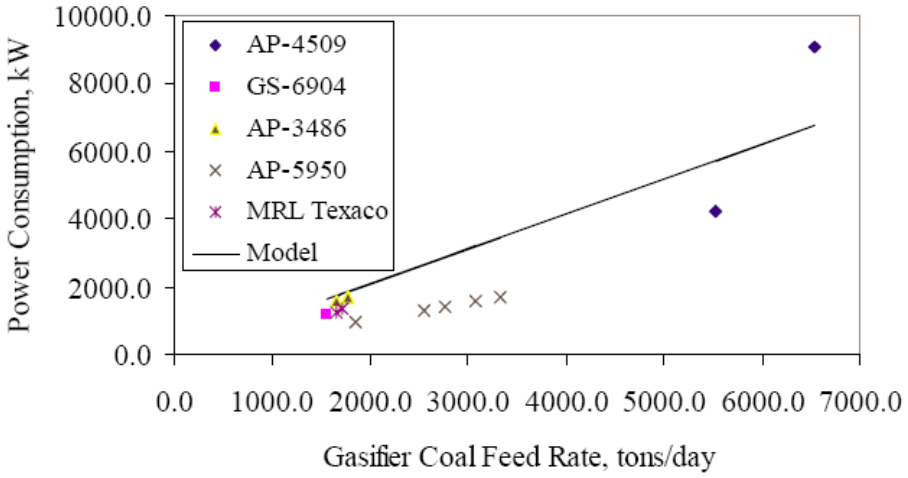

Figure 3-6. Power Requirement for the Coal Slurry Preparation Unit

Gasification

Only two data points were available for the determination of the auxiliary power consumption model for the gasification section based upon water quench high temperature syngas cooling. The two data points were obtained from studies by Matchak et al. (1984) and Robin et al. (1993). A linear model with zero intercept was developed based upon the coal flow rate (as-received basis) per gasifier train and is shown in Figure 3-7. The auxiliary model developed has a standard error of 16 kW for the entire plant and R^2 of 0.970. The R^2 variable is very high because only two data points were available.

$$W_{e,G} = 0.111\ N_{T,G}\ (m_{cf,i} / N_{O,G}) \qquad R^2 = 0.970 \qquad (3\text{-}11)$$

where,

$1300 \le m_{cf,G,i} \le 2400$ tons/day per train (as received)

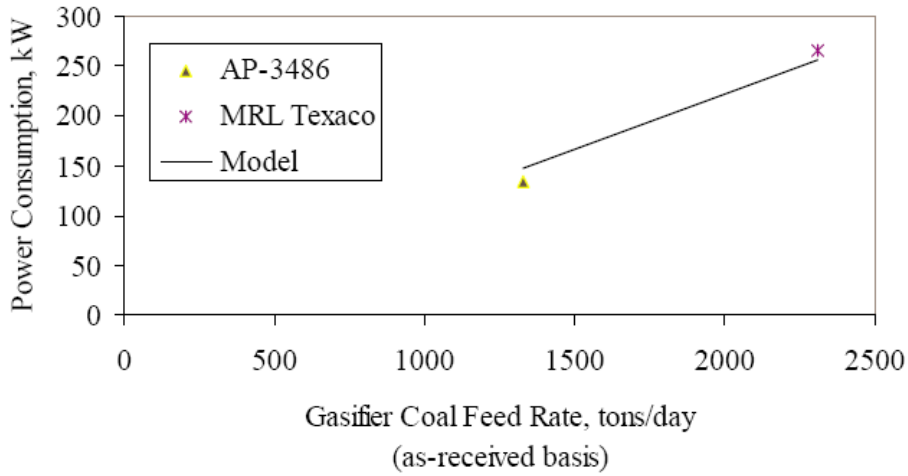

Figure 3-7. Power Requirement for the Gasification Section for Total Quench

Low Temperature Gas Cooling

The auxiliary power consumption model for the low temperature gas cooling (LTGC) section was developed using a single data point from the study by Matchak et al. (1984) and is given in MW by:

$$W_{e,LT} = 3.211 \times 10^{-5}\ m_{SN,LT,O} \qquad (3\text{-}52)$$

Process Condensate Treatment

The process condensate treatment plant has the following auxiliary power consumption model, which is developed for the present GE gasification system using a single data point from the study Matchat et al., (1984) and is given in MW by the equation:

$$W_{e,\,PC} = 9.289 \times 10^{-7}\, m_{S,BD} \qquad (3\text{-}13)$$

3.3. GE Gasifier Cost Model

3.3.1 Capital Cost

This section documents the cost model developed for the GE gasifier-based IGCC plant with total quench high temperature gas cooling. New direct capital cost models for major process sections are presented here. For the purpose of estimating the direct capital costs of the plant, the gasifier is divided into four process areas. The direct cost of a process section can be adjusted for other years using the appropriate cost index. The capital costs are provided in December 2000 dollars and can be scaled to other years with the Chemical Engineering Plant Cost Index.

Coal Handling

Coal handling involves unloading coal from a train, storing the coal, moving the coal to the grinding mills, and feeding the gasifier with positive displacement pumps. A typical coal handling section contains one operating train and no spare train. A train consists of a bottom dump railroad car unloading hopper, vibrating feeders, conveyors, belt scale, magnetic separator, sampling system, deal coal storage, stacker, reclaimer, as well as some of type of dust suppression system. Two studies (McNamee and White, 1986; Matchak et al., 1984) assumed a double boom stacker and bucket wheel reclaimer system. The studies by Smith and Heaven (1992) and Hager and Heaven (1990) assumed a combined stacker reclaimer. Pietruszkiewicz et al. (1988) specified conveyors to perform the stacking operation and a rotary plow feeder for the reclaim system.

Slurry preparation trains typically have one to five operating trains with one spare train. The typical train consists of vibrating feeders, conveyors, belt scale, rod mills, storage tanks, and positive displacement pumps to feed the gasifiers. All of the equipment for both the coal handling and the slurry feed are commercially available. This typical train design is assumed in two reports (McNamee and White, 1986; Matchak et al., 1984).

A regression model was developed for the direct capital cost of coal handling and slurry preparation using the data collected for possible independent variables affecting direct capital cost. Figure 3-8 shows the data points. A regression was developed, based on the equation developed by Frey (2001) and revised with additional data (Chase 2003, IEA 2000, Foster 2003, and Brdar 2003). Coal feed rate to gasifier on as-received basis is the most common and easily available independent variable. The direct cost model for the coal handling is based upon the overall flow to the plant rather than on per train basis. This is because a better value of R^2 was obtained in the former case. The regression model derived is:

$$DC_{CH} = 9.92 m_{cf,G,i} \qquad R^2 = 0.8 \qquad (3\text{-}14)$$

where,

$$2{,}800 \le m_{cf,G,i} \le 25{,}000 \text{ tons/day}$$

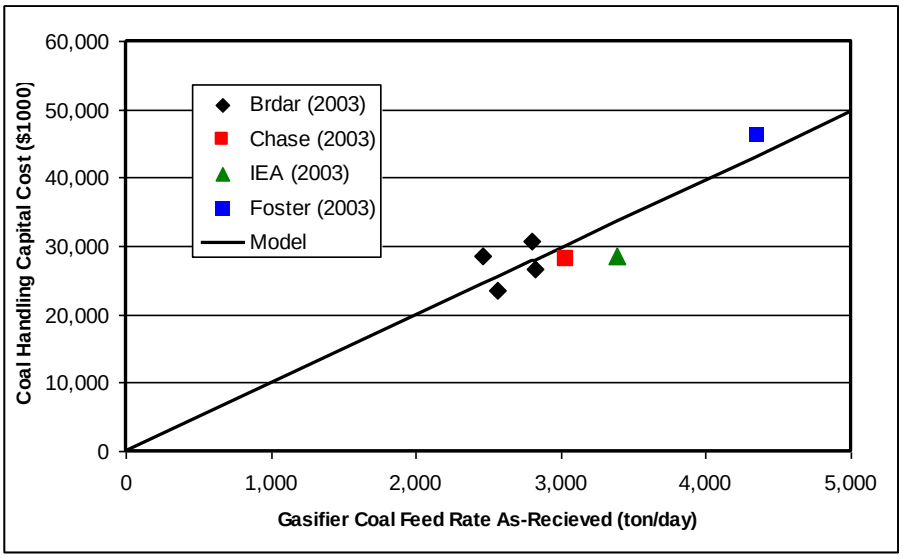

Figure 3-8. Direct Cost for the Coal Handling and Slurry Preparation Process (Cost Year = 2000)

Gasification

The GE gasification section of an IGCC plant contains gas scrubbing, gas cooling, slag handling, and ash handling. For IGCC plants of 400 MW to 1100 MW, typically four to eight operating gasification trains are used along with one spare train (Matchak et al., 1984). The direct capital cost model is a function of the as-received coal flow rate. The data is shown in Figure 3-9. The regression as shown in Equation (3-15) is based on data from IEA (2003) and Chase (2003).

$$DC_G = 15.88 * M_{CG,G,i}^{0.943} \qquad (3\text{-}15)$$

where,

$$1{,}300 \leq m_{cf,G,i} \leq 3{,}300 \text{ tons/day}$$

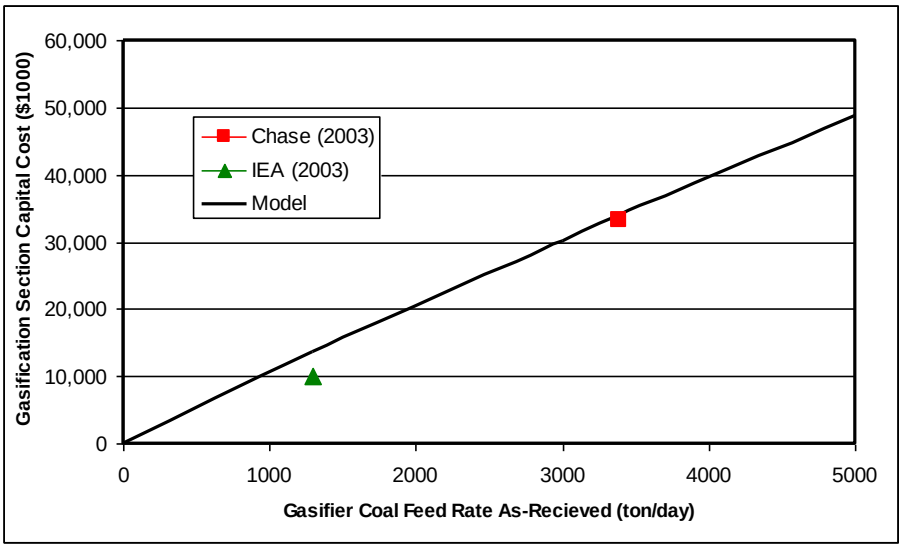

Figure 3-9. Direct Cost for Total Quench Cooled Gasifier (Cost Year = 2000)

Low Temperature Gas Cooling

In IGCC systems featuring "cold gas cleanup," the syngas is cooled to about 100 F before entering the acid gas removal plant section. Additionally, in many IGCC designs, moisture is added to the fuel gas in a fuel gas saturator to reduce NO_x formation during syngas combustion in the gas turbine.

The low temperature gas cooling section consists primarily of a series of shell and tube heat exchangers. The fuel gas saturator is a vertical column with sieve trays in which fuel gas is contacted counter-currently with hot water flowing downward.

Data for this particular plant section design was available from three studies (Chase 2003, IEA 2003, and Foster 2003). Although all "cold gas" IGCC systems have a fuel gas cooling process area, not all IGCC system designs are based on fuel gas moisturization. Alternatively, many are based on direct steam injection into the gas turbine. Equation (3-16) shows the regression results from the data. See Figure 3-10for the data and regression results.

$$DC_{LT} = 0.0156 N_{O,LT} \left(\frac{M_{syn,LT,o}}{N_{O,LT}} \right)^{1.0} \qquad R^2 = 0.99 \qquad (3\text{-}16)$$

where,

$$650{,}000 \le \left(\frac{M_{syn,LT,o}}{N_{O,LT}} \right) \le 1{,}300{,}000 \text{ lb/hr}$$

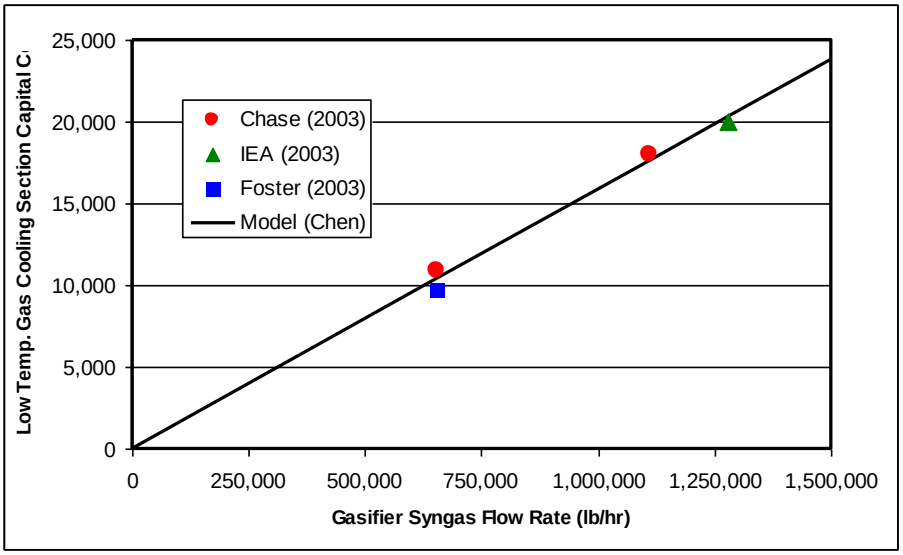

Figure 3-10. Direct Cost for Low Temperature Gas Cooling (Cost Year = 2000)

Process Condensate Treatment

The process condensate treatment section is used to treat blowdown from the particulate scrubber and process condensate from gas cooling (Fluor, 1983b; 1985). These streams contain ammonia, carbon dioxide, and hydrogen sulfide, and the scrubber blowdown also has high chlorides content. The blowdown and condensate stream are treated in separate strippers. The overhead vapor streams from both strippers are cooled in air-cooled heat exchangers and then they flow through knock-out drums prior to feed to the Claus plant sulfur furnace. The stripped bottoms product from the blowdown water stripper is cooled by the incoming process condensate water and then sent to a water treatment plant for biological treatment prior to flow to the cooling tower. The bottoms from the process condensate water stripper are sent as make up to the gas scrubbing unit.

Because the treated process condensate is used as make-up to the gas scrubbing unit, and because blowdown from the gas scrubbing unit is the larger of the flow streams entering the process condensate treatment section, it is

expected that process condensate treatment direct cost will depend primarily on the scrubber blowdown flow rate, see Figure 3-11. Because only two cost studies were identified with similar designs and sufficient detail for regression analysis, a single variate regression analysis was used and scaled to 2000$:

$$DC_{PC} = 9814\left(\frac{m_{SBD}}{300000}\right)^{0.6} \quad (3\text{-}17)$$

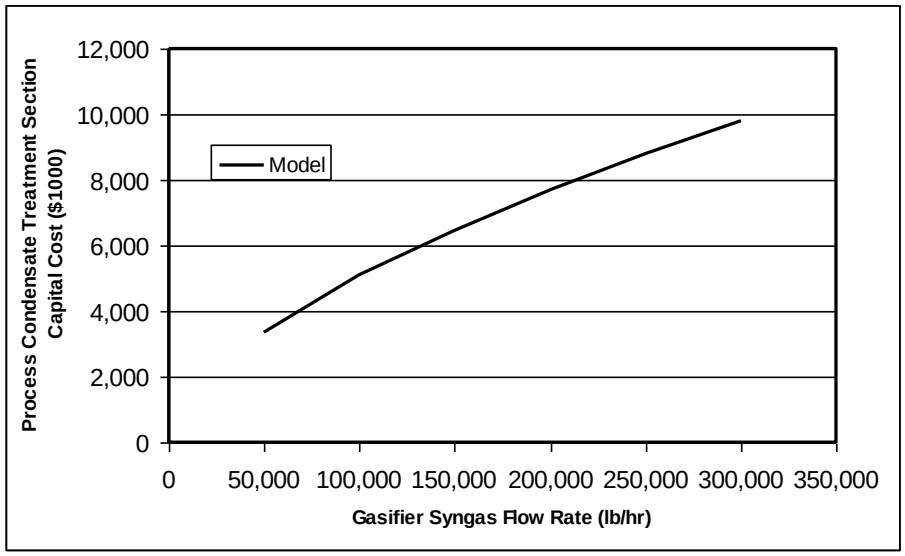

Figure 3-11. Direct Cost for Process Condensate Treatment (Cost Year = 2000)

References

Brdar R.D., Jones R.M., 2003: GE IGCC Technology and Experience with Advanced Gas Turbines, GE Power Systems, GER-4207

Chase D.L., Kehoe P.T., 2003: GE Combined-Cycle Product Line and Performance, GE Power Systems, GER-3574G

Fluor (1983b). Shell-Based Gasification-Combined-Cycle Power Plant Evaluations. Prepared by Fluor Engineers, Inc. for Electric Power Research Institute, Palo Alto, CA. EPRI AP-3129. June 1983.

Fluor (1985). Cost and Performance of Kellogg Rust Westinghouse-based Gasification-Combined-Cycle Plants. Prepared by Fluor Engineers, Inc. for Electric Power Research Institute, Palo Alto, CA. EPRI AP-4018. June 1985.

Foster A.D., Doering H.E., and Hilt M.B., 2003: Fuel flexibility in heavy-duty gas turbines, GE Company, Schenectady, New York

Frey, H.C., and N. Akunuri, "Probabilistic Modeling and Evaluation of the Performance, Emissions, and Cost of Texaco Gasifier-Based Integrated Gasification Combined Cycle Systems Using ASPEN," Prepared by North Carolina State University for Carnegie Mellon University and U.S. Department of Energy, Pittsburgh, PA, January 2001.

Hager, R.L., and D.L. Heaven (1990). Evaluation of a Dow-Based Gasification-Combined-Cycle Plant Using Bituminous Coal. Prepared by Fluor Daniel for the Electric Power Research Institute. Palo Alto, CA. EPRI GS-6904.

IEA, 2000: Modeling and simulation for coal gasification, IEA Coal Research 2000, ISBN 92-9029-354-3

IEA Greenhouse Gas R&D Program, 2003: Potential for improvement in gasification combined cycle power generation with CO_2 capture, IEA report, report number PH4/19

Matchak, T.A., A.D. Rao, V. Ramanathan et al. (1984), "Cost and Performance for Commercial Applications of Texaco-Based Gasification-Combined-Cycle Plants," AP-3486. Prepared by Flour Engineers, Inc for EPRI, Palo Alto, CA.

McNamee, G.P., and G.A. White (1986), "Use of Lignite in Texaco Gasification-Based-Combined-Cycle Power Plants," AP-4509. Prepared by Energy Conversion Systems, Inc for EPRI, Los Angeles, CA.

Pietruszkiewicz, Milkavich, Booras et al. (1988), "An Evaluation of IGCC and PCFS plants, " AP-5950. Prepared by Bechtel Group, Inc for EPRI, Palo Alto, CA.

Robin et al. (1993)

Rocha, M. F., and H.C. Frey (1997), "Cost Modeling of a Texaco Coal Gasification Combined Cycle System, " Prepared by North Carolina State University for Carnegie Mellon University and U.S. Department of Energy, Morgantown, WV, August.

Simbeck D. R., R.L. Dickenson, and E.D. Oliver (1983), "Coal Gasification Systems: A Guide to Status, Applications, and Economics," AP-3109 Prepared by Synthetic Fuel Associates, Inc for Electric Power Research Institute, Palo Alto, California.

Smith, J., and D. Heaven (1992), "Evaluation of a 510-Mwe Destec GCC Power Plant Fueled With Illinois No. 6 Coal," TR-100319. Prepared by Flour Daniel, Inc for EPRI, Irvine, CA

4. Water Gas Shift System

4.1 Water Gas Shift Process Description

4.1.1 Clean Shift Catalyst

Gases used in water gas shift reactors often contain sulfur component, such as H_2S and COS. These sulfur components have a detrimental effect on the activation of some shift catalysts, which will be poisoned and lose activation in the presence of sulfur components. On the other hand, sulfur components are necessary to maintain the activation of some other shift catalysts. For the former type of shift catalysts, sulfur components must be removed from reaction gases before the water gas shift reaction. Hence this type of catalysts is so-called "clean shift catalyst". A schematic flowsheet of coal gasification system with a clean water gas shift reaction is given in Figure 4-1. The raw syngas from the gasifier is cooled down, and fed to the soot scrubber to remove the bulk of the air-borne particulates. Then the scrubbed syngas is further cooled prior to passing through a sulfur removal process. Before passing to the shift reactors, steam is added to the clean syngas to meet requirements of a steam-to-carbon ratio. There are two shift reactors, one operating at a higher temperature and a second operating at a lower temperature. Together these form a water gas shift process. A feed/effluent heat exchanger exists between the high and lower temperature shift reactors to assure a proper lower inlet temperature to the second shift reactor.

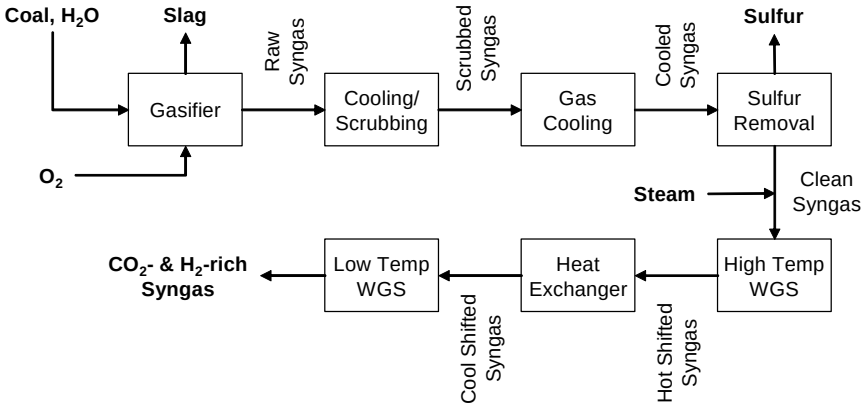

Figure 4-1. Coal gasification system with a clean water gas shift reaction

For a two-stage shift reaction with clean shift catalysts, the iron-based catalyst is the common commercially available high temperature catalyst. The commonly used low temperature clean shift catalysts are copper-based. Both high temperature and low temperature catalysts require activation by in situ pre-reduction steps. Since both catalysts burn up when exposed to air (pyrophoric), they must be sequestered during system shutdown when only air flows through the system [Frank 2003a].

The lifetimes of Cu-based catalysts and Fe-based catalysts are determined by the poison-absorbing capacity of the catalysts. These poisons are inevitably present in the process gas, such as syngas from coal gasification, or introduced with steam. As mentioned above, the key poison in syngas is sulfur. Hence a sulfur removal process is required upstream of the water gas shift reaction.

4.1.2 Sulfur Tolerant Shift Catalysts

The so-called sour shift catalysts are sulfur tolerant, and sulfur is required in the feed gas to maintain the catalyst in the active sulphided state. This type of catalyst is usually cobalt-based.

Figure 4-2 shows the schematic process of a gasifier system with a sour shift reaction. The process draws its name from the acidic or "sour" gases that remain present in the syngas through the water gas shift process before being removed. The syngas from the gasifier is quenched, and then the raw syngas is fed to the soot scrubber, removing the bulk of particulates before passing to the sour shift reactors. Before passing to the shift reactors, steam is added to the scrubbed syngas to meet the requirements of a steam-to-carbon ratio. The first shift reactor operates at high temperature and the hot shifted syngas must be cooled by a heat exchanger prior to entering the second shift reactor. After heat recovery, the cool shifted syngas from the second shift reactor and the final shifted syngas is further cooled prior to being passed to the sulfur removal system.

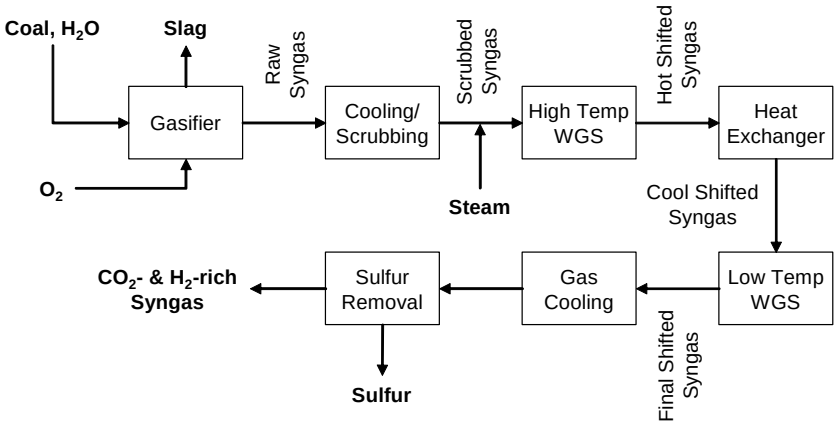

Figure 4-2. Schematic process of a gasifier system with a sour shift

The sour shift catalyst has demonstrated its high- and low-temperature performance, ranging from 210°C to 480°C, and works properly up to a pressure as high as 1160 psia [Frank, 2003b]. Because the catalyst is not impregnated with a water-soluble promoter it can be operated closer to the dew point and will not lose activity when wetted occasionally.

In a gasification plant, the average catalyst life in the first stage shift reactor was 2.5 years, and 5-8 years in the second reactor [Frank, 2003b]. The difference in catalyst life in the two reactors is highly influenced by the gas quality. These data of catalysts' lifetime are adopted for the estimation of the operation and maintenance cost of the water gas shift reaction system.

4.2 Water Gas Shift Performance Model

This section presents the performance model developed for the WGS reaction process. This is a general performance model for a two-stage shift system with either clean shift catalysts or sulfur tolerant shift catalysts. The purpose of the performance model is to characterize the change in syngas composition and flow rate as a function of inlet condition to the WGS reactor and key design parameters of the WGS system. The performance model also characterizes the heat integration between the shift reaction system and the steam cycle system.

A general water gas shift reaction process model is illustrated in Figure 4-3. The black box in this figure includes a high temperature reactor, a low temperature reactor and several heat exchangers for heat recovery. The performance of the shift reaction was first modeled in the Aspen Plus. In this model, the syngas from a gasifier is mixed with steam or quenched at a given temperature and pressure, and then fed into the high temperature reactor. Most of the CO in the syngas is converted to CO_2 in the high temperature reactor at a fast reaction rate. Because the water gas shift reaction is exothermic, the syngas from the high temperature reactor has to be cooled before being fed into the low temperature reactor. Further CO conversion is achieved in the low temperature reactor. The shifted syngas from the low temperature reactor is cooled down again for subsequent CO_2 capture in a Selexol process. Part of the heat from syngas cooling is used to heat the fuel gas from Selexol process, and the other part of the heat is integrated into the steam cycle.

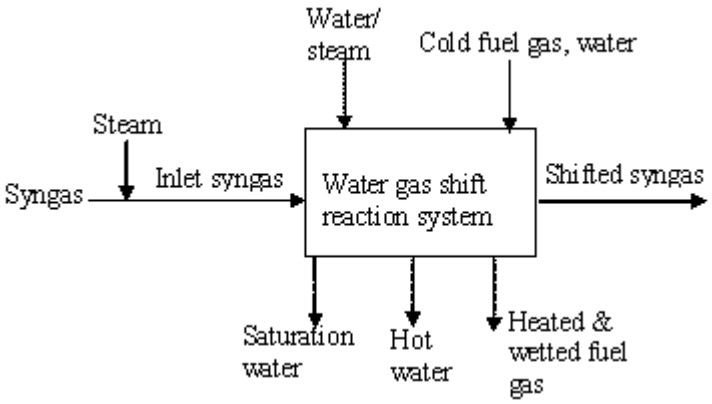

Figure 4-3. Mass and energy flow of the water gas shift reaction system

In this model, the reactions in the two reactors are assumed to achieve equilibrium states. On the other hand, the shift reaction in a real reactor only approaches an equilibrium state. In order to compensate for the difference between the equilibrium state assumption and the real state in a reactor, the approach temperature method is used to adjust the model equilibrium temperatures. The difference between the model temperature and the design reaction temperature is referred to as the approach temperature. The approach temperature is determined through comparing model outputs with practical data from shift reactors in the industry field. Thus, with the approach temperature, the reactor model is assumed to reach an equilibrium state at a higher temperature than the design temperature, which makes the CO conversion efficiency in the model to match the realistic situation.

The Aspen model had been executed thousands of times with varying the inlet temperature, pressure and syngas composition. The value ranges of these parameters are given in Table 4-1, which covers the possible ranges of gasification operation. The inlet temperature was varied in a step of 30 F, and the inlet pressure was varied by a step of 100 psia. At the same time, 50 different syngas compositions were used. A total of 9000 cases were run. Based on the Aspen simulation results, statistical regression methods were then used to develop relationships between the inlet conditions and the final products of the WGS reaction. Using these regression relationships, the entire water gas shift reaction system can be treated as a "black box" when it is used in the IECM framework.

Table 4-1. Range of model parameter values for the WGS reaction system

Parameter	Inlet temp. (F)	Inlet pres. (psia)	Volume in the syngas (vol%)				
			CO	H_2	CO_2	H_2O	CH_4
Range	440-755	150-1500	20-60	15-55	5-30	5-30	0.5-20

4.2.1 Parameters of the WGS performance model

The input and outlet parameters of this model include the temperature, pressure, and flow rates of the inlet and the outlet syngas as shown in Table 4-2. The input parameters are used to calculate reaction rates and the composition changes after the reaction.

Table 4-2. Input and output parameters of the WGS reaction system

Input parameter			Output parameter	
Syngas from gasifier	Temperature (F)		Shifted syngas	Temperature (F)
	Pressure (psia)			Pressure (psia)
	Flow rate (lb-mole/hr)			Flow rate (lb-mol/hr)
	Molar concentrations of CO, CO_2, H_2O, H_2, N_2, CH_4			Molar concentrations of CO, CO_2, H_2O, H_2, N_2, CH_4
Steam/carbon molar ratio			Reaction rate & Catalyst volume (ft^3)	
Feed water	Pressure (psia)		HP & IP steam	Temperature (F)
	Temperature (F)			Flow rate (lb-mol/hr)

4.2.2 Performance Model Output

This section discusses the performance outputs of this model. In this section, the CO to CO_2 conversion is defined and calculated using the chemical equilibrium constant. The outlet temperatures and syngas composition of the two shift reactors are regressed from Aspen model simulation results. The heat released from the syngas cooling is also quantified for the energy balance calculation of the whole IGCC system.

Shifted Syngas Composition

The water gas shift reaction is a method for further enhancing the yield of hydrogen from gasification. Syngas mixtures containing mostly hydrogen and carbon monoxide are typically generated at elevated temperatures via the combustion of coal, bio-mass, petroleum and organic wastes [Wender, 1996]. Steam is then added to the CO-H_2 feed mixture prior to being introduced to water-gas shift reactors to convert the CO to CO_2 and additional H_2. However, thermodynamic equilibrium favors high conversion of CO and steam to hydrogen and carbon dioxide at low temperatures. Therefore, the water-gas shift reaction is commonly conducted at low temperature in the presence of catalysts that enhance the reaction rate. The water-gas shift reaction is reversible and given by Equation (4-1).

$$CO + H_2O \leftrightarrow CO_2 + H_2 \qquad \Delta H = -41 kJ/mol \tag{4-1}$$

The water gas shift reaction occurring in both the high and low temperature reactors changes the concentration of syngas species and the temperature of the syngas. The CO conversion efficiency (ξ) can be used to show how much CO is converted into CO_2 in one reactor or in two reactors.

$$\xi = \frac{CO \quad flow \quad in(lb \cdot mol/hr) - CO \quad flow \quad out(lb \cdot mol/hr)}{CO \quad flow \quad in(lb \cdot mol/hr)}$$

A numerical model is set up to calculate the CO conversion in a shift reactor for given inlet parameters. Based on the definition of the CO conversion and stoichiometric factors of the reaction, the CO concentration of syngas exiting the high temperature reactor is given by,

$$[CO]_{h,o} = [CO]_0 \cdot (1 - \xi_h) \tag{4-2}$$

where

$[CO]_{h,o}$ = molar concentration of CO in the syngas exiting the high temperature reactor

$[CO]_0$ = molar concentration of CO in the syngas entering the high temperature reactor

ξ_h = CO conversion in the high temperature reactor

Based on the shift reaction shown in Equation (4-1) and the definition of CO conversion, the molar concentrations of H_2, CO_2 and H_2O after the high temperature reactor are given by,

$$[CO_2]_{h,o} = [CO_2]_0 + [CO]_0 \cdot \xi_h \quad (4\text{-}3)$$

$$[H_2]_{h,o} = [H_2]_0 + [CO]_0 \cdot \xi_h \quad (4\text{-}4)$$

$$[H_2O]_{h,o} = [H_2O]_0 - [CO]_0 \cdot \xi_h \quad (4\text{-}5)$$

Using the CO conversions definition and Equation (4-2), the CO concentration of shifted syngas after the low temperature reactor is to be given by,

$$[CO]_{l,o} = [CO]_0 \cdot (1 - \xi_{tot}) \quad (4\text{-}6)$$

where

$[CO]_{l,o}$ = molar concentration of CO in the syngas exiting the low temperature reactor

ξ_{tot} = the total CO conversion in the high and low temperature reactors

Then the concentrations of H_2, CO_2 and H_2O after the low temperature reactor are given by,

$$[H_2]_{l,o} = [H_2]_0 + [CO]_0 \cdot \xi_{tot} \quad (4\text{-}7)$$

$$[CO_2]_{l,o} = [CO_2]_0 + [CO]_0 \cdot \xi_{tot} \quad (4\text{-}8)$$

$$[H_2O]_{l,o} = [H_2O]_0 - [CO]_0 \cdot \xi_{tot} \quad (4\text{-}9)$$

Flow rate of high-pressure saturation steam

In the following two sections, temperature changes and flow rates of water and syngas are calculated, and then used for the following cost model.

Syngas from the high temperature reactor is cooled down to a temperature which is determined by the dew point of syngas before it is fed into the low temperature reactor. According to the heat integration design, heat from the exothermic reaction is recovered to generate high pressure saturated steam for the steam cycle.

The temperature of the saturation steam is determined by the high-pressure steam cycle in the power block. Using the data from the ASME steam and water table (1967), the temperature is given by the following regression equation:

$$T_{w,sat}(F) = 328.34 + 0.3565 P_{sc} - 0.0002 P_{sc}^2 + 6 \cdot 10^{-8} P_{sc}^3 - 7 \cdot 10^{-12} P_{sc}^4 \quad R^2=0.99 \quad (4\text{-}10)$$

where

P_{sc} (psia) = pressure of steam cycle, (300 ~ 3000 psia)

The heat released by the syngas after the high temperature reactor is determined by,

$$Q_{HE1}(Btu/hr) = q_{HE1} \cdot f_{SG,0} \quad (4\text{-}11)$$

where

$f_{SG,0}$ = total molar flow rate of syngas entering the high temperature reactor (lb-mole/hr);

q_{HE1} = heat released per lb-mole syngas after the high temperature reactor, which is regressed and given by (Btu/lb-mole),

$$q_{HE1}\left(\frac{Btu}{lbmol}\right) = P_0^{0.0360} T_0^{1.2874} [CO]_0^{1.14347} [CO_2]_0^{-0.4734} [H_2O]_0^{0.3150} [H_2]_0^{0.0003} [N_2]_0^{0.0139} \quad R^2=0.95 \quad (4\text{-}12)$$

where

P_0 = the pressure of syngas entering the high temperature reactor (psia)

T_0 = the temperature of syngas entering the high temperature reactor (F)

$[i]_0$ =the molar concentration of species i entering the high temperature reactor

Based on the total heat available and the saturation temperature, the flow rate of the saturation high pressure steam (**f_{HPS}**, lb-mole/hr) can be calculated by the following equation,

$$f_{HPS} = \frac{Q_{HE1}}{(h_{T_{w,sat}} - h_{T_0})} \tag{4-13}$$

where

$h_{T_{w,sat}}$ = enthalpy of steam at saturated temperature (Btu/lb-mole)

h_{T_0} = enthalpy of high-pressure feed water at inlet temperature (Btu/lb-mole).

Intermediate Pressure Steam

The syngas from the low temperature reactor is cooled to 100 F for sulfur removal, and the heat is recovered to generate the intermediate pressure steam. The total heat **Q_{tot}** (Btu/hr) released when the syngas from the low temperature reactor is cooled down to 100 °F is given by,

$$\begin{aligned} Q_{tot} = f_{l,o}(&9.255 \cdot T_{l,o} - 0.316 \cdot P_{l,o} - 1386.1 \cdot [CO]_{l,o} \\ &- 297.779 \cdot [CO_2]_{l,o} - 1485.34 \cdot [H_2]_{l,o} + 17595.87 \cdot [H_2O]_{l,o} \\ &- 1439.29 \cdot [N_2]_{l,o} - 331.533 \cdot [CH_4]_{l,o}) \end{aligned} \qquad R^2=0.95 \tag{4-14}$$

where

$f_{l,o}$ = molar flow rate of syngas exiting low temperature reactor (lb-mole/hr);

$T_{l,o}$ = syngas temperature at the outlet of the second reactor

$P_{l,o}$ = syngas pressure at the outlet of the second reactor

$[i]_{l,o}$ = molar concentration of species i at the outlet of the second reactor

In order to meet the approach temperature requirement in the superheater, the final temperature of the intermediate pressure steam (**T_{HPS}**) is set to be 10 F lower than the outlet temperature of the syngas from the second shift reactor, and the feedwater temperature is set to be 59 F. Hence the flow rate of the intermediate pressure steam (**F_{IPS}**, lb-mole/hr) is given by,

$$(f_{HPS} + f_{IPS}) \cdot (h_{IP_{sat}} - h_{FW}) + f_{IPS} \cdot (h_{IPS} - h_{IP_{sat}}) = Q_{tot} \tag{4-15}$$

where

f_{HPS} = flow rate of the high-pressure saturation steam (lb-mole/hr)

$h_{IP_{sat}}$ = enthalpy of the intermediate pressure saturation water at the inlet temperature (Btu/lb-mole)

h_{FW} = enthalpy of the feedwater (Btu/lb-mole)

h_{IPS} = enthalpy of the final intermediate pressure steam (Btu/lb-mole)

4.3 WGS Cost Models

This section presents the economic model developed for the water gas shift reaction process. The cost model is comprised of the capital cost model and the annual operating and maintenance (O&M) cost model. The capital cost of the WGS reaction system includes the following major process areas: the first stage shift reactor, the second shift reactor and the cooling units. For each of these major areas, its process facilities cost model is developed at first.

4.3.1 Process Facility Cost

The process facility cost of the reactor includes the reaction vessel, structural supports, dampers and isolation valves, ductwork, instrumentation and control, and installation costs. The reactor vessels are made of carbon steel. The process facility costs of the shift reactors are estimated based on the reactor volumes, which is assumed to be 1.2 times the catalyst volume [Doctor, 1994].

Shift Reactor Vessels

The process facility costs of the high and low temperature shift reactors are regressed as a function of reactor volume and operation pressure using the data in Table 4-3. Any of the process facility costs can be expressed for a different year using the Chemical Engineering Plant Cost Index.

$$PFC_R = 0.9927 \cdot N_{T,R}[17.6487(\frac{1.2V_{cat.}}{N_{O,R}})^{0.4883} P_R{}^{2.028}] \qquad R^2=0.9 \qquad (4\text{-}166)$$

where

PFC_R = the process facility cost of the reactor (US$ in 2000)

$N_{T,R}$ = the total number of the reactor trains

$N_{O,R}$ = the number of the reactor operating trains

$V_{cat.}$ = the volume of catalyst (m^3)

P_R = the operation pressure of the reactor (atm)

Table 4-3. Water gas shift reactor cost data adjusted to the dollar value in 2000 [Doctor, 1996]

Cost ($ in 2000)	Reactor volume(m^3)	Pressure(atm)
82864.8	22.6	31.1
38692.2	34	18.7
59189.0	9.684	31.0
21495.0	11.553	18.7

Heat Exchangers

In this model, two types of heat exchangers are used, which are the gas-liquid type, and the gas-gas type. Generally, the cost of a heat exchanger depends on its heat exchange surface, which is determined by the heat load of the exchanger and the temperature difference between the hot and cold flows. To allow for variations in these parameters, the process facility cost of the gas-liquid type heat exchanger was regressed using the data in Table 4-4,

$$PFC_{HE1} = 1.0064 \cdot N_{T,HE} \cdot [13.7528(dT_{HE})^{-0.6714} \times (\frac{Q_{HE}}{N_{O,HE}})^{0.6855}] \quad R^2=0.91 \quad (4\text{-}17)$$

where

PFC_{HE1} = process facility cost of the gas-liquid heat exchanger (US k$ in 2000)

$N_{T,HE}$ = number of total train of the heat exchanger

$N_{O,HE}$ = number of the operating train of the heat exchanger

Q_{HE} = heat load of the heat exchanger (kW)

dT_{HE} = log mean temperature difference (C)

Table 4-4. Gas-liquid heat exchanger cost data adjusted to the dollar value in 2000 [Doctor, 1996]

Cost (K$ in 2000)	Pressure (atm)	Log mean temperature difference (C)	Heat load (kW)
625.4	30.7	68.2	16421.6
615.0	30.7	90.8	21052.4
210.2	18.7	190.4	9298.0
168.2	19.4	148.6	5036.0
472.9	19.4	121.0	19534.9
315.3	19.4	13.7	1293.1
210.2	18.7	190.4	9298.0
99.8	19.4	153.5	2407.3
210.2	20.4	190.4	9298.0
634.6	68.1	52.0	12119.7
210.2	157.8	190.4	9298.0

Based on the data in Table 4-5, the process facility cost of the gas-gas type heat exchanger is given by,

$$PFC_{HE2} = 0.9927 \cdot N_{T,HE2}[24.4281 \cdot P_{HE2}^{0.2804}(dT_{HE2})^{-0.1143} \times (\frac{Q_{HE2}}{N_{O,HE2}})^{0.3881}] \quad R^2=0.94 \quad (4\text{-}18)$$

where

PFC_{HE2} = process facility cost of gas-gas heat exchanger (US k$ in 2000)

$N_{T,HE}$ = total train number of the heat exchanger

$N_{O,HE}$ = operating train number of the heat exchanger

Q_{HE} = heat load of the heat exchanger (kW)

dT_{HE} = log mean temperature difference in the heat exchanger

The process facility cost can be given in another year basis by using the Chemical Engineering Plant Cost Index.

Table 4-5. Gas-gas heat exchanger cost data adjusted to the dollar value in 2000 [Doctor, 1996]

Cost (k$ in 2000)	Pressure (atm)	Log mean temperature (C)	Heat load (kW)
1757.3	30.7	98.0	17319.5
1757.3	30.7	90.7	16776.2
2205.4	19.4	10.0	42480.7
3131.2	30.7	318.4	100832.3
2606.0	31.6	340.4	95833.1
897.1	68.1	17.2	1223.6
2193.5	18.7	31.8	25641.0
1294.8	18.7	19.4	4034.0
644.3	20.4	69.1	2407.3
849.9	20.4	71.4	5036.0
692.1	20.4	57.5	2407.3
966.5	18.7	51.2	5036.0

4.3.2 Total Capital Requirement

The total process facilities cost of the water gas shift reaction system is the summation of the individual process facility costs above plus the cost of initial catalyst charge. This is added because it is also a large and integral part of the reaction system. Following the EPRI Technical Assessment Guide (1993), the total capital requirement and O&M cost of the WGS reaction system is given in Table 4-6.

Table 4-6. Cost parameters of water gas shift process

Capital cost elements	Value
Total process facilities cost	Sum of the PFC of each equipment
Engineering and home office	10% PFC
General facilities	15% PFC
Project contingency	20% PFC
Process contingency	5% PFC
Total plant cost (TPC) = PFC+Engineering fee+General facilities+Project & Process contingency	
Allowance for funds during construction (AFDC)	Calculated based on discount rate and construction time
Royalty fees	0.5% PFC
Preproduction fees	1 month of VOM&FOM

Inventory cost	0.5% TPC
Total capital requirement (TCR) = TPC+AFDC+Royalty fees+Preproduction fee+Inventory cost	
Fixed O&M cost (FOM)	
Total maintenance cost	2% TPC
Maintenance cost allocated to labor	40% of total maintenance cost
Administration & support labor cost	30% of total labor cost
Operation labor	1 jobs/shift
Variable O&M cost (VOM)	
High temperature catalyst	$250/ft^3, replaced every 2.5 years
Low temperature catalyst	$250/ft^3, replaced every 6 years

References

Campbell, J.S., (1970): Influences of catalyst formulation and poisoning on activity and die-off of low temperature shift catalyst, Industrial & engineering chemistry process design and development, 9(4): 588, 1970.

Davis, R.J., (2003): All That Glitters Is Not AuO, Science, 301(5635), 2003.

Dmitrievich, A., (2002): Hydrodynamics, mass and heat transfer in chemical engineering. Taylor & Francis Press, New York, NY, 2002.

Doctor, R.D., (1994): Gasification combined cycle: carbon dioxide recovery, transport, and disposal**,** ANL/ESD-24, Argonne National Laboratory, Energy Systems Division, Argonne, IL, 1994.

Doctor, R.D., (1996): KRW oxygen-blown gasification combined cycle carbon dioxide recovery, transport, and disposal**,** ANL/ESD-34, Argonne National Laboratory, Energy Systems Division, Argonne, IL. 1996.

Enick, R.M. and Busfamante F., (2001): Very High-Temperature, High-Pressure Homogenous Water Gas Shift Reaction Kinetics, 2001 AIChE Annual Meeting, Reno, NV, 2001.

Frank, P., (2003a): Low Temperature Shift Catalysts for Hydrogen Production, Johnson Matthey Group, 2003.

Frank, P., (2003b): Sulfur Tolerant Shift Catalyst -Dealing with the Bottom of the Barrel Problem, Johnson Matthey Group, 2003.

Newsome, D.S., Kellogg P., (1980): The Water-Gas Shift Reaction, Cat. Rev. Sci. Eng., 21(2), 1980.

Park, J.N., Kim J.H., and Ho-In Lee, (2000): A Study on the Sulfur-Resistant Catalysts for Water Gas Shift Reaction IV. Modification of CoMo/ g-Al_2O_3 Catalyst with K, Bull. Korean Chem. Soc. 21(12), 2000.

NIST/ASME (2007), NIST/ASME Steam Properties Database Program, Version 2.21, National Institute of Standards and Technology, http://www.nist.gov/srd/nist10.htm, 2007.

Twigg, M.V., (1989): Catalyst handbook, second edition, Wolfe publishing Ltd.,

Wender, I., (1996): Reactions of Synthesis Gas, Fuel Processing Technology, Vol. 48, 189, 1996.

5. Sulfur Removal and Recovery (Cold-Gas Cleanup)

Nomenclature

$\mathbf{c_f}$ = Capacity Factor (fraction)

$M_{syn,S,i}$ = Molar flow rate of syngas entering Selexol process (lbmole/hr)

$M_{,S,C,o}$ = Molar flow rate of sulfur exiting Claus process (lbmole/hr)

$M_{HS,S,i}$ = Molar flow rate of hydrogen sulfide entering Selexol process (lb-mole/hr)

$m_{s,C,o}$ = Mass flow of sulfur from Claus plant (lb/hr)

$m_{s,BS,o}$ = Mass flow of sulfur from Beavon-Stretford plant (lb/hr)

f_{HS} = Fraction of hydrogen sulfide (by volume)

$N_{T,S}$ = Total number of Selexol trains (integer)

$N_{O,S}$ = Number of operating Selexol trains (integer)

$N_{T,C}$ = Total number of Claus trains (integer)

$N_{O,C}$ = Number of operating Claus trains (integer)

$N_{T,BS}$ = Total number of Beavon-Stretford trains (integer)

$N_{O,BS}$ = Number of operating Beavon-Stretford trains (integer)

η_{HS} = Removal efficiency of hydrogen sulfide from Selexol system (fraction)

5.1 Process Description

A number of different sulfur removal and recovery systems have been studied in IGCC and coal-to-SNG plant designs. The most common configuration is the Selexol process for sulfur removal from the raw syngas, a two-stage Claus plant for recovery of elemental sulfur, and the Shell Claus off-gas treating (SCOT) process for treatment of the tailgas from the Claus plant. However, a number of alternative designs have also been considered. These include integration of the Selexol and SCOT processes in the LONGSCOT design, as well as the use of alternative processes including the Dow GAS/SPEC MDEA and Selexl processes. The design basis assumed here is a Selexol unit for sulfur removal, a two-stage Claus plant for sulfur recovery, and either a SCOT or a Beavon-Stretford unit for Claus plant tail gas treatment. In this section, the development of a cost model for the Selexol process is discussed.

5.1.1 Selexol Sulfur Capture

The proprietary Selexol process selectively removes hydrogen sulfide from the raw syngas. Typically, about 95 percent of the hydrogen sulfide is removed through counter-current contact of the syngas with Selexol solvent. The Selexol process also removes approximately 15 percent of the carbon dioxide in the flue gas. Typically only about one third of COS in the syngas will be absorbed. H_2S and COS stripped from the Selexol solvent, along

with sour gas from the process water treatment unit is sent to the Claus sulfur plant for recovery of elemental sulfur.

The composition of the acid gas stream which is sent from the Selexol unit to a sulfur recovery plant is typically over 50 percent carbon dioxide (Bechtel , 1983a; Bechtel, 1988; Cover et al., 1985a, 1985b; Fluor, 1983a, 1983b, 1984, 1985; Parsons, 1982). The studies cited here include both IGCC and coal-to-SNG systems based on a variety of gasifiers, including KRW, Texaco, and Shell designs. From these studies, 28 individual data points were developed. Thus, the database for the Selexol cost model represents a variety of coal gas compositions.

From the available performance and cost information for the Selexol process applied to gasification systems, a database containing total direct cost, syngas inlet flow rate, syngas composition (e.g., carbon dioxide, hydrogen sulfide, carbonyl sulfide, water vapor), removal efficiency of syngas components, acid gas flow rate and composition, and syngas temperature and pressure was developed. The inlet crude syngas temperatures for these data ranged from 95 to 120ºF and the inlet pressures ranged from 315 to 557 psia.

The inlet syngas is contacted counter-currently in a packed bed with Selexol solvent. For a more detailed discussion of this process area, the reader is referred to any of the design studies used as a basis for cost model development, and in particular Fluor (1985). The absorption occurring in the absorber reduce the temperature of the syngas. The treated syngas flows through a knock-out drum to remove solvent mist and is then heated in a heat exchanger by the incoming fuel gas. The cost of the Selexol section includes the acid gas absorber, syngas knock-out drum, syngas heat exchanger, flash drum, lean solvent cooler, mechanical refrigeration unit, lean/rich solvent heat exchanger, solvent regenerator, regenerator air-cooled overhead condenser, acid gas knock-out drum, regenerator reboiler, and pumps and expanders associated with the Selexol process.

The absorption of hydrogen sulfide by the solvent is influenced by the liquid to gas molar ratio in the absorption tower, the partial pressure of the hydrogen sulfide in the syngas, the contact temperature, the number of absorption stages or trays in the tower, and the amount of residual hydrogen sulfide left in the regenerated solvent (EPA, 1983). The absorption tower must be sized based on the syngas volume flow rate and the number of trays required for contacting solvent with the syngas. The solvent circulation rate depends on both the syngas molar flow rate and the desired removal efficiency for hydrogen sulfide. As the removal efficiency is increased, the solvent circulation rate must be increased (EPA, 1983). The solvent circulation rate affects the cost of most of the process equipment in the Selexol process. However, data for the circulation rate are not reported in the design studies. Therefore, to a first order approximation, the cost of the Selexol process is assumed to depend on the syngas flow rate for the syngas temperature and pressure range of the database. The hydrogen sulfide removal efficiency is expected to have a secondary effect on cost, because it also influences the solvent circulation rate. Other parameters such as syngas temperature or the concentration of hydrogen sulfide in the syngas may also have secondary effects on the process area cost.

5.1.2 Claus Plant Sulfur Recovery

In most IGCC cost studies, sulfur recovery is assumed to be achieved using a Claus plant to produce elemental sulfur. This section presents an overview of the design features of a Claus plant in the IGCC process environment. For additional detail see (Fluor, 1985) or any of the other detailed design studies of IGCC or coal-to-SNG systems used to develop this process area cost model.

The inlet stream to the Claus plant is the acid gas from the sulfur removal section. In this study, only data for Claus plants that process the acid gas from a Selexol unit are considered. The acid gas typically contains primarily carbon dioxide and hydrogen sulfide. In order to produce elemental sulfur, a 2:1 ratio of hydrogen sulfide and sulfur dioxide is required. Therefore, a portion of the incoming acid gas is combusted in a two-stage sulfur furnace. The furnace temperature is high enough in the first stage (typically 2,500ºF) to destroy any ammonia in the acid gas. Intermediate pressure steam (e.g., 350 psia) is generated from the waste heat produced in the sulfur furnace, cooling the feed gas to the Claus converters to about 600ºF. Further cooling to 350ºF occurs in a sulfur condenser, generating low pressure steam (e.g., 55 psia). Sulfur flows to a gravity sump, and is kept molten by condensing low pressure steam that flows through coils in the bottom of the sump.

Some of the furnace gas is used to heat the feed gas from the first condenser to approximately 450ºF prior to entering the sulfur converter, where hydrogen sulfide and sulfur dioxide react in the presence of a catalyst (e.g., Kaiser S-501) to produce elemental sulfur and water. This reaction is exothermic, and the outlet temperature of

the gas is approximately 630ºF. The conversion rate is limited by thermal equilibrium. Gaseous sulfur is recovered in a second condenser. The cooling may be accomplished by heating water for fuel gas saturation. The feed gas then is mixed with remaining combustion gases and then enters the second converter. A third condenser, in which water for fuel gas saturation may be heated, is used for final sulfur recovery. The effluent gas from the Claus plant then passes through a coalescer and then on to tail gas treatment.

5.1.3 Beavon-Stretford Tail Gas Treatment

In this section, an overview of the performance and design of the Beavon-Stretford process is presented as background information for the development of a regression cost model. See (Fluor, 1983a) or (Fluor, 1983b) for a more detailed discussion of this process.

The Beavon-Stretford process is a modification of the Stretford process, which is designed to remove hydrogen sulfide from atmospheric pressure gas streams and convert it to elemental sulfur. However, the Stretford process is not appropriate for handling effluent gases containing sulfur dioxide, carbonyl sulfide, or elemental sulfur. Therefore, a Beavon unit is used to catalytically reduce or hydrolize these species to hydrogen sulfide in the presence of a cobalt molybdate catalyst.

Because hydrogen is required for the reactions occurring in the Beavon unit, flash gas from the acid gas removal section is used as a feed stream. The flash gas is partially combusted in a reducing gas generator, mixed with the Claus plant tail gas, and the total gas stream then enters the Beavon hydrogenation reactor. The hot gas from the reactor is cooled in a waste heat boiler where intermediate pressure (e.g., 100 psia) steam is generated. The gas stream is further cooled in the desuperheater section of a thermally integrated desuperheater/absorber vessel. The cooling of the gas stream is accomplished by heat transfer with cooling water, which is recirculated through an air-cooled heat exchanger. The gas stream then enters the absorber portion of the vessel, where over 99 percent of the hydrogen sulfide is removed by contact with a Stretford solution containing sodium carbonate. The treated gas is vented to the atmosphere.

The Stretford solution flows to a soaker/oxidizer, where anthraquinone disulfonic acid (ADA) is used to oxidize the reduced vanadate in the Stretford solution. The ADA is regenerated by air sparging, which also provides a medium for sulfur flotation. The sulfur overflows into a froth tank, and the underflow from the oxidizer/soaker is pumped to a Stretford solution cooling tower and then to a filtrate tank.

The sulfur from the froth tank is pumped to a primary centrifuge, where the wet sulfur cake product is reslurried and sent to a second centrifuge, after which the sulfur is again reslurried. The slurry is then pumped through an ejector mixer, where the sulfur is melted and separated in a separator vessel. The sulfur goes to a sump.

5.2 Performance Model

5.2.1 Selexol Reagent Use

Initial Solvent

The initial requirement for Selexol solvent is expected to depend primarily on the mass flow of hydrogen sulfide, the primary sulfur species in raw syngas, and on the concentration of the hydrogen sulfide. A multivariate regression yielded the following result for the initial solvent requirement, expressed in pounds:

$$CHEM_{i,S} = -25{,}200 + 16.6\left(\frac{M_{HS,S,i}^{0.935}}{f_{HS}^{1.04}}\right) \qquad R^2 = .959 \qquad n = 12$$

where,

$50 \le M_{HS,S,i} \le 900$ lbmole/hr

$0.004 \le f_{HS} \le 0.012$

The solvent requirement estimated from the regression model is compared to the reported solvent requirement in Figure 5-1.

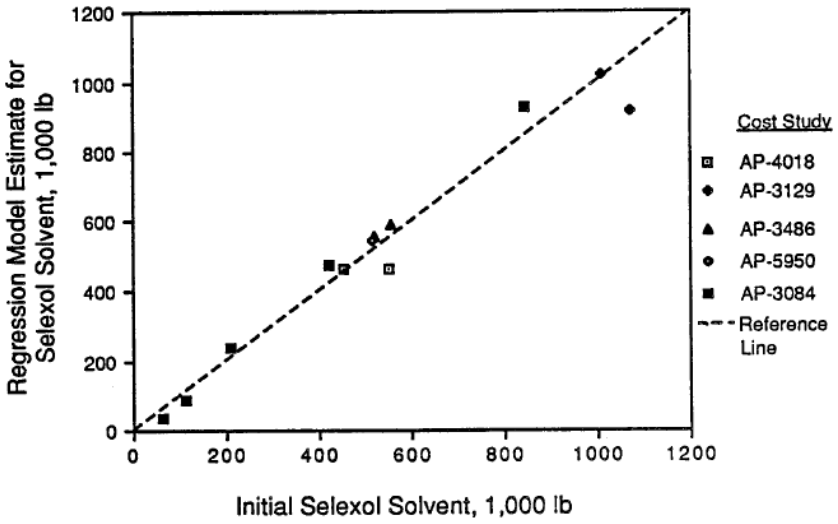

Figure 5-1. Initial Solvent Requirement for the Selexol Process.

Makeup Solvent

Selexol solvent is lost during the process and must be replenished. It is a function of the syngas flow rate, not the acid gas flow rate or capture rate. The makeup Selexol solvent flow rate is expressed in units of pounds per year. The regression shown is taken from (Frey, 2001). The regression model is shown graphically in Figure 5-2 and in equation form as:

$$m_{solv,S,i} = c_f\,(-350 + 1.58M_{syn,S,i})\ \text{lb/yr} \qquad R^2 = 0.989,\ n = 11$$

where,

$$4{,}000 < M_{syn,S,i} < 74{,}500\ \text{(lbmole/hr)}$$

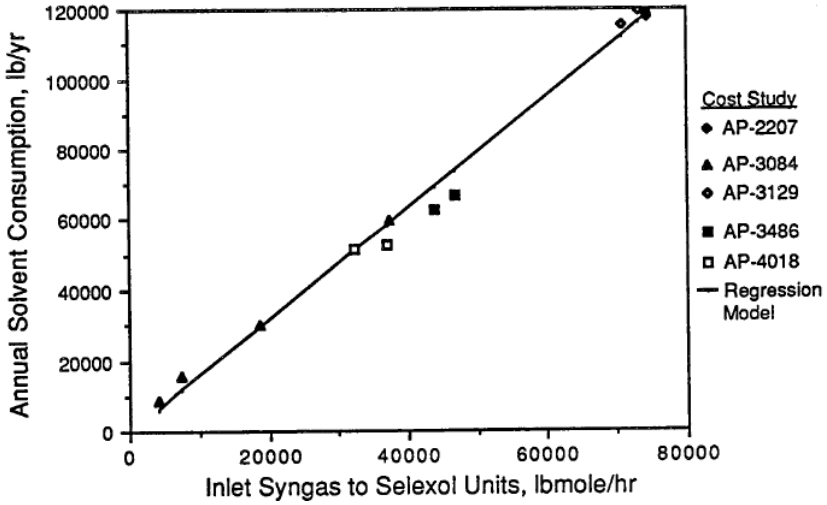

Figure 5-2. Annual Solvent Requirements for the Selexol Process

5.2.2 Claus Plant Catalyst Use

Initial Catalyst

The initial catalyst requirement for two-stage Claus plants was found to depend on the recovered sulfur mass flow rate. The initial catalyst requirement, in tons, is given by:

$$CAT_{i,C} = 5.03 * 10^{-3} m_{s,C,o}$$

$R^2 = .959$
$n = 12$

where,

$1{,}000 \le m_{s,C,o} \le 30{,}800$ lb/hr

The regression model is shown graphically in Figure 5-3.

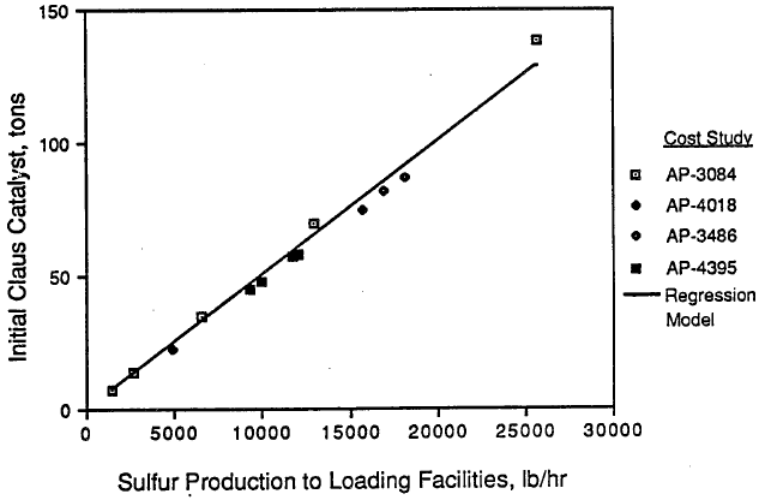

Figure 5-3. Initial Catalyst Requirement for Two-Stage Claus Plant.

Makeup Catalyst

The makeup Claus plant catalyst requirement is expressed in units of tons per year. This is the amount of catalyst that must be replaced in an average year. It is based on a regression done by (Frey, 1990).

$$m_{cat,C,i} = 0.000961 \cdot c_f \cdot m_{s,C,o}$$

$R^2 = 0.843$
$n = 13$

where,

$1{,}000 < < \mathbf{m_{s,C,,o}} <, 26{,}000$ lb/hr

The regression model is shown graphically in Figure 5-4.

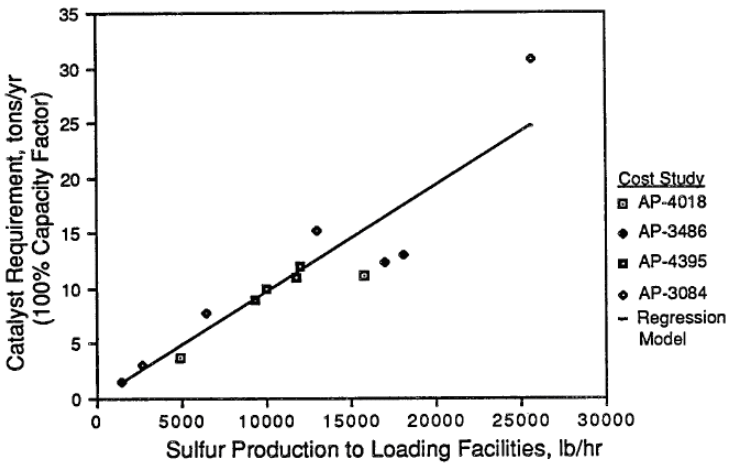

Figure 5-4. Annual Makeup Catalyst Requirement for Two-Stage Claus Plant

5.2.3 Beavon-Stretford Catalyst Use

Initial Catalyst

The Beavon-Stretford process requires a catalyst for the Beavon unit and a special chemical for the Stretford unit. The initial catalyst and chemical requirements for the Beavon-Stretford process were estimated from the values reported in (Fluor, 1983a), which includes data for a range of plant sizes. From these data, a simple linear relationship of catalyst and chemical requirements as a function of the sulfur recovered in the Beavon-Stretford unit was identified.

In the case of the Beavon catalyst (see Figure 5-5), the mass requirement as a function of sulfur flow rate can be estimated. In the case of the Stretford chemicals, the mass requirement is not given. However, the cost of the initial Stretford chemicals as a function of the recovered sulfur flow rate was developed. The resulting regression models for the initial catalyst requirement (**$CAT_{i,BS}$**), in cubic feet is:

$$CAT_{i,BS} = -1.3 + 0.641 \cdot m_{s,BS,o} \qquad R^2 = 1.00,\ n = 5$$

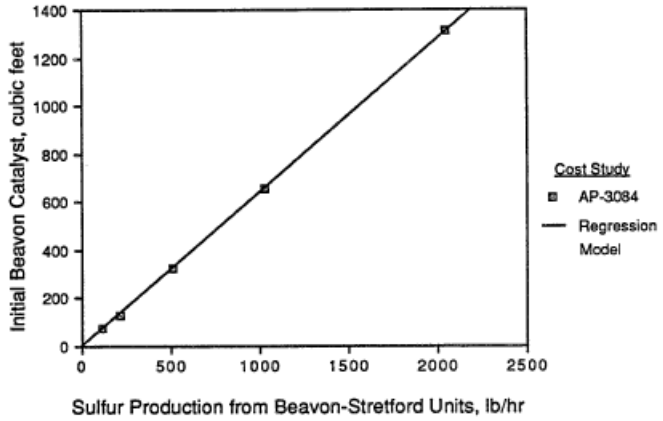

Figure 5-5. Initial Catalyst Requirement for the Beavon-Stretford Process.

Makeup Catalyst

This is the amount of catalyst that must be replaced in an average year. It is based on a regression done by (Frey, 1990). The makeup catalyst requirement is expressed in units of cubic feet per year. The data and regression are shown in Figure 5-6. Two outlier data points were excluded from the analysis, as indicated in the figure. These

points, both from the same study (Fluor, 1983b), appear inconsistent with the more extensive set of data from the other study (Fluor, 1983a).

$$m_{cat,BS,i} = 0.0856 \cdot c_f \cdot m_{s,BS,o} \qquad R^2 = 1.00, \; n = 5$$

where:

$100 < \mathbf{m}_{\mathbf{s,BS,o}} <, 2{,}000$ lb/hr

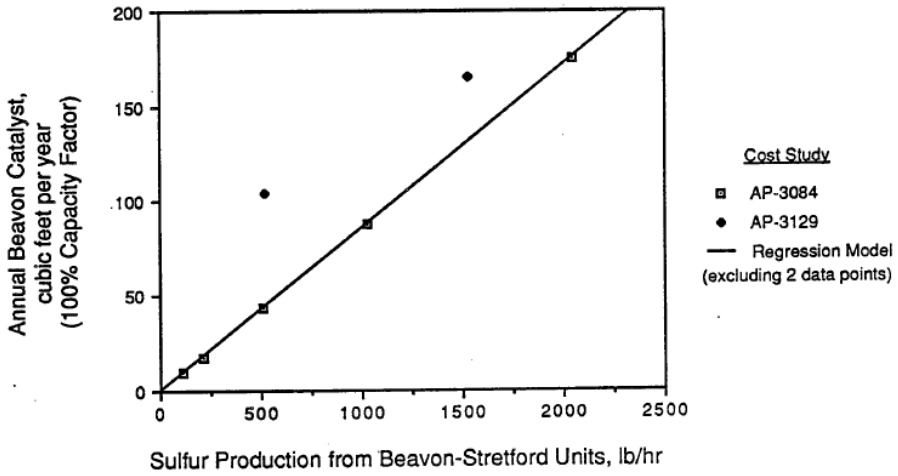

Figure 5-6. Annual Catalyst Requirement for the Beavon-Stretford Process

5.2.4 Chemical Use

Unlike the consumable catalysts, data are not available regarding the makeup mass flow rate for the Stretford chemicals. However, data are available regarding the cost of the Stretford chemicals. These calculations are provided later in this chapter with the operating and maintenance costs.

5.2.5 Energy Use

Sulfur Removal (Selexol)

The auxiliary power consumption model for the Selexol process in MW was developed by (Frey and Rubin, 1990) using 18 data points and is given by

$$W_{e,S} = 0.348 + 0.000478 \cdot \left(M_{syn,S,i}\right)^{0.839} \qquad R^2 = 0.881, \; n = 18$$

where,

$4{,}000 \leq M_{syn,S,o} \leq 74{,}500$ lb-mole/hr

The regression model is shown graphically in Figure 5-7.

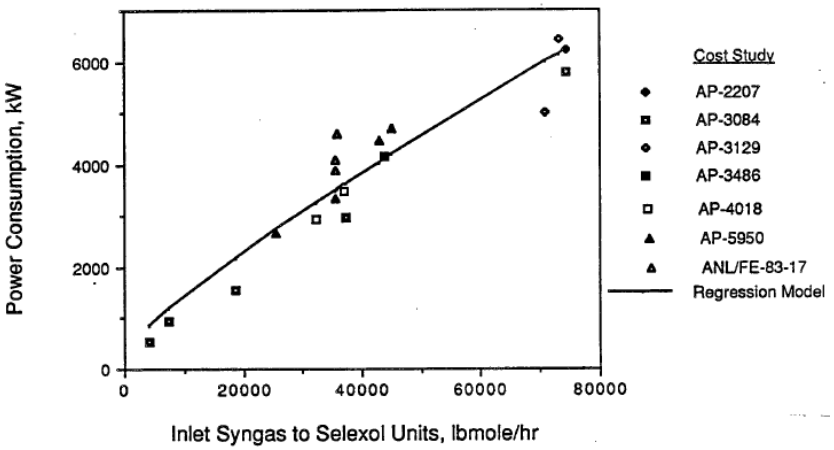

Figure 5-7. Power Requirement of the Selexol Units

Claus Plant

The auxiliary power consumption model for Claus plant in MW was developed by (Frey, 1990) using 20 data points is given by:

$$W_{e,C} = 0.000021 \cdot m_{s,C,o} \qquad R^2=0.87$$

where,

$$1{,}000 \le m_{s,C,o} \le 30{,}800 \text{ (lb/hr)}$$

The regression model is shown graphically in Figure 5-8.

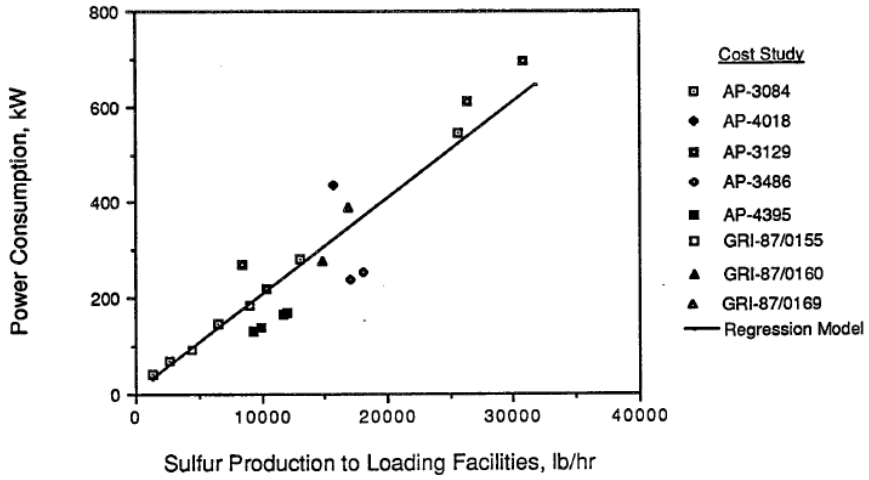

Figure 5-8. Power Requirement for Two-Stage Claus Plants

Beavon-Stretford Unit

The auxiliary power consumption model for Beavon-Stretford plant in MW was developed by (Frey, 1990) and is given by:

$$W_{e,BS} = 0.0445 + 0.00112 \cdot m_{s,BS,o} \qquad R^2=0.990, \; n = 7$$

where,

$$100 \le m_{s,BS,o} \le 2{,}000 \text{ (lb/hr)}$$

The regression model is shown graphically in Figure 5-9.

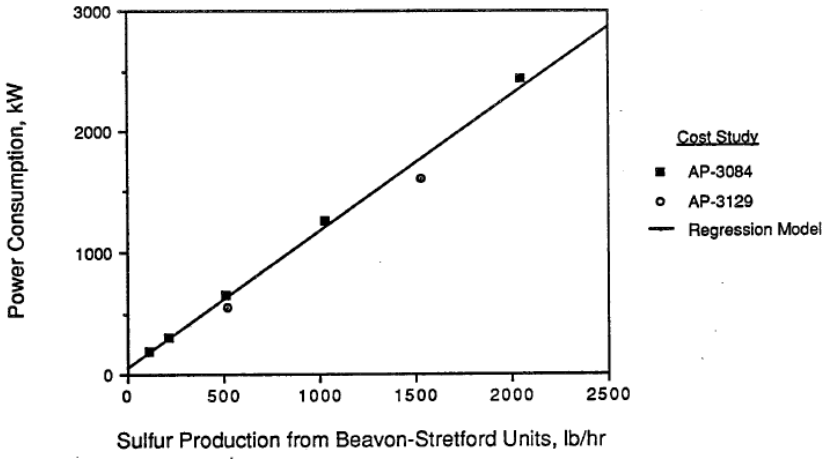

Figure 5-9. Power Requirement for the Beavon-Stretford Process

5.3 Sulfur Removal and Recovery Cost Model

5.3.1 Direct Capital Cost

Direct capital cost correlations for each process area are described in the following sections of this report. While some of the process area models may be applicable to a variety of IGCC or coal-to-SNG systems, the models are intended for the specific purpose of estimating the direct cost of the cold gas cleanup systems for capturing and recovering sulfur. The purpose here is not to recapitulate each detail of the process area design basis, but rather to document the development of the cost models. Therefore, the reader may wish to read this report in conjunction with some of the performance and cost studies cited here to obtain more detail about specific process areas.

Capital costs are given for a particular basis year. To provide the costs using a different year, the reader is encouraged to use the Chemical Engineering Plant Cost Index.

Sulfur Removal (Selexol)

Several alternative regression model formulations were attempted based on syngas flow rate, temperature, pressure, hydrogen sulfide concentration, and the removal efficiency for hydrogen sulfide. The cost of the Selexol process was found to depend primarily on the syngas flow rate entering the acid gas absorber. The cost is also influenced to a much smaller degree by the hydrogen sulfide removal efficiency. Other parameters had less significant or statistically insignificant effects in explaining the cost of the system. Therefore, these additional parameters were excluded from the model.

Hydrogen sulfide in the syngas is removed through counter-current contact with the Selexol solvent. The cost of the Selexol section includes the acid gas absorber, syngas knock-out drum, syngas heat exchanger, flash drum, lean solvent cooler, mechanical refrigeration unit, lean/rich solvent heat exchanger, solvent regenerator, regenerator air-cooled overhead condenser, acid gas knock-out drum, regenerator reboiler, and pumps and expanders associated with the Selexol process. The cost model is same as the one developed by (Frey, 1990) for a gasifier-based IGCC system with cold gas cleanup. The number of operating trains is calculated based on the syngas mass flow rate and the limits for syngas flow rate per train used to develop the regression model as given below. A minimum of two operating trains and no spare trains are typically assumed.

IGCC systems with hot gas cleanup produce a hotter gas that requires a modified Selexol system to be installed. The direct capital cost model for the Selexol section for a hot gas cleanup system in 2000 dollars is:

$$DC_S = \frac{0.4657\, N_{T,S}}{(1-\eta)^{0.059}} \left(\frac{M_{syn,S,i}}{N_{O,S}} \right)^{0.980} \qquad R^2=0.909,\ n=28$$

where,

$$2{,}000 \le \left(\frac{M_{syn,S,i}}{N_{O,S}} \right) \le 67{,}300 \text{ (lb-mole/hr)}$$

$$0.835 < \eta_{HS} < 0.997$$

The same direct cost model for Selexol section is used as that in the radiant and convective design except for a small modification of the coefficient in the equation. This modification was done to match a data point obtained from the study by (Matchak et al**.,** 1984). The direct capital cost model for the cold gas cleanup Selexol section in 2000 dollars is:

$$DC_S = \frac{0.3045\, N_{T,S}}{(1-\eta)^{0.059}} \left(\frac{M_{syn,S,i}}{N_{O,S}} \right)^{0.980}$$

where,

$$2{,}000 \le \left(\frac{M_{syn,G,i}}{N_{O,S}} \right) \le 67{,}300 \text{ (lbmole/hr)}$$

$$0.835 \le \eta_{HS} \le 0.997$$

$$200 \le W_{ST,E} \le 550 \quad \text{(MW)}$$

The range for the syngas molar flow rate per train indicates the size range for a single train. Because the scaling exponent for the syngas flow rate term is within the range typically expected for chemical process plants, extrapolation above this range may yield satisfactory results. However, the range for syngas molar flow per train is actually quite large, implying that extrapolation is unlikely in practice. Moreover, the preferred alternative to extrapolation is to adjust the number of trains so that the molar flow rate per train is within the given range. The range for the hydrogen sulfide removal efficiency should not be extrapolated. A graph comparing the regression model estimates of direct cost with the costs reported in the literature is given in Figure 5-10.

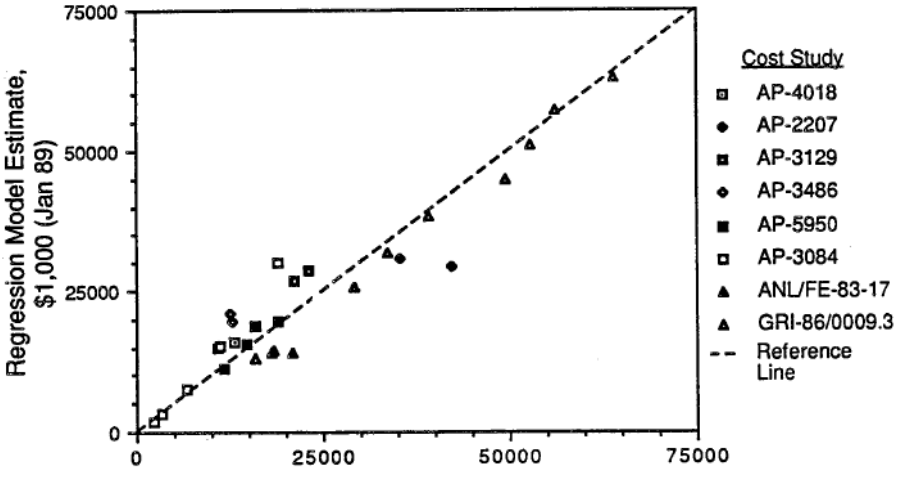

Figure 5-10. Predicted vs. Actual Costs for Selexol Acid Gas Removal

Sulfur Recovery (Claus Plant)

A direct cost correlation was developed for two-stage Claus plants based on data from a number of gasification plant studies. A number of data points are not included in this correlation because they represent either three-stage Claus plants or two-stage Claus plants with tail gas incineration and no tail gas treatment, with the incinerator costs included in the direct cost.

The cost of a Claus plant is known to scale primarily with the recovered sulfur mass flow rate capacity using the standard exponential scaling model with an exponent of approximately 0.6 (EPA, 1983b). It appears that this scaling rule may have been the basis for developing the cost estimates of Claus plants used in the design studies, because an excellent goodness-of-fit was found for a single variable regression based on sulfur recovered. The scaling exponent that was obtained in the single variate analysis was 0.668.

The regression model was further developed to represent the number of operating and spare trains for each data point in the database. The Claus plant contains a two-stage sulfur furnace, sulfur condensers, and catalysts. The cost model is same as the one developed by (Frey, 1990). The number of trains is estimated based on the recovered sulfur mass flow rate and the allowable range of recovered sulfur mass flow rate per train used to develop the regression model. The number of total trains is the number of operating trains and one spare train. Typically, one or two operating trains are used. The direct capital cost model as developed by (Frey, 1990) and scaled to 2000 dollars is:

$$DC_C = 6.96 N_{T,C} \left(\frac{M_{s,C,o}}{N_{O,C}} \right)^{0.668} \qquad R^2=0.994 \quad n=21$$

where,

$$695 \le \left(\frac{M_{s,C,o}}{N_{O,C}} \right) \le 18{,}100 \ (lbmole/hr)$$

The regression model is shown graphically in Figure 5-11.

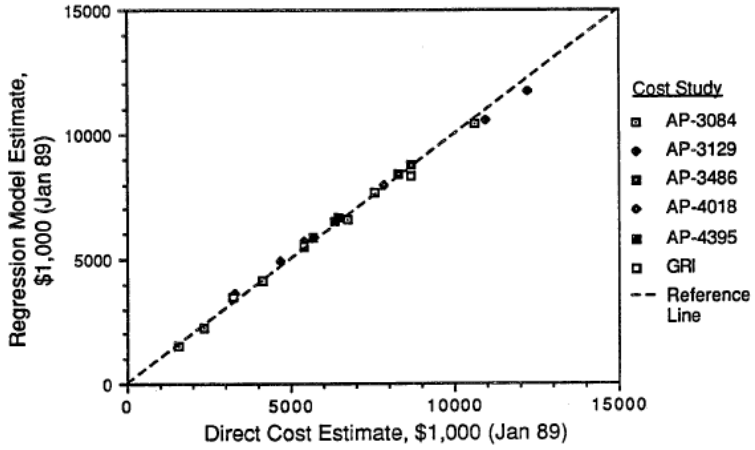

Figure 5-11. Predicted vs. Actual Costs for 2-Stage Claus Plants

As indicated above, the capacity of a single train varies by a factor of over 20. Typically, one or two operating trains and one spare train are used, each with equal capacity. Because there was a prior expectation that the cost of the Claus plant should be modeled using an exponential scaling relationship based on recovered sulfur capacity, with a coefficient near 0.6, this model can be extrapolated at the high end of the range. However, as with all other models, it is recommended that the number of trains be selected so that extrapolation is not required.

Tail Gas Treatment (Beavon-Stretford)

The process is considered commercially available. The capital cost of a Beavon-Stretford unit is expected to vary with the volume flow rate of the input gas streams and with the mass flow rate of the sulfur produced. Data from

two EPRI-sponsored studies were used to develop a regression cost model (Fluor, 1983a; 1983b). An additional two studies were reviewed for inclusion in the database, but information regarding key process parameters (e.g., recovered sulfur flow rate) was not reported. The two EPRI studies report limited performance and cost data for nine different Beavon-Stretford unit sizes. For example, there is incomplete information about inlet gas streams flow rates. Because of the limited availability of performance data, a regression analysis based only on the sulfur produced by the Beavon Stretford process was developed. However, this regression yielded an excellent fit to the data. The direct capital cost model as developed by (Frey, 1990) and scaled to 2000 dollars is:

$$DC_{BS} = 63.76 + 73.1 N_{T,BS} \left(\frac{m_{s,BS,o}}{N_{O,BS}} \right)^{0.645} \qquad R^2=0.998 \quad n=7$$

where,

$$75 \le m_{s,BS,o} \le 1{,}200 \text{ lb/hr}$$

The high coefficient of determination indicated for this model implies either that an exponential cost model is an excellent predictor of the costs of Beavon-Stretford units, or that the costs developed in the EPRI studies were based on a simple scaling model as an approximation. Therefore, it is not immediately clear if this model merely represents an accepted industry practice for developing preliminary cost estimates, or if it accurately reflects the cost of Beavon-Stretford units.

Typically, two operating and one spare train are assumed. Although the regression model is an excellent fit to the data, it is recommended that the number of trains be adjusted so that the recovered sulfur flow rate per train does not exceed the limits given above. As a default, the number of operating and total trains for this process area is assumed to be the same as for the Claus plant process area. The regression model is shown graphically in Figure 5-12.

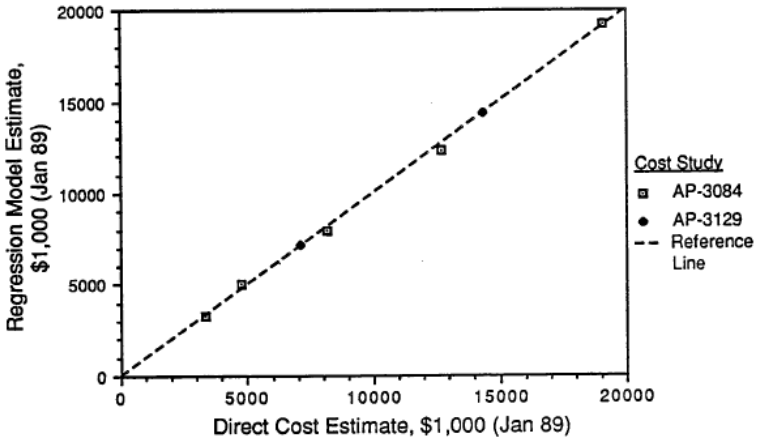

Figure 5-12. Predicted vs. Actual cost of the Beavon-Stretford Section

Hydrolyzer

A hydrolyzer may be required to convert COS to H_2S prior to the Selexol unit. At present, no detailed study has been performed. Until one is completed, the cost is assumed to be 5% of the sulfur capture system.

5.3.2 O&M Cost

Makeup chemicals or catalysts are required for the sulfur removal and recovery systems in all IGCC designs. For cold gas cleanup systems, the makeup requirements include Selexol solvent, Claus plant catalyst, Beavon-Stretford catalyst and chemicals. For the hot gas cleanup system with off-gas recycle, the only requirement is for makeup zinc ferrite sorbent. For a hot gas cleanup system with sulfuric acid recovery, makeup sulfuric acid catalyst is also required. The operating material requirements for these systems are summarized below.

To estimate the total variable operating cost, the annual material requirements appropriate to the given system must be multiplied by their respective unit costs. In the Beavon-Stretford chemical case, the unit costs are based on a process flow rate (i.e., sulfur recovered in the Beavon-Stretford unit) because the material requirements of the consumables themselves are not reported.

The total variable cost is then:

$$VOC = OC_{consumables} = \sum m_i \cdot UC_i$$

Selexol Makeup Solvent Cost

The makeup solvent cost in units of M$/yr in 2000 dollars is calculated as follows:

$$UC_{solv,S} = 1.96 \text{ \$/lb solvent}$$

$$VOM_{solv,S} = UC_{solv,S}\left(\frac{\$}{lb}\right) \cdot \mathrm{m}_{\mathrm{solv,S,i}}\left(\frac{lb}{yr}\right) \cdot 1.0e^{-6}\left(\frac{M\$}{\$}\right)$$

Claus Makeup Catalyst Cost

The makeup solvent cost in units of M$/yr in 2000 dollars is calculated as follows:

$$UC_{cat,C} = 478.08 \text{ \$/ton catalyst}$$

$$VOM_{cat,C} = UC_{cat,C}\left(\frac{\$}{ton}\right) \cdot \mathrm{m}_{\mathrm{cat,C,i}}\left(\frac{ton}{yr}\right) \cdot 1.0e^{-6}\left(\frac{M\$}{\$}\right)$$

Beavon-Stretford Makeup Catalyst Costs

The makeup solvent cost in units of M$/yr in 2000 dollars is calculated as follows:

$$UC_{cat,BS} = 184.71 \text{ \$/ton catalyst}$$

$$VOM_{cat,BS} = UC_{cat,BS}\left(\frac{\$}{ton}\right) \cdot \mathrm{m}_{\mathrm{cat,BS,i}}\left(\frac{ton}{yr}\right) \cdot 1.0e^{-6}\left(\frac{M\$}{\$}\right)$$

Beavon-Stretford Makeup Chemical Costs

The Beavon-Stretford process requires a catalyst for the Beavon unit and a special chemical for the Stretford unit. The chemical requirements for the Beavon-Stretford process were estimated from the values reported in (Fluor, 1983a), which includes data for a range of plant sizes. From these data, a simple linear relationship of chemical requirements as a function of the sulfur recovered in the Beavon-Stretford unit was identified, as shown in Figure 5-13. In the case of the Stretford chemicals, the mass requirement is not given. However, the cost of the initial Stretford chemicals as a function of the recovered sulfur flow rate was developed. The resulting regression models for the chemical requirement, in 2000 dollars, is:

$$C_{i,BS,Chem} = 85.8 \cdot m_{s,BS,o} \qquad R^2 = 1.00, \; n = 5$$

where,

$100 \le \mathbf{m_{s,BS,o}} \le 2{,}100$ (lb/hr)

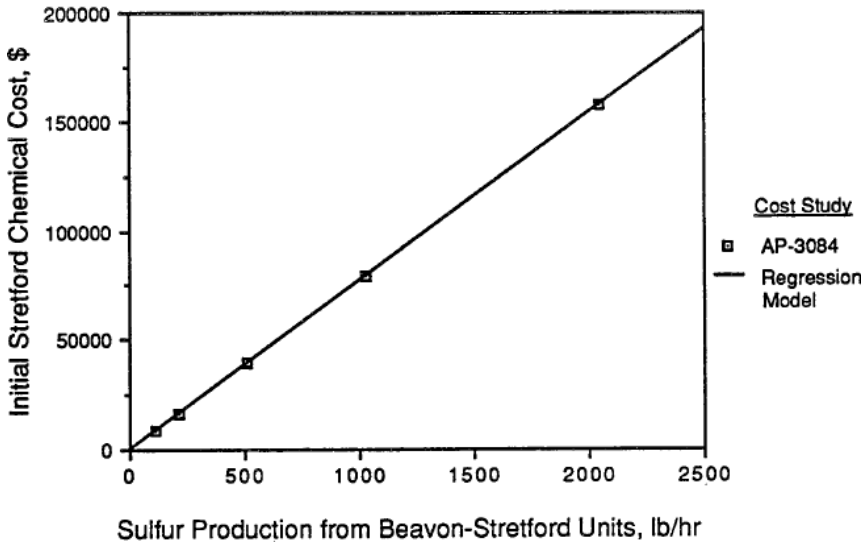

Figure 5-13. Initial Stretford Chemical Cost for the Beavon-Stretford Process.

Beavon-Stretford Makeup Chemical Costs

The regression shown below is the cost of the Stretford chemicals, in 2000 dollars, as a function of the sulfur recovered in the Beavon-Stretford process. The model is shown graphically in Figure 5-14.

$$C_{i,BS,Chem} = 170 \cdot c_f \cdot m_{s,BS,o}$$

$R^2 = 1.00$
$n = 5$

where,

$100 \leq \mathbf{m}_{\mathbf{s,BS,o}} \leq 2{,}000$ (lb/hr)

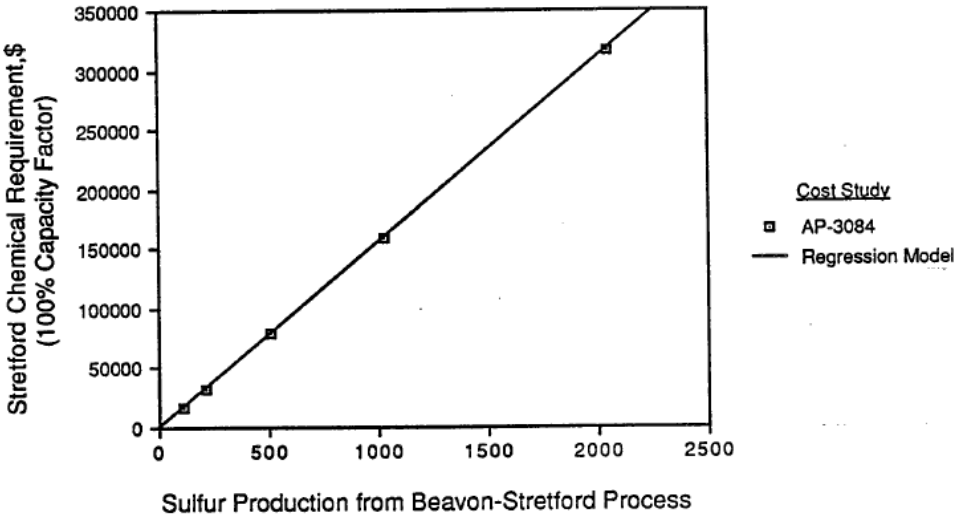

Figure 5-14. Annual Chemical Cost for the Beavon-Stretford Process

Bibliography

EPA (1983). Control Technology Appendices for Pollution Control Technical Manuals. U.S. Environmental Protection Agency, Washington, DC. EPA-600/8-83-009. April 1983.

Bechtel (1983a). Design of Advanced Fossil Fuel Systems (DAFFS), A Study of Three Developing Technologies for Coal-Fired, Base-Load Electric Power Generation: Integrated Gasification Combined Cycle Power Plant With BGC/Lurgi Gasification Process. Prepared by Bechtel Group, Inc., and Burns and Roe/Humphreys-Glasgow Synthetic Fuels, Inc. for the U.S. Department of Energy Argonne National Laboratory. Argonne, Illinois. ANL/FE-83-16. June.

Cover, A.E., D.A. Hubbard, S.K. Jain, E.W. Wong, and C.T. Baker (1985a). Design and Economics of a Lignite-to-SNG Facility Using Westinghouse Gasifiers, in Advanced Coal Gasification Technical Analysis, Final Report. Volume 3-Technical/Economic Evaluations. Prepared by Kellogg Rust Synfuels, Inc. for Gas Research Institute. Chicago, IL. GRI-86/0009.3. June 1985.

Cover, A.E., D.A. Hubbard, S.K. Jain, P.B. Koneru, and C.T. Baker (1985b). Design and Economics of a Lignite-to-SNG Facility Using Lurgi Gasifiers, in Advanced Coal Gasification Technical Analysis, Final Report. Volume 3-Technical/Economic Evaluations. Prepared by Kellogg Rust Synfuels, Inc. for Gas Research Institute. Chicago, IL. GRI-86/0009.3. November 1985.

Fluor (1983a). Economic Assessment of the Impact of Plant Size on Coal Gasification Combined Cycle Plants**.** Prepared by Fluor Engineers, Inc. for Electric Power Research Institute. Palo Alto, CA. EPRI AP-3084. May.

Fluor(1983b). Shell-Based Gasification-Combined-Cycle Power Plant Evaluations. Prepared by Fluor Engineers, Inc. for Electric Power Research Institute, Palo Alto, CA. EPRI AP-3129. June 1983.

Fluor (1984). Cost and Performance for Commercial Applications of Texaco-Based Gasification-Combined-Cycle Plants: Volume 1, Summary and Discussion of Results, and Volume 2, Design Details. Prepared by Fluor Engineers, Inc. for Electric Power Research Institute, Palo Alto, CA. EPRI AP-3486. April 1984.

Fluor (1985). Cost and Performance of Kellogg Rust Westinghouse-based Gasification-Combined-Cycle Plants. Prepared by Fluor Engineers, Inc. for Electric Power Research Institute, Palo Alto, CA. EPRI AP-4018. June 1985.

Parsons (1982**).** Evaluation of Coal Gasification-Combustion Turbine Power Plants Emphasizing Low Water Consumption**.** Prepared by Ralph M. Parsons Company for Electric Power Research Institute. Palo Alto, CA. EPRI AP-2207. January 1982.

Frey, H.C. and E.S. Rubin (1990), Stochastic Modeling of Coal Gasification Combined Cycle Systems: Cost Models for Selected IGCC Systems, Report No. DOE/MC/24248-2901 (NTIS No. DE90015345). June. Prepared by Carnegie Mellon University for U.S. Department of Energy, Morgantown, WV.

Frey, H.C. and N. Akunuri (2001), Probabilistic Modeling and Evaluation of the Performance, Emissions, and Cost of Texaco Gasifier-Based Integrated Gasification Combined Cycle Systems Using ASPEN, Prepared by North Carolina State University for Center for Energy and Environmental Studies, Carnegie Mellon University, Pittsburgh, PA.

6. Selexol System

Nomenclature

MW_{Sel} = molar weight of Selexol (280 lb/lb-mol)

$C_{p,s}$ = specific heat of Selexol (0.49 Btu/lb °F)

$C_{p,i}$ = specific heat of species **i** (Btu/lb °F)

SV_{sel} = specific volume of Selexol (32.574 gallon/lb-mol)

SV_{CO_2} = specific volume of CO_2 (377.052 SFC/lb-mol)

v_i = specific volume of CO_2 (SFC/lb-mol)

p_i = partial pressure of species i in the syngas (psia)

p_1 = pressure of syngas at the inlet of absorber (psia).

p_{CO_2} = partial pressure of CO_2 (psia)

$P_{o,1}$ = outlet pressure of power recovery turbine 1 (psia)

$P_{i,1}$ = pressure of the CO_2-rich Selexol at the inlet of turbine 1 (psia)

$P_{o,2}$ = outlet pressure of power recovery turbine 2 (psia)

$P_{i,1}$ = pressure of the CO_2-rich Selexol at the inlet of turbine 1 (psia)

$T_{SG,i}$ = syngas temperature at the inlet of the absorber (°F)

$T_{SG,o}$ = syngas temperature at the outlet of the absorber (°F)

ΔT = temperature increase of solvent in the absorber (°F)

ΔT_1 = solvent temperature increase caused by the heat transfer (°F)

ΔT_2 = solvent temperature increase due to the solution heat of gases (°F)

χ_i = solubility of species **i** in Selexol at temperature of 30+ ΔT °F

χ_{CO_2} = CO_2 solubility in the Selexol (SCF/gallon-psia)

$\chi_{CO_2,1}$ = solubility of CO_2 in Selexol at temperature 30+ ΔT (°F)

$\chi_{CO_2,4}$ = solubility of CO_2 in Selexol at temperature 30+ ΔT_1 (°F)

Q_1 = heat released by the syngas

$f_{SG,i}$ = molar flow rate of syngas at the inlet of the absorber (lb-mole/hr)

$f_{SG,i}$ = total flow rate of syngas entering the absorber (lb-mole/hr)

$[i]_1$ = molar concentration of species i in syngas at the inlet of the absorber

α = CO_2 removed from the syngas (%)

ω = Selexol flow rate (lb-mole/hr)

V_i = volume flow rate of species i captured in the Selexol (lb-mole/hr)

$V_{CO_2,res}$ = volume flow rate of residual CO_2 in the lean solvent (lb-mole/hr)

$V_{CO_2,abs}$ = volume flow rate of CO_2 captured in the absorber (lb-mole/hr)

$[CO_2]_1$ = CO_2 molar concentration at the inlet of absorber

ψ_{CO_2} = solution heat of CO_2 in Selexol (Btu/lb-solute)

hp_{tur} = power recovered through the power turbine (hp)

H_{Sel} = total dynamic head (lb/in^2)

f_{Sel_2} = flow rate of CO_2 rich Selexol entering the turbine (gal/min)

η_{tur} = efficiency of the turbine

dT_{tur} = decreased temperature of the Selexol in the power recovery turbine (°F)

dP_{tur} = decreased pressure of the Selexol in the power recovery turbine (°F)

$hp_{comp.}$ = power consumption of the CO_2 compressor (hp)

$\eta_{comp.}$ = overall efficiency of the compressor

VF_{gas} = inlet rate of the CO_2 stream (ft^3/min)

$P_{comp.,i}$ = inlet pressure of the compressor (psia)

$P_{comp.,o}$ = outlet pressure of the compressor (psia)

$$k_{gas} = \frac{C_{p,gas}}{C_{v,gas}}$$

H_s = total dynamic head (psia)

f_{Sel} = flow rate of CO_2 lean Selexol (gal/min)

η_{pump} = efficiency of the pump

$W_{ref.}$ = power consumption of the solvent refrigeration process (kW)

T_{evap} = evaporation temperature of the refrigerant (°F)

$N_{T,abs}$ = total train number of absorbers

$P_{abs,i}$ = inlet pressure of absorber (atm)

f_{Sel} = flow rate of the Selexol(lb-mole/hr)

f_{gas} = flow rate of the syngas (lb-mole/hr)

hp_{tur} = power output of the turbine (hp)

$P_{tur,o}$ = outlet pressure of the turbine (atm)

$N_{T,sump}$ = total train number of sump tanks

$N_{O,sump}$ = operating train number of the sump tanks

f_{Sel} = flow rate of Selexol entering a vessel (kg/s)

hp_{RC} = power consumption of the recycle compressor (hp)

hp_{SP} = power consumption of the Selexol pump (hp)

hp_{comp} = power consumption of the compressor (hp)

$N_{T,reft}$ = total train number of the refrigeration unit

$N_{O,reft}$ = operating train number of the refrigeration unit

ΔT_{Sel} = Selexol temperature difference between the inlet and outlet of the refrigeration unit (°C)

$N_{T,\tan k}$ = total train number of the flash tank

$N_{O,\tan k}$ = operating train number of the flash tank

6.1 Selexol System Process Description

The Selexol process uses a physical solvent to remove acid gas from the streams of synthetic or natural gas. It is ideally suited for the selective removal of H_2S and other sulfur compounds, or for the bulk removal of CO_2. The Selexol process also removes COS, mercaptans, ammonia, HCN and metal carbonyls [Epps, 1994].

In this section, the technical background information of Selexol process is reviewed. This information provides the basis for the development of a performance model of Selexol systems to control CO_2 emissions from IGCC plants.

6.1.1 History

The Selexol process, patented by Allied Chemical Corp., has been used since the late 1960s. The process was sold to Norton in 1982 and then bought by Union Carbide in 1990 [Epps, 1994]. The Dow Chemical Co. acquired gas processing expertise, including the Selexol process, from Union Carbide in 2001. The process is offered for license by several engineering companies, such as UOP [UOP, 2002].

The Selexol process has been used commercially for 30 years and has provided reliable and stable operations. As of January 2000, over 55 Selexol units have been put into commercial service [Kubek, 2000], which cover a wide variety of applications, ranging from natural gas to synthetic gas. By now, Selexol process has been the dominant acid-gas removal system in gasification projects. Moreover, increasing interests to control CO_2 emission in the world may lead to Selexol application widely, particularly for coal gasification plants. Actually, the use of the Selexol solvent has a long history in gasification process, and was chosen as the acid-gas removal technology for the pioneering work in this area. Due to its outstanding record, the Selexol process continues to be the preferred choice for acid-gas removal today, and has recently been selected for several large projects around the world [Breckenridge, 2000]. Relevant experiences for gasification are as follows [Kubek, 2000].

- About 50 Selexol units have been successfully commissioned for steam reforming, partial oxidation, natural gas, and landfill gas. Of these, 10 have been for heavy oil or coal gasifiers.
- The 100 MW Texaco/Cool Water (California) 1,000 t/d coal gasifier plant for IGCC demonstration was operated continuously for about five years in the 1980s. The Selexol unit performed extremely well. The process delivered H_2S-enriched acid gas to a Claus plant while removing 20 to 25% of the CO_2 and treating a high CO_2/H_2S ratio feed gas.

- The TVA/Muscle Shoals (Alabama) 200 t/d coal gasifier demonstration plant was operated continuously for about five years in the early 1980s. It employed a Texaco gasifier, a COS hydrolysis unit, and a Selexol unit to convert coal to clean synthesis gas, and CO_2 as an alternative feed to an existing ammonia-urea plant. The COS hydrolysis and Selexol units were stable and had a high on-stream factor. The Selexol unit delivered an H_2S-enriched acid gas to elemental sulfur production, a pure (< 1 ppmv total sulfur) synthesis gas to NH_3 synthesis, and removed part of the CO_2 to provide high-purity CO_2 for urea production.

6.1.2 Selexol Solvent

Properties

The Selexol acid gas removal process is based on the mechanism of physical absorption. The solvent used in the Selexol acid removal system is a mixture of dimethyl ethers polyethylene glycol with the formulation of $CH_3(CH_2CH_20)_nCH_3$, where n is between 3 and 9 [Epps, 1994]. The general properties of the glycol solvent is given in Table 6-1 [Sciamanna, 1988; Newman, 1985].

Table 6-1. Properties of Glycol Solvent

Property	Value
Viscosity @25C,cp	5.8
Specific gravity@25C,kg/m^3	1030
Mole weight	280
Vapor pressure @25C, mmHg	0.00073
Freezing point C	-28
Maximum operating Temp., C	175
Specific heat@25C Btu/lb F	0.49

Solubility of Acid Gases

The performance of a physical solvent can be predicted by its solubility. The solubility of an individual gas follows the Henry's law—the solubility of a compound in the solvent is directly proportional to its partial pressure in the gas phase.

Selexol is a physical solvent. Therefore, the performance of the Selexol process enhances with increasing acid gas partial pressures. As shown in Figure 6-1, chemical solvents have a higher absorption capacity at relatively low acid gas partial pressures. However, their absorption capacities plateau at higher partial pressures. The solubility of an acid gas in physical solvents increases linearly with its partial pressure. Therefore, chemical solvent technologies are favorable at low acid gas partial pressures and physical solvents are favored at high acid gas partial pressures.

Physical solvents are more efficient to regenerate, a second advantage for high acid gas partial pressure applications. The physical absorption allows for the solvent to be partially regenerated by pressure reduction, which reduces the energy requirement compared to chemical solvents.

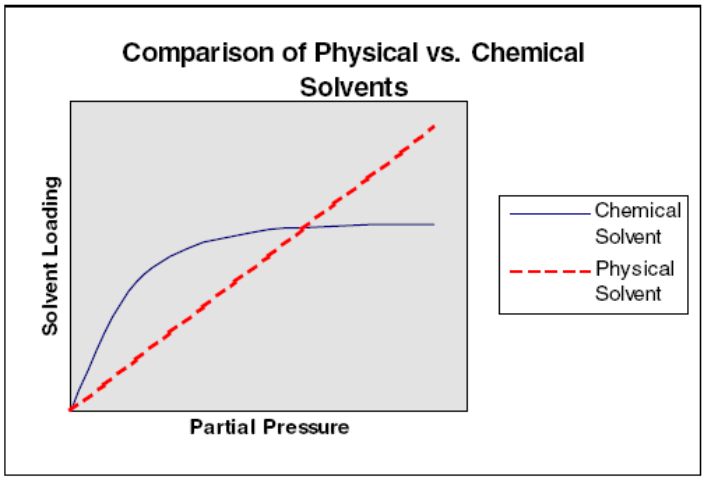

Figure 6-1. Characteristics for Chemical and Physical Solvents [Sciamanna, 1988]

Higher partial pressure leads to higher solubility in physical solvents of all components of a gas stream, so another attractive feature of the Selexol system is that it has a more favorable solubility for the acid gases versus other light gases. Compared to acid gases, H_2 and CO have much lower solubility in the solvent. For instance, as shown in Table 6-2, CO_2 is 75 times more soluble than H_2, and H_2S is 670 times more soluble than H_2 in Selexol.

Table 6-2. Relative solubility of gases in Selexol solvent [Doctor, 1994]

Gas	CO_2	H_2	CH_4	CO	H_2S	COS	SO_2	NH_3	N_2	H_2O
Solubility	1	0.01	0.0667	0.028	8.93	2.33	93.3	4.87	0	733

Table 6-3 shows the actual solubility of various gases at 25°C in the Selexol solvent. The solubility data in Table 6-3 are based on single component solubility. It would be expected that these values should be approximately the same for non-polar components even in acid gas loaded solvents [Korens, 2003].

Table 6-3. Solubility of Gases in the Selexol Solvent [Korens, 2002]

Gas	CO_2	H_2	CH_4	CO	H_2S	COS	HCN	C_6H_6	CH_3SH	H_2O
Solubility	3.1	0.03	0.2	0.08	21	7.0	6600	759	68	2200
Ncm2/g.bar @25°C										

The solvent may be regenerated by releasing the absorbed sour gases. The regeneration step for Selexol can be carried out by either thermally, or flashing, or stripping gas. In addition to its solubility, the Selexol solvent has some other positive advantages to gasification applications [Kubek, 2000].

- A very low vapor pressure that limits its losses to the treated gas
- Low viscosity to avoid large pressure drop
- High chemical and thermal stability (no reclaiming or purge) because the solvent is true physical solvent and does not react chemically with the absorbed gases [Shah, 1988]
- Non-toxic for environmental compatibility and worker safety
- Non-corrosive for mainly carbon steel construction: the Selexol process allows for construction of mostly carbon steel due to its non-aqueous nature and inert chemical characteristics
- Non-foaming for operational stability
- Compatibility with gasifier feed gas contaminants
- High solubility for HCN and NH_3 allows removal without solvent degradation

- High solubility for nickel and iron carbonyls allows for their removal from the synthesis gas. This could be important to protect blades in downstream turbine operation.
- Low heat requirements for regeneration because the solvent can be regenerated by a simple pressure letdown

6.1.3 Selexol Absorber System

This section presents a technical overview of Selexol absorption processes for acid gases removal, with particular focus on the effects of the acid gas removal requirements on the design of the Selexol process.

Standard Configuration

Although a Selexol process can be configured in various ways, depending on the requirements for the level of H_2S/CO_2 selectivity, the depth of sulfur removal, the need for bulk CO_2 removal, and whether the gas needs to be dehydrated, this process always includes the following steps:

- Sour gas absorption
- Solvent regeneration/ & sour gas recovery
- Solvent cooling and recycle

Through taking advantage of the high H_2S to CO_2 selectivity of Selexol solvent, Selexol solvent processes can also be configured to capture H_2S and CO_2 together with high levels of CO_2 recovery. This is usually accomplished by staging absorption for a high level of H_2S removal, followed by CO_2 removal. Figure 6-2 shows a Selexol process layout for synthesis gas treating where a high level of both sulfur and CO_2 removal are required. H_2S is selectively removed in the first column by a lean solvent, and CO_2 is removed from the H_2S-free gas in the second absorber. The second-stage solvent can be regenerated with air or nitrogen if very deep CO_2 removal is required.

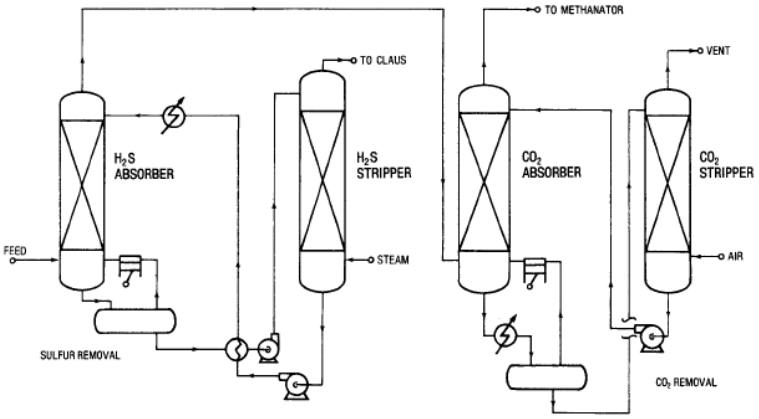

Figure 6-2. Selexol Process for Sulfur and CO_2 Removal [Kohl, 1985]

A COS hydrolysis unit may be added to the configuration shown in Figure 6-2 to achieve a higher level of removal of H_2S and COS. At the Sarlux IGCC plant in Italy, which gasifies petroleum pitch, the Selexol unit allows a COS hydrolysis step and gives an acid gas that is 50-80 vol.% H_2S to the Claus plant. This acid gas composition is the result of an H_2S enrichment factor of about 2 to 3 through the Selexol unit. The H_2S content of the purified gas from the Selexol absorber at that plant is about 30 ppmv [Korens, 2002].

Optimized Configurations

A variety of flow schemes of Selexol processes permits process optimization and energy reduction. The following is a description of an optimal design of a Selexol process which removes sulfur and CO_2 from syngas from IGCC systems. This optimal design is based on revising a Selexol process, originally designed by UOP, for H_2S and CO_2 removal from syngas for the production of ammonia (UOP, 2002).

The H_2S Absorption flowsheet for the optimized configuration is shown in Figure 6-3. Syngas from the gas cooling section of the gasification process enters the H_2S absorber where it is contacted with CO_2-saturated Selexol solvent from the CO_2-removal portion of the facility. The pre-saturated solvent from the CO_2 removal area is chilled with refrigeration before being fed into the absorber, which can increase the CO_2 and H_2S loading capacity of the solvent. The use of pre-loaded solvent prevents additional CO_2 absorption in the H_2S absorber, and it also minimizes the temperature rise across the tower, which negatively affects the H_2S solubility and the selectivity of the solvent. H_2S is removed from the syngas.

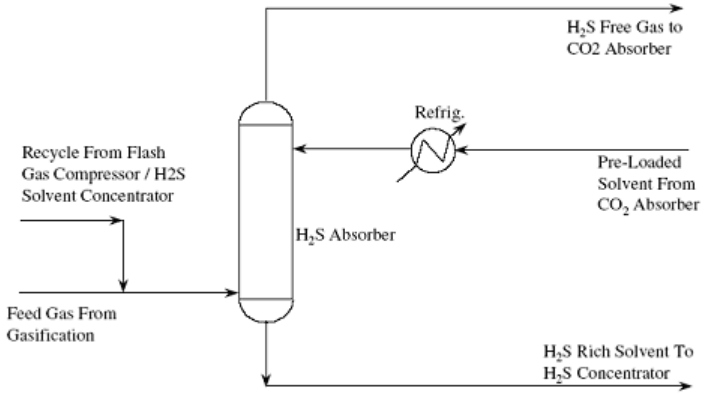

Figure 6-3. Optimized Selexol absorption process for H_2S removal

The H_2S absorber overhead stream is mixed with the entire solvent stream from the CO_2 absorber. Therefore, bulk CO_2 is removed in this pre-contacting stage which reduces the loading in the CO_2 absorber. The rich solvent from the H_2S absorber is next fed into the H_2S solvent regeneration facility.

Figure 6-4 presents a process flow diagram for the optimized H_2S solvent regeneration section. The rich solvent from the H_2S absorber is pumped to high pressure and heated in the lean / rich exchanger. The solvent then enters the H_2S solvent concentrator, which operates at a pressure higher than the H_2S absorber, thus the recycle gases can be recycled to the H_2S absorber without compression.

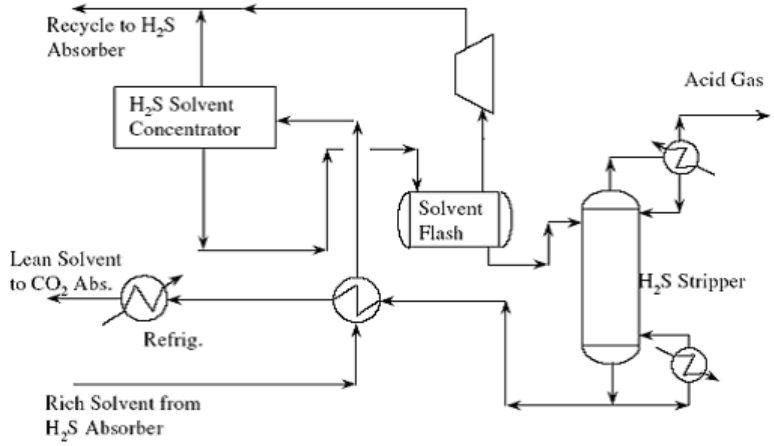

Figure 6-4. Optimized H_2S Solvent Regeneration

Due to the relative difference in solubility of CO_2 and H_2S in Selexol solvents, CO_2 is removed from solution preferentially over H_2S, which results in an enriched H_2S concentration in the solvent. The CO_2 removed in the H_2S solvent concentrator is the majority of the recycle gases back to the H_2S absorber.

The enriched solvent from the H_2S solvent concentrator is flashed down to lower pressure. The flash gas again contains a higher proportion of CO_2 than H_2S. This stream is also recycled back to the H_2S absorber. This recycle stream is relatively small because much of the CO_2 was removed at high pressure. The solvent from the flash drum enters the Selexol stripper for regeneration.

The optimized CO_2 absorption flowsheet is shown in Figure 6-5. In this optimization design, the entire CO_2 solvent flow is contacted with the H_2S absorber overhead stream in the pre-contacting stage. The heat of absorption is removed from this pre-contacting stage in a refrigeration chiller. The relatively high temperature of this stream allows setting high temperature refrigeration, which reduces the power consumption of the refrigeration system. The solvent is cooled to optimum absorption temperatures when the pressure is reduced in the flash regeneration portion of the facility.

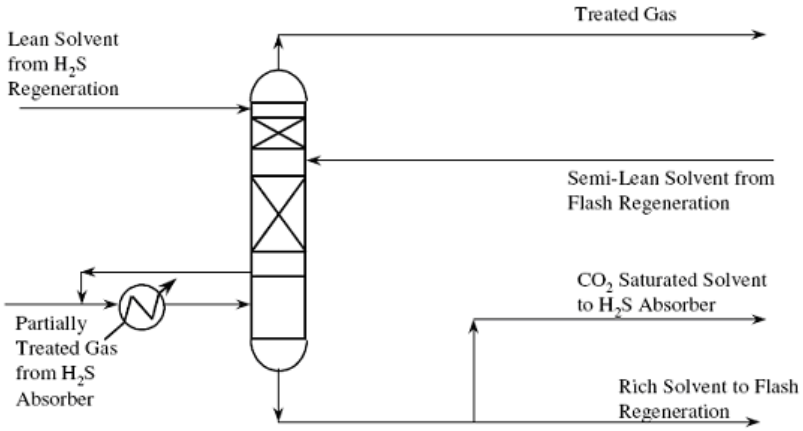

Figure 6-5. Optimized Selexol process for CO_2 absorption

A portion of the rich CO_2 solvent is returned to the H_2S absorber as pre-saturated solvent. The remainder of the solvent is flash regenerated and will be presented below. The top bed of the tower uses lean solvent from the H_2S regeneration facility to contact the syngas. This allows the CO_2 to be removed to levels lower than could be achieved using only flash regenerated (semi-lean) solvent.

Rich CO_2 is flash regenerated as shown in Figure 6-6. The flash regeneration uses one sump tank, one or two power recovery turbines, and three stages of flash. The CO_2 rich solvent leaving the bottom of the CO_2 absorber enters the sump tank at a reduced pressure, where most H_2 and a small amount of CO_2 captured in the Selexol are released and recycled back to the pre-contacting stage.

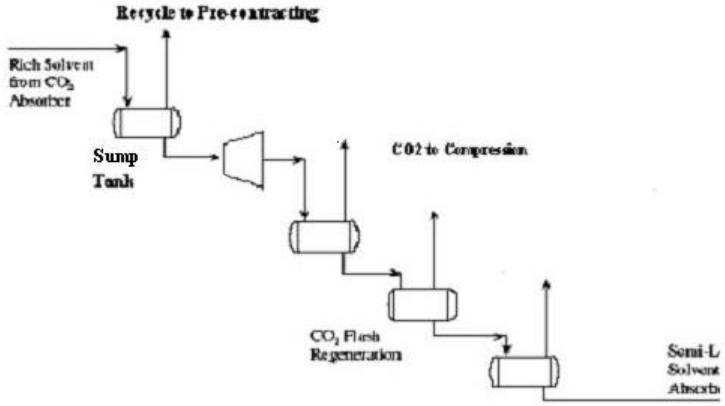

Figure 6-6. Optimized Selexol regeneration through CO_2 flash

The CO_2 rich solvent with high pressure is delivered to one or two hydraulic power recovery turbines to recover the pressure energy before it is fed into three flash drums, where CO_2 is released at staged pressures to reduce the power consumption of CO_2 compression later.

A key limitation of Selexol systems is the operating temperature requirement. The operating temperature for Selexol systems is typically approximately 100°F. Hence a reasonable location of Selexol process in an IGCC system is down stream of the syngas cooling section.

6.2 Performance Model

As a patented commercial solvent, the detailed characteristics of the Selexol solvent are not available. Hence in this section, a semi-analytical, semi-regression performance model of Selexol systems for CO_2 capture is presented. This section discusses the methodology of setting up a performance model of Selexol process for CO_2 capture. A cost model of the Selexol process, shown later, is based on this performance model.

6.2.1 Temperature Effect on Gas Solubility

The solubility of a gas in Selexol depends on its partial pressure and temperature. The solubility of CO_2 as a function of temperature is regressed based on published data [Doctor 1996, Black 2000] and given in Equation (6-1),

$$\chi_{CO_2} = 0.0908 - 0.0008T \qquad R^2 = 0.95 \qquad (6\text{-}1)$$

where

T = solvent temperature with a range of 30~77 °F

The solubility of other gases at different temperature is not available. Here the relative solubility of other gases to CO_2 at different temperature is assumed to be constant.

6.2.2 Solvent Flow Rate

The input and output parameters of this model are given in Table 6-4. For the performance simulation, the first step is to calculate the flow rate of the solvent. In order to determine the solvent flow rate, the examination of the entire Selexol process can be reduced to a simpler model, as shown in Figure 6-7.

Table 6-4. Input and output parameters of Selexol model

Input parameter				**Output parameter**		
Syngas input	Flow rate (mole/s)	f_1		Fuel gas output	Flow rate (mole/s)	f_2
	Pressure	p_1			Pressure	p_2
	Temperature	T_1			Temperature	T_2
	Molar concentrations	$[CO]_1$			Molar concentrations	$[CO]_2$
		$[CO_2]_1$				$[CO_2]_2$
		$[H_2]_1$				$[H_2]_2$
		$[CH_4]_1$				$[CH_4]_2$
		$[H_2S]_1$				$[H_2S]_2$
		$[COS]_1$				$[COS]_2$
		$[NH_3]_1$				$[NH_3]_2$
		$[H_2O]_1$				$[H_2O]_2$
CO_2 removal percentage				CO_2 flow	Flow rate (mole/s)	f_5
					Pressure	P_5
				Refrig. power	Power recovery	Comp. power

Stream S1 is the syngas fed into the absorber at a given temperature, and α percent of CO_2 is removed from the syngas. Stream S4 is the lean solvent at a design temperature. Due to heat transfer between the solvent and syngas and the absorption heat, the temperature of the rich solvent (stream S3) will be increased by ΔT. For the given CO_2 removal efficiency α, the flow rate of solvent, fuel gas and CO_2 can be calculated as follows.

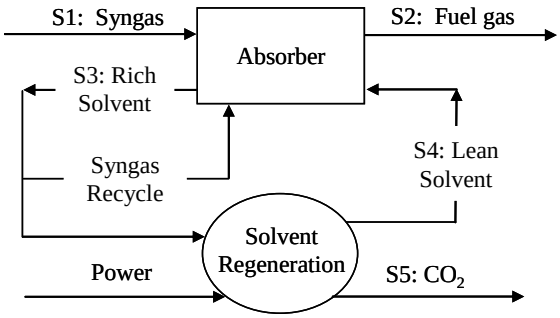

Figure 6-7. Simplified Selexol process

As mentioned in "Temperature Effect on Gas Solubility" above, the solubility of gases in Selexol is a function of temperature. For calculating the flow rate of solvent, the first step is to estimate the temperature change of solvent in the absorber.

Assuming the flow rate of solvent is ω lb-mol/hr, the temperature increase of solvent in the absorber is given by Equation (6-2):

$$\Delta T = \Delta T_1 + \Delta T_2 \tag{6-2}$$

According to the amount of heat transferred between the syngas and solvent, and the specific heat of the solvent, the temperature increase due to heat transfer is calculated by Equation (6-3):

$$\Delta T_1 = \frac{Q_1}{\omega \cdot MW_{Sel} C_{p,s}} \tag{6-3}$$

The temperature increase can be estimated according to the energy balance given by Equation (6-4):

$$\begin{aligned} Q_1 = (T_{SG,i} - T_{SG,o})\, f_{SG,i} \{ & 2.02[H_2]_1 C_{p,H_2} + 16[CH_4]_1 C_{p,CH_4} \\ & + 28[CO]_1 C_{p,CO} + 44[CO_2]_1 (1-\alpha) C_{p,CO_2} \} \\ & + 44 (T_{SG,i} - T_{SG,o} - \Delta T)\, f_{SG,i} \alpha [CO_2]_1 C_{p,CO_2} \end{aligned} \tag{6-4}$$

Specific heats $C_{p,i}$ of several gases are provided in Table 6-5.

Table 6-5. Specific heat of gases in the syngas

Gas	CO	CO_2	H_2	CH_4	Ar	N_2	H_2S	NH_3
Specific heat (Btu/lb F)	0.248	0.199	3.425	0.593	0.125	0.249	0.245	0.52

In Equation (6-2), ΔT_2 is caused by the solution heat. Equation (6-5) calculates only the solution heat of CO_2. The solution heat of other gases is negligible because the amount of other gases captured by Selexol is much less than that of CO_2.

$$\Delta T_2 = \frac{44\, f_{SG,i} [CO_2]_1 \alpha \psi_{CO_2}}{\omega MW_{Sel} C_{p,Sel}} \tag{6-5}$$

The solution heat ψ_{CO_2} of several gases is given in Table 6-6 [Korens, 2002].

Table 6-6. Solution heat (Btu/lb-solute) of gases in the Selexol

Gas	CO_2	H_2S	CH_3
Heat of solution (Btu/lb-solute)	160	190	75

In the flash tanks, the residual time is long enough to assume that equilibrium can be achieved in these tanks. In the last flash tank, the solvent temperature is about (30+ ΔT_1), hence the volume and mass flow rate of the residual CO_2 in the lean solvent (stream S4 in Figure 6-7) can be given by Equations (6-6) and (6-7) :

$$V_{CO_2,res}\left(\frac{SCF}{hr}\right) = SV_{sel}\,\omega p_{CO_2}\chi_{CO_2} \tag{6-6}$$

$$m_{CO_2,res}\left(\frac{lb\cdot mol}{hr}\right) = \frac{V_{CO_2,res}}{SV_{CO_2}} \tag{6-7}$$

According to the CO_2 capture percentage in the absorber, the amount of CO_2 that needs be captured by the solvent is given by Equation (6-8):

$$V_{CO_2,abs}\left(\frac{SCF}{hr}\right) = SV_{CO_2} f_{SG,i}[CO_2]_1\alpha \tag{6-8}$$

In the absorber, the equilibrium cannot be achieved due to the limited residual time. The flow rate of solvent used in the absorber is larger than that of the solvent required to capture α percentage of CO_2 at equilibrium. The ratio of the actual flow rate to the equilibrium flow rate of the solvent was regressed based on published data [Doctor, 1994, 1996, Sciamanna, 1988]. The ratio is given in Equation (6-9):

$$\gamma = \frac{1.26}{(1-\alpha)^{0.07}} - 0.0002\,p_1 \qquad R^2=0.8 \tag{6-9}$$

Then the flow rate of Selexol for capturing α percentage of CO_2 is given by Equation (6-10):

$$\omega\left(\frac{lb\cdot mol}{hr}\right) = \frac{\gamma(V_{CO_2,res}+V_{CO_2,abs})}{SV_{sel}\,p_1[CO_2]_1\chi_{CO_2,1}} \tag{6-10}$$

Based on the above discussion, the calculation process for the flow rate of Selexol is concluded as in the following. First assuming the temperature of the Selexol solvent in the absorber is increased by ($\Delta T_1 + \Delta T_2$), then the solubility of CO_2 at this increased temperature can be calculated. Second the solubility of CO_2 at the solvent in the last flash tank is calculated at the temperature (30+ ΔT_1). Given the amount of CO_2 needed to be required, the flow rate of the solvent is calculated based on the solubility difference between the solvent in the absorber and in the last stage flash tank. Then the new values of ΔT_1 and ΔT_2 are computed using the calculated solvent flow rate of solvent. Such calculation process continues until the flow rate of the solvent is convergent. This calculation process is represented by Figure 6-8:

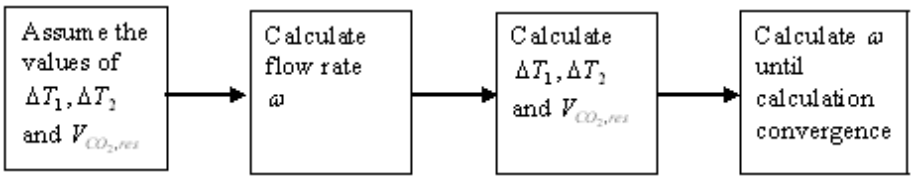

Figure 6-8. Calculation process for the flow rate of Selexol

Composition and flow rate of fuel gas

After CO_2 capture, the syngas is converted into the fuel gas, the main component of which is hydrogen. The composition and flow rate of the fuel gas can be calculated as follows.

Knowing the Selexol flow rate and solubility of gases in the Selexol, the volume and mass amount of species **i** that are captured by the solvent is given by Equations (6-11) and (6-12):

$$V_i\left(\frac{SCF}{hr}\right) = SV_{sel} \cdot \omega \cdot p_i \cdot \chi_i \tag{6-11}$$

$$m_i\left(\frac{lb \cdot mol}{hr}\right) = \frac{V_i}{v_i} \tag{6-12}$$

In the sump tank, most of the H_2, and CH_4 captured in the Selexol are released and recycled back to the absorber. Because the solubility of CO_2 is much higher, only a tiny amount of CO_2 is released in the sump tank. The operating pressure of the sump tank is a design parameter. For this study, the operating pressure is determined to keep the loss of H_2 to Selexol solvent no more than 1% of H_2 in the syngas. The calculation process for the sump tank is as the follows: assuming the operating pressure is p_{sump}, the volume of species **i** released from the sump tank is $V_i^{'}$, then the partial pressure $p_{i,sump}$ can be given by Equation (6-13). According to mass conservation, the total volume of species **i** captured in the absorber equals the volume released in the sump tank plus the volume retained in the solvent in the tank, expressed as Equation (6-14). Now recalling the Equation (6-11), the volume of species is retained in the solvent in the tank can calculated as Equation (6-15). Iteratively calculate Equations (6-13), (6-14), and (6-15) until the partial pressures are converged. If at the given operating pressure, the H_2 volume retained in the solvent does not meet the design value, then the operating pressure is adjusted and the calculation is run again. The calculation procedure is given by Figure 6-9.

$$p_{i,sump} = \frac{V_i^{'}}{\sum_i V_i^{'}} p_{sump} \tag{6-13}$$

$$V_i = V_{i,sump} + V_i^{'} \tag{6-14}$$

$$V_{i,sump}\left(\frac{SCF}{hr}\right) = 32.574\omega \cdot p_{i,sump} \cdot \chi_i \tag{6-15}$$

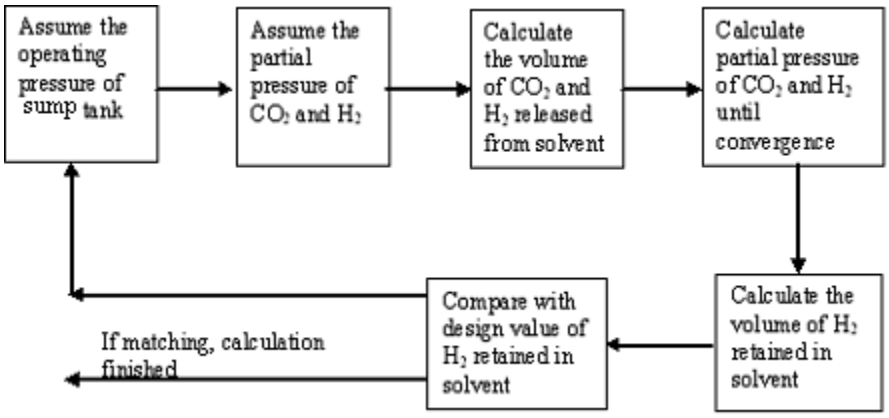

Figure 6-9. Calculation process for the operating pressure of the sump tank

Composition and flow rate of CO_2 rich flow

At each stage of the flash tanks, the flash pressure is given. At this pressure, the residual gases in the lean solvent can be calculated based on their solubility. Based on mass conservation, the composition and flow rate of CO_2 rich flow from the flash tanks can also be calculated, and the calculation procedure is similar to that shown in Figure 6-9.

6.2.3 Power Requirements

There is no heat duty in the Selexol process because the solvent is regenerated through pressure flashing, but the power input is required to compress the recycling gas from the sump tank, the lean solvent from the flash tank 3, and the CO_2 rich product. At the same time, some electricity can be generated through the power recovery hydro turbine. The total power consumption is the difference between the power input and the recovered power from the turbine.

Power recovery

In this performance model, the pressure of the high-pressure rich solvent from the absorber is reduced and the energy is recovered through one or two hydro turbines. According to the designs in other studies [Doctor, 1994, 1996, Sciamanna, 1988, Black, 2000], a thumb rule of design is concluded here. If the pressure of CO_2 rich Selexol flow is larger than 240 psia, two power recovery turbines will be used. Otherwise, only one power recovery turbine will be used. Generally, this outlet pressure ($P_{o,1}$, psia) of the turbine can be determined based on the system pressure as shown in Equation (6-16):

$$P_{o,1} = 0.0402 P_{i,1}^{1.415} \tag{6-16}$$

where

$$(150 \le p_{i,1} \le 1000)$$

If the pressure of the CO_2 rich Selexol flow is larger than 240 psia, then the outlet pressure of the second turbine is given by Equation (6-17):

$$p_{o,2} = 35.619 \ln(p_{i,1}) - 169.88 \tag{6-17}$$

where

$$(240 \le p_{i,1} \le 1000)$$

The power recovered from the liquid solvent is calculated from the following expression [Doctor, 1994],

$$hp_{tur} = H_{Sel} \cdot \frac{f_{Sel_2}}{1714} \cdot \eta_{tur} \tag{6-18}$$

The temperature change of the solvent in the turbine can be calculated based on the change in enthalpy, which equals flow work, $\int vdp$. For the default efficiency of turbines, 78%, the temperature can be given by,

$$dT_{tur} = 0.0047 \cdot dP_{tur} - 0.0715 \tag{6-19}$$

CO_2 Compression

There are three flashing pressure levels for CO_2 release. The design of the flashing pressures in the three flashing tanks is an optimal problem, but a preliminary study showed that the effect of flashing pressures on the power consumption of the Selexol processes is not considerable. Hence, some default values are adopted here for the process design. If the system pressure is larger than 240 psia, the first flashing pressure equals the outlet pressure of the second turbine. If the system pressure is less than 240 psia, the first flashing pressure is set to be 25 psia. The second flashing pressure is set to be 14.7 psia, and the last flashing pressure is set to be 4 psia.

In each flashing tank, the gases released from solvent are calculated. CO_2 released from flash tank 2 and tank 3 is compressed to the flashing pressure of tank 1. The CO_2 stream is finally compressed to a high pressure (>1000psia) for storage using a multi-stage, inter-stage cooling compressor. The power required by the CO_2 compressors is estimated by [Doctor, 1994],

$$hp_{comp.} = \frac{0.00436}{\eta_{comp.}} VF_{gas} P_{comp,i} \left(\frac{k}{k-1} \right) \left[\left(\frac{P_{comp.,o}}{P_{comp.,,i}} \right)^{\left(\frac{k_{gas}-1}{k_{gas}} \right)} - 1 \right] \quad (6\text{-}20)$$

Solvent compression work

The CO_2-lean solvent is pumped back to the absorber operating pressure by a circulation pump. The power required by the circulation pump is estimated in a similar way as done in Equation (6-18):

$$hp_{pump} = H_s \frac{f_{Sel}}{1714 \eta_{pump}} \quad (6\text{-}21)$$

Recycle gas compression work

The gases from the sump tank are recycled to the absorber. A compressor is used to compress the gases to the operating pressure of the absorber. The power of the compressor is estimated using Equation (6-20).

Solvent refrigeration

Before the CO_2-lean solvent fed into the absorber, it has to be cooled down to the absorber operating temperature (30 °F) by refrigeration. The refrigeration power in kW is estimated by [Doctor, 1994],

$$W_{ref.} = \frac{refrigeration \quad load \left(\frac{Btu}{hr} \right)}{1000 \left(9 + \frac{T_{evap}(^{o}F)}{10} \right)} \quad (6\text{-}22)$$

Makeup of the Selexol solvent

The vapor pressure of the Selexol solvent is 1.35×10^{-5} psia at 77 °F, which is very low. The real vapor pressure is even lower because the operating temperature is usually lower than 77 °F. Hence, the loss of solvent due to evaporation is negligible. On the other hand, due to leakage, especially in the start on and turn off processes, a certain amount of solvent is lost. Here the annual loss of solvent is assumed to be approximate 10% of the total solvent in the system [UOP, 2003].

6.3 Capital Costs

The outputs of this cost model include the process facility cost, total plant cost, total plant investment, total capital requirement, and O&M cost.

6.3.1 Process Facility Costs

The major process facility costs of the Selexol system for CO_2 capture are considered in the following sub-sections. Each is determined from actual costs and key performance parameters.

CO_2 Absorption Column

Using the data in Table 6-7, the process facility costs of the absorption column are regressed as a function of the operating pressure, the flow rates of the solvent and syngas. The process facility cost for the absorber in 1,000 US$ for 2000$ is:

$$PFC_{abs} = N_{T,abs}\left[\begin{array}{l} -1375.356 + 16.536 \cdot P_{abs,i} \\ +\,0.127628\left(\dfrac{f_{Sel} + f_{gas}}{2}\right) \end{array}\right] \qquad R^2 = 0.90 \qquad (6\text{-}23)$$

Table 6-7. Absorber cost data adjusted to the dollar values in 2000 [Doctor, 1996]

PFC (2000$)	P(atm)	Flow rate of syngas (lb-mol/h)	Selexol flow rate (lb-mol/hr)
6.3E+05	30.35	11771.88	11815.53
9.2E+05	10.21	12418.46	20802.84
1.5E+06	16.88	17614.58	23000
1.3E+06	68.05	17614.58	6900

Power Recovery Turbine

Based on the data in Table 6-8, the process facility cost of the power recovery turbine is given in 1,000 US$ for 2000$ as follows:

$$PFC_{tur} = 219.086 + 0.080912 hp_{tur} + 0.020086 P_{tur,o}^2 \qquad R^2 = 0.91 \qquad (6\text{-}24)$$

Table 6-8. Power recovery turbine cost data adjusted to the dollar value in 2000 [Doctor, 1996]

PFC (2000 k$)	Outlet pressure	Power output(hp)
277.23	13.60	649
235.64	3.40	404
246.66	5.10	293
263.21	3.40	451
246.66	1.70	293
317.14	51.03	567
317.14	6.80	567

Sump Tank

The process facility cost of the sump tank is regressed as a function of the solvent flow rate as given in Table 6-9. The cost in 1,000 US$ for 2000$ is as follows:

$$PFC_{slump} = 2.0049 N_{T,slump}\left(\frac{f_{Sel}}{N_{O,slump}}\right)^{0.7446} \qquad R^2 = 0.87 \qquad (6\text{-}25$$

where

f_{Sel} ~ 400 – 800 kg/s per train

Table 6-9. Sump tank cost data adjusted to the dollar value in 2000 [Doctor, 1996]

PFC (2000 k$)	Selexol flow rate (kg/s)
179.04	416.85
272.83	733.92
205.11	811.44
205.22	811.44

Recycle Compressor

The process facility cost of the recycle compressor (Table 6-10) can be determined as a function of the recycle compressor capacity hp_{RC} in 1,000 US$ for 2000$ is given by,

$$PFC_{RC} = 4.45519 hp_{RC}^{0.7784} \qquad R^2 = 0.98 \qquad (6\text{-}26)$$

Table 6-10. Recycle compressor cost data adjusted to the dollar value in 2000 [Doctor, 1996]

PFC (2000 1,000 US$)	Compressor Capacity (hp)
576.64	537
361.19	259
212.55	151
212.55	151.3

Selexol Pump

The process facility cost of the Selexol pump (Table 6-11) can be determined from the Selexol pump capacity hp_{SP}. The cost in 1,000 US$ for 2000$ is given by,

$$PFC_{SP} = 1.2286 hp_{SP}^{0.7164} \qquad R^2 = 0.92 \qquad (6\text{-}27)$$

Table 6-11. Selexol pump cost data adjusted to the dollar value in 2000 [Doctor, 1996]

PFC (2000 1,000 US$)	Pump capacity (hp)
301.52	2205
207.29	1282
326.63	2388
326633.3	2388

CO_2 Compressor

The process facility cost of the CO_2 compressor (Table 6-12) is determined as a function of the compressor capacity hp_{comp}. The cost in 1,000 US$ for 2000$ is given by,

$$PFC_{comp1} = 7.0321 hp_{comp}^{0.6769} \qquad R^2 = 0.83 \qquad (6\text{-}28)$$

Table 6-12. CO_2 compressor cost data adjusted to the dollar value in 2000 [Doctor, 1996]

PFC (2000, 1,000 US$)	Compressor capacity (hp)
323.1754	600.41
311.5061	255
216.2418	155.52
190.1031	120.54
1026.139	1086
576.6455	539.71

CO_2 Final Product Compressor

The process facility cost of the multi-stage CO_2 compressor is calculated similar to the CO_2 compressor cost in Equation (6-28). Using the data in Table 6-13, the cost of the final product compressor in US$ for 2000$ is given by,

$$PFC_{comp2} = 13.0969 hp_{comp}^{0.64} \qquad R^2 = 0.85 \qquad (6\text{-}29)$$

Table 6-13. CO_2 final compressor cost data adjusted to the dollar value in 2000 [Doctor, 1996]

PFC (2000 k$)	Compressor Capacity (hp)
2162.421	2582
2851.544	2913
2565.347	3369
2382.109	3217

Refrigeration

The process facility cost of the refrigeration unit is regressed as,

$$PFC_{refr} = 1.0019 N_{T,refr}\left[16.4796\left(\frac{f_{Sel}}{N_{O,refr}}\right)^{0.3618}(\Delta T_{Sel})^{0.4064}\right] \qquad R^2 = 0.97 \qquad (6\text{-}30)$$

where

$7{,}000 < f_{Sel} < 23{,}000$ kg/s per train

$1 < \Delta T_{Sel} < 5$ °C

Flash tank

The process facility cost of flash tanks (Table 6-14) is given by,

$$PFC_{\tan k} = 0.9832 \cdot N_{T,\tan k}\left(\frac{f_{Sel}}{N_{O,\tan k}}\right)^{0.8005} \qquad R^2 = 0.89 \qquad (6\text{-}31)$$

where

$400 < f_{Sel} < 800$ kg/s per train

Table 6-14. Flash tank cost data adjusted to the dollar value in 2000 [Doctor, 1996]

PFC (2000 $)	Solvent flow rate (kg/s)
129745.5	416.85
197707.4	733.92
205227.8	811.44

6.3.2 Other Costs

Here the default values for the indirect capital cost calculations are provided. They are given by the relationships shown in Table 6-15.

Table 6-15. Parameters for TCR of Selexol process

Indirect Capital Cost Parameter	Definition or Unit Cost
Engineering and home office	10% PFC
General facilities	15% PFC
Project contingency	15% PFC
Process contingency	10% PFC
Total plant cost (TPC) = sum of the above values	
Interest during construction	Calculated
Royalty fees	0.5% PFC
Preproduction fees	1 month fee of fixed & variable O&M
Inventory cost	0.5% TPC
Total capital requirement (TCR) = sum of above values	
Fixed O&M cost (FOM)	
Total maintenance cost	2% TPC
Maintenance cost allocated to labor	40% of total maintenance cost
Administration & support labor cost	30% of total labor cost
Operation labor	2 jobs/shift
Variable O&M cost (VOM)	
Selexol solvent	$ 1.96/lb

References

Black W.B., Pritchard V., Holiday A., Ong J.O. and Sharp C., 2000: Use of SELEXOL Process in Coke Gasification to Ammonia Project By Presented at the Laurance Reid Gas Conditioning Conference, The University of Oklahoma, Norman, Oklahoma

Doctor R.D., 1994: Gasification combined cycle: carbon dioxide recovery, transport, and disposal, ANL/ESD-24, Argonne National Laboratory, Energy Systems Division, Argonne, Illinois

Doctor R.D., 1996: KRW oxygen-blown gasification combined cycle carbon dioxide recovery, transport, and disposal, ANL/ESD-34, Argonne National Laboratory, Energy Systems Division, Argonne, Illinois

Epps R., 1994: Use of Selexol Solvent for Hydrocarbon Dewpoint Control and Dehydration of Natural Gas, presented at the Laurance Reid Gas Conditioning Conference, Norman, OK

Korens N., Simbeck D.R., Wilhelm D.J., 2002: Process Screening Analysis of Alternative Gas Treating and Sulfur Removal for Gasification, Revised Final Report, December 2002, Prepared by SFA Pacific, Inc. Mountain View, California

Kubeck D. J., E. Polla and F.P. Wilcher, 2000: Purification and Recovery Options for Gasification, UOP LLC, Des Plaines, IL

Newman S. A., 1985: Acid and sour gas treating processes: latest data and methods for designing and operating today's gas treating facilities, Gulf Publishing Co.

Sciamanna S. and Lynn S., 1988: Solubility of hydrogen sulfide, sulfur dioxide, carbon dioxide, propane, and n-butane in poly(glycol ethers), Ind. Eng., Chem. Res., 27

Shah V.A., 1988: Low-cost ammonia and carbon recovery, Hydrocarbon Process., 67(3)

UOP, 2002: Use of SELEXOL Process in Coke Gasification to Ammonia Project, UOP report

Personal communication with UOP, 2003

7. Power Block

Nomenclature

English Letter Symbols

P_a = Ambient pressure of inlet air

r_p = Pressure ratio, ratio of compressor outlet pressure to compressor inlet pressure

T_a = Ambient temperature of inlet air

$T_{T,in}$, = Turbine inlet temperature

y_i = Mole fraction of compound i

Greek Letter Symbols

$\Delta h_{r,i}$ = Enthalpy of reaction for compound I (j/gmole)

Δp_{back} = turbine back pressure (psi)

η_C = Adiabatic compressor efficiency

η_T = Adiabatic turbine efficiency

7.1 Power Block Process Description

7.1.1 Boiler Feedwater System

The boiler feedwater system consists of equipment for handling raw water and polished water in the steam cycle. This equipment includes a water demineralization unit for raw water, a demineralized water storage tank, a condensate surge tank for storage of both demineralized raw water and steam turbine condensate water, a condensate polishing unit, and a blowdown flash drum. The major streams in this process section are the raw water inlet and the polished water outlet. Data on the cost of the boiler feedwater section and the flow rates of the raw water and polished water streams is available from five studies for 14 plant sizes. These studies include Texaco-based, Shell-based, and KRW-based IGCC systems (Fluor, 1983a; 1983b; 1984; 1985; 1986). Because all of these studies were developed by the same contractor using a consistent approach, they provide an excellent basis for developing a cost model. The boiler feedwater section is generic to the steam cycle.

7.1.2 Gas Turbine

The most commonly assumed gas turbine in early IGCC performance and cost studies is the General Electric (GE) model MS7001F, also referred to as the "Frame 7F" (see Chapter 10 for more recent updates). This gas turbine is designed for a turbine inlet temperature of 2,300 °F and has a power output of about 125 to 150 MW. By contrast, typical gas turbines have firing temperatures in the range of 2,020 to 2,150 °F. The thermal efficiency of gas turbines increases as the firing temperature increases. The higher firing temperature is the result of advances in turbine blade manufacturing. The Frame 7F turbine blades are manufactured using a process known as "directional solidification," which has been used on smaller aircraft engine turbine blades. Because of improvements in molding technology, the process can now be applied to the larger turbine blades of the Frame 7F.

Further advances in manufacturing techniques may lead to the capability to cast turbine blades as single crystals with no grain boundaries, permitting an additional 50 to 150 °F increase in firing temperature (Smock, 1989).

The first Frame 7F has completed factory tests at General Electric and has been delivered to a Virginia Power site in Chesterfield, VA as part of a combined-cycle power plant. General Electric has rated this machine at 150 MW with a heat rate of 9,880 Btu/kWh. Figure 7-1 shows the schematic of the turbine with the associated compressor and combustor.

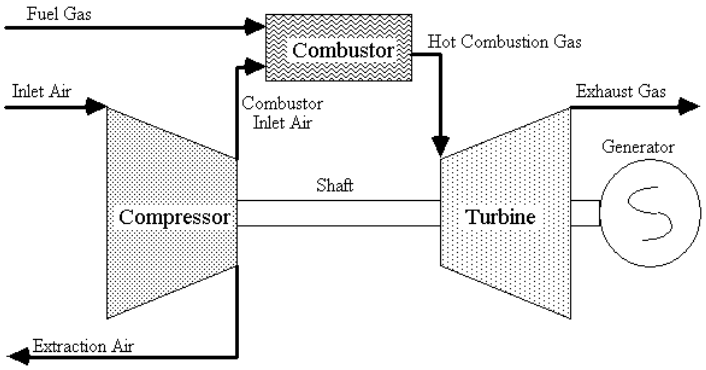

Figure 7-1. Simple Schematic of Gas Turbine Mass Balance with Compressor Air Extraction

There are a number of design factors that affect the cost of a gas turbine in an IGCC process environment. For example, the firing of medium-BTU coal gas, as opposed to high-BTU natural gas, requires modification of the fuel nozzles and gas manifold in the gas turbine (BGE, 1989). Some additional concerns associated with firing coal gas are discussed by Cincotta (1984). The presence of contaminants in the syngas may affect gas turbine maintenance and long-term performance. Liquid droplets may cause uneven combustion or may burn in the turbine first-stage nozzles, causing damage. Solids can deposit on fuel nozzles or cause erosion in the hot gas path of the gas turbine (e.g., combustor, turbine). Alkali materials that deposit on hot gas path parts cause corrosion. It is expected that, at fuel gas temperatures less than 1,000 °F, that alkali material is essentially condensed on any particulate matter in the raw syngas, and that the alkali removal efficiency is approximately the same as the particle removal efficiency. For sufficiently high particle removal efficiencies, erosion is not expected to be a problem. Corrosion is not expected to be any worse than for distillate oil firing. Deposition of particles is expected to be within the allowance of reasonable maintenance schedules. The design for an advanced high firing temperature gas turbine employs advanced air film cooling which could be affected by the ash content of combustion products.

Another design issue is the gas turbine fuel inlet temperature. A study by Fluor (Earley and Smelser, 1988) assumes that hot desulfurized syngas from an advanced hot gas cleanup process is fed directly to the gas turbine at 1,200 °F. The Fluor study indicates that General Electric expects that a fuel system capable of a 1,200 °F fuel inlet temperature could be developed by 1994. The maximum fuel temperature test to date has been at 1,000 °F. An earlier study with hot gas cleanup included a hot gas cooler to reduce the gas temperature to 1,000 °F (Corman, 1986). For the KRW (now KBR) system with cold gas cleanup, the coal gas temperature is within the limits of current technology. However, the gas turbine costs developed here should not be used in conjunction with IGCC systems featuring hot gas cleanup without some adjustments to account for the uncertainty in using a higher fuel inlet temperature.

Unfortunately, there is currently a lack of reported data from which to develop a detailed gas turbine cost model that is explicitly sensitive to the type of factors discussed above. In preliminary cost estimates, the typical approach to accounting for these uncertainties in performance, or for the possibility of increased capital cost due to design modifications, is through process contingency factors. The approach taken here is to use the available cost data for the GE Frame 7F to develop a cost estimate for a single gas turbine. In the use of this cost estimate for actual case studies in a later task, judgments about the uncertainty in cost, and about the likelihood of cost increases for applications with coal gases, have been encoded using process contingency factors.

7.1.3 Heat Recovery Steam Generator

The heat recovery steam generator (HRSG) is a set of heat exchangers in which heat is removed from the gas turbine exhaust gas to generate steam. Typically, steam is generated at two or three different pressures, and associated with the HRSG is one steam drum for each steam pressure level. High pressure superheated steam is generated for use in the steam turbine, and typically the exhaust from the steam turbine first stage is reheated. The input streams to the HRSG section include the gas turbine exhaust and boiler feedwater to the deaerator. The major output stream is the high-pressure steam to the steam turbine. Several parts of the HRSG must be sized to accommodate the high-pressure steam flow, including the superheater, reheater, high pressure steam drum, high pressure evaporator, and the economizers.

Most studies of IGCC systems aggregate the cost of the HRSG units with the cost of the gas turbine and the steam turbine. Only four studies were identified in which the cost of the HRSG units were reported as a separate line item. A study of Texaco and British Gas/Lurgi IGCC systems includes performance and cost estimates for several sizes of HRSGs used in combination with reheat steam turbines (Parsons, 1982). These HRSG units include two steam pressure levels, and are used in conjunction with a conventional gas turbine. The high-pressure steam varies from 650 psia to 1520 psia for these HRSGs. The exhaust gas flow rate and temperature indicate that the gas turbine is a GE Frame 7E or equivalent. A study by Bechtel and WE (1983c) for a KRW-based system included an HRSG design with three pressure levels using a large 130 MW gas turbine with a high exhaust gas temperature. A study of Texaco-based IGCC systems included performance and cost estimates for reheat steam turbines and HRSGs with two pressure levels (Fluor Technology, 1986). A recent study of Dow-based IGCC systems includes performance and cost estimates for two-pressure level reheat HRSGs applied in conjunction with large advanced gas turbines (Fluor Daniel, 1989).

A detailed approach to estimating the cost of HRSGs is reported by Foster-Pegg (1986). This approach requires detailed performance and design information for each heat exchanger in the HRSG. The necessary design values were not reported in the performance and cost studies, nor was sufficient detail about performance available to develop such a model. Furthermore, the level of detail in the Foster-Pegg model is not justifiable for the applications envisioned for this model for several reasons. The technical and cost growth risks of IGCC systems reside primarily in process areas such as gasification, gas cleanup, and advanced gas turbine designs. The HRSG is a conventional, commercially available component. Therefore, the priorities for cost model development should be with the more innovative systems. Secondly, in comparative studies of IGCC systems, the cost of HRSGs will be similar, and will not be a factor in distinguishing one system from another. Instead, differences in the gasification process area, gas cleanup, and byproduct recovery, as examples, are expected to be important in distinguishing alternative systems. Third, the purpose of this model is not to develop detailed, final estimates of site-specific costs for a particular project, but to develop preliminary cost estimates for the purpose of research planning. Therefore, there is not a need for a highly detailed cost model for this particular process area.

7.1.4 Steam Turbine

A typical steam turbine for an IGCC plant consists of high-pressure, intermediate-pressure, and low-pressure turbine stages, a generator, and an exhaust steam condenser. The high-pressure stage receives high pressure superheated steam from the HRSG. The outlet steam from the high-pressure stage returns to the HRSG for reheat, after which it enters the intermediate pressure stage. The outlet from the intermediate pressure stage goes to the low-pressure stage.

7.2 Detailed Analysis of Gas Turbines

7.2.1 Commercial Offerings for 2,300 °F Gas Turbines

In this research, the modeling of IGCC systems is intended to include performance representative of typical high-firing temperature gas turbine technology. However, the intent is not to attempt to model exactly the performance of any one proprietary gas turbine model.

Instead, the goal is to achieve reasonable accuracy in reproducing the key performance characteristics of this class of gas turbines.

As of 1989, there were two 2,300 °F turbine inlet temperature heavy-duty gas turbine models which are expected to be offered commercially in the next year or two. These are the General Electric MS7001F and the Westinghouse/Mitsubishi 501F. Some characteristics and design assumptions for these gas turbines are given in Table 7-1. The MS7001F is designed to fire either natural gas or distillate oil at design point conditions of 59 °F ambient temperature, 14.7 psia ambient pressure, and 60 percent relative humidity. The use of coal gas represents a departure from the design fuel. Because coal gas has a substantially lower heating value than natural gas, the fuel mass flow rate is significantly larger than the design basis for the gas turbine. Typically, the mass flow at the turbine inlet nozzle is limited by choking. Therefore, an increase in the fuel mass flow rate must be compensated by a reduction in the compressor air flow rate, for a given pressure ratio and firing temperature. This results in off-design operating conditions for the gas turbine, which has implications for gas turbine performance, such as efficiency, exhaust temperature, and other parameters.

Table 7-1. Representative 2,300 °F Firing Temperature Heavy-Duty Gas Turbine Commercial Offerings

Design Specification (Fuel: Natural Gas)	General Electric MS7001F	Westinghouse/Mitsubishi 501F
Net Power, kW	150,000	145,000
Heat Rate, BTU/kWh	9880	10,000
Compressor Inlet Air, pps	918.7	912
Pressure Ratio	13.5	14.2
Exhaust Temp., ºF	1,081	1,061
Compressor Stages	18	16
Inlet Guide Vanes	Yes	Yes
Variable Stator Vanes	No	No
Compressor Cooling Air		
Extraction (stage no.)	13, 17, discharge	13, 10, 6, discharge
Compressor Bleed (stage no.)	13	6,10,13
No. of Combustor Cans	14	16
Standard Combustor Design	multiple fuel nozzles	pre-mix, two-stage
(Natural Gas firing)	wet injection--NO_x	lean-burn low-NO_x
	("quiet" combustor)	
Turbine Stages	3	4
Turbine Cooling:		
Row 1 rotor vanes	internal convection	film, impingement, pin fin
Row 2 rotor vanes	internal convection	similar to Row 1
Row 3 rotor vanes	uncooled	inlet cavity convection
Row 4 rotor vanes	N/A	uncooled

NOTES: Brandt, 1988; Brandt, 1989; Scalzo et al., 1989
- The GE MS7001F apparently uses film cooling on the turbine stator vanes ("nozzles"), but not on the rotor vanes ("buckets"). Both offerings use corrosion coatings on the hot gas path components.
- Later updates to this chapter appear in Chapter 10.

Many IGCC studies were developed prior to the testing and delivery of the prototype MS7001F. In these studies, a variety of assumptions regarding the projected performance of this unit were made regarding firing temperature, pressure ratio, efficiency, and other measures of performance. In most cases, these assumptions have proven to be different from the actual unit. This is an example of the difficulty involved in trying to predict the commercial

scale performance of an advanced system for which no commercial experience is yet available. In many cases, the assumptions may have been unnecessarily conservative, while in other cases they may have been optimistic.

The studies appear to give only superficial consideration to the off-design nature of gas turbine operation on coal gas. Furthermore, the studies appear to give only superficial consideration to other factors associated with firing coal gas in a gas turbine.

Although a MS7001F is now in commercial service, the performance of this model with coal gas has yet to be demonstrated.

7.2.2 Operating Strategies for Coal Gas Firing

The primary issues discussed in this section are the interactions between fuel flow, compressor performance, and compressor air extraction.

A gas turbine is designed to meet a set of goals for a specific set of operating conditions. When any of these conditions are changed, the turbine is said to be in an "off-design" mode. The response of the gas turbine to changes in operating conditions requires detailed knowledge which is specific to each machine. This type of information is closely held proprietary information. The design of a gas turbine, and prediction of its performance, involves a significant amount of empirical information. In many cases, off-design information must be obtained from testing under various conditions, which is expensive. At a minimum, some testing is required to verify the accuracy of theoretical models. Because of the expense of testing needed to support gas turbine design and to verify the operation the gas turbine once built, detailed information about gas turbine design, such as compressor operating maps, are not published (Eustis and Johnson, 1990). Furthermore, gas turbine manufacturers usually try to adopt existing successful designs where feasible into new models, or to modularize the system (in the case of combustor cans, for example) so that a change in one component requires only a simple substitution and no changes in other components (Cohen et al**.,** 1987; Brandt, 1988; Scalzo et al**.,** 1989).

Because of the expense of developing and testing gas turbines, it is unlikely that, in the near term, the gas turbine industry will develop a machine designed specifically for operation with coal gas. Instead, they will try to develop an understanding of how a machine designed for larger markets (e.g., natural gas firing) will behave when firing coal gas. The manufacturers may be required to offer some modifications, such as for fuel valves or combustors. However, the manufacturers are also likely to impose limitations on fuel composition or gas turbine operation to which a customer must adhere. The development of such limitations is presumably based on some type of technical risk analysis of the gas turbine, supported either by theoretical models, empirical testing, both or neither.

Uncertainties are likely to remain, however, regarding the long-term maintainability and performance of the gas turbines when firing coal gas. In particular, problems such as loss of output or shorter maintenance cycles (e.g., more frequent reblading) may be encountered in machines fired with coal gas for long periods of time (a complete life cycle). In some cases, these uncertainties can be represented solely as uncertainties in cost. However, there may be trade-offs between changing operating conditions and maintenance costs. A major concern for reliable operation of an integrated plant is the stability of the compressor and the control system, particularly when air is extracted for use in the gasifier.

A key difference between natural gas firing and coal gas firing is the heating value of the fuel. Natural gas has a heating value of about 1,000 BTU/scf. Medium-BTU coal gas (MBG) has a heating value of 300 to 500 BTU/scf, and low-BTU coal gas (LBG) has heating values around 100 BTU/scf. As a result, the mass flow rate of fuel required to supply a given amount of chemical energy is significantly larger for LBG than for natural gas.

The factor that usually limits the mass flow in a gas turbine is the area of the turbine inlet nozzles (Eustis and Johnson, 1990). When the flow is choked (sonic) the mass flow is at its maximum, and the maximum mass flow for an ideal gas is given by:

$$m_{\max} = P\, A^{*} \sqrt{\frac{MW}{T}} \sqrt{\frac{\gamma}{R}\left(\frac{2}{\gamma+1}\right)^{\frac{\gamma+1}{\gamma-1}}} \qquad (7\text{-}1)$$

where,

m_{max} = maximum mass flow rate

P = total pressure

A^* = critical area where flow is choked

MW = molecular weight of gas

T = total temperature

R = universal gas constant

γ = ratio of specific heats for the gas

The molecular weight of the exhaust gas varies within about two percent for all three cases compared to the natural gas design point. The term under the radical varies about 5 percent as the ratio of specific heats varies from 1.2 to 1.4. At 2,000 °F, the ratio of specific heats of nitrogen, the largest component in the exhaust gas, is about 1.3. The mass flow into the gas turbine is proportional to the critical area (which is fixed for a given gas turbine model) for a given pressure ratio and firing temperature.

For natural gas-fired operation, the air flow into the GE MS7001F compressor is about 919 lb/sec. The natural gas flow rate is about 20 lb/sec, yielding an exhaust flow rate of about 939 lb/sec. However, in the case of low-BTU coal gas, the fuel flow rate is likely to be on the order of 200 lb/sec. This would imply a turbine flow rate of over 1,100 lb/sec, or a compressor flow rate of about 720 lb/sec, depending on the operating strategy employed and whether a substantially redesigned gas turbine is assumed.

Eustis and Johnson (1990) discuss several strategies for firing coal gas in a gas turbine. These options include:

- Increase the pressure ratio. This increases the maximum mass flow rate in the turbine nozzle. However, the compressor may not have enough surge margin to do this. Also, the increased mass flow would increase the thermal loads on the turbine blades and vanes, which may require a reduction in firing temperature.
- Reduce compressor mass flow using inlet guide vanes (IGV). This reduces the compressor mass flow to compensate for the increased fuel flow. The flow reduction is limited by the compressor design. Compressors with variable stators and intermediate air bleed points in addition to IGVs are better able to achieve flow reductions without inducing stalling in any of the compressor stages.
- Increase the inlet turbine nozzle critical area. This is a major redesign and would require a new gas turbine model. As a practical matter, it is unlikely that gas turbine manufacturers would develop such a machine.
- Reduce the turbine inlet temperature. This would reduce the gas turbine efficiency and power output, but allow increased turbine mass flow.
- Bleed air from the compressor. This is possible only where there is a use for high pressure air elsewhere in the plant. Otherwise, it is wasteful, and reduces plant efficiency.

In this study, a combination of Strategies 2 and 5 is assumed. Both the GE MS7001F and the Westinghouse/Mitsubishi 501F have IGVs. They do not have variable stator vanes. For the low-BTU coal gas systems, a portion of the compressor discharge air is assumed to be extracted for use as gasifier blast air. However, as noted in Table 7-1, the ratio of extraction air to the fuel flow is about 0.5 to 0.6. The extraction air does not fully compensate for the increased fuel mass flow. Thus, at full load, the IGVs would have to be partially closed.

IGVs are often used to respond to part load conditions without having to reduce firing temperature. At the point where the IGVs are "fully" closed, firing temperature must then be reduced to further reduce the load. In a coal gasification application, because the IGVs are already partially closed at full load, the gas turbine will be less efficient at part load operation, as the point at which firing temperature must be reduced will be at a higher load condition than for natural gas.

The partial closure of IGVs will slightly affect the gas turbine pressure ratio. However, because the gas turbine model used in these case studies is based on mass and energy balances only, and not the aerodynamic characteristics of a gas turbine, pressure ratio is not predicted. Any change in pressure ratio must be specified by the model user.

Closure of IGVs also affects the compressor surge margin. At surge conditions, the compressor is no longer able to generate a steady high pressure exit stream. Thus, any downstream pressurized gas, such as that in the combustor, will backflow into the compressor, possibly causing severe vibration and damage. Compressors are usually designed to operate at a point sufficiently removed from the "surge line" to reduce the possibility of encountering surge. However, the operation of the machine with IGVs closed may reduce the margin between the operating conditions and surge conditions (Eustis and Johnson, 1990).

The determination of the surge line and the compressor characteristics requires extensive testing under a variety of loads, corrected speeds, IGV settings, and mass flow rates. These data are summarized in compressor "maps." These maps are proprietary information, due to the expense of developing them and the importance of the information to the competitive position of the manufacturer. General Electric reports that the MS7001F has a better surge margin than the MS7001E, which has been commercially available for years. GE reports that no in-service surges of the MS7001E have been reported. Thus, GE expects a superior surge margin for the MS7001F (Brandt, 1989). This may alleviate any concerns about using the IGVs to reduce the compressor mass flow. However, without a compressor map, it is difficult to make any quantitative assertions.

The use of air extraction for the low-BTU coal gas cases helps to improve the surge margin of the compressor, by reducing the amount of IGV closure needed at full load conditions. However, air extraction poses significant control problems for the IGCC plant, because it imposes a coupling between the gas turbine and the gasifier. Changes in coal composition can affect the fuel/air ratio, but can also affect the gasifier blast air requirement. This requires a sophisticated control system to regulate the IGVs, extraction air flow rate, and fuel flow rate. Advanced control systems may be required (Corman, 1986).

7.2.3 Fuel Valve

The pressure drop across the fuel valve system has an important effect on system efficiency. The gasifier pressure must be high enough to compensate for all pressure losses between the gasifier outlet and the gas turbine combustor. The pressure in the combustor is determined based on the gas turbine pressure ratio. Pressure losses in the system include the fuel gas piping, fuel valve, particulate removal devices (e.g., cyclones), and sulfur removal devices (e.g., zinc ferrite absorbers). Increasing the gasification pressure above that required for fuel gas delivery can reduce the system efficiency (Simbeck et al., 1983).

Reduction in the fuel valve pressure drop was reported to be one goal of a proposed demonstration plant. The typical pressure drop in the fuel valve was reported at about 70 psi. The goal was to achieve about 10 psi. The demonstration project proposes to use a GE MS7001E with a fuel gas temperature of about 1,000 °F. The material requirements for this system were claimed not to be a major problem (Hester and Pless, 1990).

A design study of an IGCC system with hot gas cleanup assumed a gas turbine fuel inlet temperature of 1,200 °F. The basis for this assumption was reported to be GE's expectation that by 1994 a fuel system for 1,200 °F gas could be developed, although the highest fuel gas temperature tested to date has been 1,000 °F (Earley and Smelser, 1988).

The presence of particles in the fuel gas could lead to erosion or deposition in the fuel nozzles. Based on two-stage high-efficiency cyclones, a GE study concludes that the particle concentration and size distribution in the fuel gas would allow for "adequate" nozzle and control valve lives. However, any solids that deposit in the fuel nozzle can alter flow characteristics. This can result in reduced combustion efficiency. Solids deposits can also interfere with fuel valve operation. Naphthas, tars, and phenols can build up on valve internals (Cincotta, 1984).

Any liquids entering the combustor as large droplets may not burn completely within the combustor. They may carry over to, and burnout in, the first stage turbine nozzle. This can cause damage to the turbine (Cincotta, 1984).

The fuel control system poses a design challenge for an IGCC plant. The control system must account for changes in the heating value of the fuel gas during plant operation, as well as differences in the load-following capability of the gasifier and gas turbine. The fuel control system could potentially depressurize the gasifier by demanding more fuel than the gasifier can supply during ramp-up (Cincotta, 1984). The addition of gas turbine air extraction for gasifier blast air further complicates the control system (Corman, 1986).

In the modeling studies, the effect of pressure drop in the fuel gas valve can be explicitly included in the ASPEN performance simulation. The effect of exotic fuel valve materials or designs on gas turbine cost can be incorporated in the cost model through, for example, a direct capital cost multiplier factor.

7.2.4 Combustion and Emissions

Gas turbine combustors have been developed in an empirical-based manner. Mathematical analysis and scale model testing apparently have been inadequate predictors of full-scale combustor performance (Dawkins et al**.,** 1986). As a result, heavy-duty gas turbines have been developed using multiple modular "can" combustors. Typically, many of these combustors are arranged around the circumference of the machine between the compressor and the turbine. As part of a development program only one can combustor needs to be used in testing (Cincotta, 1984). In a commercial-scale gas turbine, such as the ones summarized in Table 7-1, perhaps 16 to 18 combustor cans are utilized. Each one can be changed out for maintenance and repair. The standard combustor can also be replaced by improved versions as they become available. The same combustor design can be used in different size machines by using an appropriate number of the combustor cans.

There are a number of pollutant species that may be contained in the hot gas exiting the combustor which have received attention in the literature. These are:

- Thermal NO_x resulting from thermal fixation of oxygen and nitrogen in air.
- Fuel NO_x resulting from conversion of chemically bound nitrogen in the fuel (e.g., ammonia).
- SO_2 resulting from hydrogen sulfide, carbonyl sulfate, and sulfur contained in naphtha, tars, oils, and phenol.
- CO resulting from incomplete carbon conversion in the combustor.
- Uncombusted particles passing through the combustor.
- Alkali (sodium and potassium compounds) which may cause turbine blade corrosion.

The design of gas turbine combustors is undergoing changes in response to environmental constraints on NO_x and CO emissions and an increasing array of potential gas turbine fuels. Currently, most efforts are focused on developing low- NO_x combustors for natural gas applications (Angello and Lowe, 1989). However, some theoretical studies, bench scale research, and a few commercial-scale demonstrations have involved medium- and low-BTU gases, such as those derived from coal gasification. The design of combustors for coal gas applications may be fundamentally different from those for natural gas applications, particularly with respect to NO_x emissions.

7.2.5 NO_x Emissions

NO_x emissions result primarily from the thermal fixation of nitrogen and oxygen in the inlet combustion air and from conversion of chemically-bound nitrogen in the fuel. The former is referred to as "thermal" NO_x, while the latter is referred to as "fuel" NO_x. Thermal NO_x formation is sensitive mainly to the flame temperature of the burning fuel. Poor mixing of fuel and air can lead to localized "hot spots" which generate high flame temperatures and, hence, high thermal NO_x emissions. Uniform mixing of fuel and air leads to more uniform flame temperatures, which reduces thermal NO_x formation. In addition, other measures which reduce flame temperatures, such as staged lean combustion or the addition of diluents such as water or steam, will reduce thermal NO_x emissions (Davis et al**.,** 1987; Touchton, 1984)

Fuel NO_x arises from the conversion of ammonia, HCN, or other nitrogen-containing chemical species in the fuel. The formation of fuel NO_x is relatively insensitive to temperature compared to thermal NO_x formation. Fuel NO_x formation depends primarily on the concentration of fuel-bound nitrogen in the fuel gas and the method of fuel/air contacting (Folsom et al**.,** 1980). To reduce fuel NO_x formation, two-stage rich/lean combustion has been proposed and tested by several (e.g., Folsom et al**.,** 1980; Sato et al**.,** 1989; Unnasch et al**.,** 1988). In the rich combustion stage, fuel bound nitrogen is converted mostly to diatomic nitrogen. In the lean stage, fuel burnout is completed under conditions which minimize the formation of thermal NO_x.

The most widely used gas turbine fuel is natural gas, which contains negligible fuel-bound nitrogen. Most major gas turbine manufacturers are attempting to develop dry low- NO_x combustors, to reduce the formation of "thermal" NO_x by premixing the fuel and air and use of lean-burn or lean-lean two-staged combustion. The Westinghouse/Mitsubishi 501F will be offered with a low NO_x combustor featuring fuel and air premixing and a lean-burn combustor (Scalzo et al., 1989). The GE MS7001F is offered with a multiple fuel nozzle combustor can (Brandt, 1988). This is not a low- NO_x design per se, but it does allow increased levels of water or steam injection to achieve low NO_x emissions with fuels that do not contain fuel-bound nitrogen. The multiple nozzle design has been referred to as the "quiet" combustor because it has a lower vibration and noise level than GE's single fuel-nozzle combustor. The reduced vibrations permit higher levels of water injection.

Medium-BTU Coal Gas

IGCC systems that feature "cold" gas cleanup effectively remove any ammonia, the primary fuel-bound nitrogen species, from the raw coal gas. Thus, fuel NO_x emissions are not expected to be a problem for this application. Thermal NO_x emissions are of concern, however. MBG may have flame temperatures similar to that of distillate oil, and thus uncontrolled NO_x emissions from firing MBG may be comparable or greater than uncontrolled emissions from firing distillate oil (Davis et al**.,** 1987).

Most conceptual design studies assume that steam injection and/or fuel gas saturation can be used to reduce the combustor flame temperature and, hence, NO_x emissions to meet current New Source Performance Standards (NSPS) for gas turbines (e.g., Gallaspy et al., 1990 and many of the other EPRI design studies). Wet injection is a standard technique for natural gas and oil-fired gas turbines. The thermal diluent, steam or water, results in a reduction in peak combustion temperatures, thus reducing thermal NO_x formation (e.g., Davis et al., 1987; Touchton, 1984; Touchton, 1985). Both steam injection and fuel gas saturation have been tested at the Cool Water demonstration plant, which uses MBG from a Texaco gasifier (Cool Water, 1988; Holt et al., 1989).

The NSPS is often quoted as 75 ppm at 15 percent oxygen on a dry basis, but the standard actually includes a correction for plant efficiency. Thus, the actual allowable emissions under NSPS for a particular gas turbine model may be higher.

However, it is controversial whether the gas turbine NSPS is the applicable standard for IGCC power plants, or whether it is even a relevant standard. More likely, IGCC plants will be subject to local or EPA-mandated procedures such as Best Available Control Technology (BACT), which is determined on a plant-by-plant basis. The procedure for BACT analysis that is becoming increasingly common is known as the "top-down" approach. In this approach, a facility is asked to use the most stringent control system that has been demonstrated unless there are energy, environmental, or economic reasons to do otherwise. For natural gas-fired gas turbines, BACT may include combinations of low- NO_x combustors, wet injection, and post-combustion NO_x control using selective catalytic reduction (Smock, 1989; Moore-Staub et al., 1990). It is likely that an actual IGCC plant will be required to achieve very low NO_x emissions on the order of 10 ppm, rather than the 75 ppm (corrected) often assumed. Thus, SCR may be required. SCR has been applied to or required for a number of natural gas- and oil-fired gas turbines in California and a few other states (Radin and Boyles, 1987; Moore-Staub et al., 1990). SCR is expected to be capable of reducing IGCC system NO_x emissions to 5 ppm (Holt et al., 1989). At least one IGCC plant, a proposed demonstration plant in Florida, is to be permitted with SCR (Hester, 1990). This may set a BACT precedent for other IGCC plants.

For the purposes of the current study, fuel gas saturation and/or steam injection for combustion NO_x control is assumed for medium-BTU coal gases with no fuel-bound nitrogen. The effect of SCR would primarily be to increase the capital and operating costs of the system, with a slight penalty on plant efficiency due to increased HRSG backpressure and the auxiliary power requirements of the SCR ammonia injection and control systems. SCR may be more advantageous for application with fuel gases containing significant concentrations fuel-bound nitrogen.

The applicability or efficacy of dry low- NO_x combustors designed for natural gas when converted to coal gas firing may merit some testing and evaluation. Whether the combustors can be used "as is", other than modifications for the fuel nozzles, might be the subject of further research.

Low-BTU Coal Gas

Thermal NO_x is not expected to be a major concern with LBG gases because of their low adiabatic flame temperatures resulting from the presence of thermal diluents in the fuel such as N_2. The thermal NO_x emissions from LBG are often dismissed in the literature as being insignificant, particularly if peak flame temperatures are limited to less than 2,800 °F (Davis et al., 1987; Folsom et al., 1980; Notestein, 1989; Sato et al., 1989; Unnasch et al., 1988). Uncontrolled thermal NO_x emissions from LBG combustion may in fact be on the order of 10 to 50 ppm, as suggested by some small-scale combustor tests (e.g., Unnasch et al., 1988).

A confounding factor for thermal NO_x emissions from LBG is the expected high gas turbine fuel valve inlet temperatures associated with hot gas cleanup (HGCU) systems. Also, increasing pressure ratios for gas turbines may promote thermal NO_x emissions (Folsom et al., 1980). Increasing the fuel gas temperature will tend to increase thermal NO_x production because the flame temperatures will be marginally higher. However, this is not expected to significantly increase thermal NO_x emissions for the fuel temperatures of current interest (1,000 to 1,200 °F).

The primary concern regarding NO_x emissions from LBG is fuel NO_x resulting from ammonia, HCN, or other fuel bound nitrogen species. LBG is derived from air-blown gasification systems. Air-blown gasification is commonly envisioned in conjunction with HGCU. HGCU systems typically are based on dry pollutant removal processes, such as cyclones or barrier filters for particulate control and chemical sorption for sulfur control. Unlike "cold" gas cleanup wet scrubbing processes, these dry processes do not remove ammonia, the primary fuel-bound nitrogen specie, in the fuel gas. In conventional gas turbine combustors, most of the ammonia would be converted to NO_x. For example, Cincotta (1984) states that the conventional GE MS7001E combustor would convert about 70 percent of ammonia in a Lurgi fuel gas to NO_x. Another study reports a similar finding (Sato et al., 1989). In a conventional combustor, the conversion rate of ammonia to NO_x may vary from 50 to 90 percent depending on the concentration of ammonia in the fuel gas (Pillsbury, 1989).

The ammonia concentration in the fuel gas depends on the gasifier type and operating conditions. Notestein (1989) indicates typical ranges of ammonia concentration in coal gas as 200 to 600 ppmv for fluidized bed gasifiers operating at 1,300 to 1,800 °F, 2,000 ppm for entrained flow gasifiers, and up to 5,000 ppm for fixed bed gasifiers operating below 1,200 °F. Holt et al. (1989) suggest that about 50 to 60 percent of coal-bound nitrogen is converted to ammonia in fixed bed gasifiers, while only 10 to 15 percent is converted in entrained-flow gasifiers. Some typical concentrations from ASPEN simulation models are given in Table 7-1.

The most likely near-term solution for reducing fuel NO_x emissions from LBG combustion appears to be staged rich/lean combustion (Cincotta, 1984; Folsom et al., 1980; Sato et al., 1989; Unnasch, 1988). In rich/lean combustion, the rich stage is used to convert ammonia to nitrogen, and the second stage is used for fuel burnout. The combination of a rich and lean stage also reduces the peak flame temperatures in the combustor, thereby reducing thermal NO_x emissions.

Some of the findings of several combustor research efforts have been:

- **Temperature**. Fuel NO_x formation is relatively insensitive to temperature (Holt et al., 1989). Variation in fuel heating value appears to have little effect on conversion of ammonia to NO_x (Folsom et al., 1980).
- **Fuel-nitrogen concentration**. The fraction of fuel-bound nitrogen converted to NO_x decreases with increasing fuel-bound nitrogen concentration (Folsom et al., 1980; Sato et al., 1989; Unnasch et al., 1988). In the Unnasch et al. (1988) tests, it was found that above 5,000 ppm ammonia concentration, there was very little marginal increase in NO_x emissions.
- **Stoichiometry**. Fuel NO_x formation is sensitive to the reaction stoichiometry. In an oxygen-deficient environment, a substantial portion of fuel-bound nitrogen can be converted to diatomic nitrogen. The optimal reactant stoichiometry (fuel/air ratio) in the rich stage to maximize conversion of fuel-bound nitrogen to N_2 (minimize fuel NO_x) is influenced by reaction temperature (Folsom et al., 1980).
- **Pre-Mixing**. Uniform pre-mixing of fuel and air may be required to assure a uniform fuel/air ratio throughout the reaction mixture (Folsom et al., 1980).
- **Hydrocarbons**. The presence of hydrocarbons, such as methane, appears to promote the formation of fuel NO_x, due to reactions with intermediate reaction products which interfere with N_2 formation.

However, a hydrocarbon gas does appear to promote the conversion of NO to N_2. This may have implications for the second stage (Folsom et al., 1980).

- **Burnout**. A rich stage for fuel-bound nitrogen "cracking" to N_2 requires a second lean stage for fuel burnout (Folsom et al., 1980).
- **Thermal** NO_x. The lean mixture in the second stage can be adjusted to reduce or minimize thermal NO_x formation (Folsom et al., 1980). However, the rich/lean combustor may not reduce thermal NO_x as effectively as a lean/lean combustor would for fuels without nitrogen compounds (Holt et al., 1989). Unnasch et al. (1988) found that MBG combustion yielded higher thermal NO_x emissions than LBG, and speculated that this was attributable to higher flame temperatures.
- **Turbulence**. Fuel NO_x formation is expected to increase in turbulent flames. A laminar diffusion flame appears to allow for good conversion of ammonia to N_2 (Folsom et al., 1980).
- **Fuel heating value**. If fuel heating value is too low, combustion may not start in the fuel-rich zone. If combustion begins in the fuel-lean zone, conversion of ammonia to NO_x may be very high (Sato et al., 1989).
- **Pressure**. As combustor pressure increases, the conversion of ammonia to NO_x appears to decrease slightly, based on testing from 1 to 14 atm using a half-scale conventional combustor model (Sato et al., 1989).
- **Efficacy**. Rich/lean combustor tests using small scale combustors at relatively low pressures have achieved up to 95 percent conversion of ammonia to N_2 (Folsom et al., 1980; Unnasch, 1988; Notestein, 1989). Folsom et al. attempted to develop ideal combustors of various designs on the bench-scale, but indicated that full-scale commercial designs may not be as successful in achieving NO_x reductions. The tests by Sato et al. (1989) did not appear to achieve such high conversion rates. These tests involved perhaps more realistic full- and half-scale gas turbine combustors. In the Sato tests, ammonia conversion to N_2 was increased from a nominal value of 30 percent to a nominal value of 50 percent. This may be contrasted with the value of 30 percent typical of conventional combustors, discussed previously. These results imply that the efficacy of a commercial scale rich/lean combustor in reducing fuel NO_x emissions may be in doubt.
- **CO emissions**. In the Sato et al. (1989) tests, CO emissions were below 100 ppm.

Another concept that has received some attention is catalytic combustion. However, in the near term, rich/lean combustion appears to be receiving more attention and testing. Therefore, for this study, rich/lean combustion is assumed as the most likely alternative for fuel NO_x control.

7.2.6 Combustion Efficiency and CO Emissions

CO emissions, which result from incomplete combustion of hydrocarbons or no combustion of CO in the fuel gas, are an indicator of poor combustion efficiency. Many of the measures which reduce NO_x emissions, such as reducing flame temperature through wet injection or staged combustion, also tend to increase CO emissions by reducing the combustion efficiency. Most heavy-duty natural gas-fired and distillate oil-fired gas turbines have very low CO emissions (less than 5-10 ppm).

CO emissions increase at part load as the gas turbine combustor firing temperature is reduced during load-following (Entrekin and Edwards, 1987). Becker and Shulten (1985) report on part-load gas turbine combustion of low-BTU blast furnace gas in which it was difficult to achieve conversion of CO in the gas. However, coal gas has a higher hydrogen content than blast furnace gas, and may tend to combust more completely.

At the Cool Water demonstration plant, CO emissions were low with wet injection or fuel gas saturation. However, there are limits to fuel gas moisturization. As moisturization increases, the combustor flame becomes increasingly unstable, leading to pressure oscillations which can reduce the life of the combustor. At very high injection or moisturization rates, the combustion flame will ultimately blow out. Prior to the loss of flame, combustion efficiency will be low and CO emission will be high (Holt et al., 1989). The maximum fuel moisturization level is thus usually determined based on the point at which CO emissions begin to increase significantly.

A post-combustion flue gas CO catalyst can be used to convert CO to CO2. The CO catalyst is relatively low cost, compared to SCR catalyst for NO_x control. However, the combination of reduced combustion efficiency and the exhaust gas pressure drop across the CO catalyst leads to reduced plant efficiency (Holt et al**.,** 1989). The effects of flue gas from coal gas combustion on CO catalyst, such as catalyst masking or poisoning, may need to be assessed to determine the economics of CO catalysts in an IGCC process environment.

Incomplete combustion may occur due to local chilling of the flame, such as at points of secondary air entry (Cohen et al**.,** 1987) or due to wet injection.

One advantage that coal gases have compared to natural gas or distillate oil with respect to combustion efficiency is the presence of hydrogen, which has a very high flame speed. This results in early ignition and promotes complete combustion (Holt et al**.,** 1989).

CO Emissions With MBG

For a medium-BTU gas, CO emissions are not expected to be a major concern at baseload operation, particularly if there is hydrogen in the fuel gas. CO emissions could become a problem at part load if firing temperature is significantly reduced, or could become significant if high levels of water injection or fuel moisturization are used.

CO Emissions with LBG

CO emissions are more of a concern for LBG than MBG. Corman (1986) reports an estimate for baseload CO emissions from a 100-MW class gas turbine firing LBG with a heating value of less than 150 BTU/scf to be approximately 10,000 tons/year. Corman implies the emissions would be higher for part-load gas turbine operation. However, in a phone conversation (1990) Corman appeared to have no concern about CO emissions with LBG. Pillsbury (1989) indicated that heating value is not the proper determinant of combustion efficiency, particularly because hydrogen is highly flammable and will tend to promote complete combustion even in LBG. Pillsbury and Corman both stated that the expected CO emissions are on the order of 10 ppm or less when firing LBG at baseload conditions.

7.2.7 Combustor Pressure Drop

The combustor pressure drop is one of the significant losses in the gas turbine system. Pressure losses are due to skin friction and turbulence. The rise in temperature during combustion increases velocity and momentum of the gases in the combustor, which leads to temperature-related pressure losses. However, the pressure drop due to turbulence is usually much higher than the pressure loss associated with the temperature ratio in the combustor. The build-up of carbon or other deposits on the combustor liner may also affect skin friction and/or turbulence-related pressure losses. Furthermore, aerodynamically excited vibrations in the combustor could lead to deposits breaking away, which could result in turbine damage (Cohen et al**.,** 1987).

7.2.8 Particles

The particle loading in the fuel gas may be considered to consist of refractory materials or carbonaceous materials. Refractory particles may pass through the combustor without alternation. They can split into smaller particles, or possibly agglomerate into larger particles. Carbonaceous material may be fully or partially combusted, leaving perhaps ash residues (Cincotta, 1984). The particle discharge from the combustor may affect turbine maintenance.

7.2.9 Combustor Life

The combustor life has an effect on maintenance and repair work and, hence, the cost of maintaining the gas turbine. For industrial gas turbines, combustor chamber lives of 100,000 hours are desirable (Cohen et al**.,** 1987). However, deposition, erosion, corrosion, and vibrations can shorten the life of combustor components such as the liners, requiring more frequent liner replacement or more expensive materials. The modular nature of the combustor cans makes this type of maintenance routine. However, the cost will increase with the frequency of maintenance and repair. The possible presence of particulates and alkalis in the coal gas may lead to more costly maintenance compared to clean fuel (e.g., natural gas) fired gas turbines.

7.2.10 Turbine

The heavy-duty high firing temperature gas turbines assumed for this study typically employ three or four turbine rotor stages. The first two or three stages are subject to high thermal loadings due to the high temperature exhaust gas. Improvements in turbine rotor blade cooling technology have made possible increases in gas turbine firing (turbine inlet) temperatures while maintaining essentially constant bulk metal temperatures in the rotors and stators of the first turbine stage. Possible future improvements in materials and manufacturing processes (such as making turbine blades from a single crystal with no grain boundaries) may allow higher blade bulk metal temperatures, due to the improved strength of the material, and further increases in firing temperature (Smock, 1989).

A number of potential problems with the effect of hot combustion gas on the turbine have been identified in various reports. These include:

- Corrosion of hot gas path components from alkali metals
- Erosion of material from airfoils (rotor and stator blades) due to ash particles of sufficient size and quantity. This would likely exacerbate corrosion as well, as the airfoils are often coated with a corrosion resistant layer.
- Deposition of ash on hot gas path components, changing the aerodynamic characteristics of the turbine and resulting in loss of efficiency. This would also affect film cooling and the heat transfer from the hot gas to the airfoils.
- Blockage of film cooling holes, reducing the efficiency of blade cooling. This could lead to localized thermal stresses arising from thermal gradients in the blade material, affecting the operating life and/or sustainable firing temperature of the turbine

All of these possible problems would affect the gas turbine maintenance cycle, thereby affecting maintenance costs. Some or all of these affects could also require changes in gas turbine operation, such as a reduction in firing temperature or strict specifications on fuel gas composition.

7.2.11 Advanced Cooling Technology

Aircraft derivative gas turbines, and particularly military engines, have employed a variety of advanced turbine cooling techniques. These machines fire clean jet fuel, and as such are not subject to the exhaust gas contaminants expected in coal gas-fired units. Turbine blades and stator vanes subject to high temperature environments may have hollow internal cooling passages, through which compressed air is passed for convective cooling. These passages may have pin fins, to promote heat transfer from the metal to the cooling air. The cooling air is typically exhausted from the blade through holes in the blade tip or the trailing edge of the blade. The cooling air exhausted at the blade tip does provide some aerodynamic advantages by blocking against external bypass flow of exhaust gases between the blade tip and the rotor shroud. To further promote heat transfer in the internal cooling circuits, high velocity impingement of cooling air against the inside surface of a highly heated area may be used (referred to as impingement cooling). In addition, film cooling, in which some cooling air from inside the blade is vented near the leading edge of the blade, may also be employed. Film cooling results in a boundary layer of cooling air over the blade surface (Cohen et al**.,** 1987; Dawkins et al**.,** 1986).

The amount of cooling air required depends on the firing temperature, cooling air temperature, heat transfer features of the rotor and stator vanes, the material properties, and the design life of the system (Dawkins et al**.,** 1986).

Based on testing of a prototype MS7001F engine with high (2,300 °F) firing temperature, GE reports that they expect their minimum hot gas component life design requirement to be met. The basis for this assertion is measurement of hot gas path metal temperatures to be 30 to 50 °F below the design values. The test was conducted with natural gas (Brandt, 1989). The gas path metal temperatures in a coal gas application may be affected by deposition or hole plugging, which is discussed in a later section.

The design of blades is complicated due to the changes in hot gas temperature across the blade surfaces, and the changes in temperature of cooling air inside the blade. Thus, the design must account for thermal gradients. Stresses in the blades may arise from thermal gradients (Cohen et al**.,** 1987).

Any particles or liquid droplets which pass through the combustor and burn-out in the turbine nozzle or turbine first-stage may have deleterious effects on the thermal stresses in the hot gas path components.

7.2.12 Turbine Blade Materials

The selection of firing temperature for a gas turbine depends on both the turbine blade cooling technology employed and the blade materials. Three key criteria for selecting hot gas path materials, particularly for rotor blades, are: (1) creep-rupture properties; (2) hot corrosion resistance; and (3) hot oxidation resistance. The creep strength of a metal is a function of the bulk metal temperature. The time to obtain a standard 0.2 percent creep strain decreases as temperature increases. Also, the fatigue strength of a metal subject to cyclic stresses decreases as temperature increases. To provide blade strength, nickel-based superalloys may be used for rotor blades. To provide corrosion and oxidation resistance, coatings may be applied to the blade surfaces. Typical coatings include platinum-chromium-aluminide (Dawkins et al**.,** 1986).

The GE MS7001F is reported to use a first-stage coating alloy containing cobalt, chromium, aluminum, and yttrium (Brandt, 1988). The blades for the GE turbine are reported to be manufactured using a technology called directional solidification that has been used for 20 years to make jet engine blades. In this casting method, the grain boundaries in the crystal structure of the metal are oriented to improve tensile strength, ductility, and fatigue strength. The use of this molding technology has permitted an increase in firing temperature of about 150 °F. Possible future improvements would be the casting of a single-crystal blade with no grain boundary, which would permit another 50 to 150 °F improvement in firing temperature (Smock, 1989). Increases in firing temperature permit increased simple cycle efficiency. Such a design improvement is likely to be a long-term development objective.

7.2.13 Deposition

Deposition of ash on surfaces in the hot gas path can restrict air flow, thus reducing turbine efficiency. Deposition of ash particles is expected to some extent in coal-fueled gas turbines (Cincotta, 1984). Deposits can also lead to plugging of cooling air outlet holes, particularly those used for film cooling, on the turbine rotor blades (Becker and Schulten, 1985; Dawkins et al**.,** 1986). This can lead to increased localized temperature gradients that can result in thermal stress cracking, and can be exacerbated by the stress riser effect of the cooling air holes themselves. Also, film cooling can be affected by deposits on the turbine blades and hot gas channels. Such deposits, of certain size and consistency, can significantly alter the flow and heat transfer characteristics of the blades (Becker and Schulten, 1985).

Hot gas path blockage is generally expected with any gas turbine application involving a fuel containing ash particles. GE predicted a blockage rate of about 0.4 percent of the first-stage turbine nozzle area per 100 hours of operation at a 2,300 °F firing temperature, based on a system with two-stages of high efficiency cyclones (Cincotta, 1984). This implies nozzle cleaning every 2,500 hours, if up to 10 percent blockage is allowed. The assumption appears to be that this cleaning can be accomplished using off-line water washing, for example.

GE conducted some tests with a turbine simulator to determine possible effects of ash deposition. No measurable deposits were found on the airfoils. However, the tests were only 57 hours in duration (Corman, 1986).

Evaluation of deposition appears to require a long-term testing program, which in reality may not be realized until a demonstration plant is built and operating. The effect of deposition on the heat transfer characteristics of the turbine blades might be to require a reduction in firing temperature or to increase the frequency of blade replacements. Thus, either performance and/or cost may be affected by these types of problems.

7.2.14 Erosion

Erosion occurs due to contact of particles with sufficient mass or velocity to remove material from hot gas path surfaces, particularly rotor and stator vanes. Some possible sources of particles contributing to erosion include: particles not removed from the fuel gas in cyclones or barrier filters; break-away deposits from the fuel nozzle, fuel valves, combustor lining, transition piece, or turbine nozzles; and carry-over of sorbent material from the zinc ferrite sorbent bed and, if included in the system, alkali removal sorbent bed. GE reported that they expect to

achieve a particle size distribution and loading using two-stages of high efficiency cyclones to be within the erosion tolerance of the gas turbine materials (Cincotta, 1984).

However, some speculate that cyclones are insufficient to avoid the build up of particles and, hence, pressure drop in the zinc ferrite absorber bed. Therefore, barrier filtration upstream of the zinc ferrite unit may be required, in lieu of a single-stage cyclone. There is also speculation that a cyclone downstream of the zinc ferrite absorber may not be needed. Most design studies assume a cyclone between the absorber and the gas turbine combustor to capture any catastrophic loss of sorbent or unusual entrainment of sorbent, as well as to provide for additional removal of particles still present from the gasifier.

7.2.15 Corrosion

The most widely expressed concern regarding hot gas path corrosion is due to the presence of alkali in the exhaust gas. For systems with cold gas cleanup, alkali are not expected to pose a corrosion threat because it is believed that below 1,200 to 1,400 °F, alkali condense onto particles in the gas stream (METC, 1987; Notestein, 1989), which are in turn removed very effectively by wet scrubbing. For hot gas cleanup systems using the zinc ferrite process, the fuel gas temperature in the particulate removal device is typically expected to be about 1,100 °F. The removal efficiency of alkali which condense on particles depends on the alkali concentration on the particles as a function of particle size, and the particle removal efficiency as a function of particle size. The expectation is that, because the smaller particles have a larger surface area per unit mass, there will be a larger concentration of condensed alkali on the smaller particles (Cincotta, 1984).

Several have reported that there is evidence that the alkali in coal gas may not pose as much of a threat as an equivalent concentration of alkali in petroleum fuels. The suggestion is that alkali in the coal gas are "gettered" by aluminosilicate ash materials (METC, 1987; Notestein, 1989). This, combined with the absence of "catalytic" elements, such as vanadium and molybdenum, are believed to reduce the ability of the coal gas alkali to cause corrosion.

In the event that particulate removal proves to be insufficient for alkali control, several alkali control technologies for hot gas cleanup systems have been explored (Notestein, 1989). Perhaps the most promising of these is an absorber utilizing emathlite, a naturally occurring clay (Bachovchin, 1987).

7.3 Power Block Performance Model

7.3.1 Simple Cycle Gas Turbine: Mass and Energy Balance

The simple cycle gas turbine (SCGT) mass and energy balance model is based upon the air-standard Brayton cycle, as described in Wark (1983). The case study examples are based upon data reported by General Electric for the Frame 7F gas turbine design (Brooks, 2000).

A SCGT is comprised of three major components, including the compressor, combustor, and turbine, as shown in Figure 7-2. Air, at ambient pressure P_a and ambient temperature, T_a, enters the compressor. The ratio of the compressor exit pressure to the inlet ambient air pressure is defined as the pressure ratio, r_p. Compression takes place approximately adiabatically. Therefore, the temperature of the compressed air is higher than the ambient temperature of the inlet air. The performance of an ideal adiabatic and isentropic compressor can be calculated using straight-forward thermodynamic principles. However, because real compressors are subject to inefficiencies, their performance will not be as good as the ideal case. Therefore, an adiabatic compressor efficiency, η_c, is defined to more accurately represent the real world performance of a compressor.

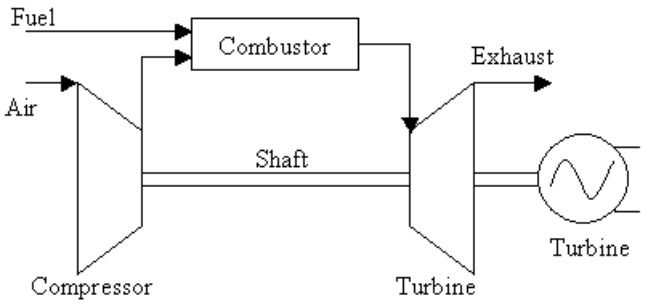

Figure 7-2. Simplified Schematic Diagram of a Simple Cycle Gas Turbine

The compressed air enters a combustor, where it is mixed with high pressure gaseous fuel. The fuel and air are burned at essentially constant pressure. The conventional fuel for SCGT systems is natural gas, which is comprised mostly of methane. However, other fuels may be burned in a gas turbine, including syngas obtained from a gasification process. Syngas typically contains carbon monoxide (CO), hydrogen (H_2), methane (CH_4), carbon dioxide (CO_2), nitrogen (N_2), and water vapor (H_2O) as the primary constituents. Syngases also may contain relatively small amounts of hydrogen sulfide (H_2S), carbonyl sulfide (COS), and ammonia (NH_3). These latter three components are significant in terms of the formation of SO_2 and NO_x emissions, but are less important in terms of calculating the mass and energy balance of the system because they comprise only a small portion of the total fuel flow rate and the total fuel heating value. The combustor typically has a small pressure drop. Therefore, the exit pressure from the combustor is slightly less than that compared to the compressor outlet.

The high-pressure hot product gases from the combustor enter the turbine, or expander, portion of the SCGT system. In the turbine, the gases are reduced in pressure, resulting in a corresponding reduction in temperature. The heat-removal process associated with expansion and cooling of the hot gases in the turbine results in an energy transfer from the gases to shaft work, leading to rotation of a shaft. In many heavy duty SCGT designs, the compressor, turbine, and a generator turn on the same shaft. The turbine must supply enough rotational shaft energy to power the compressor. The net difference between the work output of the turbine and the work input to the compressor is available for producing electricity in the generator. The ratio of compressor work to turbine work is referred to as the back work ratio.

The turbine inlet temperature is carefully controlled to prevent damage or fatigue of the first stage stator and rotor blades. The turbine inlet temperature and the pressure ratio are the two most important parameters that impact on system efficiency.

The expected operating practice for gas turbines in IGCC service is to adjust the air flow through the gas turbine compressor such that the flow at the turbine inlet nozzle is (approximately) choked. This usually involves the use of compressor inlet guide vanes to adjust the compressor air flow based on fuel flow and compressor air extraction (if any) to obtain design flow in the turbine.

As noted by Frey and Rubin (1991), the mass flow through a gas turbine is limited by the critical area of the turbine inlet nozzle. The critical area of the turbine inlet nozzle is a constant for a given make and model of gas turbine. Gas turbine operation on natural gas typically involves a relatively small fuel mass flow rate compared to the compressor mass flow rate. However, when operating on syngas, which may have a heating value substantially smaller than that of natural gas, a larger fuel mass flow rate is needed in order to supply approximately the same amount of energy to the gas turbine. The mass fuel-to-air ratio will be larger for a low BTU fuel than for a high BTU fuel. However, the total mass flow at the turbine inlet remains approximately the same. Therefore, the mass flow at the compressor inlet must be reduced to compensate for the higher fuel-to-air ratios needed for low BTU syngases.

The mass air flow at the turbine inlet nozzle is estimated, assuming choked flow conditions, based upon the following relationship (Frey and Rubin, 1991):

$$m_{act} = m_{ref}\left(\frac{P_{act}}{P_{ref}}\right)\sqrt{\left(\frac{MW_{act}}{MW_{ref}}\right)\left(\frac{T_{ref}}{T_{act}}\right)} \qquad (7\text{-}2)$$

The reference values are determined based upon calibration to published data for gas turbine operation on natural gas. The actual values are determined based upon the desired simulated conditions. The pressure, temperature, and molecular weight in Equation (7-1) are evaluated at the turbine inlet nozzle.

The design specification adjusts the compressor air flow so that the ratio of the actual turbine inlet gas flow to the reference value, adjusted for temperature, pressure, and gas molecular weight, approaches unity to within a specified tolerance.

The effect of this new design specification is that the turbine inlet nozzle mass flow rate remains relatively constant even for varying values of fuel gas heating value and compressor air extraction. Thus, the gas turbine is more properly sized compared to the cost model.

The mass and energy balance for each of the following components are presented in the following sections: (1) compressor; (2) combustor; (3) turbine; and (4) generator. The calculation of overall SCGT performance is also discussed.

Compressor

The outlet pressure of a compressor is specified by multiplying the pressure ratio and the inlet pressure:

$$P_{C,out} = P_{C,in}\, r_p \tag{7-3}$$

The outlet temperature is estimated via a multi-step procedure. The first step is to estimate the entropy of the inlet air based upon a regression relationship of thermodynamic data as given in Figure 7-3. Based upon the estimated entropy of the inlet air and the pressure ratio, the entropy of the compressor outlet air is estimated:

$$s_{C,out} = s_{C,in} + (R/MW_{air}) \ln(r_p) \tag{7-4}$$

For example, if the inlet temperature is 295 K, then the entropy of the inlet air is estimated to be 1.682 kJ/(kg-K). Suppose that the pressure ratio is 6, and that the molecular weight of air is approximately 29. The estimated outlet air entropy will be 2.196 kJ/(kg-K). By comparison, the exact value reported in Wark (1993) for the same case is 2.199 kJ/(kg-K). Thus, the regression-based approach here agrees well with the published case study.

Using the estimate of the entropy of the outlet air, a regression expression shown in Figure 7-4 is used to estimate the temperature of the outlet air. In this example, the temperature is estimated to be 488 K, compared to a value of 490 K as reported by Wark (1983). With knowledge of the temperature of the outlet air, the enthalpy of the outlet air is estimated based upon the regression expression shown in Figure 7-5. The estimated enthalpy is 489.9 kJ/kg, versus a reported value of 492.7 kJ/kg. This procedure is based upon an isentropic compressor.

To take into account the irreversibilities in an actual compressor, the actual enthalpy of the outlet air is estimated based upon the following relationship:

$$h_{C,out} = h_{C,in} + (h_{C,out,isentropic} - h_{C,in})/\eta_c \tag{7-5}$$

If the adiabatic compressor efficiency is assumed to be 0.82, then the estimated enthalpy at the compressor outlet is:

$$h_{C,out} = 294.8 + (489.9-294.8)/\ 0.82 = 532.7 \text{ kJ/kg} \tag{7-6}$$

The value reported by Wark (1983) is 536.1 kJ/kg. Based upon the estimated enthalpy for the actual compressor outlet air, the actual outlet temperature is estimated based upon the regression equation given in Figure 7-6. The estimated outlet temperature is 528 K, versus a reported value of 532 K. Thus, although there is some error in the estimation procedure, the result is within a few degrees of the reported value.

The work input requirement for the compressor is given by the mass flow of air multiplied by the difference in enthalpy between the outlet and inlet.

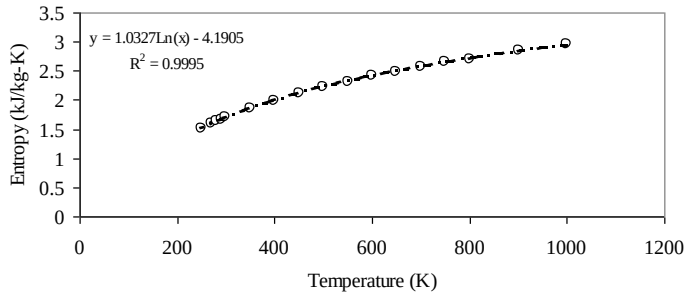

Figure 7-3. Regression Results for Entropy as a Function of Temperature for Air

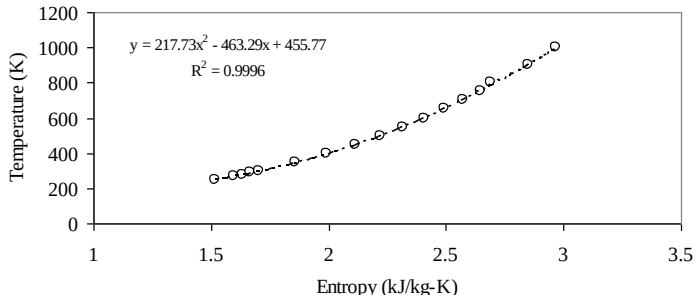

Figure 7-4. Regression Results for Temperature as a Function of Entropy for Air

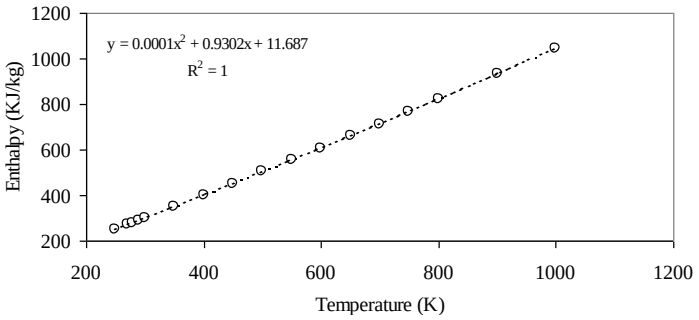

Figure 7-5. Regression Results for Enthalpy as a Function of Temperature for Air

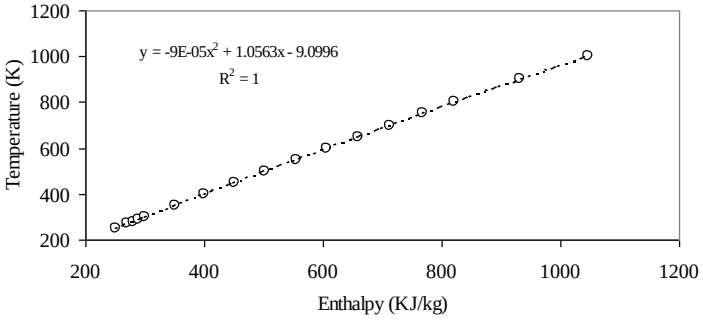

Figure 7-6. Regression Results for Temperature as a Function of Enthalpy for Air

Combustor

For the combustor, we assume that in general the fuel contains the following major components:

- carbon monoxide (CO)
- hydrogen (H_2)
- methane (CH_4)

- carbon dioxide (CO_2)
- nitrogen (N_2)
- water vapor (H_2O)

Although syngases also may contain relatively small amounts of hydrogen sulfide (H_2S), carbonyl sulfide (COS), and ammonia (NH_3), we will assume that these three components contribute negligibly to the mass and energy balance. These latter three components are significant in terms of the formation of SO_2 and NO_x emissions.

The volume percent (or, equivalently, mole fraction) of each of the six major components will be known. Therefore, a heating value can be estimated for the fuel. Based upon date reported by Flagan and Seinfeld (1988), the enthalpy of reaction of CO is estimated as 283,400 J/gmole, the enthalpy of reaction of H_2 is estimated as 242,200 J/gmole, and the enthalpy of reaction of CH_4 is estimated as 803,500 J/gmole. These are estimated on a lower heating value basis, assuming that H_2O produced is in the form of vapor. The other three major components are assumed to be non-reactive. The heating value of the syngas, on a J/gmole basis, is given by:

$$\Delta h_{r,SG} = y_{CO}\,\Delta h_{r,CO} + y_{H2}\,\Delta h_{r,H2} + y_{CH4}\,\Delta h_{r,CH4} \qquad (7\text{-}7)$$

The syngas is represented by a mixture of the six constituent gases. Air is a mixture primarily of oxygen and nitrogen. For every mole of oxygen in the air, there are approximately 3.76 moles of nitrogen. The major products of combustion are carbon dioxide, water vapor, nitrogen, and excess oxygen. Therefore, the mass balance for stoichiometric combustion is given by:

$$[y_{CO}\,CO + y_{H2}\,H_2 + y_{CH4}\,CH_4 + y_{CO2}\,CO_2 + y_{N2}\,N_2 + y_{H2O}\,H_2O] + a\,O_2 + 3.76\,a\,N_2 \rightarrow b\,CO_2 + c\,H_2O + d\,N_2 \qquad (7\text{-}8)$$

The mass balance is given on the basis of one mole of syngas mixture. Thus, the units of each stoichiometric coefficient are moles of the respective compound per mole of syngas mixture. The mole fractions of each component in the syngas are known. Therefore, the unknowns are the stoichiometric coefficients a, b, c, d, and e. These can be solved based upon elemental balances:

Carbon:	$y_{CO} + y_{CH4} + y_{CO2} = b$
Hydrogen:	$2\,y_{H2} + 4\,y_{CH4} + 2\,y_{H2O} = 2c$
Oxygen:	$y_{CO} + 2\,y_{CO2} + y_{H2O} + 2a = 2b + c$
Nitrogen:	$2\,y_{N2} + 2(3.76)\,a = 2\,d$

Based upon these four equations, the solutions for a, b, c, and d are:

$$a = \tfrac{1}{2}\,y_{H2} + 2\,y_{CH4} + \tfrac{1}{2}\,y_{CO} \qquad (7\text{-}9)$$

$$b = y_{CO} + y_{CH4} + y_{CO2} \qquad (7\text{-}10)$$

$$c = y_{H2} + 2\,y_{CH4} + y_{H2O} \qquad (7\text{-}11)$$

$$d = y_{N2} + 3.76\,a \qquad (7\text{-}12)$$

However, gas turbine combustors operate with a significant amount of excess air. The mass balance for the case with excess air can be developed based upon the stoichiometric mass balance by introducing a new variable for the fraction of excess air, e_a. The fraction of excess air is given by:

$$e_a = (\text{Total air} - \text{stoichiometric air}) / (\text{Stoichiometric air}) \qquad (7\text{-}13)$$

The mass balance for excess air is:

$$[y_{CO}\,CO + y_{H2}\,H_2 + y_{CH4}\,CH_4 + y_{CO2}\,CO_2 + y_{N2}\,N_2 + y_{H2O}\,H_2O] + a(1+e_a)O_2 + 3.76a(1+e_a)N_2 \rightarrow b\,CO_2 + c\,H_2O + d'\,N_2 + (a)(e_a)O_2 \qquad (7\text{-}14)$$

The solutions for a, b, and c are the same as in Equations (7-9), (7-10), and (7-11). The solution for d is replaced by the solution for d':

$$d' = y_{N2} + 3.76\,a\,(1+e_a) \qquad (7\text{-}15)$$

For example, suppose that a fuel contains, on a mole or volume percentage basis, 24.8% hydrogen, 39.5 % carbon dioxide, 1.5 % methane, 9.3 % carbon dioxide, 2.3 % nitrogen, and 22.7 % water vapor. Stoichiometric combustion of this fuel would require 0.3515 moles of oxygen per mole of syngas mixture, and 1.32 moles of nitrogen in the inlet air. The exhaust gas would contain 0.50 moles of carbon dioxide, 0.50 moles of water vapor, and 1.34 moles of nitrogen, all based upon one mole of syngas combusted. If the fuel were burned with 100 percent excess air, then the exhaust gas would contain 0.50 moles of carbon dioxide, 0.50 moles of water vapor, and 2.67 moles of nitrogen, and 0.35 moles of oxygen, all based upon one mole of syngas combusted.

The actual amount of air that is needed to combust the fuel depends upon the desired turbine inlet temperature. Therefore, it is necessary to solve an energy balance in order to estimate the fuel to air ratio. The turbine inlet temperature, $T_{T,in}$, is a known design parameter. The temperature of the air from the compressor is known based upon the compressor pressure ratio and adiabatic compressor efficiency, as explained in the previous section. The syngas temperature would also be known. The only unknown is the excess air ratio. Thus, the energy balance is:

$$b\,H_{CO2}(T_{T,in}) + c\,H_{H2O}(T_{T,in}) + d'\,H_{N2}(T_{T,in}) + (a)(e_a)H_{O2}(T_{T,in}) - [y_{CO}\,H_{CO}(T_{SG}) + y_{H2}\,H_{H2}(T_{SG}) + y_{H2}\,H_{H2}(T_{SG}) + y_{CO2}\,H_{CO2}(T_{SG}) + y_{N2}\,H_{N2}(T_{SG}) + y_{H2O}\,H_{H2O}(T_{SG})] - a(1+e_a)\,H_{O2}(T_{C,out}) - 3.76a(1+e_a)\,H_{O2}(T_{C,out}) = \Delta h_{r,SG} \quad (7\text{-}16)$$

Because all of the terms in this equation are known except for the excess air fraction, the equation can be rearranged in terms of excess air fraction as follows:

$$b\,H_{CO2}(T_{T,in}) + c\,H_{H2O}(T_{T,in}) + \{y_{N2} + 3.76\,a\,(1+e_a)\}\,H_{N2}(T_{T,in}) + (a)(e_a)H_{O2}(T_{T,in}) - [y_{CO}\,H_{CO}(T_{SG}) + y_{H2}\,H_{H2}(T_{SG}) + y_{H2}\,H_{H2}(T_{SG}) + y_{CO2}\,H_{CO2}(T_{SG}) + y_{N2}\,H_{N2}(T_{SG}) + y_{H2O}\,H_{H2O}(T_{SG})] - a(1+e_a)\,H_{O2}(T_{C,out}) - 3.76a(1+e_a)\,H_{N2}(T_{C,out}) = \Delta h_{r,SG} \quad (7\text{-}17)$$

For convenience, we create the following groups of terms:

$$H_{fuel} = y_{CO}H_{CO}(T_{SG}) + y_{H2}\,H_{H2}(T_{SG}) + y_{CH4}H_{CH4}(T_{SG}) + y_{CO2}H_{CO2}(T_{SG}) + y_{N2}H_{N2}(T_{SG}) + y_{H20}\,H_{H20}(T_{SG}) \quad (7\text{-}18)$$

$$H_{air,stoich} = aH_{O2}(T_{C,out}) + 3.76aH_{N2}(T_{C,out}) \quad (7\text{-}19)$$

$$H_{products,stoich} = bH_{CO2}(T_{T,in}) + cH_{H2O}(T_{T,in}) + \{y_{N2} + 3.76a\}\,H_{N2}(T_{T,in}) \quad (7\text{-}20)$$

The solution for the excess air fraction is given by:

$$e_a = \frac{H_{fuel} + H_{air,stoich} + \Delta h_{r,SG} - H_{products,stoich}}{a\left[3.76\left\{H_{N2}(T_{T,in}) - H_{N2}(T_{C,out})\right\} + \left\{H_{O2}(T_{C,out})\right\}\right]} \quad (7\text{-}21)$$

For example, suppose that the turbine inlet temperature is specified as 1,100 K. For the same syngas composition as previously assumed, and for the same compressor outlet temperature of 528 K, the estimated excess air ratio is 4.218. This excess air ratio was verified in two ways. First, the excess air ratio was substituted into the final mass balance, and an energy balance was calculated using Equation (7-14). The energy balance was properly closed. Second, the same assumptions were input into an independently developed spreadsheet that uses a different set of equations for estimating enthalpy. The results agreed to within a few degrees for the predicted turbine inlet temperature calculated by the independent software.

Turbine

The energy balance for the turbine is estimated in a manner similar to that for the compressor. However, a key difference is that the exhaust gas is not air, and therefore the thermodynamic data for air are not strictly applicable for use with the turbine. In addition, pressure losses in the combustor and the turbine back pressure must be accounted for when estimating the work capability of the turbine.

The pressure at the combustor outlet, which is assumed to be same pressure as for the turbine inlet, is given by:

$$P_{C,out} = P_{T,in} = P_a(r_p) - \Delta p_{comb} \quad (7\text{-}22)$$

The pressure at the turbine outlet is given by:

$$P_{T,out} = P_a + \Delta p_{back} \quad (7\text{-}23)$$

Therefore, the pressure ratio for the turbine is given by:

$$r_{p,turb} = P_{T,in} / P_{T,out} = (P_a(r_p) - \Delta p_{comb})/(P_a + \Delta p_{back}) \quad (7\text{-}24)$$

Because nitrogen comprises approximately 70 percent or more (by volume) of the exhaust gases from the gas turbine, we use nitrogen as the basis for the calculations to determine the turbine exhaust temperature. Figure 7-7 and Figure 7-8 display the regression equations for entropy as a function of temperature, and for temperature as a function of entropy, respectively. For example, temperature is equal to 4.9161×10^{-4} (entropy)$^{6.9277}$ with an R^2 = 0.9999. The entropy at the turbine inlet is estimated based upon the turbine inlet temperature. For example, if the turbine inlet temperature is 1,100 K, then the estimated entropy from the Equation in Figure 7-7 will be 8.253 kJ/kg-K. If the turbine pressure ratio is equal to 6, then the entropy at the turbine outlet is estimated as:

$$s_{T,out} = s_{T,in} + 8.3144/28 \ln(1/r_{p,turb}) \quad (7\text{-}25)$$

$$s_{T,out} = 8.253 + 8.3144/28 \ln(1/6) = 7.721 \text{ kJ/kg-K}$$

At this value of entropy, the temperature is calculated, based upon the regression equation given in Figure 7-8, to be 694 K. This temperature is exactly the same as that reported by Wark (1983) for a similar calculation based upon air.

If the turbine is not isentropic, then the turbine outlet temperature will be higher than that predicted based upon the above isentropic calculation. The isentropic turbine work output is given by the difference between the enthalpies of the inlet and outlet under isentropic conditions. The enthalpy of exhaust gas is estimated based on the regression equation shown in Figure 7-9.

$$h_{T,I,out,isentropic} = 5.9731 \times 10^{-S} T^2 + 1.0373T - 10.1939 \quad (7\text{-}26)$$

The estimated enthalpy is 738.5 kJ/kg when the outlet temperature is 694°K. This procedure is based on an isentropic turbine. If the inlet temperature is 1,100°K, then the enthalpy at the turbine inlet is estimated to be:

$$h_{T,in} = 5.9731 \times 10^{-S} \, 1100^2 + 1.0373 \times 1100 - 10.1939$$
$$= 1{,}203.1 \text{ kJ/kg}$$

To take into account the efficiency of an actual expander, the actual enthalpy of the outlet gas is estimated based on the following relationship:

$$h_{T,i,out} = h_{T,i,in} + (h_{T,i,out,isentropic} - h_{T,i,in})\eta_{Ti} \quad (7\text{-}27)$$

If the adiabatic turbine efficiency is assumed to be 0.95, then the estimated enthalpy at the turbine outlet is:

$$h_{T,i,out} = 1{,}203.1 + (738.5 - 1{,}203.1) \times 0.95 = 761.7 \text{ kJ/kg}$$

The actual temperature at the outlet is estimated based upon the regression expression shown in Figure 7-10.

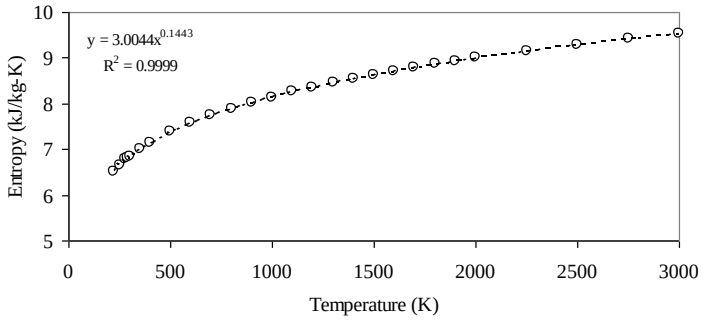

Figure 7-7. Regression Results for Entropy as a Function of Temperature for Nitrogen (N_2)

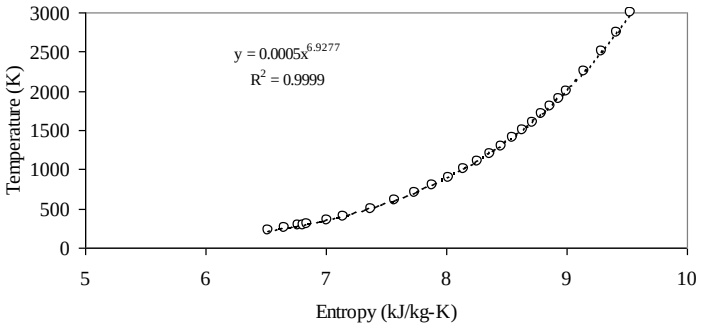

Figure 7-8. Regression Results for Temperature as a Function of Entropy for Nitrogen (N_2)

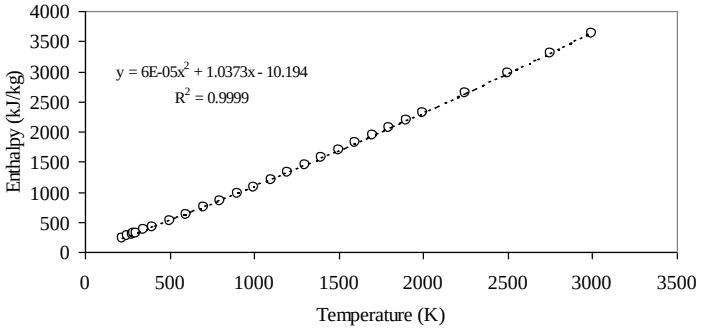

Figure 7-9. Regression Results for Enthalpy as a Function of Temperature for Nitrogen (N_2)

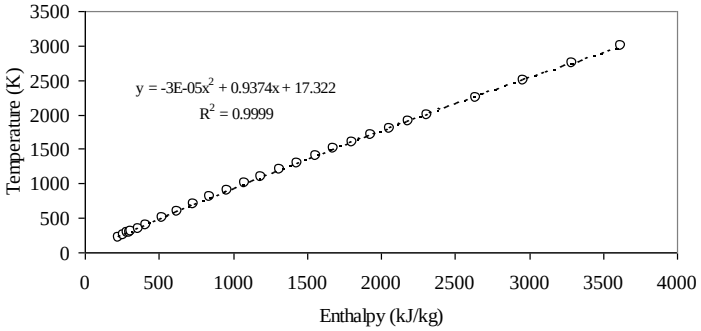

Figure 7-10. Regression Results for Temperature as a Function of Enthalpy for Nitrogen (N_2)

Calibration of the Gas Turbine Model

In order to calibrate the gas turbine model, a simple cycle system was simulated for natural gas and one gas turbine and key input assumptions in the simulation were varied in order to match published specifications for the exhaust gas temperature, simple cycle efficiency, and net power output for a commercial gas turbine. The simple cycle efficiency, power output, and exhaust gas temperature vary with the isentropic efficiencies of compressors and expanders of the gas turbine, as illustrated in Figure 7-11, Figure 7-12, and Figure 7-13. The curves shown in these three figures were obtained from sensitivity analysis of the simple cycle gas turbine model. For natural gas firing, published data are available for a "Frame 7F" type of gas turbine. For example, the published values for a General Electric MS7001F gas turbine are a simple cycle efficiency of 36.35 percent on a lower heating value basis, a power output of 169.9 MW, an exhaust mass flow of 3,600,000 lb/hr, and an exhaust gas temperature of 1,116 ºF (Farmer, 1997). The required turbine isentropic efficiency is selected from Figure 7-11 based upon the desired exhaust temperature; in this case, an isentropic efficiency of 87.2 percent was selected. A compressor isentropic efficiency of 91.8 percent is selected based on Figure 7-12 in order to obtain the correct simple cycle efficiency. The reference mass flow at the turbine inlet is adjusted to 3,470,000 lb/hr obtain the desired power output. The estimated power output of 170.0 MW, obtained from the ASPEN gas turbine model with the selected values of isentropic efficiencies, is within 0.11 percent of the published data. A similar procedure was used to

calibrate the gas turbine to data for a coal gasification application. The isentropic efficiencies obtained in the case of syngas are 0.81 and 0.919 for gas turbine compressors and gas turbine expanders respectively.

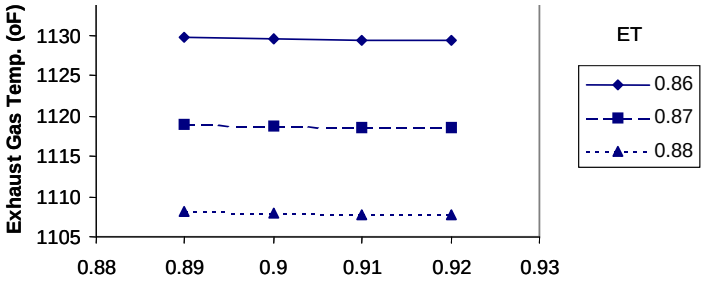

Figure 7-11. Exhaust Gas Temperature versus Gas Turbine Compressor isentropic Efficiency

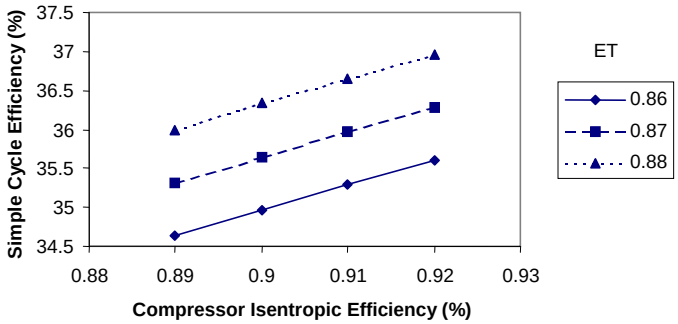

Figure 7-12. Simple Cycle Efficiency versus Gas Turbine Compressor isentropic Efficiency

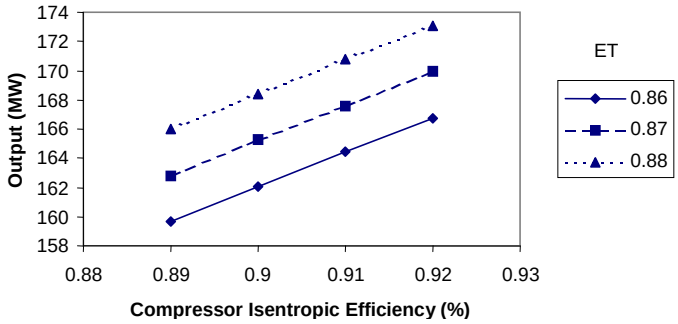

Figure 7-13. Output versus Gas Turbine Compressor Isentropic Efficiency. Note: ET = Gas Turbine Expander Isentropic Efficiency

7.3.2 Fuel Saturation/Combustor

Thermal NO_x constitutes a major portion of the total NO_x emissions from a gas turbine combustor fired on syngas. To control the formation of thermal NO_x, water vapor must be introduced along with the cleaned gas into the combustors of gas turbines. The water vapor lowers the peak flame temperatures. The formation of NO from nitrogen and oxygen in the inlet air is highly temperature sensitive. Lowering the peak flame temperature in the combustor by introducing water vapor results in less formation of thermal NO and hence, lowers NO emissions.

Another advantage of fuel gas moisturization is to increase the net power output of the gas turbine. The introduction of moisture into the syngas lowers the syngas heating value and requires an increase in fuel mass flow in order to deliver the same amount of total heating value to the gas turbine engine. Because the mass flow of combustor gases is constrained by choked flow conditions at the turbine inlet nozzle, the inlet air flow has to be reduced to compensate for the increased fuel flow. This results in less power consumption of power by the gas turbine compressors, resulting in an increase in the net gas turbine output.

The saturation of fuel gas takes place in a saturator vessel, which is adiabatic. The clean gas from the acid gas removal system enters the saturator from the bottom while hot water, which is at a higher temperature than that of

the syngas, is sprayed from the top of the vessel, as shown in Figure 7-14. The typical temperature of the hot water is 380 ºF, while that of the syngas is 85 ºF before saturation. The saturated gas is heated to a temperature of approximately 350 ºF and exits from the saturator from the top of the vessel while the hot water gets cooled and exits from the bottom of the vessel. The heat needed for heating the water is transferred from low temperature gas cooling units and the heat recovery steam generators to the fuel gas saturation unit as shown in Figure 7-15. A portion of the cold water leaving the fuel gas saturator is sent to heat exchangers in low temperature gas cooling section, where it get heated while cooling the hot syngas from the gas scrubbing section. The remaining portion of cold water is heated by heat exchange with boiler feedwater from the heat recovery steam generation system. Both the portions of heated water are combined to form the hot water spraying from the top of the saturator vessel. The clean, medium BTU gas from the fuel gas saturator is combusted in the gas turbine combustors.

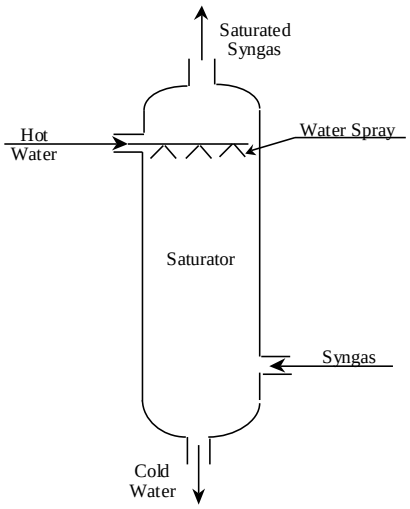

Figure 7-14. Fuel Gas Saturator

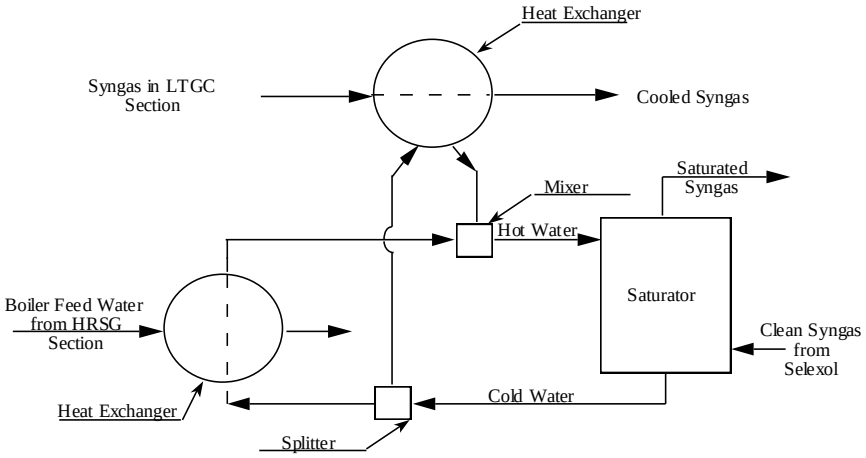

Figure 7-15. Simplified Schematic of Fuel Gas Saturation

Figure 7-15 shows the details of the fuel gas saturation unit. The syngas leaving the Selexol acid gas recovery unit, is saturated with moisture before the gas enters the gas turbine combustor. This is done with the intent of raising the net plant power output and to control NO_x emissions from the gas turbine. The steam saturation increases the mass throughput and the heat capacity of the inlet pressurized fuel gas stream to the gas turbine resulting in an increase in the gas turbine power output. The amount of water required to saturate the clean syngas to 40 weight percent moisture is calculated.

7.3.3 Gas Emissions

Environmental Emissions

SO_2 emissions from IGCC systems are controlled by removing sulfur species from the syngas prior to combustion in the gas turbine. NO_x emissions tend to be low for this particular IGCC system for two reasons. The first is that there is very little fuel-bound nitrogen in the fuel gas. The second reason is that thermal NO formation is low because of the low syngas heating value and correspondingly relatively low adiabatic flame temperature. A primary purpose of the gas cleanup system is to protect the gas turbine from contaminants in the fuel. Hence, no post-combustion control is assumed. However, it is possible to further control NO_x emissions, for example, through use of Selective Catalytic Reduction (SCR) downstream of the gas turbine. The emission rates of these pollutants are lower than for conventional power plants and for many advanced coal-based power generation alternatives. CO_2 emissions are lower than for conventional coal-fired power plants because of the higher thermal efficiency of the IGCC system (e.g., nearly 40 percent in this case versus typical values of 35 percent for conventional pulverized coal-fired power plants).

NO_x Emissions

The generation of NO and NO_2 from the gas turbine has been modeled in Frey and Akunuri (2001). Both the fuel NO_x as well as thermal NO_x have been taken into consideration for the estimation of NO and NO_2. The default assumptions made for these estimations are that fuel NO is 95 percent by volume of the fuel NO_x, and that the fraction of ammonia that is converted to fuel NO_x is 0.90. The conversion rate of nitrogen to NO_X during the gas turbine combustion is assumed to be 0.00045. Atmospheric emission rates are calculated on a lb/MMBTU basis as part of the model output.

Particulate Matter Estimations

PM emissions are controlled in the syngas cleanup system prior to the gas turbine and therefore, particulate matter emissions from the gas turbine are not modeled in the present model.

CO and CO_2 Emissions

CO emissions from the power plant are assumed to come from the gas turbine section of the plant. The fraction of CO that is converted to CO_2 in the gas turbine is assumed to be 0.99985. Aside from the gas turbine, CO_2 is also emitted by the Beavon-Stretford tail gas treatment unit. The emissions are expressed in terms of lb/kWh.

SO_2 Emissions

SO_2 emissions from the IGCC system are assumed to the result from combustion of syngas in the gas turbine. The SO_2 emissions from the gas turbine are due to oxidation of H_2S and COS in the fuel gas. The amount of H_2S and COS in the fuel gas can be varied by changing the removal efficiency of the Selexol process. The emissions are calculated on a lb/MMBTU basis.

7.3.4 Energy Use

HRSG Feedwater System

Boiler Feed Water Treating

$$W_{e,BF} = 20.8 + 2.13x10^{-4}m_{pw} \qquad \begin{matrix} R^2 = 0.975 \\ n = 14 \end{matrix} \qquad (7\text{-}28)$$

where,

$$234{,}000 \leq m_{pw} \leq 3{,}880{,}000 \text{ lb/hr}$$

The standard error of the estimate is 38 kW. The regression model is shown graphically in Figure 7-16.

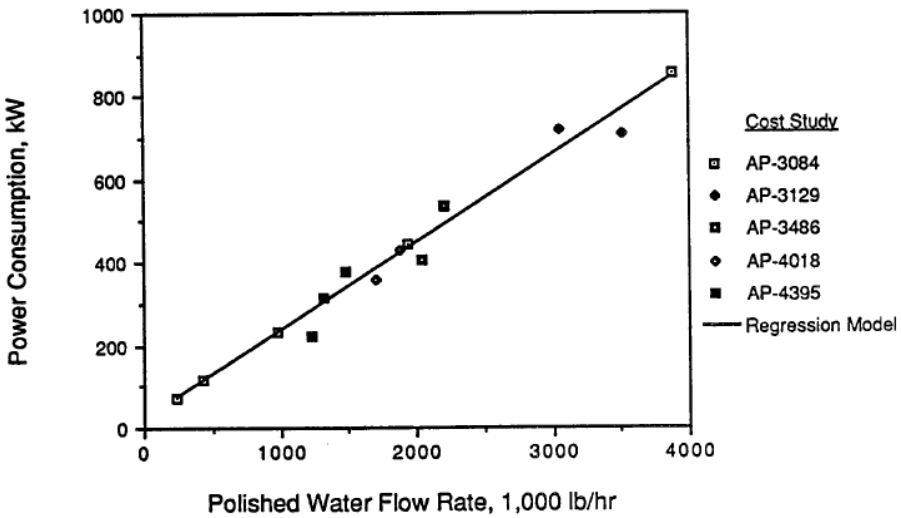

Figure 7-16. Power Requirement for Boiler Feed Water Treating

Process Condensate Treatment

$$W_{e,PC} = 7.34x10^{-4}m_{sbd} \qquad R^2 = 1.00,\ n = 3 \qquad (7\text{-}29)$$

where,

$$196{,}000 \leq m_{sbd} \leq 237{,}000 \text{ lb/hr}$$

The standard error of the estimate is negligible. The regression model is shown graphically in Figure 7-17.

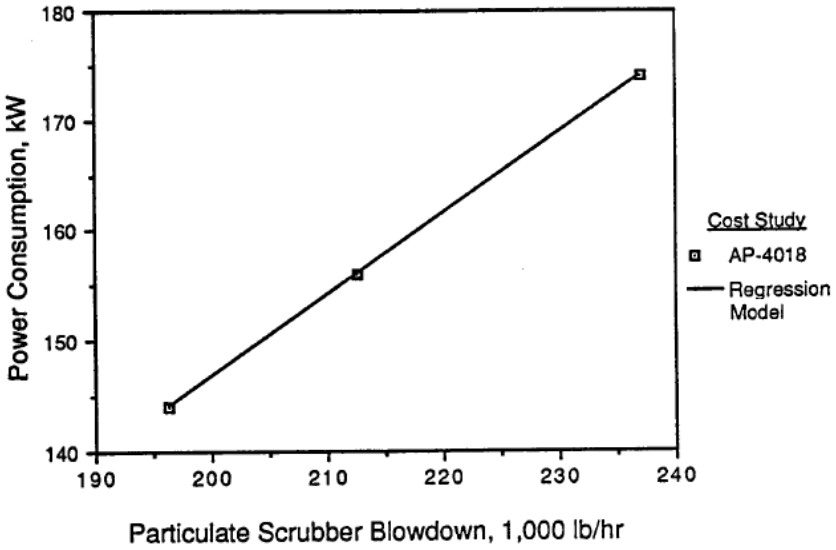

Figure 7-17. Power Requirement for Process Condensate Treatment

7.4 Power Block Cost Model

7.4.1 Power Block Capital Cost

Gas Turbine

There are a number of design factors that affect the cost of a gas turbine in an IGCC process environment. For example, the firing of medium-BTU coal gas, as opposed to high-BTU natural gas, requires modification of the fuel nozzles and gas manifold in the gas turbine (BGE, 1989). Some additional concerns associated with firing coal gas are discussed by Cincotta (1984). The presence of contaminants in the syngas may affect gas turbine maintenance and long-term performance. Liquid droplets may cause uneven combustion or may burn in the turbine first-stage nozzles, causing damage. Solids can deposit on fuel nozzles or cause erosion in the hot gas path of the gas turbine (e.g., combustor, turbine). Alkali materials that deposit on hot gas path parts cause corrosion. It is expected that, at fuel gas temperatures less than 1,000 °F, that alkali material is essentially condensed on any particulate matter in the raw syngas, and that the alkali removal efficiency is approximately the same as the particle removal efficiency. For sufficiently high particle removal efficiencies, erosion is not expected to be a problem. Corrosion is not expected to be any worse than for distillate oil firing. Deposition of particles is expected to be within the allowance of reasonable maintenance schedules. The design for an advanced high firing temperature gas turbine employs advanced air film cooling which could be affected by the ash content of combustion products.

Another design issue is the gas turbine fuel inlet temperature. A study by Fluor (Earley and Smelser, 1988) assumes that hot desulfurized syngas from an advanced hot gas cleanup process is fed directly to the gas turbine at 1,200 °F. The Fluor study indicates that General Electric expects that a fuel system capable of a 1,200 °F fuel inlet temperature could be developed by 1994. The maximum fuel temperature test to date has been at 1,000 °F. An earlier study with hot gas cleanup included a hot gas cooler to reduce the gas temperature to 1,000 °F (Corman, 1986). For the KRW system with cold gas cleanup, the coal gas temperature is within the limits of current technology. However, the gas turbine costs developed here should not be used in conjunction with IGCC systems featuring hot gas cleanup without some adjustments to account for the uncertainty in using a higher fuel inlet temperature.

Unfortunately, there is currently a lack of reported data from which to develop a detailed gas turbine cost model that is explicitly sensitive to the type of factors discussed above. In preliminary cost estimates, the typical approach to accounting for these uncertainties in performance, or for the possibility of increased capital cost due to design modifications, is through process contingency factors. The approach taken here is to use the available cost data for the GE Frame 7F to develop a cost estimate for a single gas turbine. This cost estimate has been encoded using process contingency factors.

Although cost estimates of the GE Frame 7F are available in a number of IGCC cost studies, recent cost estimates are significantly higher than older estimates. However, the more recent estimates are expected to be more reliable, because the Frame 7F was at or near commercialization at the time of the recent studies. In four recent site-specific IGCC studies performed for EPRI (BGE, 1989; Fluor Daniel, 1988, 1989; FPL, 1989), the cost of the Frame 7F in the first phase of a phased IGCC construction schedule ranged from $30.8 to 33.6 million, with an average of $32.0 million (Jan 89). This cost excludes equipment associated with combined cycle systems, which are discussed in the following two sections. In two other studies (JCP&L, 1989; NUSCo, 1988), the cost of the Frame 7F for application in natural gas-fired combined cycle plants was estimated at $28.3 and $26.8 million, respectively. The higher estimate of $32.0 million per unit is consistent with the expectation that the cost of the gas turbine modified to fire medium-BTU coal gas will be higher than for the standard natural gas-fired unit. This high estimate will be used in the cost model:

$$DC_{GT} = 32{,}000\ N_{T,GT} \tag{7-30}$$

A competitor to the GE Frame 7F is under development by Mitsubishi Heavy Industries and Westinghouse Electric. The prototype model 501F is expected to achieve a rating of 148.8 MW and a turbine inlet temperature of 2,300 °F. This model was made available in 1992 (GTW, 1989). No cost data are currently available for this model; however, competition between the Frame 7F and the 501F could result in similar prices for both machines.

A Kraftwerk Union (KWU) gas turbine, model 84.2, was analyzed in an EPRI study (Fluor Daniel, 1988). This is a commercially available, moderate firing temperature machine that is rated at approximately 100 MW with a cost of about $24.2 million per unit. The combustor features a low-NOx design, and does not require water injection when operated on natural gas.

Heat Recovery Steam Generator

The cost of the HRSG is expected to depend on factors such as the high-pressure steam flow rate to the steam turbine, the pressure of the steam, the gas turbine exhaust gas volume flow rate, the number of steam drums, and, to a lesser extent, the boiler feed water or saturated steam flowrates in each of the heat exchangers in the HRSG. A variety of regression models were investigated to represent these potential predictive parameters. However, because only 10 data points are included in the database, only a limited number of predictive parameters can be reasonably included in the model, based on statistical considerations. Furthermore, some parameters that are expected to be important in determining HRSG cost, such as the gas turbine exhaust flow rate, are not statistically important for this data set. When the gas turbine exhaust flow rate, high pressure inlet steam flow rate to the steam turbine, and the steam pressure are included in a regression model, the exponent for exhaust flow rate is small and is not statistically significant. The exhaust gas flow rate is not an influential predictive parameter because the cost studies are based primarily on either GE Frame 7E or 7F gas turbines; therefore, there was not a large range of variation for the exhaust gas flow rate. A simple regression model based only on the high-pressure steam flow rate to the steam turbine yielded a high coefficient of determination. A multivariate regression based on the high-pressure steam flow to the steam turbine and the pressure of the steam yielded satisfactory results:

$$DC_{HR} = 11350 \times N_{T,HR}\left(\frac{P_{hps,HR,o}}{1500}\right)^{1.526} \times \left(\frac{\frac{m_{hps,HR,o}}{N_{O,HR}}}{600000}\right)^{0.242} \qquad \begin{matrix} R^2 = 0.966 \\ n = 10 \end{matrix} \qquad (7\text{-}31)$$

where,

$$650 \le P_{hps,HR,o} \le 1{,}545 \text{ psia; and}$$

$$66{,}000 \le \frac{m_{hps,HR,o}}{N_{O,HR}} \le 640{,}000 \text{ lb/hr}$$

The regression model is shown graphically in Figure 7-18.

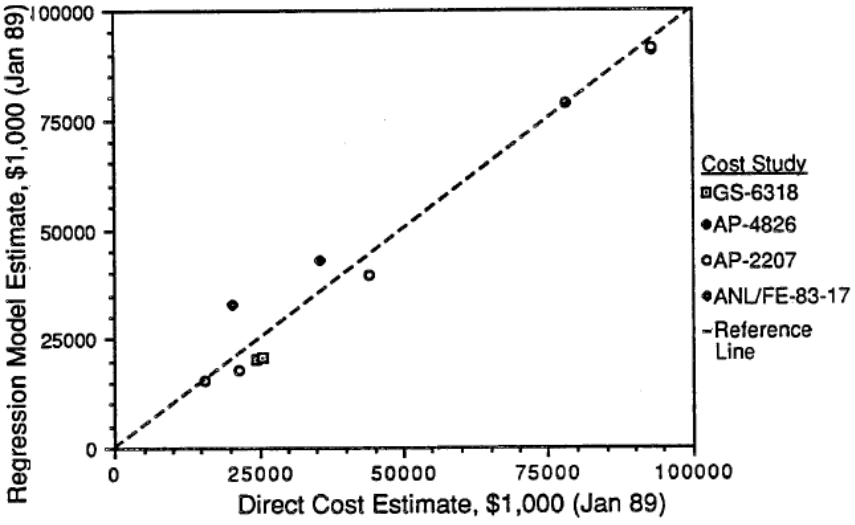

Figure 7-18. Predicted vs. Actual Cost for Heat Recovery Steam Generators.

Steam Turbine

A typical steam turbine for an IGCC plant consists of high-pressure, intermediate-pressure, and low-pressure turbine stages, a generator, and an exhaust steam condenser. The high-pressure stage receives high pressure superheated steam from the HRSG. The outlet steam from the high-pressure stage returns to the HRSG for reheat, after which it enters the intermediate pressure stage. The outlet from the intermediate pressure stage goes to the low-pressure stage.

The cost of a steam turbine is expected to depend on the mass flow rate of steam through the system, the pressures in each stage, and the generator output, among other factors. Nine cost estimates for the steam turbine were available from four studies. A single-variate regression based on the generator output was found to yield reasonable results:

$$DC_c = 158.7 \cdot W_{ST,E} \qquad \begin{matrix} R^2 = 0.958 \\ n = 9 \end{matrix} \qquad (7\text{-}32)$$

where,

$$200 \le W_{ST,E} \le 550 \ \text{MW}$$

Only one steam turbine is used in most IGCC designs. A graphical representation of the regression model is shown in Figure 7-19.

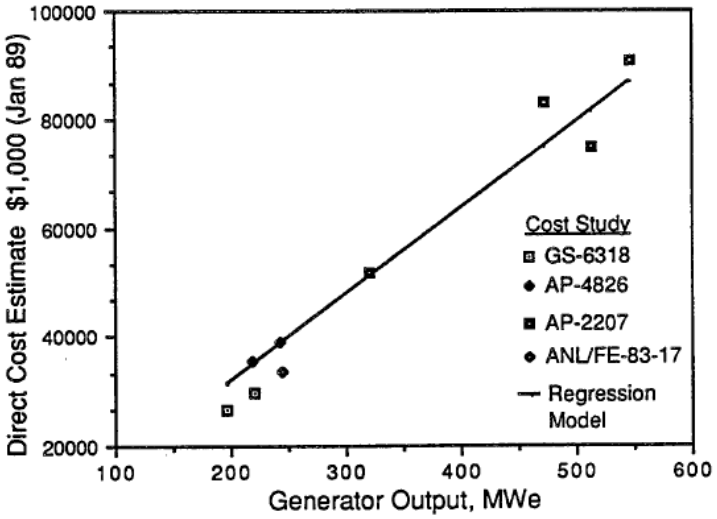

Figure 7-19. Direct Cost for the Steam Turbine-Generator Section

HRSG Feedwater System

The boiler feedwater system consists of equipment for handling raw water and polished water in the steam cycle. This equipment includes a water demineralization unit for raw water, a demineralized water storage tank, a condensate surge tank for storage of both demineralized raw water and steam turbine condensate water, a condensate polishing unit, and a blowdown flash drum. The major streams in this process section are the raw water inlet and the polished water outlet. Data on the cost of the boiler feedwater section and the flow rates of the raw water and polished water streams is available from five studies for 14 plant sizes. These studies include Texaco-based, Shell-based, and KRW-based IGCC systems (Fluor, 1983a; 1983b; 1984; 1985; 1986). Because all of these studies were developed by the same contractor using a consistent approach, they provide an excellent basis for developing a cost model. The boiler feedwater section is generic to the steam cycle.

The cost of the boiler feedwater section is expected to depend on both the raw water flow rate through the demineralization unit and the polished water flow rate through the polishing unit. The polished water flow rate includes primarily both the raw water and the steam turbine condensate. The steam cycle condensate is typically larger than the raw water flow rate. A two-variable regression model of the boiler feed water system cost as a function of the raw water and polished water flow rates was found to yield good results. The cost in 2000 dollars is:

$$DC_{BF} = 0.16 m_{rw}^{0.307} m_{pw}^{0.435} \qquad \begin{matrix} R^2 = 0.991 \\ n = 14 \end{matrix} \qquad (7\text{-}33)$$

where,

$$24{,}000 \le m_{rw} \le 614{,}000 \text{ lb/hr}$$
$$234{,}000 \le m_{pw} \le 3{,}880{,}000 \text{ lb/hr}$$

For this model, a nonlinear variable transformation was used. The error of the linearized model is approximated by a normal distribution. Therefore, the error of the nonlinear model shown above is represented by a lognormal distribution. The median of the errors is 1.0, with a mean of 1.002 and a standard deviation of 0.063. The 90 percent probability range for the error is approximately 0.9 to 1.1, implying a 90 percent confidence band of 90 to 110 percent of the nominal cost estimate.

Typically, only one train of equipment is used in this section, and all the equipment is commercially available. A comparison of the regression model cost estimates and the direct cost estimates from the detailed cost studies is shown in Figure 7-20. This model should not be extrapolated beyond the range of the predictive variables as indicated above. However, because the cost of the boiler feed water section is a very small portion of the total direct cost for a typical IGCC plant, the effect of any errors introduced by modest extrapolations may be acceptable for some purposes.

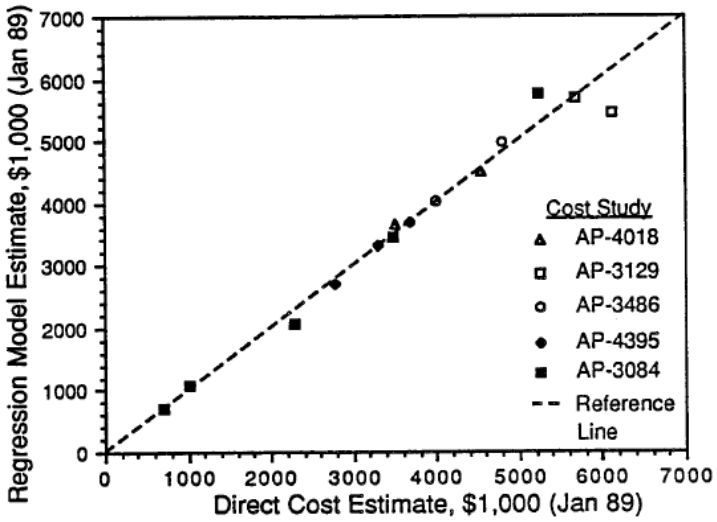

Figure 7-20. Predicted vs. Actual Direct Costs for the Boiler Feedwater Section

References

Bachovchin, D.M., M.A. Alvin, and L. M. Day (1987). "A Study of High Temperature Removal of Alkali in a Pressurized Gasification System." In Proceedings of the Seventh Annual Gasification and Gas Stream Cleanup Systems Contractors Review Meeting, Volume II. U.S. Department of Energy. Morgantown, WV. June, 1987. p. 495-504

Bechtel and WE (1983c). Design of Advanced Fossil Fuel Systems (DAFFS), A Study of Three Developing Technologies for Coal-Fired, Base-Load Electric Power Generation: Integrated Gasification Combined Cycle Power Plant With Westinghouse Gasification Process. Prepared by Bechtel Group, Inc., and Westinghouse Electric Corporation, Synthetic Fuels Division, for the U.S. Department of Energy Argonne National Laboratory. Argonne, Illinois. ANL/FE-83-17. June. 1983

Becker, B., and W. Schulten (1985). "Advanced Gas Turbines for Efficient and Reliable Combined-Cycle Plants." In Proceedings: Conference on Coal Gasification Systems and Synthetic Fuels for Power Generation, Volume 2. Electric Power Research Institute. AP-4257-SR. December 1985. p. 25-1 to 25-21.

BGE (1989). Baltimore Gas and Electric Company's Study of a Shell-Based GCC Power Plant. Prepared by Baltimore Gas and Electric Company for Electric Power Research Institute, Palo Alto, CA. EPRI GS-6283. March 1989.

Brandt, D.E (1988). "The Design and Development of an Advanced Heavy-Duty Gas Turbine" Journal of Engineering for Gas Turbines and Power 110 (1988): 243-250.

Brandt, D.E (1989). "MS7001F Prototype Test Results." ASME Paper No. 89-GT-102. 1989.

Brooks, F.J. (2000), "GE Gas Turbine Performance Characteristics," GER-3567H, GE Power Systems, Schenectady, NY.

Cincotta, G.A. (1984). Gas Turbine Systems Research and Development Program. Prepared by the General Electric Company for the U.S. Department of Energy Morgantown Energy Technology Center. Morgantown, WV. DOE/MC/20315-1767-Exec. Summ. September 1984.

Cohen, H., G.F.C. Rogers, and H.I.H. Saravanamuttoo (1987). Gas Turbine Theory, 3rd Ed. Longman Scientific and Technical. New York. 1987.

Cool Water (1988). Cool Water Coal Gasification Program: Fifth Annual Progress Report. Prepared by Cool Water Coal Gasification Program, Bechtel Power Corporation, and Radian Corporation for the Electric Power Research Institute, Palo Alto, CA. EPRI AP-4832. October. 1988

Corman, J.C. (1986). System Analysis of Simplified IGCC Plants, Topical Report. Prepared by General Electric Company for U.S. Department of Energy, Morgantown Energy Technology Center, Morgantown, West Virginia. DOE/ET/14928-2233. September 1986.

Dawkins, R.P., et al. (1986). Screening Evaluation of Advanced Power Cycles. Prepared for Electric Power Research Institute by Fluor Technology, Inc. AP-4826. November 1986.

Davis, L.B., M.B. Hilt, and R.B. Schiefer (1987). "NOx Emissions from Advanced Gas Turbines Fired on MBTU Gases." In Proceedings: Sixth Annual EPRI Contractors' Conference on Coal Gasification. Electric Power Research Institute. AP-5343-SR. October 1987. p. 16-1 to 16-16.

Earley, P.I., and S.C. Smelser (1988a). Design and Economics of a Coal-to-Pipeline-Gas Facility Using KRW Gasifiers with Reduced Carbon Conversion. Prepared by Fluor Technology, Inc. for Gas Research Institute. Chicago, Illinois. GRI-87/0169. January 1988. OR Earley, P.I. and S.C. Smelser (1988b). Design and Economics of a Plant to Convert Eastern Bituminous Coal to Pipeline Gas or Power Using KRW Gasifiers With In-Bed Desulfurization. Prepared by Fluor Technology, Inc. for Gas Research Institute. Chicago, Illinois. GRI-87/0166. September 1988.

Entrekin, H.D., and T.R. Edwards (1987). Effects of Load Following on Gas Turbine Emissions and Ambient Air Quality. Presented at the 80th Annual Meeting of the Air and Waste Management Association, New York, NY. June 21-26.

EPRI (1986). TAG(tm) - Technical Assessment Guide, Volume 1: Electricity Supply - 1986. EPRI P-4463-SR. Electric Power Research Institute, Inc. December 1986

Eustis, F. H. and M.S. Johnson (1990), "Gas Turbine Effects on Integrated-Gasification-Combined-Cycle Power Plant Operations," GS/ER-6770, Prepared by Stanford, University for Electric Power Research Institute, Inc, Palo Alto, CA, March.

Farmer, R (1997); Gas Turbine World; Pequot Publishing Inc., Fairfield, CT; Vol 18., p 44.

Flagan, R.C. and Seinfeld, J.H. (1988). Fundamentals of air pollution engineering. Prentic Hall.

Fluor (1983a). Economic Assessment of the Impact of Plant Size on Coal Gasification Combined Cycle Plants. Prepared by Fluor Engineers, Inc. for Electric Power Research Institute. Palo Alto, CA. EPRI AP-3084. May.

Fluor(1983b). Shell-Based Gasification-Combined-Cycle Power Plant Evaluations. Prepared by Fluor Engineers, Inc. for Electric Power Research Institute, Palo Alto, CA. EPRI AP-3129. June 1983.

Fluor (1984). Cost and Performance for Commercial Applications of Texaco-Based Gasification-Combined-Cycle Plants: Volume 1, Summary and Discussion of Results, and Volume 2, Design Details. Prepared by Fluor Engineers, Inc. for Electric Power Research Institute, Palo Alto, CA. EPRI AP-3486. April 1984.

Fluor (1985). Cost and Performance of Kellogg Rust Westinghouse-based Gasification-Combined-Cycle Plants. Prepared by Fluor Engineers, Inc. for Electric Power Research Institute, Palo Alto, CA. EPRI AP-4018. June 1985.

Fluor (1986). Planning Data Book for Gasification Combined Cycle Plants: Phased Capacity Additions. Prepared by Fluor Engineers, Inc. for Electric Power Research Institute. Palo Alto, CA. EPRI AP-4395. January 1986.

Fluor Daniel (1988). Evaluation of a Texaco Gasification Combined Cycle Plant with Kraftwerk Union Gas Turbines. Prepared by Fluor Daniel, Inc. for Electric Power Research Institute, Inc. Palo Alto, CA. EPRI GS-6160. December 1988.

Fluor Daniel (1989). Evaluation of a Dow-Based Gasification Combined Cycle Plant Using Low-Rank Coals. Prepared by Fluor Daniel, Inc. for Electric Power Research Institute, Inc. Palo Alto, CA. EPRI GS-6318. April 1989.

Fluor Technology (1986b). Screening Evaluation of Advanced Power Cycles. Prepared by Fluor Technology, Inc. for Electric Power Research Institute, Palo Alto, CA. EPRI AP-4826. November 1986.

Folsom, B.A., C.W. Courtney, and M.P. Heap (1980). "The Effect of LBG Composition and Combustor Characteristics on Fuel NOx Formation." Journal of Engineering for Power 102 (1980):459-467.

Foster-Pegg R. W., 1986, “Capital Cost of Gas-Turbine Heat Recovery Boilers“, Chemical Engineering, Vol. 93, n. 14, pp. 73-78.

FPL (1989). Florida Power and Light Company's Study of Shell-Based GCC Power Plants. Prepared by Florida Power and Light Company for Electric Power Research Institute, Inc. Palo Alto, CA. EPRI GS-6176. January 1989.

Frey, H.C. and N. Akunuri (2001), “Probabilistic Modeling and Evaluation of the Performance, Emissions, and Cost of Texaco Gasifier-Based Integrated Gasification Combined Cycle Systems Using ASPEN, Prepared by North Carolina State University for Center for Energy and Environmental Studies, Carnegie Mellon University, Pittsburgh, PA.

Frey, H.C. and E.S. Rubin (1991), “Development and Application of a Probabilistic Evaluation Method for Advanced Process Technologies,” DOE/MC 24248-3105 (DE91002095), Prepared by Carnegie Mellon University for U.S. Department of Energy, Morgantown, WV, April.

Farmer, R. (1989). "150 MW Class 501F Design to Begin Full Load Factory Testing This Summer," Gas Turbine World. May-June 1989. pp 12-17

Hester, J.C., and D.E. Pless (1990). Proposed Demonstration of An Air Blown Coal Gasification Combined Cycle Gas Turbine Concept. Presented at the Seventh Annual International Pittsburgh Coal Conference. September, 1990.

Holt, N.A., E. Clark, and A. Cohn (1989). "NOx Control in Coal Gasification Combined Cycle Systems." In 1989 Symposium on Stationary Combustion Nitrogen Oxide Control, Volume 1. Electric Power Research Institute. GS-6423. July 1989. p. 5A-17 to 5A-28.

METC (1987). Gas Stream Cleanup: Technology Status Report. Morgantown Energy Technology Center, U.S. Department of Energy. Morgantown, WV. DOE/METC-87/0255. October.

Moore-Staub, A.L., et al**.** (1990). Gas Turbine Cogeneration Unit PSD BACT Determination: A 1990 Case Study. Presented at the 83rd Annual Meeting of the Air and Waste Management Association. Pittsburgh, PA. June

Notestein, J.E (1989). "Update on Department of Energy Hot Gas Cleanup Programs." In Eighth Annual EPRI Conference on Coal Gasification. Electric Power Research Institute. GS-6485. August 1989. p. 14-1 to p. 14-43

Parsons (1982). Evaluation of Coal Gasification-Combustion Turbine Power Plants Emphasizing Low Water Consumption. Prepared by Ralph M. Parsons Company for Electric Power Research Institute. Palo Alto, CA. EPRI AP-2207. January 1982.

Pillsbury, P (1989). Westinghouse. personal communication.

Sato, M., et al**.** (1989). "Development of a Low-NOx LBG Combustor for Coal Gasification Combined Cycle Power Generation Systems." ASME Paper No. 89-GT-104. 1989.

Scalzo, A.J. et al. (1989). "A New 150 MW High-Efficiency Heavy-Duty Combustion Turbine." Journal of Engineering for Gas Turbines and Power 111 (1989): 211-217.

Simbeck, D.R., R.L. Dickenson, and E.D. Oliver (1983). Coal Gasification Systems: A Guide to Status, Applications, and Economics. Prepared by Synthetic Fuels Associates for the Electric Power Research Institute, Palo Alto, CA. AP-3109. June.

Smock, R. "Gas Turbines Dominate New Capacity Ordering," Power Engineering Magazine. August 1989. pp 23-28.

Touchton, G.L (1984). "An Experimentally Verified NOx Prediction Algorithm Incorporating the Effects of Steam Injection." Journal of Engineering for Gas Turbines and Power 106 (1984): 833-840.

Touchton, G.L (1985). "Influence of Gas Turbine Combustor Design and Operating Parameters on Effectiveness of NOx Suppression by Injected Steam or Water" Journal of Engineering for Gas Turbines and Power 107 (1985): 706-713.

Unnasch, S., R. Chang, and H. Mason (1988). Study of Ammonia Removal in Coal Gasification Processes Using Integrated Systems Approach. Final Report. Prepared by Acurex Corporation for U.S. Department of Energy Morgantown Energy Technology Center. Morgantown, West Virginia. DOE/MC/23275-2589. March.

Wark, K. (1983). Thermodynamics, Fourth Edition. McGraw-Hill Book Company: New York.

8. CO_2 Transport

Abstract

The modeling of carbon dioxide (CO_2) transport via pipeline is important as pipeline is the primary mode by which CO_2 captured from power plants can be moved from the plant site to the sequestration site. The cost of CO_2 transport has been estimated by developing performance and cost models for CO_2 transport by pipeline. The performance model estimates the required pipeline diameter as a function of engineering and design parameters, such as pipeline length and design CO_2 mass flow. The economics model estimates the capital, and operating and maintenance cost of CO_2 transport by pipeline as a function of parameters such as the project lifetime, discount rate, and operating and maintenance charges. The cost model has been developed by regressing data on actual U.S. pipeline construction projects (for natural gas) Using these models with a set of illustrative parameters, the cost of transporting 5 million tonnes per year of CO_2, which is approximately the annual emissions of a 600 MW (net) pulverized coal fired power plant capturing 90% of the CO_2 produced, over 100 km in the Midwest is $1.2 per tonne. The cost of CO_2 transport decreases non-linearly with increasing amounts of CO_2 transported, and increases non-linearly with the length of the pipeline. For longer pipeline lengths, the cost of CO_2 transport can also be lowered by adding booster stations. A sensitivity analysis on several design and economic parameters has shown that the median cost to transport 5 million tonnes per year of CO_2 over 100 km is between $1.1 and $1.9 per tonne depending on the geographic region of the U.S. The sensitivity analysis has shown the parameters that most affect the transport cost are, in decreasing order of importance: load factor, capital recovery factor, labor escalation factor, and inlet pressure.

Nomenclature

p = Absolute pressure (Pa)

$\mathbf{p_r}$ = Reduced pressure

$\mathbf{p_c}$ = Critical pressure (K)

R = Gas constant (m^3 Pa/mol/k)

ρ = Fluid density (kg/m^3)

ν = Specific volume (m^3/kg)

$\dot{\nu}$ = Molar volume (m^3/mol)

T = Absolute temperature (K)

$\mathbf{T_r}$ = Reduced temperature

$\mathbf{T_c}$ = Critical temperature (K)

Z = Compressibility factor

M = Molecular mass (g/mol)

ω = Pitzer acentric factor

$\mathbf{k_{ij}}$ = Peng-Robinson binary interaction parameter

g = Acceleration due to gravity (m/s^2)

$\mathbf{g_c}$ = Gravitational constant

$\mathbf{h_i}$ = Height at location **i** (m)

u = Average fluid velocity (m/s)

η = Pump efficiency

$\mathbf{f_F}$ = Fanning friction factor

L = Pipe segment length (m)

D = Pipe inner diameter (m)

$\dot{m}$ = Mass flow rate (Kg/s)

ε = Pipe roughness (mm)

Re = Reynolds number

μ = Viscosity (Pa s)

$\dot{Q}$ = Volumetric flow rate (m^3/s)

P = Pump power (W)

$\mathbf{D_1}$ = Initial segment diameter (m)

$\mathbf{D_n}$ = n^{th} segment diameter (m)

$\mathbf{N_S}$ = Number of segments

$\mathbf{N_B}$ = Number of booster pumping stations

$\mathbf{C_P}$ = Cost of power ($/MWh)

8.1 Introduction

Government regulators, policy-makers (public and private), and other interested parties require methods to estimate the cost of potential global climate change mitigation measures. One possible measure to reduce emissions of carbon dioxide (CO_2) to the atmosphere is carbon capture and storage (CCS). This report details the development of a model that calculates the pipeline transport cost of CO_2 from the site of capture to the location of storage. This model will complement and link to the previously developed Integrated Environmental Control Model (IECM), which can be used to assess CO_2 capture options for various types of power plants (Rao, et al. 2004).

Pipeline transport has been selected as the mode of CO_2 transportation for this model because of it is the only reasonable method for terrestrial transport of the large quantities of CO_2 involved (Skovholt, 2003; Svensson et al. 2004). Furthermore, there is considerable experience in the transport of CO_2 by pipeline, as upwards of 50 million tonnes per year of CO_2 is transported over nearly 3100 km of pipelines primarily for use in EOR operations (Gale et al. 2004; Smith et al. 2001; Bock et al. 2003; Doctor et al. 2005; Kinder Morgan, 2002).

In this report, the pipeline transport model is used to estimate the cost per tonne of transporting CO_2 from a range of power plant sizes over variable distances and, to assess the effect of additional booster compression stations on the transport cost. Furthermore, in an attempt to quantify the sensitivity of the model to uncertainty and variability in the parameters, a probabilistic analysis has been performed, which shows the range of costs that could occur and the probability associated with these costs for specific scenarios.

8.2 Pipeline Transport Process Description

The performance model takes as input engineering design parameters, such as pipeline length and design CO_2 mass flow and calculates the required pipe diameter. The transport performance model is based on previous work by the Massachusetts Institute of Technology (MIT) for the United States Department of Energy (DOE) and has been revised to include a comprehensive physical properties model for CO_2 and other fluids of interest (e.g., H_2S) and to account for the compressibility of CO_2 during transport; booster pumping station options; segment elevation changes, and; probabilistic assessment capabilities (Bock et al. 2004). Figure 8-1 shows the inputs and outputs from the performance model, and how the performance model interacts with the pipeline cost model and the CO_2 properties model.

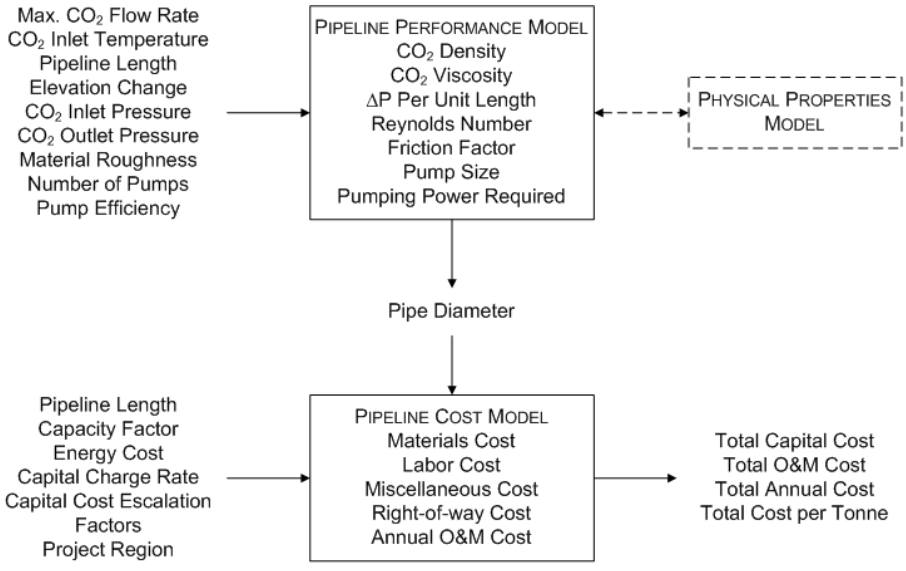

Figure 8-1. The boundaries, inputs, and output from the pipeline model

8.2.1 Physical Properties of Carbon Dioxide

At ambient temperatures and pressures, CO_2 is a gas with a density higher than that of air. However, efficient transport of CO_2 via pipeline requires that CO_2 is compressed and cooled to the liquid state. Transportation at lower densities (i.e., gaseous CO_2) is inefficient because of the large volumes that need to be moved. In pipeline transport, the density of CO_2 varies between 800 kg/m^3 and 1000 kg/m^3. For comparison, the density of water under these conditions is approximately 1000 kg/m^3. Figure 8-2 shows the density of CO_2 as a function of temperature for several isobars in the transport region.

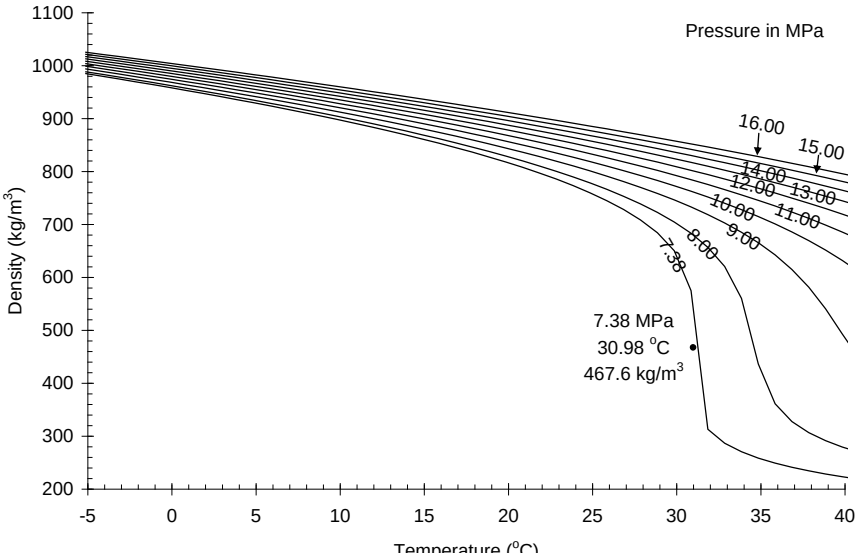

Figure 8-2. The density of carbon dioxide as a function of temperature for several isobars in the transport range.

The typically long length of a CO_2 pipeline means that it can be treated approximately as an isothermal system, where the CO_2 is at the temperature of the earth surrounding the pipeline.

In northern countries, the soil temperature varies from a few degrees below zero in the winter to 6-8 ^oC in summer (Skovholt, 1993). In warmer countries, the soil temperature may reach up to 20 ^oC (Skovholt, 1993). Under these temperature conditions, CO_2 liquefies at pressures greater than 3 MPa to 5 MPa. However, in a pipeline crossing hilly terrain, the pressure at the tops of the hills may drop below 3 MPa to 5 MPa, which would result in two-phase flow, i.e., slugs of both liquid and gas in the pipeline. Two-phase flow is highly undesirable as slugs of fluid can damage flow metering and pumping or compression equipment. Thus, as can be seen in Figure 8-3, if the pipeline is operated at pressures greater than the critical pressure of CO_2, which is 7.38 MPa, two-phase flow is not possible at any temperature. Skovholt calls this the "dense phase condition." (Skovholt, 1993)

To ensure that the flow in the pipeline remains liquid under all conditions it is recommended that the CO_2 pipeline operating pressure not be allowed to drop below 8.6 MPa at 4°C (Mohitpour, 2003). Conversely, for pipe with ASME-ANSI 900# flanges the maximum allowable operating pressure is 15.3 MPa at 38°C (Mohitpour et al. 2003).

The design of CO_2 pipelines is dependent on the physical and transport properties (e.g., density and viscosity) of CO_2, thus it is necessary to use accurate representations of the phase behavior, density, and viscosity of CO_2 in their design. Other models, such as the MIT model (Bock, 2003), have used correlations that approximate the density and viscosity of CO_2. The shortcoming of these types of correlations is that they are only accurate over a small range of pressure and temperature and for pure CO_2. Conversely, chemical & petroleum industry process simulators (e.g., Aspen Plus or HYSYS) use generalized equations of state to represent the physical properties of multi-component liquid and gas mixtures accurately across a wide range of pressures and temperatures.

This model calculates physical properties of CO_2 and CO_2 containing mixtures using a cubic equation of state with Peng-Robinson parameters, and mixing rules employing a binary interaction parameter (Reid, 1987). Equation (8-1) shows the form of the cubic equation of state for a fluid mixture of **n** pure components.

$$p = \frac{RT}{\hat{v} - b_m} - \frac{a_m}{\hat{v}^2 + 2b_m\hat{v} - b_m^2} \tag{8-1}$$

In Equation (8-1), **p** is the system pressure, R is the ideal gas constant, **T** is the absolute temperature of the system, $\hat{v}$ is the molar volume of the system, and, **am** and **bm** are constants defined below.

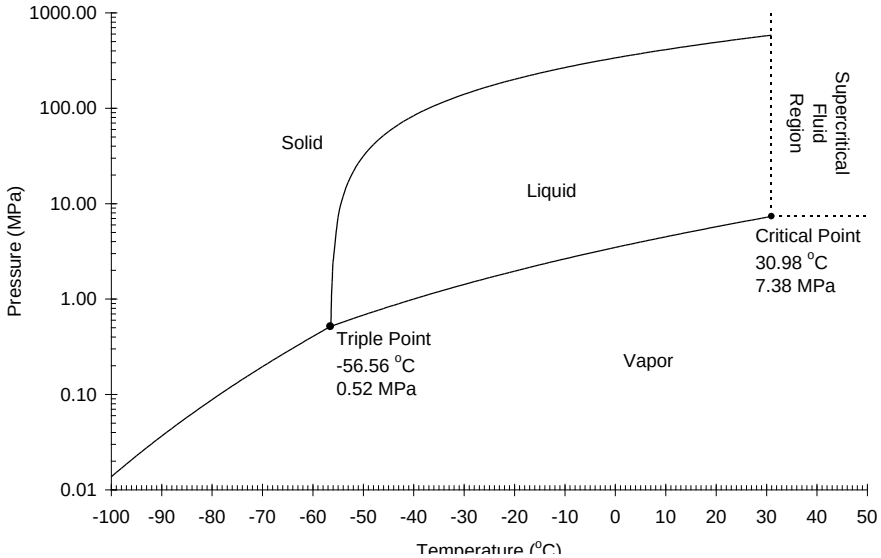

Figure 8-3. Phase diagram for CO2 showing the sublimation, melting, and boiling curves as well as the triple point and the critical point.

Equations (8-2) and (8-3) show the Peng-Robinson parameters for pure component **i**, and Equation (8-4) shows the mixing rules used to arrive at the mixture parameters for use in Equation (8-1).

$$a_i = \frac{0.45724 R^2 T_{c,i}^2}{p_{c,i}} \left[1 + f(\omega_i)\left(1 - T_{r,i}^{1/2}\right)\right]^2 \tag{8-2}$$

where,

$$f(\omega_i) = 0.37464 + 1.54226\omega_i - 0.26992\omega_i^2$$

$$b_i = \frac{0.07780 R T_{c,i}}{p_{c,i}} \tag{8-3}$$

$$a_m = \sum_i^n \sum_j^n y_i y_j \left(a_i a_j\right)^{1/2} \left(1 - k_{ij}\right)$$

$$b_m = \sum_i^n y_i b_i \tag{8-4}$$

In Equations (8-2) through (8-4), **i** and **j** denote different pure components, $\mathbf{T_r}$ is the reduced temperature of the pure component, **ω** is the Pitzer acentric factor for the pure component, and $\mathbf{k_{ij}}$ is the Peng-Robinson binary interaction parameter for the fluid pair.

The model uses an analytical method to solve Equation (8-1) for the specific volume of the fluid, which can then be easily converted to density. For pure CO_2, the relative error between the density predicted by the reference equation of state developed by Span and Wagner (Span et al. 1986) and the density of CO_2 estimated by the Equation (8-1) is less than 9% in range of interest for the transport model, and averages approximately 2%. Figure 8-4 shows the relative error over this range.

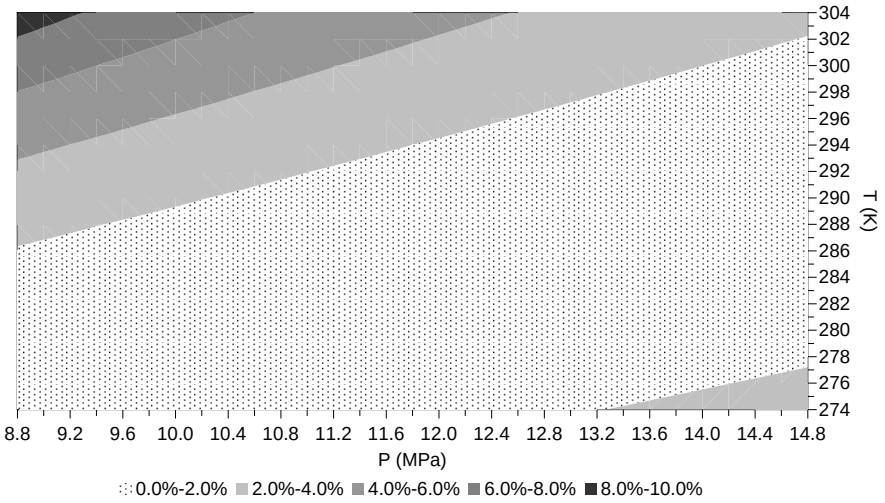

Figure 8-4. Relative error between the density of CO_2 calculated by the Peng-Robinson equation of state and the density of CO_2 as predicted by the Span and Wagner equation of state in the range of pressures and temperatures of interest for the transport model.

The viscosity of CO_2 and CO_2-containing mixtures is calculated via the Chung et al. method (Chung, 1988), extended to high pressures by Reid, Prausnitz, and Poling (Reid et al. 1987). This method, like the Peng-Robinson equation of state, is fundamentally based on the thermodynamic properties of the fluid mixture. However, unlike the Peng-Robinson Equation of state it requires the solution of over a dozen equations. For the details of this method, see Reid, Prausnitz, and Poling (Reid et al. 1987).

For pure CO_2, the relative error between the viscosity predicted by the reference equation of state developed by Vesovic (Vesovic et al. 1990) and modified by Fenghour (Fenghour et al. 1998) and the viscosity of CO_2 estimated by Equation (8-1) is less than 11% in range of interest for the transport model, and averages approximately 4%. Figure 8-5 shows the relative error over this range.

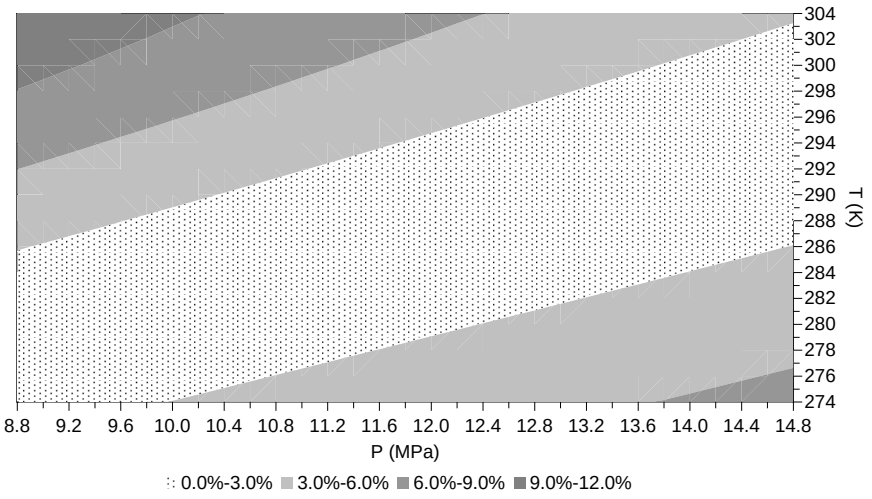

Figure 8-5. Relative error between the viscosity calculated by the Chung et al. method and the viscosity predicted by the model of Vesovic et al. (modified by Fenghour et al) for the range of temperatures and pressures of interest in the transport model.

8.2.2 Pipe Segment Engineering and Design

While liquid CO_2 is relatively incompressible when compared with gaseous CO_2, the small compressibility of the liquid over the relatively long distance of the pipeline can result in non-trivial error if the CO_2 is assumed to be incompressible. For example, for a 100 km long pipeline with the same inlet and outlet pressures, the diameter predicted by a model that does not consider compressibility is 2 in less than the diameter predicted by a model which considers compressibility.‡ Thus, liquid CO_2 is considered a compressible fluid in the model. Additionally, as mentioned previously, the pipeline flow process and pumping processes are treated as isothermal.

The required pipe diameter is calculated from an energy balance on the flowing CO_2. Equation (8-5) shows the differential form of this energy balance, which will be integrated in following steps by making several simplifying assumptions. Equation (8-5) accounts for changes in kinetic energy, pressure-volume work, changes in potential energy, and energy loss due to skin friction.

$$\frac{c}{g_c v}du + \frac{1}{v}dp + \frac{g}{g_c v^2}dh + \frac{2 f_F c^2}{g_c D}dL = 0 \tag{8-5}$$

In Equation (8-5): **c** is a constant equal to the product of density, **ρ**, and fluid velocity, **u**; **g** is acceleration due to gravity; $\mathbf{g_c}$ is the conversion factor converting force units (in the SI system of units, this is equal to unity); **v** is the specific volume of fluid; **p** is pressure; **h** is height; $\mathbf{f_F}$ is the fanning friction factor (McCabe, 1993); **D** is the pipeline diameter; and **L** is the length of the pipe segment.

Each term in Equation (8-5) has to be integrated over the length of the pipe segment between the upstream and downstream conditions, represented as points 1 and 2, respectively. The first term in Equation (8-5) to integrate is the kinetic energy term, which is integrated with a simple substitution in Equation (8-6).

$$\int_1^2 \frac{c}{g_c v}du = \frac{c^2}{g_c}\ln\left(\frac{u_2}{u_1}\right) \tag{8-6}$$

Integration of the pressure-volume work term in Equation (8-5) is somewhat more complex, and requires substitution of the compressibility for specific volume, and definition of average pressure and temperature conditions. For any fluid, compressibility is defined as:

$$Z = \frac{pvM}{RT} \tag{8-7}$$

where, **R** is the ideal gas constant, **T** is the absolute temperature of the fluid, and **M** is the molecular weight of the fluid. Thus, the specific volume can be rewritten in terms of the compressibility as:

$$v = \frac{ZRT}{pM} \tag{8-8}$$

Substituting the definition of specific volume given above in Equation (8-8) into the pressure-volume work term of Equation (8-5) results in Equation (8-9):

$$\int_1^2 \frac{1}{v}dp = \int_1^2 \frac{pM}{ZRT}\,dp = \frac{M\left(p_2^2 - p_1^2\right)}{2Z_{ave}RT_{ave}} \tag{8-9}$$

The average temperature, $\mathbf{T_{ave}}$, and pressure, $\mathbf{P_{ave}}$, required in Equation (8-9) are defined in Equations (8-10) and (8-11), respectively. The derivation of the average pressure definition can be found (Mohitpour et al. 2003):

$$T_{ave} = \frac{T_1 + T_2}{2} \tag{8-10}$$

‡ All units in this report are in *SI* units with the exception of pipe diameter, which is commonly measured in inches (in).

$$P_{ave} = \frac{2}{3}\left(p_2 + p_1 - \frac{p_2 p_1}{p_2 + p_1} \right) \tag{8-11}$$

Integration of the potential energy term is relatively simple using the definitions of average temperature and pressure, and the result is given in Equation (8-12).

$$\int_1^2 \frac{g}{g_c v^2}\, dh = \frac{g p_{ave}^2 M^2}{g_c Z_{ave}^2 R^2 T_{ave}^2}\left(h_2 - h_1\right) \tag{8-12}$$

The friction loss term is integrated in Equation (8-13).

$$\frac{2 f_F c^2}{g_c D}\int_1^2 dL = \frac{2 f_F c^2}{g_c D} L \tag{8-13}$$

The result of integrating Equation (8-5), is then given below:

$$\frac{c^2}{g_c}\ln\left(\frac{u_2}{u_1}\right) + \frac{M\left(p_2^2 - p_1^2\right)}{2 Z_{ave} R T_{ave}} + \frac{g p_{ave}^2 M^2}{g_c Z_{ave}^2 R^2 T_{ave}^2}\left(h_2 - h_1\right) + \frac{2 f_F c^2 L}{g_c D} = 0 \tag{8-14}$$

where, for pipe with a circular cross section:

$$c = \frac{4\dot{m}}{\pi D^2} \tag{8-15}$$

Solving Equation (8-14) for the internal diameter results in the following equation:

$$D = \left\{ \frac{-64 Z_{ave}^2 R^2 T_{ave}^2 f_F \dot{m}^2 L}{\pi^2\left[g_c M Z_{ave} R T_{ave}\left(p_2^2 - p_1^2\right) + 2 g P_{ave}^2 M^2 \left(h_2 - h_1\right)\right]} \right\}^{1/5} \tag{8-16}$$

Where $\dot{m}$ is the design (i.e., maximum annual) mass flow rate of CO_2. Thus, Equation (8-16) can be used to calculate the pipe diameter required for a given pressure drop. Complicating this, however, is the Fanning friction factor, which is a function of the pipe diameter. The Fanning friction factor cannot be solved for analytically, thus an explicit approximation for Fanning friction factor is given by Equation (8-17) (Zigrang et al. 1982):

$$\frac{1}{2\sqrt{f_F}} = -2.0 \log\left\{ \frac{\varepsilon/D}{3.7} - \frac{5.02}{\mathrm{Re}} \log\left[\frac{\varepsilon/D}{3.7} - \frac{5.02}{\mathrm{Re}} \log\left(\frac{\varepsilon/D}{3.7} + \frac{13}{\mathrm{Re}} \right) \right] \right\} \tag{8-17}$$

where ε is the roughness of the pipe, which is approximately 0.0457 mm for commercial steel pipe (Boyce, 1997), and Re is the Reynolds number. The Reynolds number is given by Equation (8-18):

$$\mathrm{Re} = \frac{4\dot{m}}{\mu \pi D} \tag{8-18}$$

Where **μ** is the viscosity of the fluid. As a result, Equations (8-16), (8-17), and (8-18) must be solved iteratively to determine the pipe diameter. In the iteration scheme, Equation (8-18) is first calculated using an initial guess for the pipe diameter, and then the calculated Reynolds number is substituted into Equation (8-17). The Fanning friction factor is then substituted into Equation (8-16), which leads to an updated diameter, which is compared with the value at the previous iteration. The values for the diameter converge to within 10^{-6} m in less than 10 iterations.

8.2.3 Booster Pump Engineering and Design

Booster pumping stations may be required for longer pipeline distances, or for pipelines in mountainous or hilly regions with large increases in elevation. Additionally, in some cases the use of booster pumping stations may allow a smaller pipe diameter to be used, reducing the cost of CO_2 transport.

The pumping station size is developed from the energy balance on the flowing CO_2, Equation (8-5), in a manner similar to the calculation of the pipe segment diameter. However, both the pumping station size and pipeline diameter are calculated on the basis of the maximum design mass flow rate of CO_2, while the pumping station annual power consumption is calculated on the basis of the nominal (i.e., annual average) mass flow rate of CO_2. The nominal mass flow rate of CO_2 is the product of the pipeline load factor and the design mass flow rate of CO_2. Pumping station size is required to determine the capital cost of the pump, while the pumping station annual power requirement is required to calculate operating cost.

For the calculation of the pumping station size, liquid phase CO_2 is considered an incompressible fluid and pumping processes are treated as isothermal. In addition to the assumption of incompressibility, the assumptions in the derivation of the pumping station size and power requirement are: no elevation change, and no change in velocity between the inlet and the outlet of the pump. Equation (8-19) results from simplifying the energy balance using these assumptions:

$$P = \frac{\dot{Q}\Delta p}{\eta} \tag{8-19}$$

Where P is the required pump power, $\dot{Q}$ is the volumetric flow rate, and **η** is the pump efficiency, which accounts for all frictional losses.

8.2.4 Illustrative Performance Model Results

Figure 8-6 shows the internal diameter in inches of a pipeline carrying pure CO_2 as a function of the CO_2 mass flow rate, as calculated by Equations (8-16), (8-17), and (8-18). This figure shows discrete steps in pipeline diameter because pipe is generally only available in certain common diameters, referred to as Nominal Pipe Sizes (NPS). In addition, the pipe wall thickness must be accounted for to determine the inner diameter of the line pipe used in the calculations. The conversions between NPS and maximum inner diameter of line pipe are listed in Table 8-1.

For example, a pipeline spanning a distance of 100 km, designed to carry 5 million tonnes per year of CO_2 at a pressure drop of 28 kPa/km, requires an internal diameter of 15 inches, based on Equations (8-16), (8-17), and (8-18). However, since this size is not a common line pipe size, the next largest NPS is selected by the model, which is 16 inches, resulting in an internal diameter of about 15.5 inches.

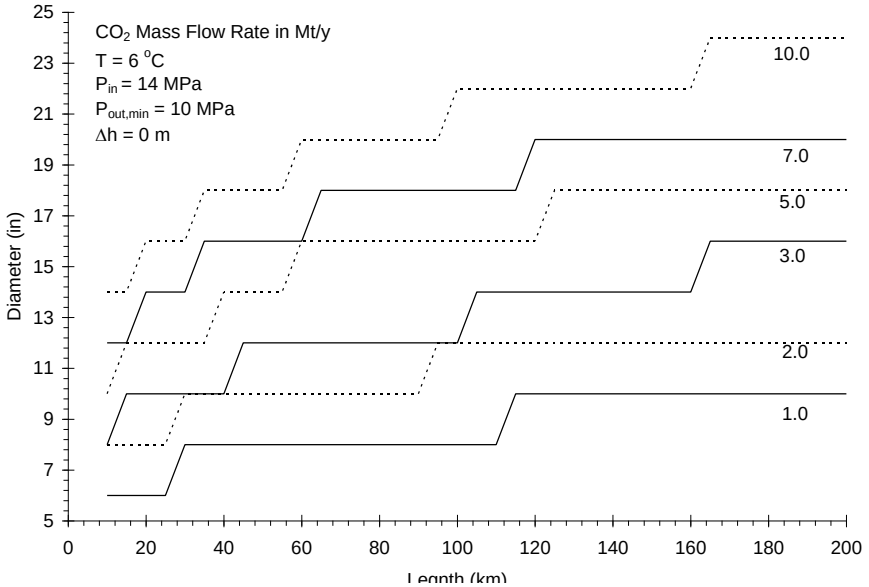

Figure 8-6. Pipeline diameter as a function of length for several flow rates in Mt/y for isothermal flow at 12ºC.

Table 8-1. Conversions between NPS and maximum inner pipe diameter (Mohitpour, 2003)

Nominal Pipe Size (NPS)	Pipe OD (inch)	Minimum Wall Thickness (inches)	Maximum Pipe ID (inch)
4	4.5	0.126	4.248
6	6.626	0.126	6.312
8	8.626	0.157	8.312
10	10.752	0.189	10.374
12	12.752	0.189	12.374
14	14	0.209	13.582
16	16	0.220	15.560
18	18	0.220	17.560
20	20	0.220	19.560
22	22	0.236	21.528
24	24	0.252	23.496
26	26	0.264	25.472
30	30	0.287	29.426
34	34	0.311	33.378
36	36	0.323	35.354
42	42	0.354	41.292
48	48	0.402	47.196

8.3 Pipeline Transport Cost Models

The pipeline transport economic models take output from the performance model (i.e., pipeline diameter) combined with a user-specified pipeline length and the pipeline project region to estimate the capital cost and annual operating costs of the pipeline, as shown in Figure 8-1.

Cost data for actual CO_2 pipelines are not readily available; nor are such projects as prevalent as oil or natural gas pipelines. For these reasons, the data set used to develop the pipeline capital cost models is based on natural gas pipelines; however, there are many similarities between transport of natural gas and CO_2. Both CO_2 and natural gas are transported at similar pressures, approximately 10 MPa (or greater), and assuming that the CO_2 is dry, both pipelines will require similar grades of steel. Thus, at the level of a preliminary analysis where predicted costs might differ from actual costs by approximately 30%, using models based on natural gas pipelines is a reasonable approximation.

8.3.1 Pipeline Data Set

The CO_2 pipeline model cost regression is based on natural gas pipeline project costs published in the **Oil and Gas Journal** between 1995 and 2005 (True, 1995; True, 1996; True, 1997; True, 1998; True, 1999; True, 2000; True, 2001; True, 2002; True, 2003; True, 2004; Smith et al. 2005). The project costs published are based on Federal Energy Regulatory Commission (FERC) filings from interstate gas transmission companies.[§] The entire data set contains the "as-built" costs for 263 on-shore pipeline projects in the contiguous 48-states and excludes costs for pipelines with river or stream crossings and lateral projects (i.e., a pipeline of secondary significance to the mainline system, such as a tie-in between the mainline and a power plant). Data from each year's **Oil and Gas**

[§] When these companies want to modify their pipeline system, they must apply for a "certificate of public convenience and necessity" that specifies what the company estimates the construction will cost. Additionally, these companies must report back to FERC with the actual cost of construction after completion of the project.

Journal report have been inflated to 2004 dollars using the Marshall and Swift equipment cost index (published monthly in **Chemical Engineering**).

The pipeline data set contains information on the year and location of the project and the length and diameter of the pipeline. The locations are listed by state; however, to develop the regression, the states have been grouped into six regions. The project regions used here are the same as those used by the Energy Information Administration for natural gas pipeline regions (EIA, 2005), and are shown in Figure 8-7.

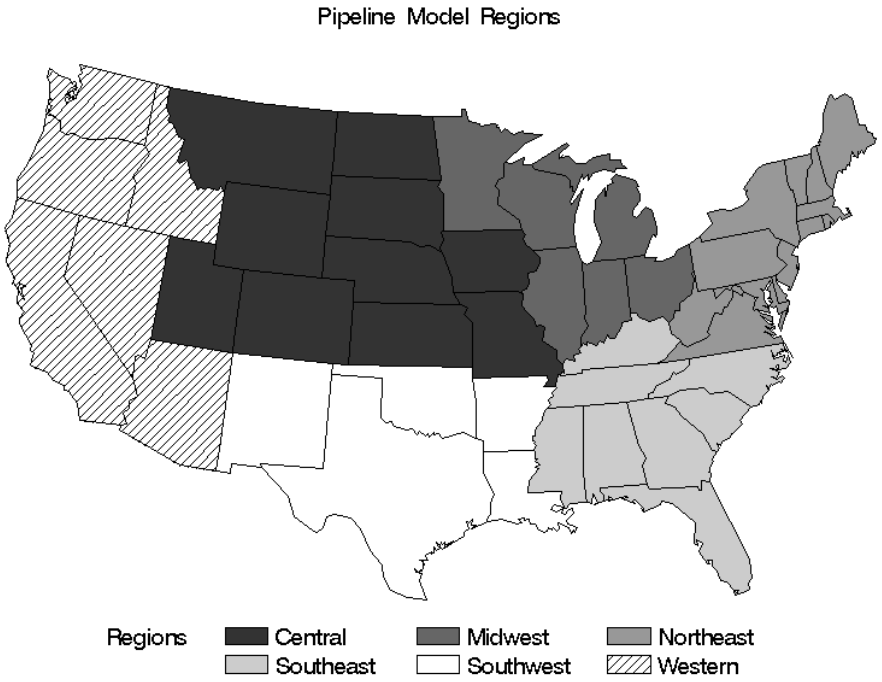

Figure 8-7. The breakdown of states in each EIA natural gas pipeline region.

The total cost for each project is broken down into four categories, which are: materials, labor, miscellaneous charges, and right-of-way (ROW). The materials category includes the cost of line pipe, pipe coatings, and cathodic[**] protection. Labor covers the cost of labor during pipeline construction. Miscellaneous includes the costs of: surveying, engineering, supervision, contingencies, telecommunications equipment, freight, taxes, allowances for funds used during construction (AUFDC), administration and overheads, and regulatory filing fees. ROW covers the cost of obtaining right-of-way for the pipeline and allowance for damages to landowners' property during construction.

Figure 8-8 shows the distribution of pipeline projects by pipeline diameter, Figure 8-9 shows the distribution of projects by region, and Figure 8-10 shows the distribution of projects by length. Figure 8-8 clearly shows clearly that only certain pipe diameters are chosen for construction. This is because line pipe is manufactured only in discrete diameters, as noted earlier. Figure 8-9 shows that while most projects in the data set have been built in the Northeast region, the data set contains at least some projects in all regions. Finally, Figure 8-10 shows that the distribution of pipeline lengths in the data set is skewed towards shorter lengths, which is corroborated by the average pipeline length of 31 km being nearly 20 km longer than the median length.

[**] Cathodic protection prevents corrosion of the pipeline by connecting the pipeline with a sacrificial anode that is intended to corrode in place of the pipeline—these systems can be either galvanic or imposed current systems.

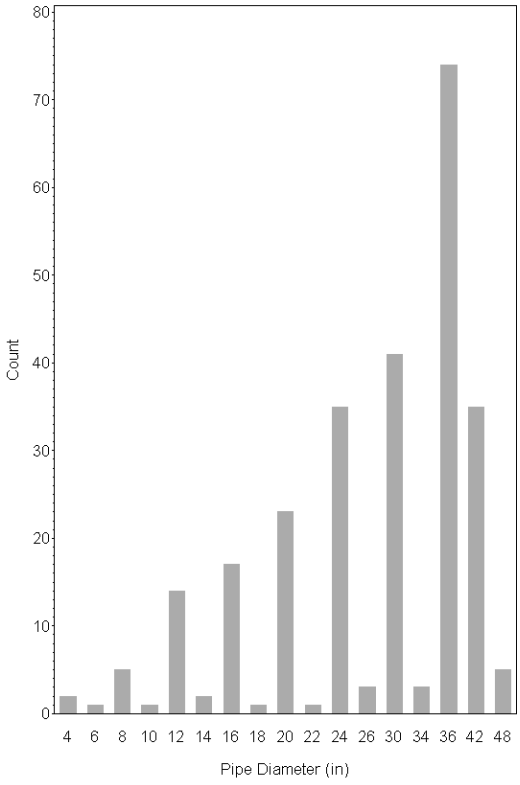

\

Figure 8-8. The frequency distribution of pipeline diameters.

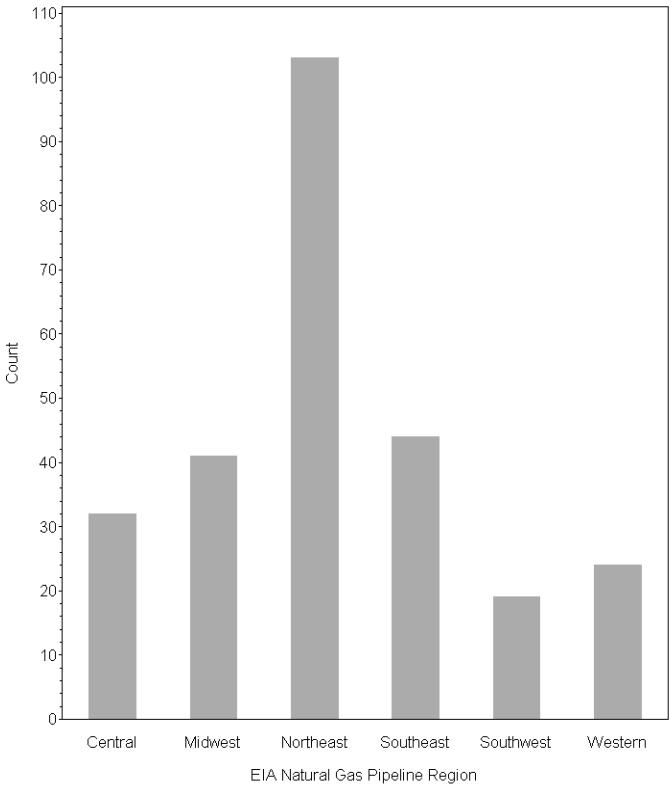

Figure 8-9. The frequency distribution of projects by region

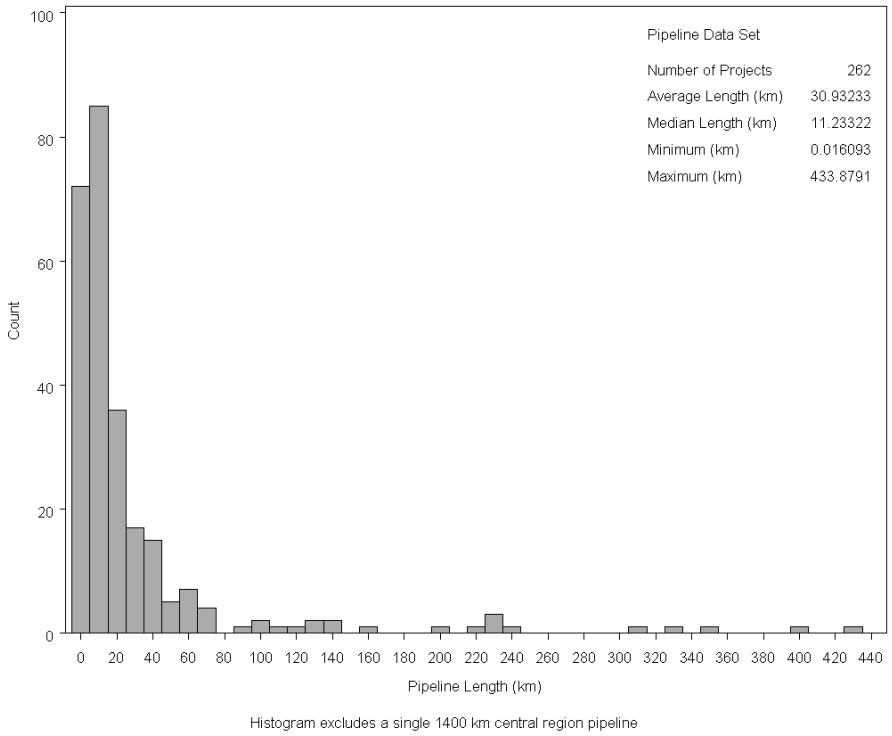

Figure 8-10. The histogram of pipeline lengths, which excludes one 1400 km project for clarity

8.3.2 Capital Cost Models

Separate cost models have been developed for materials, labor, miscellaneous charges, and ROW costs. The capital cost models take the general form shown in Equation (8-20):

$$\log(Cost) = \delta + \eta NE + \lambda SE + \omega C + \nu SW + \tau W + \beta \log(Length) + \gamma \log(Diameter) \quad (8\text{-}20)$$

Where **NE, SE, C, SW,** and **W** are binary variables that take a value of 1 or 0 depending on the region and adjust the estimated cost up or down from the Midwest value, which is the basis for the regression. Regional variables exist in the cost model only if they are statistically significant predictors of the cost, thus different models include different sets of regional variables. The regression intercept accounts for the fixed cost associated with a pipeline project of any length or diameter in the Midwest.

In Equation (8-20), the dependent variable is the base-10 logarithm of the component capital cost and the independent variables are the base-10 logarithm of pipeline distance and pipeline diameter. Log-transformed variables have been used in the regression as opposed to the untransformed variables to reduce heteroskedasticity of the residuals. Heteroskedasticity of the residuals is caused by clustering of data and can result in poor estimates of the regression coefficients. For example, Figure 8-11 shows clustering of pipeline projects at short distances and relatively low total capital costs, while Figure shows that the log-transformed variables are more evenly distributed.

If the intercept and regional variables in Equation (8-20) are collected into a single term, the cost model can be rewritten as shown below:

$$\log(Cost) = \log(\alpha) + \beta \log(Length) + \gamma \log(Diameter) \quad (8\text{-}21)$$

where,

$$\log(\alpha) = \delta + \eta NE + \lambda SE + \omega C + \nu SW + \tau W$$

By reorganizing and taking the anti-logarithm of Equation (8-21), the cost model can be written in Cobb-Douglas form:††

$$Cost = \alpha Length^{\beta} Diameter^{\gamma} \tag{8-22}$$

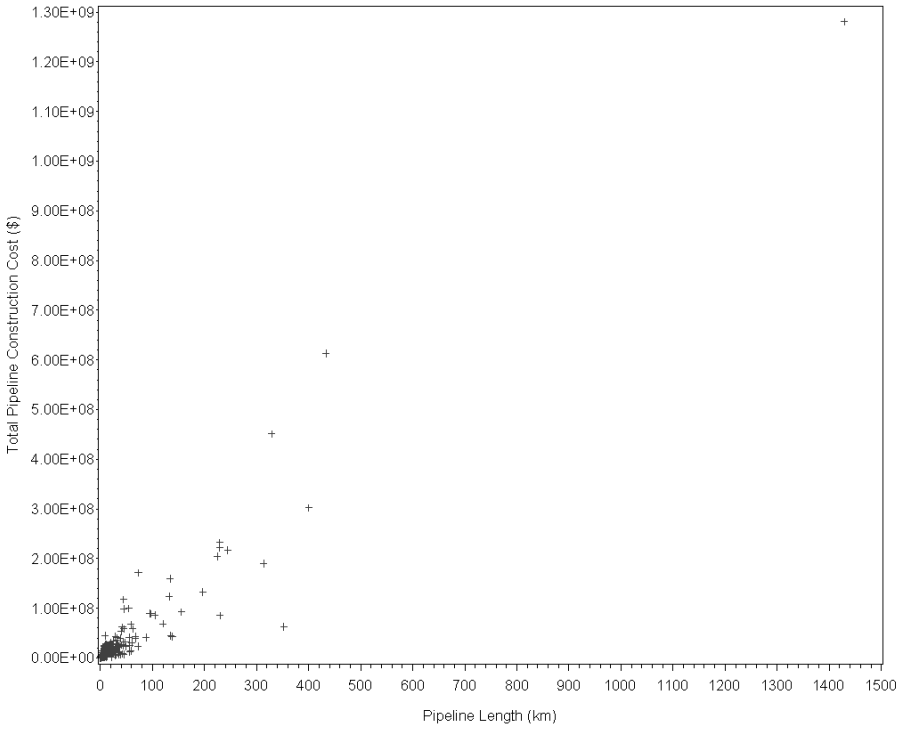

Figure 8-11. Total pipeline capital cost as a function of pipeline length, showing the clustering of variables at relatively low costs and short lengths

There are several interesting properties of Cobb-Douglas functions that are interesting in the context of the cost models. If the sum of β and γ is equal to one, the total cost exhibits constant returns to scale; if the sum is less than one, decreasing returns to scale, and; if the sum is greater than one, increasing returns to scale. Moreover, the values of β and γ are the elasticity of cost with respect to length and diameter, respectively.

The use of separate cost models for each aspect of the capital cost allows real capital cost escalation factors to be applied to individual elements of the capital cost that can be used to scale the results to account for higher or lower than expected project specific costs (e.g., due to changes in the cost of steel) (Figure 8-12). All of the capital cost models developed here report costs in 2004 dollars and the results of these models are subject to the aforementioned escalation factors.

†† In economic theory, a Cobb-Douglas production function has the form $f(K,L) = AK^{a}L^{b}$, where *K* and *L*, refer to capital and labor.

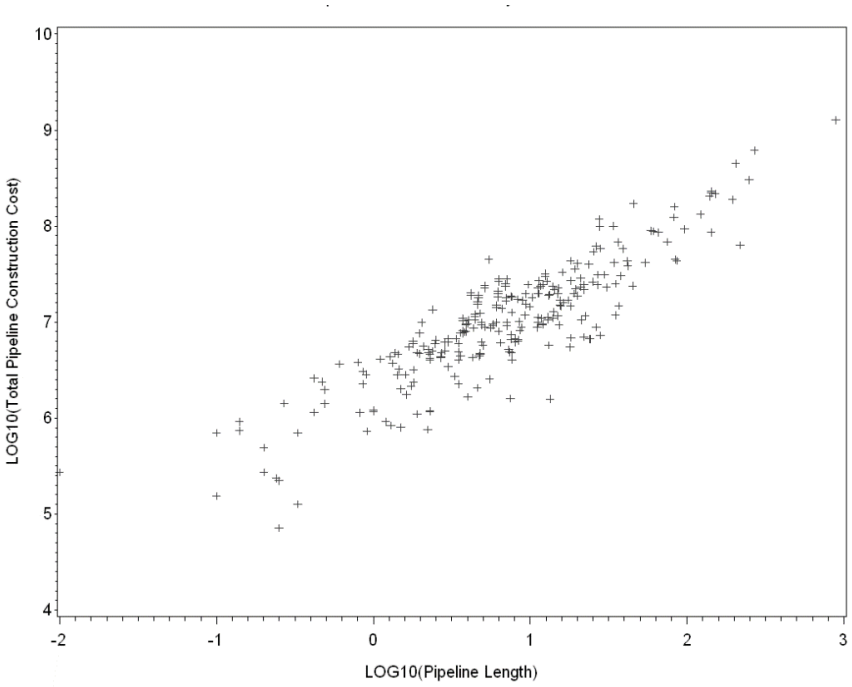

Figure 8-12. The logarithm of total pipeline construction cost and pipeline length showing a reduction in clustering of data points compared to the untransformed plot

Pipeline Materials Cost Model

The pipeline materials cost takes the form given in Equation (8-23):

$$\log(MaterialsCost) = \delta + \lambda SE + \beta \log(Length) + \gamma \log(Diameter) \quad (8\text{-}23)$$

Where **Diameter** is in inches, **Length** is in miles, and SE is a binary variable. The SE regional variable has been included in the regression, however all others have been discarded as they are not significant at the **p=0.05** level.

The regression model in Equation (8-23) is statistically significant, **F(3,244)=2318, p<0.001,** and has an adjusted $\mathbf{R^2}$ value of 0.97.[‡‡] 15 projects were removed from the regression data set when performing the regression because they were found to be outliers based upon their deleted studentized residuals.[§§] Table 8-2 shows the parameter estimates for Equation (8-23), along with the associated 95% confidence interval, **t**-values, and **p**-values.

Table 8-2. Parameter estimates for Equation (8-23), and their standard errors, t-values, and p-values.

Parameter	Value	95% CI (Low)	95% CI (High)	t-value	p-value
δ	3.29813	3.16753	3.42873	49.74	<0.001
β	0.90131	0.87755	0.92507	74.72	<0.001
γ	1.59000	1.50162	1.67838	35.44	<0.001
δ	0.07352	0.03214	0.11491	3.50	<0.001

[‡‡] The F-value is an indicator of the significance of the regression—that is, that there is a significant relationship between the dependent and independent variables—while the R^2 value is a measure of the goodness-of-fit of the regression, with higher values indicating that the model is a more accurate predictor of the dependent variable

[§§] Deleted studentized residuals are a measure of an observations influence on the parameters of the regression, where larger values can indicate undue influence on the regression parameters. A value of 3 has been used as a cutoff for acceptable deleted studentized residuals.

Based on the regression results, several general observations can be made. The materials cost exhibits increasing returns to scale, which means that multiplying both the length and diameter by a constant **n** multiplies the materials cost by a factor greater than **n**. In this case, a doubling of both length and diameter results in a nearly 6-fold increase in materials cost. The elasticity of substitution for length is approximately 0.9, thus a doubling in pipeline length results in slightly less than a cost doubling. Conversely, the elasticity of substitution for diameter is approximately 1.6, thus a doubling in pipeline diameter results in a three-fold cost increase.

Pipeline Labor Cost Model

The pipeline labor cost model takes the form given in Equation (8-24):

$$\log(LaborCost) = \delta + \eta NE + \omega C + \nu SW + \beta \log(Length) + \gamma \log(Diameter) \quad (8\text{-}24)$$

Where **Diameter** is in inches, **Length** is in miles, and **NE**, **SW**, and **C** are binary variables that adjust the total cost of the pipeline if it is constructed in the Northeast, Southwest, or Central regions. The other two pipeline regions have not been included because they have been found not to be statistically significant predictors at the **p=0.05** level.

The regression model in Equation (8-24) is statistically significant, **F(5,253)=361, p<0.001,** and has an adjusted $\mathbf{R^2}$ value of 0.87. Two projects were removed from the regression data set when performing the regression because they were found to be outliers based upon its deleted studentized residual. Table 8-3 shows the parameter estimates for Equation (8-24), along with the associated 95% confidence intervals, **t**-values, and **p**-values.

Table 8-3. Parameter estimates for Equation (8-24), and their standard errors, t-values, and p-values.

Parameter	Value	95% CI (Low)	95% CI (High)	t-value	p-value
δ	4.65680	4.44281	4.87080	42.86	<0.001
β	0.81986	0.77514	0.86458	36.10	<0.001
γ	0.93951	0.78728	1.09174	12.15	<0.001
η	0.07526	0.01175	0.13877	2.33	0.020
ω	-0.18719	-0.28094	-0.09345	-3.93	<0.001
ν	-0.21633	-0.33169	-0.10098	-3.69	<0.001

The labor cost model shows increasing returns to scale—a doubling of length and diameter results in a 3-fold increase in labor costs. Both the elasticity of substitution for length and diameter are less than one, thus doubling the length or diameter results in a less than doubling in total cost.

Pipeline Miscellaneous Cost Model

The miscellaneous cost model takes the form given in Equation (8-25):

$$\log(Cost) = \delta + \eta NE + \lambda SE + \omega C + \tau W + \beta \log(Length) + \gamma \log(Diameter) \quad (8\text{-}25)$$

Where **Diameter** is in inches, **Length** is in miles, and, as in the previous model the variables **NE**, **SE**, **C**, and **W** are binary variables that adjust the total cost of the pipeline if it is constructed in the Northeast, Southeast, Central, or West regions. The Southwest pipeline region has not been explicitly included it is not a statistically significant predictor at the **p=0.05** level.

The regression model in Equation (8-25) is statistically significant, **F(6,252)=185, p<0.001,** and has an adjusted **R2** value of 0.82. Four projects were removed from the regression data set when performing the regression because they were found to be outliers based upon their deleted studentized residual. Table 8-4 shows the parameter estimates for Equation (8-25), along with their 95% confidence interval, **t**-values, and **p**-values.

The miscellaneous cost model shows increasing returns to scale—a doubling of length and diameter results in an approximately 3-fold increase in labor costs. Both the elasticity of substitution for length and diameter are less than one, thus doubling the length or diameter results in a less than doubling in total cost.

Table 8-4. Parameter estimates for Equation (8-25), and their standard errors, t-values, and p-values.

Parameter	Value	95% CI (Low)	95% CI (High)	t-value	p-value
δ	4.55194	4.29304	4.81084	34.63	<0.001
β	0.78345	0.73114	0.83577	29.50	<0.001
γ	0.79067	0.61242	0.96893	8.74	<0.001
η	0.14543	0.05643	0.23443	3.22	0.002
ω	-0.36877	-0.48889	-0.24866	-6.05	<0.001
τ	-0.37723	-0.50661	-0.24785	-5.74	<0.001
λ	0.13236	0.02510	0.23963	2.43	0.0158

Pipeline Right-of-Way Cost

The ROW model takes the form given in Equation (8-26):

$$\log(Cost) = \delta + \omega C + \beta \log(Length) + \gamma \log(Diameter) \tag{8-26}$$

Where **Diameter** is in inches, **Length** is in miles, and the variable **C** is a binary variable that adjusts the total cost of the pipeline if it is constructed in the Central region. The other four pipeline regions have not been included because they have been found not to be statistically significant predictors at the **p=0.05** level.

The regression model in Equation (8-26) is statistically significant, **F(3,239)=168, p<0.001,** and has an adjusted $\mathbf{R^2}$ value of 0.67. This $\mathbf{R^2}$ value is considerably less than for any of the other models. This is likely because of the greater variability in ROW costs, which depend on a number of factors not explicitly included in the model, such as property values along the pipeline route, etc.

Six projects were removed from the regression data set when performing the regression because they were found to be outliers based upon their deleted studentized residual. Table 8-5 shows the parameter estimates for Equation (8-26), along with their 95% confidence intervals, **t**-values, and **p**-values.

Table 8-5. Parameter estimates for Equation (8-26) and their standard errors, t-values, and p-values.

Parameter	Value	95% CI (Low)	95% CI (High)	t-value	p-value
δ	4.16650	3.68692	4.64607	17.11	<0.001
β	1.04935	0.95493	1.14377	21.89	<0.001
γ	0.40306	0.07409	0.73204	2.41	0.017
ω	-0.38195	-0.56547	-0.19842	-4.10	<0.001

The ROW cost model shows increasing returns to scale—a doubling of length and diameter results in an approximately 3-fold increase in labor costs. The elasticity of substitution for length is approximately one, thus doubling the length results in a doubling in total cost. This seems reasonable, as the cost per unit of land required for the pipeline ROW would not change due to the length of the pipeline. However, the elasticity of substitution for pipeline diameter is less than 1, which indicates that a doubling of pipeline diameter will result in less than a doubling of cost.

Pumping Station Capital Cost

The total capital cost of a pumping station has been estimated by the IEA for a European study involving the pipeline transmission of CO_2 (EIA, 2002). That cost is given by the regression in Equation (8-27):

$$PumpCost = 7.82P + 0.46 \tag{8-27}$$

where the result is in millions of U.S. dollars (2002), and P is the installed booster station power in MW. This correlation yields a cost slope of $7,820 per kW of installed capacity.

Illustrative Model Results

The behavior of the capital cost models is shown in Figure 8-13, where the category cost model results are stacked to indicate the total cost of a 16-inch diameter pipeline for distances from 10 mi to 60 mi located in the Midwest. For reference, a 16-inch pipeline could transport approximately 5 million metric tonnes of CO_2 per year over a 100 km distance, which would be approximately the maximum annual emissions of a 600 MW (net) pulverized coal fired plant with 90% CO_2 capture.

Figure 8-13 shows that the labor cost accounts for over 50% of the total cost of a 16" pipeline across all distances between 10 mi and 60 mi. The next largest cost category is materials, followed by ROW, and miscellaneous. However, the size breakdown shown in Figure 8-13 is dependent on the pipeline diameter. For example, the material cost increases more rapidly with pipeline diameter than the miscellaneous cost, thus for a 36 in pipeline, the materials cost is much a much larger fraction of the total cost than the miscellaneous cost.

The regional dependence of the labor, miscellaneous, and ROW models means that the predicted cost of projects in some regions will be either higher or lower than the cost of equivalent projects in other regions. The difference in cost between the Midwest and the other five regions is summarized in Table 8-6 for a 16-inch diameter pipeline that is 100 km long. The results in this table show that, when compared to the Midwest, pipelines in the Northeast and Southeast are more expensive to construct, and pipelines in the Central and Southwest are less expensive to construct.

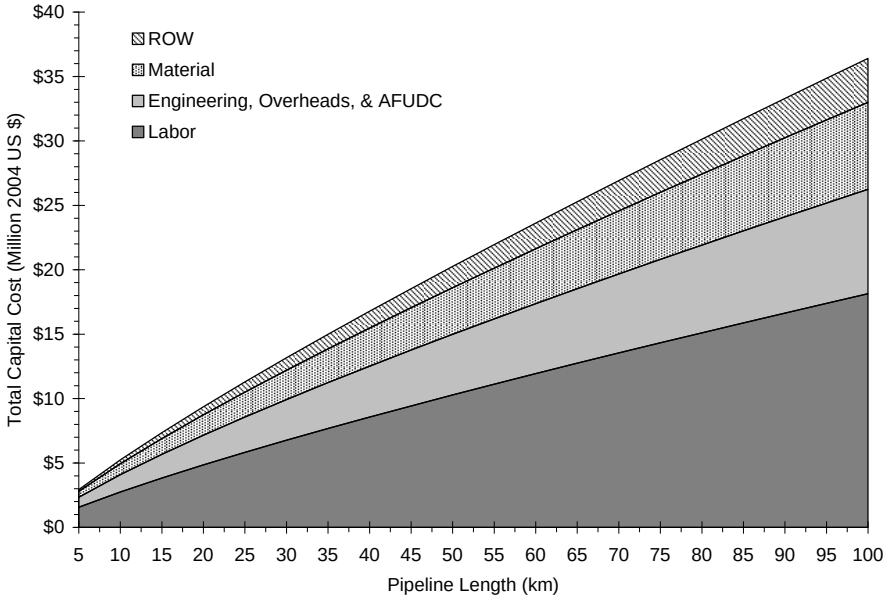

Figure 8-13. The capital cost of a 16-inch pipeline located in the Midwest over varying lengths

Table 8-6. The cost of construction of a 100 km, 16-inch pipeline in the Midwest, and the regional differences relative to the Midwest cost, where values in brackets are negative.

	Midwest Cost	Difference from Midwest				
		NE	SE	SW	West	Central
Material	$6,745,996	$0	$1,244,359	$0	$0	$0
Labor	$18,129,240	$3,430,305	$0	($7,112,589)	$0	($6,348,038)
Miscellaneous	$8,109,657	$3,225,629	$2,889,578	$0	($4,707,358)	($4,640,432)
ROW	$3,417,320	$0	$0	$0	$0	($1,999,126)
Total	$36,402,213	$6,655,934	$4,133,937	$(7,112,589)	$(4,707,358)	$(12,987,596)

8.3.3 Operating & Maintenance Cost Model

While operating and maintenance (O&M) costs are not large in comparison to the annualized capital cost of pipeline transport, they are nonetheless significant. For a 100 km long pipeline, transporting approximately 5 million tonnes per year of CO_2 with no booster pumping stations, the O&M cost would account for approximately 6% of the total cost per tonne of transportation.

Operating & Maintenance Cost Components

In the United States, pipeline maintenance activities are regulated under title 49 of the Code of Federal Regulations (CFR), section 195, subsections 400 through 452. These regulations specify requirements for training, inspections, and repairs. Routine activities that fall under the category of maintenance activities include (Mohitpour, 2005):

- ROW and facilities environmental protection
- ROW and site maintenance
- Pipeline depth of cover maintenance
- Aerial inspection/patrol and leak detection
- ROW erosion control and stabilization
- Cathodic protection monitoring and maintenance
- Pipeline integrity assessment
- Pipeline repair and modifications
- Pipeline encroachment assessment
- Equipment operational test and routine maintenance
- Aesthetics and landscaping

In addition to these activities, title 49 of the CFR, section 195, subpart 452, requires the operator of a CO_2 pipeline to develop and maintain an integrity management program that addresses risks along each segment of their pipeline system. This program is particularly addressed to address risks in high consequence areas (i.e., a populated place or navigable waterway).

Pipeline O&M Cost Model

Bock et al. (2003) report that the O&M cost of operating a 480 km CO_2 pipeline is between $40,000 and $60,000 per month. Thus, on an annual basis, this amounts to approximately $3,100 per kilometer of pipeline in 2003 dollars.

Based on the EPRI Technical Assessment Guide (EPRI, 1993), the O&M charges associated with the booster pumping stations are assumed to be 1.5% of their original capital cost, annually.

8.3.4 Pipeline Routing Considerations

In most situations, the straight-line distance from a CO_2 source to a CO_2 sink will not result in the lowest cost pipeline, thus the actual pipeline length used in the model will be longer than the straight-line distance. Moreover, ROW cost and, to some extent, materials cost are dependent on the pipeline routing and this is not explicitly accounted for by the cost models.

Pipeline routing depends heavily on the locations of existing ROW's. Use of existing right-of-ways, particularly those for power lines, which are frequently owned by a utility company, can significantly reduce the cost of the pipeline. On the other hand, if the pipeline operator must use an existing or new easement on landowners' properties, the pipeline operator must negotiate with the landowner for the right to create or use an already existing easement for a new purpose. If negotiations between the pipeline operator and the landowner break down, the pipeline operator may be able to acquire the ROW through eminent domain. However, regulations surrounding the use of eminent domain vary from state-to-state. For example, a recent Midwest Geological Sequestration Consortium report discusses the use of eminent domain in the State of Illinois for CO_2 pipelines (Nyman et al. 2004).

In addition to consideration of existing ROW's, the pipeline route should consider features, such as: elevation changes; river, road, and rail crossings, and; population density. Locations with higher population density and locations at which the pipeline crosses roads and railway with result in the use more stringent pipeline design factors (Mohitpour et al. 2003). The use of more stringent design factors will increase grade of line pipe required for sections of the project and, thus, increase the total materials cost.

In the pipeline cost models, the additional costs of routing the pipeline through different areas and terrains are averaged into the regional dummy variables. Thus, pipelines in the Northeast have a more expensive ROW cost because they, on average, are built in areas with higher population densities. However, depending on the specifics of a pipeline project, use of escalation factors to account for some routing considerations may be necessary.

8.4 Model Implementation

The pipeline model algorithm has been developed using Visual Basic in Microsoft Excel; more recently, it has also been implemented in the IECM framework. The basic input and output screen is shown in Figure 8-14. From this input screen all of the pipeline parameters can be modified, and the model output viewed.

Pipeline Transport Model: Model Summary

July 31, 2006

Model Inputs		Model Outputs	
Pipeline Parameters*		**Segment Parameters**	
Mass Flow (t/yr)	5.00E+06	Pipe Segments	1
Plant Capacity Factor (%)	100%	Segment Legnth	100
Ground Temperature (°C)	12	Outlet Pressure (Mpa)	10.90
Inlet Pressure (MPa)	13.79	ΔP/ΔL (Pa/m)	28.89
Minimum Outlet Pressure (MPa)	10.30	Average CO_2 Density (kg/m^3)	928.38
Total Pipeline Length (km)	100	Average CO_2 Viscosity (μPa s)	100.04
Pipline Elevation Change (m)	0	Reynolds Number	5.11E+06
Material Roughness (mm)	0.0457	Fluid Velocity (m/s)	1.40
		Errosional Velocity (m/s)	13.14
Pumping Station Parameters		NPS (in)	16
Number of Booster Stations	0		
Pump Efficiency (%)	75%	**Pumping Parameters**	
		Length Between Stations (km)	-
Economic Parameters		Compression Ratio	1.26
Annual O&M ($/km/y)	$ 3,100	Pump Size (kW)	668
Annual Pump O&M (% of Capital)	1.5%	Annual Power Requirement (MWh)	5762
COE ($/MWh)	$ 40.00		
Capital Recovery Factor (%)	15%	**Economic Parameters**	
Project Region	US Midwest	Total Capital Cost ($)	$ 36,402,213
		Annualized Capital Cost ($/y)	$ 5,460,332
Capitalc Real Cost Escalation Factors		Total O&M ($/y)	$ 310,000
Materials (%)	100%	Total Energy Cost ($/y)	$ -
Labor (%)	100%	Total Annual Cost ($)	$ 5,770,332
ROW (%)	100%	Total Cost ($/t)	$ 1.15
Engineering, Overheads, AFUDC (%)	100%		
Pumping (%)	100%		

*See "Detailed Calculations" for fluid composition

Click the base case button to the right to reset the model inputs and results to the base case values — Base Case

Calculate pipeline diameter — Calculate

Figure 8-14. The CO_2 pipeline transport model input screen in the Excel

8.4.1 Combining Performance and Cost

The cost model is dependent on the diameter of the pipeline as calculated by the performance model. Thus, the model must first calculate the pipeline diameter based on the users' inputs.

In order to accommodate the booster stations, the pipeline is broken up into segments, each being equal in length. The segment length, **L**, and number, **NS**, of the pipe segments is determined by the number of booster stations specified by the user, **NB**, and the total pipeline length, **L**. The number of pipe segments is one greater than the number of booster stations and the segment length is the total length divided by the number of segments. For example, for a 30 km pipeline if there are two booster pumping stations specified there are then three-10 km long pipe segments. For all segments, the inlet pressure and minimum outlet pressure are given by the Inlet Pressure and Minimum Outlet Pressure fields in the model input.

The calculation of the desired pipeline diameter for a pipeline segment is a three-step process. These steps are shown in Figure 8-15 along with other steps in the overall algorithm. The first step iteratively calculates the pipeline diameter based on the pressure difference between the inlet pressure and the minimum outlet pressure, using Equations (8-16), (8-17), and (8-18). This diameter is then compared with a list of commonly available diameters of line pipe, and then the next largest size is chosen (see Table 8-1). Finally, the new outlet pressure is iteratively calculated based on the available pipe diameter.

Following determination of the pipeline segment diameter, the booster pumping station size is calculated using Equation (8-19). Based on the pumping station size and the pipeline capacity factor, the annual power requirement for each booster pumping station is calculated.

Using the pipeline segment diameter, total length, and pipeline region, the capital cost is then calculated using the correlations presented earlier. If booster pumping stations are selected, then the cost of these stations is included in the total capital cost. The capital costs for materials, labor, miscellaneous, ROW and pumping costs are then multiplied by their respective capital cost escalation factors to account for any anticipated project specific deviations from the capital cost models. The total capital cost is then annualized using the capital charge rate, and divided by the annual expected amount of CO_2 handled annually to determine the cost of transport.

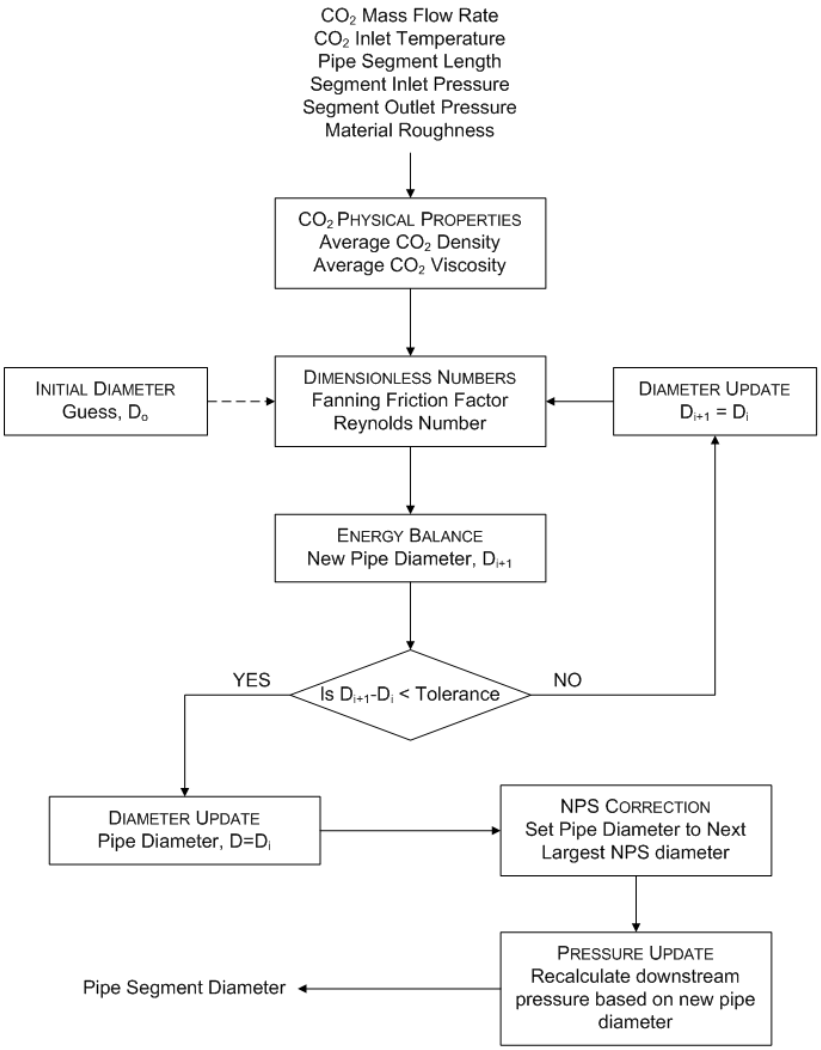

Figure 8-15. Flowchart showing the method used to calculate the pipe diameter.

8.4.2 Sensitivity Analysis Tools

Sensitivity of the model to uncertainty and variability in the input parameters is assessed via Monte Carlo simulation. In Monte Carlo simulation, a large number of cases are run; each case with parameter values independently and randomly selected from distributions that characterize the uncertainty or variability of the particular parameter. From the results of the simulation, a cumulative distribution function is generated that shows the probability of an outcome given the uncertainty and variability in the inputs. Furthermore, plots of the model response as a function of the input parameters can be generated which show the sensitivity of the model to variation in the input.

The model's Monte Carlo input screen is shown in Figure 8-16. From this screen the input parameters can either be deterministic, uniformly distributed between an upper and lower bound, or distributed according to a triangular distribution (between an upper and lower bound with a median). The number of iterations can also be specified depending on the needs of the user.

Pipeline Transport Model: Sensitivity										
July 31, 2006										
Parameters	Distribution	a	b	c	Distribution					
Mass Flow (t/yr)	Deterministic				5.00E+06					
Plant Capacity Factor (%)	Deterministic	50%	100%	75%	Triangular					
Ground Temperature (°C)	Deterministic				12					
Inlet Pressure (MPa)	Deterministic	12	15		Uniform					
Minimum Outlet Pressure (MPa)	Deterministic				10.3					
Total Pipeline Length (km)	Deterministic				100					
Pipline Elevation Change (m)	Deterministic				0					
Material Roughness (mm)	Deterministic				0.0457					
Number of Booster Stations	Deterministic				0					
Pump Efficiency (%)	Deterministic				75%					
Annual O&M ($/km/y)	Deterministic	$ 2,000	$ 4,200		Uniform					
Annual Pump O&M (% of Capital)	Deterministic				1.5%					
COE ($/MWh)	Deterministic				$ 40.00					
Capital Recovery Factor (%)	Deterministic	10%	20%	15%	Triangular					
Escalation Materials (%)	Deterministic	75%	125%		Uniform					
Escalation Labor (%)	Deterministic	75%	125%		Uniform					
Escalation ROW (%)	Deterministic	75%	125%		Uniform					
Escalation Engineering, Overheads, AFUDC (%)	Deterministic	75%	125%		Uniform					
Escalation Pumping (%)	Deterministic	75%	125%		Uniform					
Project Region	US Midwest									
Monte Carlo										
Number of Runs	100									

To run the Monte Carlo analy
the Monte Carlo button. Hittii
cancel the analysis underwa

Trial	Mass Flow (t/yr)	Plant Capacity Factor (%)	Ground Temperature (°C)	Inlet Pressure (MPa)	Minimum Outlet Pressure (MPa)	Total Pipeline Length (km)	Pipline Elevation Change (m)	Material Roughness (mm)	Number of Booster Stations
1	5000000	0.8087495	12	12.8035474	10.3	100	0	0.0457	0
2	5000000	0.59902386	12	13.1801823	10.3	100	0	0.0457	0
3	5000000	0.57317955	12	13.07695	10.3	100	0	0.0457	0

Figure 8-16. The input screen for the transport model sensitivity analysis.

8.4.3 Illustrative Results

Figure 8-17 shows typical results when the model is used to estimate the cost of transport for the U.S. Midwest region. From Figure 8-17, we can see that the cost per tonne of CO_2 transported increases with distance, and decreases for a fixed distance with increasing design capacity. However, the increase with distance is less than linear; that is, the cost per kilometer of a longer pipeline is less than the cost per kilometer for a shorter pipeline.

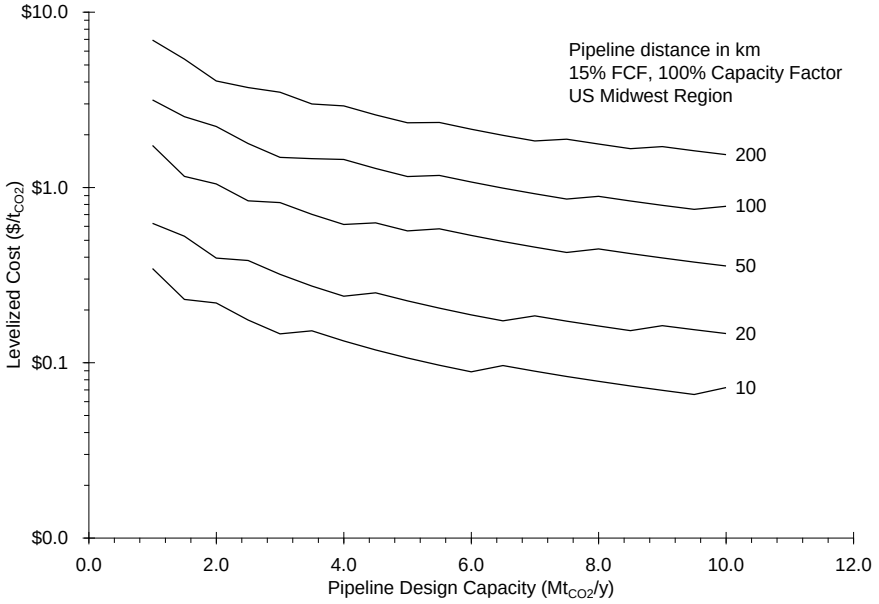

Figure 8-17. Cost per tonne of CO2 transported across the U.S. Midwest via pipeline as estimated by the model for varying pipeline distances (in km) and annual design capacities.

8.5 Comparison with Other Models

Differences between the model developed here (referred to as the CMU model) and other models stem from differences in the performance model (i.e., the way the required pipeline diameter is calculated), as well as in the cost model. To better explain differences between available models, differences in the performance model, cost model, and overall results will be discussed separately.

8.5.1 Performance Model Comparison

The CMU performance model, described earlier, is compared in Figure 8-18 with a model developed by MIT described in a report for the DOE (Bock et al., 2003). The MIT model allows for continuous pipe sizes and does not account for the compressible nature of the flowing CO_2.

Figure 8-21 shows that for the same conditions, the CMU model tends to predict a larger pipe diameter than the MIT model. There are likely several reasons for this difference, the primary one being that accounting for compressibility will result in a larger pipe diameter being required. Moreover, the MIT model calculates the properties of the flowing CO_2 at the inlet of the pipeline, rather than averaged over the entire length of the pipeline as in the CMU model, resulting in a smaller calculated pipe diameter.

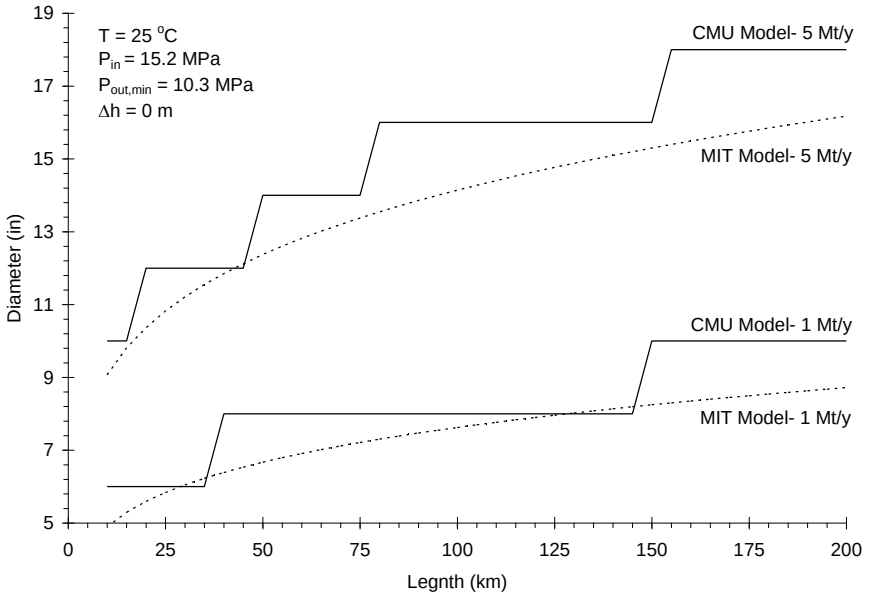

Figure 8-18. A comparison between the MIT model and the CMU model, showing that the CMU model generally predicts a larger pipe diameter for a range of flow rates (1-5 Mt/y)

A further comparison can be made with the rules of thumb proposed by Skholvolt (1993), which are based on relatively low pressure compared to the pressures that would likely be used in a CO_2 constructed today. The parameters used by Skovholt are presented in Table 8-7.

Table 8-7. Parameters used by Skovholt to determine rules of thumb for pipe diameter

Pipeline Parameter	Value
Segment Length (km)	250
Ground Temperature (°C)	6
Maximum Pressure (MPa)	11
Minimum Pressure (MPa)	9

Using these parameters, the diameters calculated by Skovholt are compared with diameters calculated by the CMU model for the same conditions in Table 8-8. In this case, the diameters calculated by the CMU model are consistently larger for all mass flow rates. Moreover, the CMU model cannot accommodate the case of 110 million tonnes per year in one pipeline. The reasons for the difference between the diameters presented by Skovholt and those calculated by the CMU model are not clear, as Skovholt does not describe the methods used to calculate the rules of thumb.

Table 8-8. The pipe diameters proposed by Skholvolt compared with those calculated by the CMU model (all diameters in inches)

Design Mass Flow (Mt_{CO2}/y)	Skholvolt	CMU Model
3	16	18
20	30	36
35	40	48
110	64	N/A

8.5.2 Cost Model Comparison

The CMU cost model can be compared with the cost model from the previously mentioned MIT study (Bock et al., 2003), cost models developed in a study for the IEA (IEA, 2002), and models developed for the Midwest Geological Carbon Sequestration (MGSC) Partnership (Nyman et al., 2004). This comparison is shown in Figure 8-19 for the case of a 16-inch pipeline.

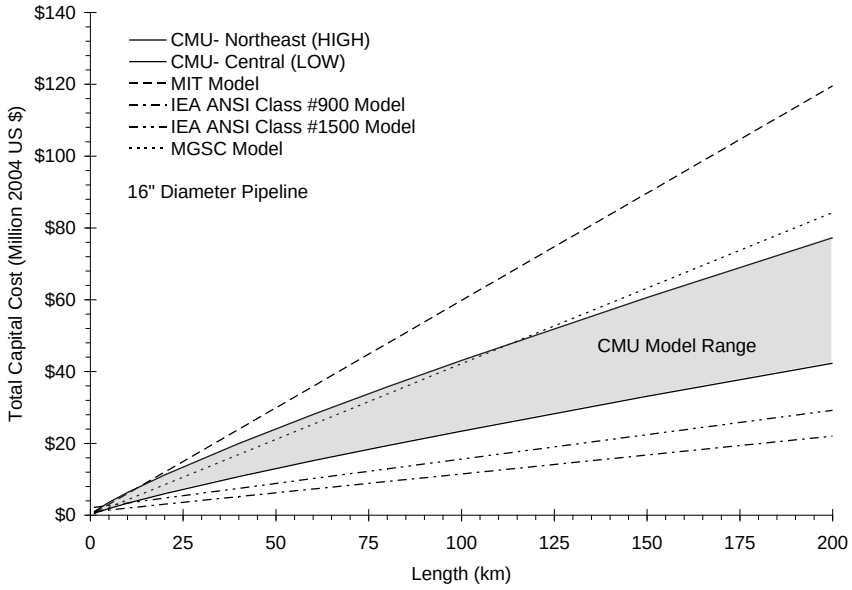

Figure 8-19. The range of capital costs possible from the CMU cost models, depending on region, compared with the capital costs possible from the MIT and IEA models for a 16" NPS pipeline.

Figure 8-19 shows the total capital cost of a 16-inch NPS pipeline for a range of distances as calculated by the MIT model, which uses a simple slope factor ($/in/km); the MGSC model, which uses discrete slope factors ($/km) for diameters between 4 and 24 inches, and; the IEA models, which depends on the operating pressure of the pipeline as well as length and diameter. The IEA ANSI Class #900 model is for pipelines with an operating pressure up to approximately 14 MPa, while the Class #1500 model is for pressures up to about 23 MPa. The figure shows that the CMU model predicts costs that are less than those predicted by the MIT model, on the low side of the MGSC model, and higher than either of the IEA models. Moreover, Figure 8-19 shows that the MIT,

IEA, and MGSC models are linear in length, but the CMU model is slightly non-linear. In the CMU model, the cost per unit length decreases slightly with increasing pipeline length.

The differences between the CMU, MIT, IEA, and MGSC models are likely due to the differing approaches taken in their development. Both the IEA and MGSC models are based on "bottom-up" cost estimates, developed from private design studies of pipeline projects. On the other hand, the MIT model is based on similar data to the CMU model, but with a smaller set of projects, no variation by region, and no accounting for the non-linear effects of length on cost.

8.5.3 Overall Model Comparison

Results from the MIT model and the CMU model can be compared over a range of lengths. Unfortunately, the overall results of the IEA and MGSC model cannot be compared in the same way—the IEA model implementation is not amenable to sensitivity analysis, while the MGSC has not developed a design model. Figure 8-20 shows the results of the comparison between the MIT and CMU models for a fixed mass flow rate of 5 Mt/y, and a charge factor of approximately 16%.

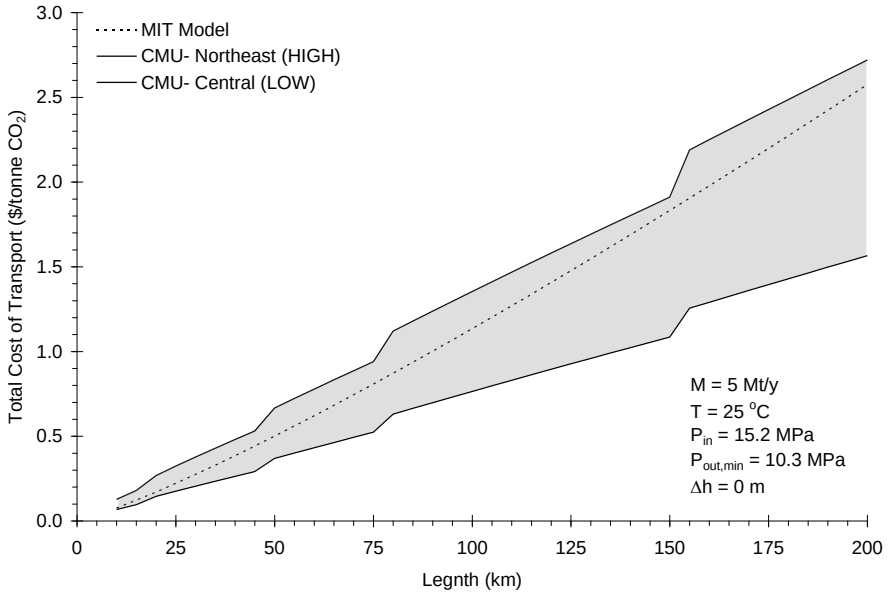

Figure 8-20. A comparison of results from the CMU pipeline transport model and the MIT pipeline transport model

This figure shows that the lower costs and the larger pipe diameters predicted by the CMU transport model compared with the MIT cost model cancel out somewhat, depending on the region selected in the CMU model. Nonetheless, there are significant differences between the costs predicted by the models, particularly at long lengths for pipelines in the Central, West, and Southwest, where the cost predicted by the CMU model is at least 20% less than the cost predicted by the MIT model.

The CMU model is also compared in Figure 8-21 against the results presented in the IPCC Special Report on Carbon dioxide Capture and Storage in Figures 4.2 and 4.5 (Doctor et al. 2005).

The CMU model results shown in Figure 8-21 (top) generally agrees with the results presented in the IPCC Special Report, repeated in Figure 8-21 (bottom). However, costs for projects in the central region are lower than the lower "onshore" bound in Figure 8-21. This may be because the results represented in the IPCC Special Report figure are not region specific. Moreover, the pipeline inlet pressure, outlet pressure, and temperature could be adjusted to change the required pipe diameter, altering the costs presented in Figure 22(a).

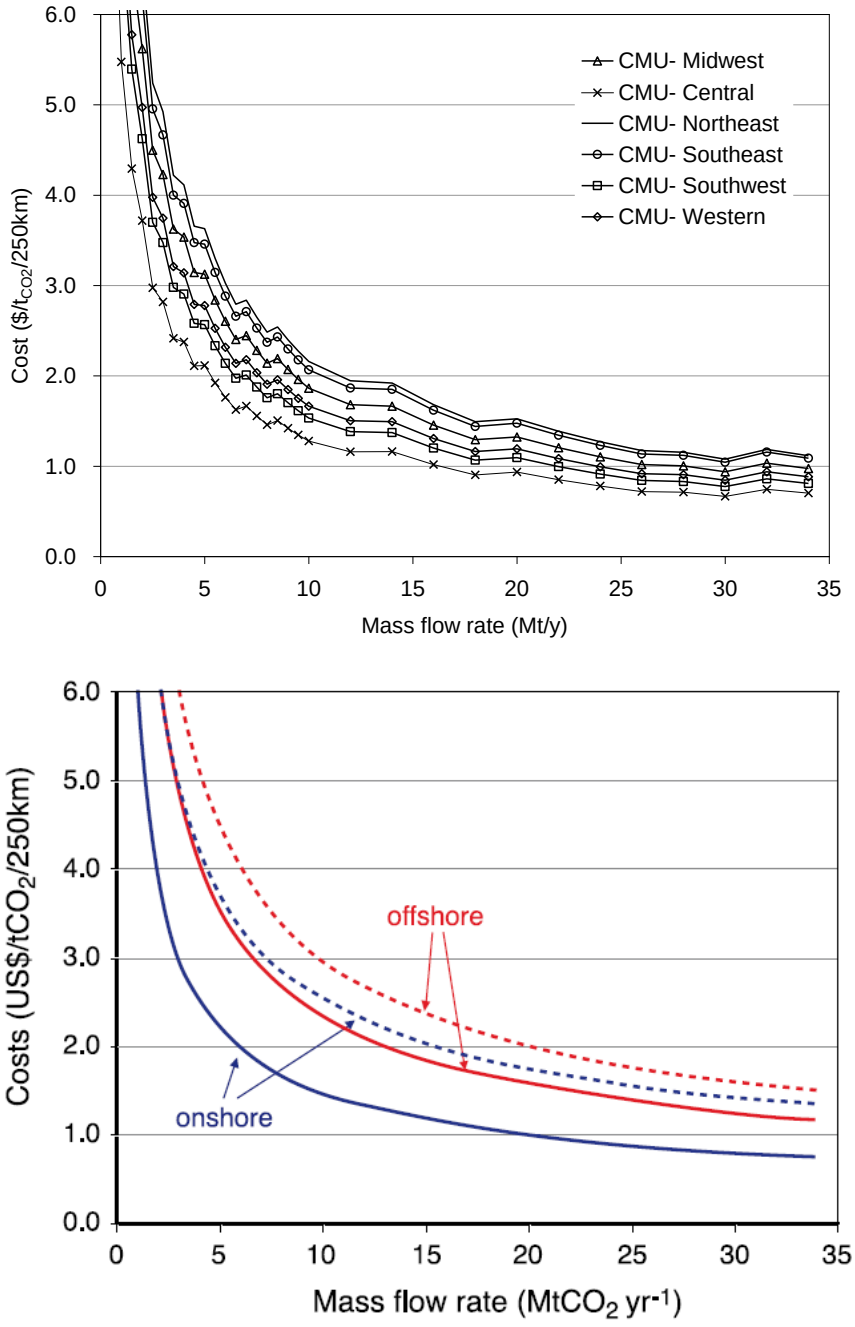

Figure 8-21. Comparison of results from the CMU model (top) and results presented in Figure 4.2 of the IPCC Special Report (bottom)

8.6 Illustrative Case Parameters

The parameters for the illustrative case have been selected to be representative of a typical coal-fired power plant in continental North America. Table 8-9 lists these parameters and the source for the parameter estimates. Several of the parameters were taken from the Integrated Environmental Control Model (IECM) software (CMU, 2004), and in these cases, the default software parameters were used. Additionally, all of the capital cost escalation factors were unity. However, Table 8-9 excludes the CO_2 mass flow rate and pipeline length, as these parameters are addressed separately.

Table 8-9. The illustrative case parameters for the model

Pipeline Parameters	Value	Source
Load Factor (%)	100%	-
Ground Temperature (°C)	12	Skovholt (1993)
Inlet Pressure (MPa)	13.79	IECM (CMU, 2004)
Minimum Outlet Pressure (MPa)	10.3	TVA (Bock, 2003)
Pipe Roughness (mm)	0.0457	Boyce (1997)
Pumping Parameters		
Number of Booster Stations	0	-
Pump Efficiency (%)	75%	IECM (CMU, 2004)
Economic Parameters		
Annual O&M ($/km/y)	$ 3,100	TVA (Bock, 2003)
Annual Pump O&M (% of Capital)	1.5%	EPRI (1993)
COE ($/MWh)	$ 40.00	IECM (CMU, 2004)
Capital Recovery Factor (%)	15%	IECM (CMU, 2004)
Project Region	Midwest	-

Design CO_2 mass flow rate is a function of the plant size and the plant technology. For illustration, a pipeline designed to handle 5 million tonnes per year of CO_2 (at maximum flow rates) from a power plant, would be appropriate for an approximately 600 MW pulverized coal (PC) or integrated gasification combined cycle (IGCC) plant. The distance between the plant and the storage site is highly site dependent, but will be assumed to be 100 km for illustrative purposes. Nonetheless, the amount of CO_2 handled by the pipeline and the length of the pipeline will be varied parametrically.

8.7 Illustrative Results

For a CO_2 pipeline project with the parameters defined in Table 8-9, running 100 km and transporting 5 million tonnes per year, the CMU project model predicts a cost of approximately $1.2 per tonne CO_2 for a 16-inch NPS pipeline. Figure 8-22 results from varying the pipeline length and CO_2 mass flow rate, while continuing to assume that no booster stations are required.

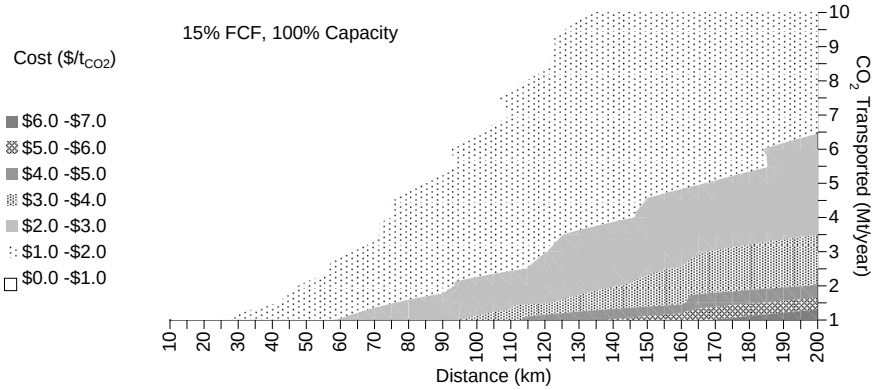

Figure 8-22. The transport cost surface for a coal fired plant with no booster stations

From Figure 8-22 it is clear that economies of scale exist; for a fixed distance, the cost of transport per tonne decreases non-linearly as the net plant size increases. For example, for a 200 km pipeline, the cost of transporting 1 million tonnes per year via pipeline is nearly $7 per tonne, whereas for 5 million tonnes per year the cost is approximately $2.3 per tonne, and for 10 million tonnes per year the cost decreases to approximately $1.5 per tonne.

8.7.1 Cost Minimization Behavior

Incorporating pumping stations into the design can result in cost savings and in many cases will be necessary due to the terrain over which the pipeline is laid. Cost savings can occur with the installation of pumping stations, particularly over longer distances, because the required pipeline diameter, and associated capital cost, decreases as booster stations are installed. Of course, the decreased capital cost must offset increased operating costs from pumping stations.

Figure 8-23 compares the cost of transport with and without the optimum number of cost minimizing booster stations for different annual CO_2 flow rates and distances. This figure illustrates that the cost savings that are achieved by adding booster stations decrease with increasing amounts of CO_2 handled, and increases with pipeline length. The optimum number of compressors in Figure 8-23 was arrived at through a "brute force" optimization method. In this method the number of compressors for a given flow rate and distance is increased in integer steps from zero to find the number of compressors that minimizes cost.

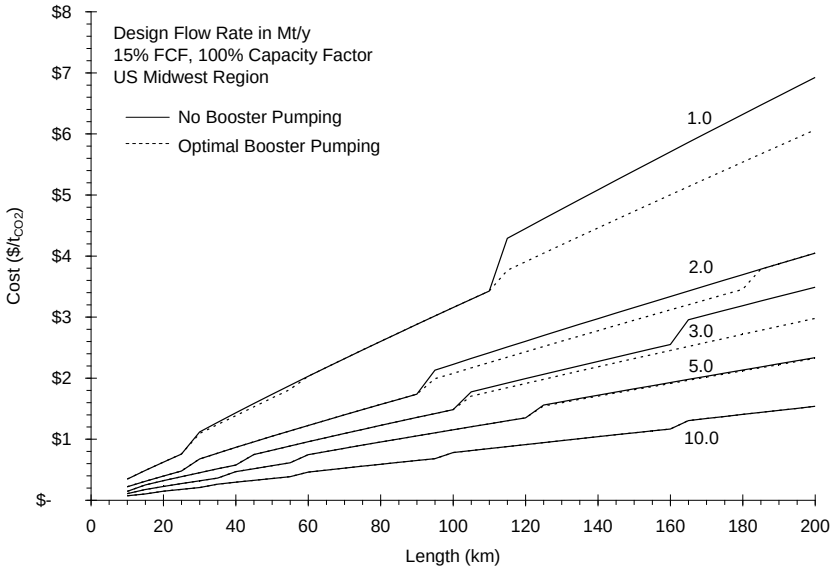

Figure 8-23. The transport cost as a function of length for amounts of CO2 transported for cases with no booster stations (solid line), and the cost minimizing optimum number of booster stations (dotted line)

8.8 Model Sensitivity Analysis Results

To assess the sensitivity of the model to changes in multiple simultaneous design parameters and financial parameters, parameters of interest have been drawn from uniform distributions over a series of Monte Carlo trials and the cost of pipeline transport calculated. The uniform distribution has been selected to model the range of input distributions because there is no prior information that would suggest choosing a more complex distribution (e.g., triangular, lognormal, etc.). The design parameters of interest are the ground temperature, and inlet pressure, while financial parameters include: load factor, capital recovery factor, and annual pipeline O&M cost. The input parameters for the sensitivity analysis are shown in Table 8-10.

Increasing numbers of runs for the Monte Carlo sensitivity analysis will give results with better resolution; however, this also takes increased amounts of time. For this analysis, 1,000 runs have been completed, which takes about 10 minutes. From these runs a cumulative distribution (CDF) for transport cost has been generated, shown in Figure 8-24.

Table 8-10. Parameters for the sensitivity analysis.

Pipeline Parameters	Illustrative Value	Minimum	Maximum	μ
Design Mass Flow (Mt/y)	5	-	-	-
Pipeline Length (km)	100	-	-	-
Load Factor (%)	100%	50%	100%	75%
Ground Temperature (°C)	12	0	20	10
Inlet Pressure (MPa)	13.79	12	15	13.5
Minimum Outlet Pressure (Mpa)	10.3	-	-	-
Pipe Roughness (mm)	0.0457	-	-	-
Pumping Parameters				
Number of Booster Stations	0	-	-	-
Pump Efficiency (%)	75%	-	-	-
Economic Parameters				
Annual O&M ($/km/y)	$ 3,100	$ 2,000	$ 4,200	$ 3,100
Annual Pump O&M (% of Capital)	1.50%	-	-	-
COE ($/MWh)	$ 40	-	-	-
Capital Recovery Factor (%)	15%	10%	20%	15%
Escalation Materials	1	0.75	1.25	1
Escalation Labor	1	0.75	1.25	1
Escalation ROW	1	0.75	1.25	1
Escalation Engineering, Overheads, & AFUDC	1	0.75	1.25	1
Escalation Pumping	1	0.75	1.25	1
Project Region	Midwest	-	-	-

Figure 8-24 shows that depending on the selection of input parameters, for a Midwest pipeline project transporting 5 million tonnes of CO_2 annually over 100 km, the probability of the cost falling between approximately $1 and $2.6 per tonne of CO_2 transported is 90%. The minimum cost and maximum cost predicted by the model are $0.7

and \$3.4 per tonne of CO_2 transported; however, these values are highly sensitive to the number of Monte Carlo runs performed. A less sensitive measure is the median cost of transport, which is \$1.6 per tonne under these conditions.

Using the cost models for different regions changes the results of the sensitivity analysis, as shown in Figure 8-24. As expected, a project in the Central U.S. region will have costs less than a project in the Midwest or Northeast for all combinations of input parameters. The median cost of a project in the Central U.S. transporting 5 million tonnes of CO_2 annually over 100 km is \$1.1 per tonne. In the Northeast, the project cost could approach that of the Midwest for some combinations of input parameters. The median cost of this project in the Northeast is \$1.9 per tonne.

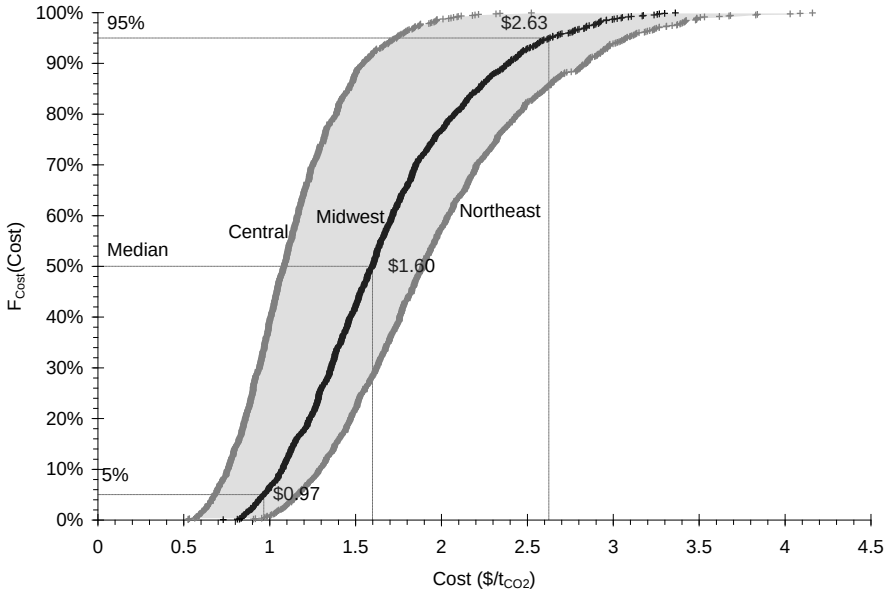

Figure 8-24. The CDF generated from the Monte Carlo sensitivity analysis on the transport model.

The relative importance of the variable input parameters in contributing to the variability of the transport is not clear from the CDF presented in Figure 8-24. In order to assess the relative contribution of variability to the cost calculated by the transport model, Spearman rank-order correlation coefficients were calculated. The rank-order correlation (ROC) coefficients are shown in Figure 8-25.

The dotted horizontal lines above and below the abscissa in Figure 8-25 indicate the 95% two-tailed confidence interval for the calculated rank-order correlation coefficients. Thus, variability in the annual pipeline O&M cost (**ROC = 2%**) and ground temperature (**ROC = -1%**) do not appear to affect the distribution of transport costs significantly. Variability in the ROW (**ROC = 5%**), engineering, overheads, and AFUDC (**ROC = 8%**), and materials escalation factors (**ROC = 9%**), has a limited effect on the distribution of the transportation cost. Consequently, the four parameters that drive the variability in the transportation cost are, in decreasing order of importance: load factor, capital recovery factor, labor escalation factor, and inlet pressure.

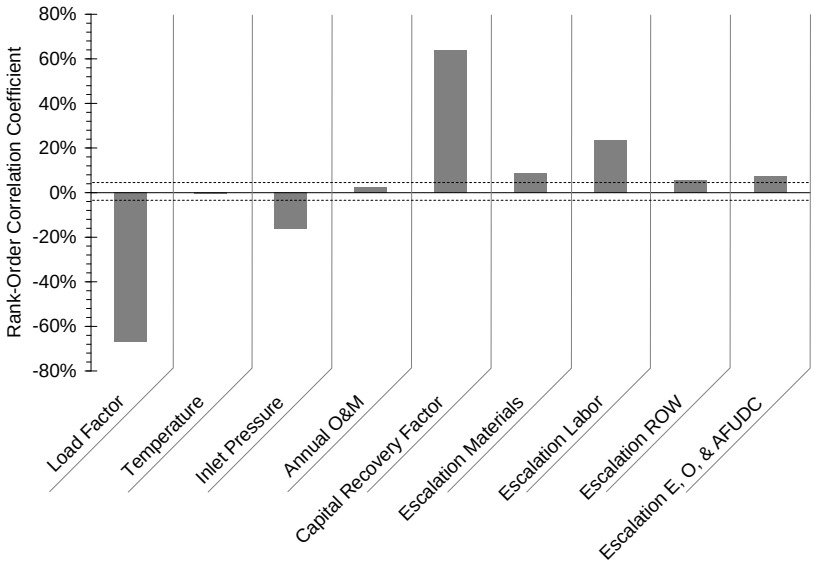

Figure 8-25. Rank-order correlation between the input parameters and the output parameters, showing the relative importance of variability in the input parameters to the cost of transport

8.9 Conclusions

The objective of this work is to develop an engineering-economic model for the transport of CO_2. At pressures greater than 9 MPa and typical ground temperatures, large amounts of CO_2 can be transported via pipeline in the liquid state. This report described the development of a performance model that accounts for compressible flow of liquid CO_2 based on a physical properties model for CO_2 and CO_2-containing mixtures. The report also describes the development of model that estimates material, labor, miscellaneous, and right-of-way costs, which is region specific and non linear in pipeline length.

Comparing the performance and cost models developed here against pipeline transport models developed by the IEA, MGSC, and MIT shows that all of the performance and cost models show similar trends. However, there are significant differences in the absolute cost estimated produced by the models. These differences are mainly due to two factors: the CMU cost model is non-linear in length, whereas the other models are linear, and; the CMU model accounts for regional differences, while the others do not. For example, for a pipeline transporting approximately 5 million tonnes per year of CO_2 over 100 km, the cost of transport in the Central region is nearly half that of the Northeast region, while the cost predicted in the Southwest region within 10% of that predicted by the MIT model.

The models developed here have been applied to an illustrative case of a pipeline constructed in the Midwest U.S., designed to transport 5 million tonnes of CO_2 per year over a distance of 100 km. For this base case, the model estimates a pipeline diameter of 16 inches and a cost of approximately $1.2 per tonne of CO_2 transported. For longer pipelines, however, it is possible to minimize the cost of transport by using booster pumping stations, because the required pipeline diameter decreases as pumping stations are added.

To assess the sensitivity of the model to changes in multiple simultaneous design and financial parameters, Monte Carlo methods have been used. The design parameters of interest are: ground temperature, and inlet pressure. Financial parameters of interest are: load factor, capital recovery factor, annual pipeline O&M cost, and cost model escalation factors. The results shown that, depending on region, the median cost is between $1.1 and $1.9 per tonne of CO_2 transported, and the most important parameters are, in decreasing order of importance: load factor, capital recovery factor, labor escalation factor, and inlet pressure.

The results presented in the report suggest that this model can be used to inform decision makers about the cost of CO_2 transport, particularly in the electric power industry. Future work includes incorporating this model into the Integrated Environmental Control Model (IECM) and coupling it with storage models to assess the full cost of carbon capture and storage (CCS).

References

Rao, A.B., E.S. Rubin, M.B. Berkenpas, 2004. *An Integrated Modeling Framework for Carbon Management Technologies*. Final report to US Department of Energy (U.S. DOE), Carnegie Mellon University, Pittsburgh, PA, 173 pp.

Skovholt, O., 1993: CO_2 Transportation System. *Energy Convers. Mgmt.* 34, 1095-1103.

Svensson, R., M. Odenberger, F. Johnsson, L. Stromberg, 2004. Transportation systems for CO_2 – application to carbon capture and storage. *Energy. Convers. Manage.* 45, 2243-2353.

Gale, J., J. Davison, 2004. Transmission of CO_2- safety and economic considerations. *Energy*. 29, 1319-1328.

Smith L, N. Gupta, B. Sass, T. Bubenik, 2001: *Carbon Dioxide Sequestration in Saline Formations- Engineering and Economic Assessment*. Final Report to U.S. Department of Energy (U.S. DOE), Battelle Memorial Institute, Columbus, OH, 92 pp.

Bock B, R. Rhudy, H. Herzog, et al., 2003: *Economic Evaluation of CO_2 Storage and Sink Enhancement Options*. Final Report to U.S. Department of Energy (USDOE), TVA Public Power Institute, Muscle Shoals, TN, 500 pp.

Doctor, R., A. Palmer, D. Coleman, et al., 2005: Transport of CO_2. In *IPCC Special Report on Carbon Dioxide Capture and Storage*. B. Metz, O. Davidson, H. C. de Coninck, M. Loos, and L. A. Meyer (eds.), Cambridge University Press, Cambridge, pp. 181-192

Kinder Morgan, Inc, 2002: *Kinder Morgan CO_2 Company*. http://www.kne.com/business/co2/transport.cfm#co2_pipelines, 23 Dec 2004

Mohitpour, M., H. Golshan, A. Murray, 2003: *Pipeline Design & Construction*. ASME Press, New York, NY, 648 pp.

Reid, R.C., J.M. Prausnitz, B.E. Poling, 1987: *The Properties of Gases and Liquids*. McGraw-Hill Book Company, New York, NY, 741 pp.

Span, R., W. Wagner, 1996: A New Equation of State for Carbon Dioxide Covering the Fluid Region from the Triple-Point Temperature to 1100 K at Pressures up to 800 MPa. *J. Phys. Ref. Data*, 25, 1509-1596.

Chung, T.H., M. Ajlan, L.L. Lee, K.E. Starling, 1988: Generalized Multiparameter Correlation for Nonpolar and Polar Fluid Transport Properties. *Ind. Eng. Chem. Res.*, 27, 671-679.

Vesovic, V., W.A. Wakeham, G.A. Olchowy, J.V. Sengers, J.T.R. Watson, J. Millat, 1990: The Transport Properties of Carbon Dioxide. *J. Phys. Ref. Data*, 19, 763-808.

Fenghour, A., W.A. Wakeham, V. Vescovic, 1998: The Viscosity of Carbon Dioxide. *J Phys. Ref. Data*, 27, 31-44.

McCabe, W.L., J.C. Smith, P. Harriott, 1993: Unit Operations of Chemical Engineering. 5th ed. McGraw-Hill, New York, NY, 1130 pp.

Zigrang, D.J., N.D. Sylvester, 1982. Explicit Approximations to the Solution of Colebrook's Friction Factor Equation. *AIChE Journal*, 28, 514-515.

Boyce, M.P, 1997. Transport and Storage of Fluids. In *Perry's Chemical Engineers Handbook*. R.H. Perry, D.W. Green, (eds.), McGraw-Hill, New York, NY, Ch. 10, pp. 1-152.

True, W.R., 1995: U.S. Interstate Pipelines Ran More Efficiently in 1994. *Oil & Gas Journal*, 93(48), 39-58.

True, W.R., 1996: U.S. Pipelines Continue Gains Into 1996. *Oil & Gas Journal*, 94(48), 39-58.

True, W.R., 1997: Construction Plans Jump; Operations Skid in 1996. *Oil & Gas Journal*, 95(31), 37-58.

True, W.R., 1998: Weather, Construction Inflation Could Squeeze North American Pipelines. *Oil & Gas Journal*, 96(35), 33-55.

True, W.R., 1999: U.S. Pipelines Experience Another Tight Year, Reflect Merger Frenzy. *Oil & Gas Journal*, 97(34), 45-69.

True, W.R., 2000: More Construction, Higher Costs. *Oil & Gas Journal*, 98(36), 68-86.

True, W.R., 2001: Profitable 2000, Higher Demand Push U.S. Natural Gas Construction Plans. *Oil & Gas Journal,* 99(36), 66-85.

True, W.R., 2002: Fed Data Solid 2001 For US Pipeline Companies. *Oil & Gas Journal*, 100(38), 52-75.

True, W.R., 2003: US Pipeline Companies Solidly Profitable in 2002, Scale Back Construction Plans. *Oil & Gas Journal,* 101(34), 60-90.

True, W.R., 2004: US Construction Plans Slide; Pipeline Companies Experience Flat 2003, Continue Mergers. *Oil & Gas Journal,* 102(32), 52-67.

Smith, C.E., W.R. True, J. Stell, 2005: US Gas Carriers See 2004 Net Jump; Construction Plans Rebound. *Oil & Gas Journal*, 103(34), 50-71

Energy Information Administration, 2005: *Changes in U.S. Natural Gas Transportation Infrastructure in 2004*: http://www.eia.doe.gov/pub/oil_gas/natural_gas/feature_articles/2005/ngtrans/ngtrans/pdf.

International Energy Agency (IEA) Greenhouse Gas R&D Programme, 2002: *Pipeline Transmission of CO_2 and Energy Transmission Study- Report*. Report Number PH4/6, IEA, Cheltenham, UK, 61 pp.

Mohitpour, M., J. Szabo, T.V. Hardeveld, 2005: *Pipeline Operation & Maintenance- A Practical Approach.* ASME Press, New York, NY, 600 pp.

Electric Power Research Institute (EPRI), 1993: *Technical Assessment Guide Volume 1: Electricity Supply*. EPRI, Palo Alto, CA.

Nyman, D.J., J.S. Dracos, R. Varagani, 2004: Carbon Dioxide Capture and Transportation Options in the Illinois Basin—Task 3: Assess Carbon Dioxide Transportation Options in the Illinois Basin. Report to the USDOE, Midwest Geological Sequestration Partnership (MGSC), 82 pp.

Carnegie Mellon University, 2004: Center for Energy and Environmental Studies, http://www.iecm-online.com/cees_models.htm, 23 May 2004.

Appendix: Properties of CO_2 and Fluids of Interest

Table 8-11. Physical properties of CO_2 and other fluids relevant to the transport model

Fluid	M (g/mol)	T_c (K)	p_c (Mpa)	V_c (cm^3/mol)	ω	μ (debyes)
O_2	32	154.581	5.043	73.37	0.0222	0
N_2	28.01	126.192	3.4428	89.4143	0.0372	0
H_2O	18.02	647.096	22.064	55.948037	0.3443	1.855
CO_2	44.0098	304.128	7.3773	94.1	0.22394	0
CH_4	16.04	190.564	4.5992	9.629	0.01142	0
CO	28.01	132.8	3.4935	92.17	0.051	0.1
SO_2	64.06	430.64	7.884	122.026	0.256	1.6
H_2S	34.08	373.6	9.008	98.203	0.1012	0.9
NH_3	17.03	405.5	11.333	72	0.25	1.47

Table 8-12. Binary interaction parameters for the Peng-Robinson equation used in the transport model

k_{ij}	O_2	N_2	H_2O	CO_2	CH_4	CO	SO_2	H_2S	NH_4
O_2	0	-0.0119	0	0	0	0	0	0	0
N_2	-0.0119	0	0	-0.017	0.0311	0.0307	0.08	0.1767	0.2193
H_2O	0	0	0	0.12	0	0	0	0.04	-0.2589
CO_2	0	-0.0170	0.1200	0	0.0919	0	0	0.0974	0
CH_4	0	0.0311	0	0.0919	0	0.03	0.1356	0	0
CO	0	0.0307	0	0	0.0300	0	0	0.0544	0
SO_2	0	0.0800	0	0	0.1356	0	0	0	0
H_2S	0	0.1767	0.0400	0.0974	0	0.0544	0	0	0
NH_3	0	0.2193	-0.2589	0	0	0	0	0	0

9. Regression Analysis

Regression analysis is used to help understand the interrelationships among a given set of variables. The use of regression analysis here is oriented toward developing useful and reasonable relationships between process area costs and key performance parameters. The emphasis is not on the use of extensive formal statistical tests but rather on the practical application of regression analysis for cost model development. Thus, some statistical tests, along with engineering judgments and the availability of data, are used to guide the selection of parameters, the representation of relationships in the regression models, and validation of the models. The "goodness" of the regression models are indicated with common summary statistics, graphical comparison of the model predictions with the actual data, and evaluation of the appropriateness of the model relationships with a priori engineering expectations.

This section will briefly discuss issues related to developing and interpreting the regression models. The issues related to developing the regression models include developing a data set for analysis, selecting parameters for inclusion in the model, and validating the model. Specific issues related to the development and use of the models in this study are then discussed.

9.1 Overview of Multivariate Linear Least Squares

The discussion in this section draws on Ang and Tang (1975), Chatterjee and Price (1977), DeGroot (1986), Dillon and Goldstein (1984), Edwards (1976), Montgomery and Peck (1982), and Weisberg (1985). An overview of key concepts is presented; details of multivariate regression can be obtained elsewhere in many texts such as the ones cited here.

$$C = B\left(\frac{A_{cap}}{B_{cap}}\right)^{n} \tag{9-1}$$

In general, regression analysis involves describing the mean and variance of a random variable, Y, as a function of the value of another variable, X, or a set of variables $X=(X_1, X_2, X_3,..., X_k)$. The variables in the vector X may take on specific values $x=x_i(x_1,i, x_2,i, x_3,i,...,x_k,i)$. For each value x_i in an actual data set, there is a corresponding value y_i. We use the notation $E(Y|X=x_i)$ to indicate the mean, or expected value, of Y associated with a specific vector of values xi of the variables X. The notation Var(Y|X) represents the conditional variance of Y on X. If we expect that the value of Y can be estimated from a weighted linear combination of the k variables in X, and if the conditional variance of Y is independent of the specific values xi of X, then:

$$E\left(Y\middle|X = x\right) = \alpha + \beta_1 X_1 + \beta_2 X_2 + \mathrm{K} + \beta_k X_k \tag{9-2}$$

$$Var\left(Y\middle|X\right) = \sigma^2 = constant \tag{9-3}$$

The parameters in the linear equation are estimated, based on a limited number, n, of observed pairs of (x_i, y_i), using multi-variable linear regression with constant variance. The linear regression model is written as:

$$E\left(Y'\middle|X = x_i\right) = a + b_1 X_1 + b_2 X_2 + \mathrm{K} + b_k X_k \tag{9-4}$$

or as:

$$Y' = a + b_1 X_1 + b_2 X_2 + \mathrm{K} + b_k X_k + \varepsilon \tag{9-5}$$

The linear fit is usually obtained by selecting the values of a and b_i to minimize the sum of the square of the errors between $E(Y'|X=x_i)$ from Equation (9-4) and the values of Y from actual data, y_i. Equation (9-5) differs from Equation (9-4) in that the model is used to predict the conditional random values of Y', rather than the conditional expected value of Y'. Equation (9-5) includes an error term, ε, which represents the variance in Y that is unexplained by the model. Thus, for a specific data point x_i, there is a corresponding data value y_i, a conditional

mean value $E(Y'|X=x_i)$, and a conditional random distribution for Y'. Using the method of least squares, as documented in any standard text, we obtain estimates for the coefficients of the regression model. It is important to recall that the coefficients of the model, a and b_i, known as the partial regression coefficients, and the values of $E(Y'|X=x_i)$ or the parameters of the conditional distribution for Y' calculated using the model, are only estimates of the respective "true" population values of the parameters α and β_i and the "true" population of the values of Y associated with each value x_i.

Common statistical measures of the adequacy of the regression model in describing the data set (X, Y) include the standard error of the estimate, the coefficient of determination, the t-test for significance of each partial regression coefficient, and the F-test for the significance of the regression model and coefficient of determination. Confidence intervals, in addition to significance tests, can also be used. Proper application of these statistics requires the existence of certain properties in the data set (X, Y) and in the regression model. Several of these key assumptions are:

- random sample of n paired values (X, Y) (e.g., values of X are not pre-selected or screened)
- X and Y are multivariate normal
- for each value of x, there is an associated normal population of Y
- for each value of x, the variance of Y is constant
- no error in the measurement of X
- residual errors are not auto correlated
- residual errors are normally distributed
- residual errors have constant variance

While these assumptions are often only approximately satisfied when developing regression models, the use of statistical evaluation methods based on these assumptions may provide some insight to guide the development of the model, even if a strict interpretation of the results is not correct. Therefore, blind application of significance tests to accept or reject parameters may not be appropriate. The most important consideration in selecting variables for use in a model, and for selecting the functional form of the model, is the analyst's knowledge of the substantive area under study and of each of the variables. The analyst will generally have expectations regarding the sign and magnitude of the coefficient for each variable, as well as which variables should be most significant in predicting the dependent variable.

The use of statistical tests is thus viewed here as an aid to, but not as a substitute for, the judgment of the analyst regarding the relationships among the variables. For example, it is common to test the significance of a model parameter by determining whether it is possible to reject a hypothesis that its coefficient is equal to zero. However, in many practical regression situations, it is known, based on theory or experience, that the coefficient must be greater than zero and, therefore, such a significance test is not particularly relevant. The potential inability to reject the hypothesis that a coefficient is zero in a regression model may be more an artifact of a small number of data points than due to a lack of relationship between Y and the predictive variable of concern.

Statistical tests are useful in identifying the independent variables which are relatively more important in predicting Y than others for the available data. For example, one can examine a correlation matrix of X and Y to determine which variables X_i are most highly correlated with Y. These variables are logical candidates for inclusion in the regression model. However, if a potential predictive variable X_i is also highly correlated with another variable X_i, then the inclusion of both may not significantly improve the model and may lead to counter-intuitive results in terms of the sign or magnitude of the coefficient for one of the variables. In such cases, one of the variables would be excluded from the model. Statistical tests can be used to identify independent variables that have only a weak predictive power. These variables would also typically be excluded from the model. A few of the statistical measures used to evaluate regression models will be discussed here, with an indication of how they are used in this study.

The issues of statistical tests and model validation are closely linked. Statistical tests are used to determine the adequacy of the model in representing a known data set. To the extent that the model is used only to interpolate information from within the data set, checking the adequacy of the model is the same as model validation. A regression model can be used for prediction beyond the range of the original data set only if there is some basis in

prior experience, industry practice, or physical theory for the relationships between variables. If the form of the regression model is not based on theoretical or expert judgment about the relationship between the dependent and independent variables, the model should not be used for extrapolation. The user is cautioned that the primary purpose of the models developed in this study is for interpolation within the range of data values used to develop the models. Furthermore, the user is cautioned that the models are intended for application with very specific systems. Throughout the report, the limitations on the ranges of predictive variables and discussion of the design basis for process areas will be presented.

In using multiple regression models, it is easy to inadvertently extrapolate beyond the original domain for X, because that domain is jointly defined by the pairing of the values of each independent variable used to generate the model. Therefore, range checks on each independent variable separately will not guarantee the avoidance of "hidden" extrapolation. However, because the regression models are developed with some engineering basis for the relationship between variables, hidden extrapolation may be acceptable and individual range checks on the independent variables will be used as a practical convenience.

9.1.1 Standard Error

The standard error of the estimate is the standard deviation of the residual errors ε for Y'. The standard error is a measure of the variability in Y that is not captured by the model. If the functional form of the regression model is "correct", this variability can be attributed to factors that are not quantified in the database and therefore cannot be investigated quantitatively. If the functional form of the regression model is not appropriate, then some portion of the standard error may be associated with an incorrect choice of the model, rather than unexplainable variability in the data set. Therefore, it is often useful to compare alternative functional forms of the model in terms of the standard error.

The standard error is estimated based on the residual sum of squares and the degrees of freedom of the residuals. The residual sum of squares is the sum of the squares of the difference between the values of $E(Y'|X=x_i)$ estimated by the model in Equation (9-4) and the values y_i from the data. The degrees of freedom of the regression model are the number of variables, k. The degrees of freedom of the residuals are the number of data points less the number of partial regression coefficients, including the intercept term. Thus, the standard error is given by:

$$s = \sqrt{\frac{\sum_{i=1}^{n}\left[E\left(Y'\middle|X = x_i\right) - y_i\right]^2}{n-k-1}} \tag{9-6}$$

This is an unbiased estimate of the standard deviation of the error. The error is assumed to be normally distributed with a mean of zero. In practice, this assumption may be difficult to verify, particularly for a small number of observed data points. Typical methods for evaluating the normality of the error include plotting the residuals against the fitted values $E(Y'|X=x_i)$, or plotting the errors on normal probability paper. A normality test may also be based on a one-sample Kolmogorov-Smirnov test (e.g., see DeGroot, 1986). In this test, the estimated cumulative probability distribution (cdf) for the errors is compared to a cdf based on the standard normal distribution. The maximum difference between the values of the sample and normal cdf's, adjusted for sample size, is the basis for estimating the test statistic. If the test statistic is larger than a specified value, based on the acceptable significance level for the test, then the hypothesis that the errors are normally distributed is rejected.

The estimate of the standard error is dependent on the actual data as well as the number of data points. As the quantity (n-k-1) becomes small, the estimate of the standard error will tend to increase. The standard error can be used to place a confidence interval on the values of Y' using Equation (9-4) or to generate conditional random values of Y' using Equation (9-5) and a probabilistic modeling capability. In the envisioned application of the regression models developed in this work, the standard error will be used as a basis for generating conditional random values of Y'.

9.1.2 Coefficient of Determination

The most commonly used measure of the adequacy with which a regression model fits the data is the coefficient of determination, R^2, which is defined as:

$$R^2 = 1 - \frac{\sum_{i=1}^{n} \left(y_i - E\left(Y' \middle| X = x_i\right)\right)^2}{\sum_{i=1}^{n} \left(y_i - E\left(Y'\right)\right)^2} \tag{9-7}$$

The numerator of the fractional term is the sum of the square of the residual errors between the actual data and the predicted conditional expected values of Y' from Equation (4). The denominator is the sum of the square of the differences between the actual data and the sample mean. The value of the coefficient of determination is interpreted as the proportion of the total variance in Y which is explained by the regression model, and it varies from 0 to 1, with values near 1 typically considered to represent "good" fits. The coefficient of determination is the square of the multiple correlation coefficient, R, between Y and the regression model. The multiple correlation coefficient is a measure of the degree of linear relationship between the dependent variable Y' and the linear combination of predictive variables.

The coefficient of determination is not a sufficient measure of the goodness of the model. At a minimum, evaluation of a regression model should include consideration of how reasonably the functional form and values of the coefficients represent the expected relationships between variables, the significance level of the coefficients and the regression model as a whole, and a graphical comparison of the model results with the actual data. The coefficient of determination may be highly influenced by extreme data points. If those data points are removed, the correlation coefficient may be drastically altered. The addition of a new data point may lead to a large change in the value of the coefficient of determination. Also, if the range of the predictive variables is reduced or increased, the correlation coefficient may change considerably.

9.1.3 Statistical Significance of the Model

It may be appropriate to consider a significance test for the correlation coefficient. A significance test based on the t-statistic can be used for this purpose to test the hypothesis that the correlation is not significantly different from zero. The hypothesis that a parameter is equal to zero is known as the null hypothesis. The likelihood that a parameter is significantly different from the null hypothesis is determined using a test statistic, such as the t-test. The value of the test statistic computed from the data is then compared to the value of the statistic estimated for the significance level of the test. It is common to use significance levels of 0.05 or 0.01 as the basis for comparison. If the probability of a obtaining a value of the test statistic is less than the significance level (e.g., 5 percent or 1 percent), then the null hypothesis is rejected as being sufficiently improbable that it is regarded as false.

The null hypothesis for the correlation coefficient is a hypothesis that the correlation is zero. A correlation of zero implies that the regression model is not useful, and that the best predictor for the value of Y is the mean of Y. Instead of doing a significance test, it is also possible to use a transformation of the correlation coefficient for use in developing a confidence interval for the correlation (Edwards, 1976). However, statistical tests on the correlation coefficient are related to statistical tests on the coefficient of determination. Furthermore, a test of the null hypothesis for the coefficient of determination is implicitly a test of the null hypothesis that the regression coefficients for the predictive parameters are all zero (Edwards, 1976; Dillon and Goldstein, 1984). This hypothesis is commonly tested using the F test statistic. Thus, an F test implicitly is a test of the null hypothesis for the coefficient of determination as well as for the partial regression coefficients for the predictive parameters.

The F test involves first computing the F-ratio of the regression model, which is related to the coefficient of determination as follows:

$$F = \frac{\left(\frac{R^2}{k}\right)}{\left(\frac{1 - R^2}{n - k - 1}\right)} \tag{9-8}$$

As the coefficient of determination becomes large, the value of the F-ratio increases. The value of the F-ratio is then compared to the value of the F-distribution (published in many texts) for a selected significance level based on the degrees of freedom of the numerator (k) and denominator (n-k-1) of the F-ratio. Therefore, the F-test is influenced by both the number of data points and the number of predictive parameters included in the model. If the F-ratio is larger than the selected value of the F-distribution, then it is possible to reject the hypothesis that all the regression coefficients are equal to zero. However, rejection of this hypothesis does not imply that all of the regression coefficients are significantly different from zero; it only implies that at least one coefficient is significantly different from zero. Furthermore, even if the regression model is statistically significant, it may not necessarily be the best model of the data or even a theoretically valid model of the data. In this study, the F-ratio is compared to a significance level of 0.001 as the basis for rejecting the null hypothesis. In cases where the significance level is higher than 0.001, the significance level of the F-ratio is reported.

To test the significance of individual regression coefficients, a commonly used technique is a t-test. For each regression coefficient, most computer regression packages will report the results of a t-test of the hypothesis that the individual regression coefficients are significantly different from zero. If a regression coefficient is not significantly different from zero, it can be deleted from the model with usually little effect on the residual error. In addition, the standard error for each coefficient is generally reported, which permits the evaluation of confidence intervals for the coefficients, using the t-distribution.

9.2 Application of Regression Analysis to Model Development

In general, the models developed here have high coefficients of determination and meet the F-test of significance at a significance level below 0.001. These results are not unexpected, because the development of the models is based on prior engineering knowledge of the primary relationships between performance, design, and cost. In this section, issues specifically related to the development of the regression models in this report are discussed. These issues relate to the number of observations available in each model data set, the use of transformation of variables to develop nonlinear models using linear regression, the selection of predictive parameters, the collection of data, and the reporting of results.

9.2.1 Number of Observations

The number of data points used to develop the regression model has an important effect on variable selection and interpretation of model results. As the number of data points becomes small, the number of independent variables that can be used may become constrained. It is often possible to obtain a model with a high coefficient of determination by selecting a large number of independent parameters; however, such a model may contain counter-intuitive relationships, or relationships that violate principles of engineering. This often occurs when the range of a predictive variable is small, when other important predictive variables have not been included in the model, or when there is correlation or co-linearity between predictive variables. It is often appropriate to include only a small set of independent parameters that are expected to be fundamentally important and robust as more data are gathered, rather to include all possible variables for which data are currently available. To select the most important parameters, one may begin by including all possible predictive variables in the model. Those variables with regression coefficients that fail the t-test for significance are then deleted to yield a new model with fewer predictive variables. The deletion or inclusion of a variable may be tempered by judgment regarding relationships that must be included in the model, assuming that the coefficients of the particular variable are of the correct sign and magnitude.

For small numbers of data, the estimates for the standard error, and the significance levels for the F-ratio, will tend to increase, because the degrees of freedom are reduced. Therefore, confidence intervals on the regression coefficients and the estimate for Y will usually be larger than when more data are available. As more data become available, the regression models can be redeveloped. While the specific values of the regression coefficients would likely change, they would be expected to remain within the confidence intervals, unless the new data are from a different sample population than the original data. In this case, the original regression model is not an appropriate representation of the new data. It is important, therefore, to ascertain if the basis for the new data is the same as for the older data (e.g., same design for process area equipment, same battery limits for the process

area). In some cases, it may not be appropriate to add the new data without also including other predictive variables to capture the differences in the basis for the new and old data.

9.2.2 Transformation of Variables

While linear regression analysis has been used for the regression models developed in this report, in many cases variable transformations have been used because the relationship between the dependent and predictive variables is non-linear. For example, the simplest cost model involves exponential scaling of a performance parameter to estimate cost, as presented in Equation (9-1). This functional form is standard in the chemical process industry, and cost capacity exponents for standard process plants are published in various sources (e.g., Peters and Timmerhaus, 1980; Ulrich, 1984; Humphreys and Wellman; 1987). The exponential scaling rule can be converted to linear form using the natural logarithm to transform the variables. A typical assumption for the functional form of the cost models is:

$$Y = aX_1^{b_i} X_2^{b_2} \text{K}\ X_k^{b_k} \tag{9-9}$$

This model represents the expected exponential scaling relationship between key process flow rates or design parameters and cost. In most cases, the exponent is expected to be less than one, representing the "economy of scale" of building larger units compared to smaller units. Typically, the exponent of one of the parameters will be much larger than for the other parameters. This result is expected, for example, when the flow rate of one material stream is expected to have a major influence in cost, while other parameters, such as temperature, may have only a secondary effect. The model in Equation (9-9) can be transformed to linear form using the natural logarithm:

$$\ln(Y) = \ln(a) + b_2 \ln(X_1) + b_2 \ln(X_2) + \text{K} + b_k \ln(X_k) \tag{9-10}$$

A linear regression is then developed based on the transformed variables. The transformation of variables affects the interpretation of distribution of the errors. If the errors for Equation (9-10) are normally distributed, which is the underlying assumption for the statistical tests discussed in the previous section, then the errors for Equation (9-9) will be lognormally distributed. The statistical tests are applied to the transformed model of Equation (9-10). These cases are noted in the text.

Recall that the probability density function (pdf) for the normal distribution is given by:

$$f(x) = \frac{1}{\sigma\sqrt{2\pi}} \exp\left(-\frac{[x-\mu]^2}{2\sigma^2}\right);\ -\infty \le x \le \infty \tag{9-11}$$

where μ is the mean and σ is the standard deviation. If y is lognormally distributed, then ln(y) is normally distributed. The pdf for the lognormal distribution is given by:

$$f(y) = \frac{1}{\phi_y\sqrt{2\pi}} \exp\left(-\frac{[\ln(y)-\xi]^2}{2\phi^2}\right);\ 0 \le y \le \infty \tag{9-12}$$

The parameters of the lognormal distribution are ξ and ϕ. These parameters correspond directly to the mean and standard deviation of the normal distribution for ln(y). The mean and variance of the lognormal distribution are given by:

$$\mu_y = \exp\left(\xi + \frac{\phi^2}{2}\right) \tag{9-13}$$

$$\sigma_y^2 = \omega(\omega-1)\exp(2\xi) \tag{9-14}$$

where,

$$\omega = \exp(\phi^2)$$

Using these relationships, the parameters of the lognormal distribution of errors for the nonlinear regression models can be estimated from the parameters of the normal distribution for the errors of the linearized model. Therefore, the statistical model based on the functional form in Equation (9-9) is given by:

$$Y' = aX_1^{b_i} X_2^{b_2} \text{K}\ X_k^{b_k} \varepsilon \tag{9-15}$$

where the error term is multiplicative and lognormal, not additive and normal as with the linear model in Equation (9-5). The mean of ln(ε) is zero and the standard deviation is the standard error of the estimate for the linearized model. These parameters for ln(ε) are used to estimate the mean and standard deviation for the lognormal distribution of ε using the relationships shown in Equations (9-12), (9-13), and (9-14). The median of the lognormal error term in Equation (9-15) will always be 1. The mean of the error term will typically be a value close to, but larger than, 1 and the standard deviation will typically be less than 1. The parameters that are reported for lognormal error terms in this report are the mean and standard deviation given by Equations (9-13) and (9-14).

9.2.3 Two-Step Regressions

In many cases, the relationship between cost and performance parameters is expected to be nonlinear, as described by Equation (9-15). However, the cost is also directly proportional to the number of trains of equipment for a given process area. To capture both the nonlinear relationships between performance and cost and the linear relationship between the number of trains and cost, a two-step approach to developing the regression models may be required. The primary reason for the two-step approach is because it is not possible to specify that the exponent of the number of trains must be equal to one when developing the nonlinear model. In the first step, a linearized regression of cost and performance parameters as just described is developed on the basis of a single train of equipment. In the second step, the predicted values from the nonlinear model for a single train are combined with information about the number of trains to predict the total cost of the process area. Thus, the final regression model from this process contains predictive variables for both performance and the number of total and operating trains.

The first step in the process involves estimating the coefficient and exponents of a model of the form of Equation (9-9) on the basis of a single train of equipment. The values of Y estimated in this fashion are then multiplied by the corresponding total number of trains to form a new predictive variable. This predictive variable is then used in a simple linear regression model. The first regression yields a model of the form:

$$Y^1 = a\left(\frac{X_1}{N_0}\right)^{b_1}\left(\frac{X_2}{N_0}\right)^{b_2} \text{K}\ \left(\frac{X_k}{N_0}\right)^{b_k} \tag{9-16}$$

Note that this is a general functional form; in some cases, the predictive performance parameters (such as temperature or pressure) do not depend on the number of trains, and therefore would not be divided by the number of operating trains. The estimated values of cost from Equation (9-16) represent the cost per operating train. However, we are ultimately interested in the total cost for the process area. Therefore, we calculate a new predictive variable which is the estimated cost for all operating and spare trains:

$$X^{(2)} = N_T Y^1 \tag{9-17}$$

We then use this new variable as the basis for a simple linear regression of the form:

$$Y' = a^{(2)} + b^{(2)} X^{(2)} + \varepsilon \tag{9-18}$$

Typically, the value of b(2) from this model is close to 1.0. The value of a(2) may occasionally be small enough (or statistically insignificant) to exclude from the model by estimating the regression without a constant. Note that the error term here is in the linear space. If the errors conform to a hypothesis of normality, then the error can be represented as normally distributed with a mean of zero. Based on Equations (9-16), (9-17),and (9-18), we can write the final regression model as:

$$Y' = a^{(2)} + b^{(2)}\left[N_T a \left(\frac{X_1}{N_0}\right)^{b_1} \left(\frac{X_2}{N_0}\right)^{b_2} \mathrm{K} \left(\frac{X_k}{N_0}\right)^{b_k} \right] + \varepsilon \qquad (9\text{-}19)$$

where the term within the square brackets is treated as a single variable in the simple linear regression. Thus, the first regression is essential a method for grouping a number of performance parameters into a single aggregate predictive term, while the second regression permits the addition of the linear relationship between cost and the number of trains of equipment. This approach permits the calculation of model statistics based on total, rather than per train, process area costs, which are the ultimate measures of interest.

9.2.4 Selection of Predictive Variables

Direct capital cost regression models for each IGCC plant section, and in some cases estimates of annual operating requirements, have been developed based on an analysis of approximately 30 detailed performance and cost studies of IGCC and coal-to-SNG (synthetic natural gas) systems. These models have been developed based on analysis of plant section direct costs and key plant section performance parameters. In each regression model, the parameters selected for inclusion in the model and the analytic relationships between model inputs and outputs were based on engineering judgments, statistical analysis, and data availability. These regression models relate the total direct cost (which includes delivered equipment cost, installation labor, and installation materials) to the statistically most significant performance parameters influencing cost. These parameters are typically mass flow rates, although in some cases parameters such as removal efficiency, pressure, or temperature were found to be statistically significant. In cases where parameters that are expected to be important were not found to be statistically significant, the variation in these parameters often is small for the available data samples (e.g., most gasifier designs are at a specific pressure and temperature), or the variation in these parameters is highly correlated with variations in the statistically most significant parameter (e.g., the syngas output from the gasification section is highly correlated with the coal feed rate). Similarly, some parameters that are expected to be important in influencing cost may yield counter-intuitive results in the regression models (e.g., cost inversely proportional to mass flow rate). This, too, occurs when two parameters are highly correlated.

9.3 Collecting Data

Performance and cost data were collected into separate data bases for each plant section, based on similarity of plant section definitions. Only direct equipment costs were collected. Direct costs include equipment, material, and labor costs associated with installing plant equipment. Because indirect costs are treated differently in different studies (e.g., EPRI vs. GRI), these were not included in the cost data bases. All direct costs were adjusted to a common year using the Chemical Engineering plant cost index (January 1989 = 351.5). Because the studies varied in the amount of detail for each plant section, only a few performance parameters may be reported in common among studies for a given plant section. This limits the number of parameters that are candidates for regression analysis.

9.3.1 Reporting Results

For each plant section, the direct capital cost model is reported along with the error of the regression, the coefficient of determination, the number of data points used in developing the regression, and the range of values over which the regression was developed. The error term is typically expressed as a normal distribution with a mean of zero and a standard deviation estimated from the difference between the direct costs available in the literature and the direct costs estimated from the regression model. In cases where a non-linear variable transformation was used, the error is reported as a lognormal distribution. The error term provides a measure of the variance of the direct cost estimate. In principle, the variance would be zero if the model accounted for all the parameters that influence costs and if the model were of an appropriate functional form. However, because the models are simplified and include only one or a few parameters, not all of the variation in cost is captured. The variance represents differences in plant location, design, or performance parameters that are not included in the cost model.

References

Chatterjee, S., and B. Price (1977). Regression Analysis by Example. John Wiley and Sons, New York. 1977.

DeGroot, M.H. (1986). Probability and Statistics, Second Edition. Addison-Wesley, Reading, MA. 1986.

Dillon, W.R., and M. Goldstein (1984). Multivariate Analysis: Methods and Applications. John Wiley and Sons, New York. 1984.

Edwards, A.L. (1976). An Introduction to Linear Regression and Correlation. W.H. Freeman and Company, San Francisco, CA. 1976.

Montgomery, D.C., and E.A. Peck (1982). Introduction to Linear Regression Analysis. John Wiley and Sons, New York. 1982.

Peters, M.A., and K.D. Timmerhaus (1980). Plant Design and Economics for Chemical Engineers. Third Edition. McGraw-Hill, New York. 1980.

Ulrich, G.D. (1984). A Guide to Chemical Engineering Process Design and Economics. John Wiley and Sons, New York. 1984.

Weisberg, S. (1985). Applied Linear Regression. John Wiley and Sons, New York. 1985.

10. Updates to IGCC Models in IECM

Introduction

In this part of the report, 2008 updates to the technologies, technical parameters and cost parameters for IGCC models in the IECM are presented. Technologies such as Shell gasifier, Sulfinol sulfur removal and GE 7FB gas turbine are added to IECM. Cost models are updated to be in tune with recent figures as of 2008. Case studies with application of IECM to different conditions are presented at the end. Documentation of process performance models developed using Aspen Plus is given in the Appendix.

10.1 Modifications to IECM – Technology Models

This section lists the technology-related modifications done to IECM. The modifications range from inclusion of new technologies to changing of technical parameters in the existing ones. Documentation of process performance model for Shell gasification technology is given in the Appendix.

10.1.1 Shell Gasification Technology

The earlier versions of IECM used only the GE quench type gasification technology in its IGCC models. Now, Shell gasification system, a dry-feed gasification technology, is also added. Radiant syngas cooling is used for non-capture cases and a quench cooling system is used for capture cases. Following is the description of modifications to IECM user-interface to include Shell technology as an option

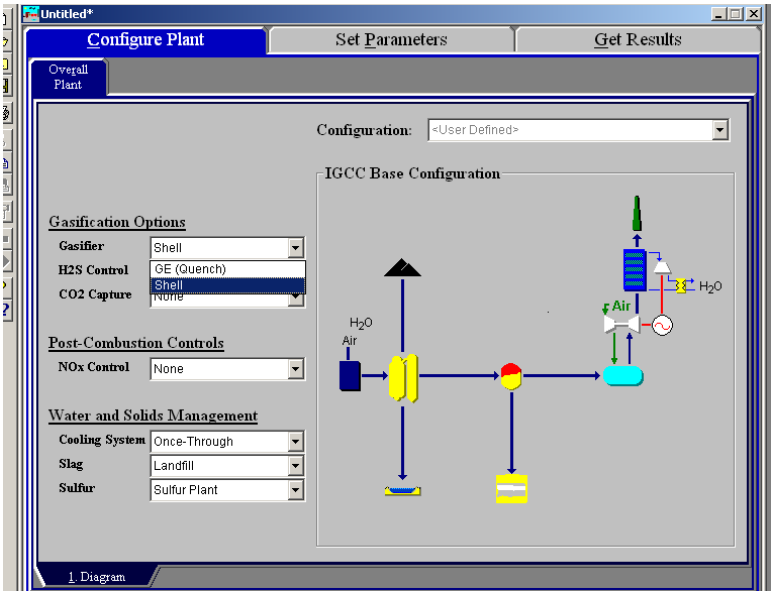

Figure 10-1. Gasifier type choices - GE (Quench) and Shell

Figure 10-1 shows the Configure Plant tab where the user can choose between GE (Quench) or Shell gasifier technologies.

By selecting the Shell gasifier technology, the gasifier area screen in the Set Parameters tab updates the variables correspondingly. Shell gasifier is a dry-feed gasifier, operating at a temperature of 2600 ºF (line 2 in the Gasifier Area tab) and 615 psia (line 3 in the Gasifier Area tab. In IECM, temperature can be varied by +/- 100 ºF, as shown in Figure 10-2.

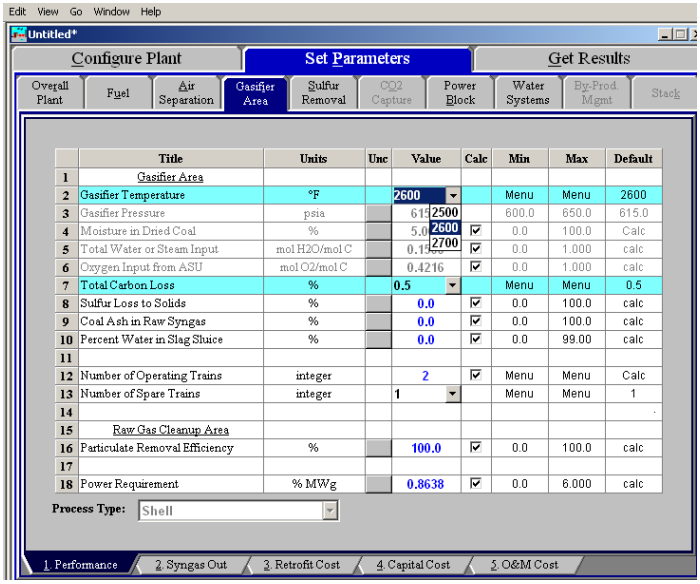

Figure 10-2. Gasifier area: temperature is 2600 ºF, with options of 2500 ºF and 2700 ºF

Figure 10-3 shows other default operating parameters. Shell gasifier is a dry-feed system. Bituminous coals have to be dried to 5% moisture content (line 4 in the Gasifier Area tab). Sub-bituminous coals and lignite are dried to 6% and 12% moisture levels respectively. A small amount of steam is also input to the gasifier, such that the mole ratio of water to carbon in coal is 0.15 (line 5 in the Gasifier Area tab). Oxygen input from the ASU is fixed such that the mole ratio of oxygen to carbon in coal is 0.4216 (line 6 the Gasifier Area tab). Total carbon loss is given as a function of carbon in slag. The default is 0.5% by weight but it can be changed to 1% or 1.5% (line 7 the Gasifier Area tab).

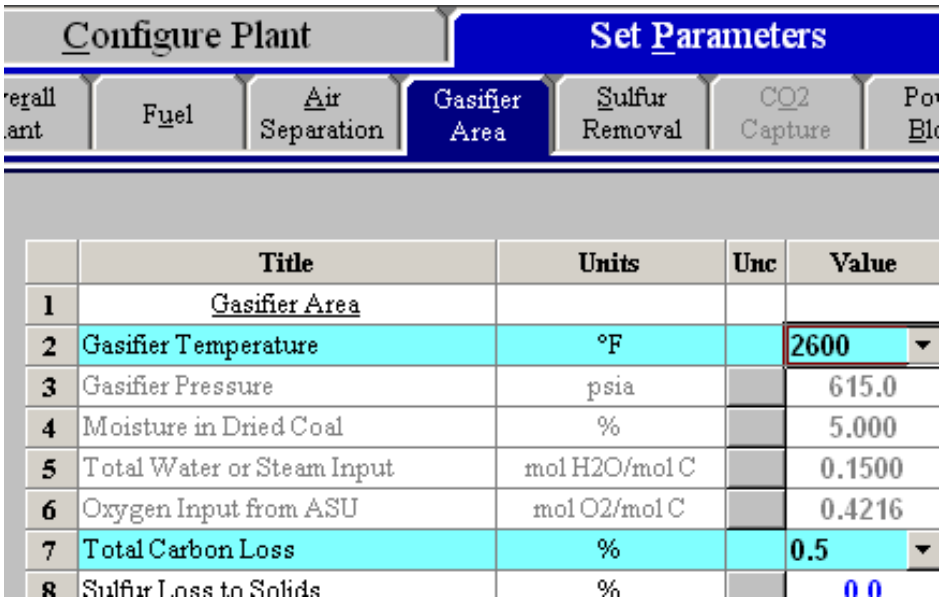

Figure 10-3. Default operating parameters of a Shell gasifier

Figure 10-4 shows the syngas composition for Illinois#6 coal, gasifier operating temperature of 2600 °F and carbon loss percentage of 0.5%. The composition changes when one or more of input specifications like coal type, gasifier temperature or carbon loss are changed.

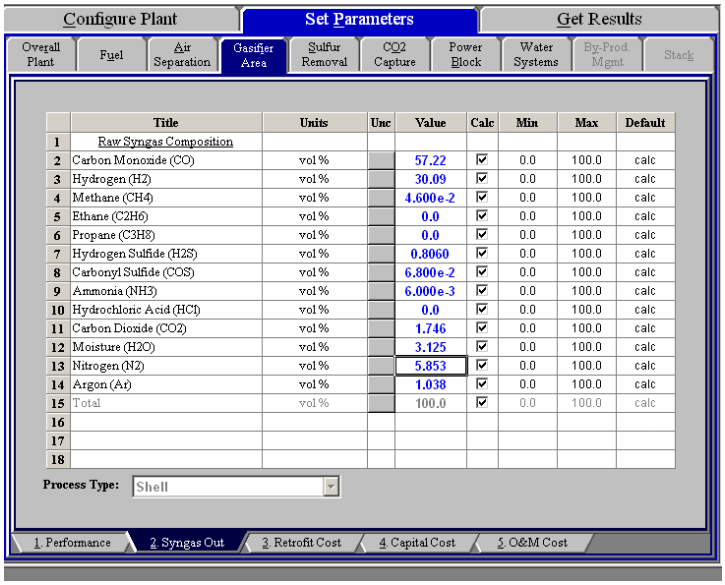

	Title	Units	Unc	Value	Calc	Min	Max	Default
1	Raw Syngas Composition							
2	Carbon Monoxide (CO)	vol %		57.22	☑	0.0	100.0	calc
3	Hydrogen (H2)	vol %		30.09	☑	0.0	100.0	calc
4	Methane (CH4)	vol %		4.600e-2	☑	0.0	100.0	calc
5	Ethane (C2H6)	vol %		0.0	☑	0.0	100.0	calc
6	Propane (C3H8)	vol %		0.0	☑	0.0	100.0	calc
7	Hydrogen Sulfide (H2S)	vol %		0.8060	☑	0.0	100.0	calc
8	Carbonyl Sulfide (COS)	vol %		6.800e-2	☑	0.0	100.0	calc
9	Ammonia (NH3)	vol %		6.000e-3	☑	0.0	100.0	calc
10	Hydrochloric Acid (HCl)	vol %		0.0	☑	0.0	100.0	calc
11	Carbon Dioxide (CO2)	vol %		1.746	☑	0.0	100.0	calc
12	Moisture (H2O)	vol %		3.125	☑	0.0	100.0	calc
13	Nitrogen (N2)	vol %		5.853	☑	0.0	100.0	calc
14	Argon (Ar)	vol %		1.038	☑	0.0	100.0	calc
15	Total	vol %		100.0	☑	0.0	100.0	calc
16								
17								
18								

Figure 10-4. Syngas composition at gasifier exit. This varies with the coal type and operating conditions like temperature and carbon loss percentage.

10.1.2 Sulfinol Sulfur Removal System

A Sulfinol sulfur removal system model is also added to the IGCC model. This is in addition to the Selexol system model that already exists in IECM. The user can choose between Sulfinol and Selexol processes, as shown in Figure 10-5. When the Sulfinol option is selected, CO_2 capture option is deactivated (Figure 10-6). CO_2 capture works only if Selexol is chosen for H_2S capture (Figure 10-7).

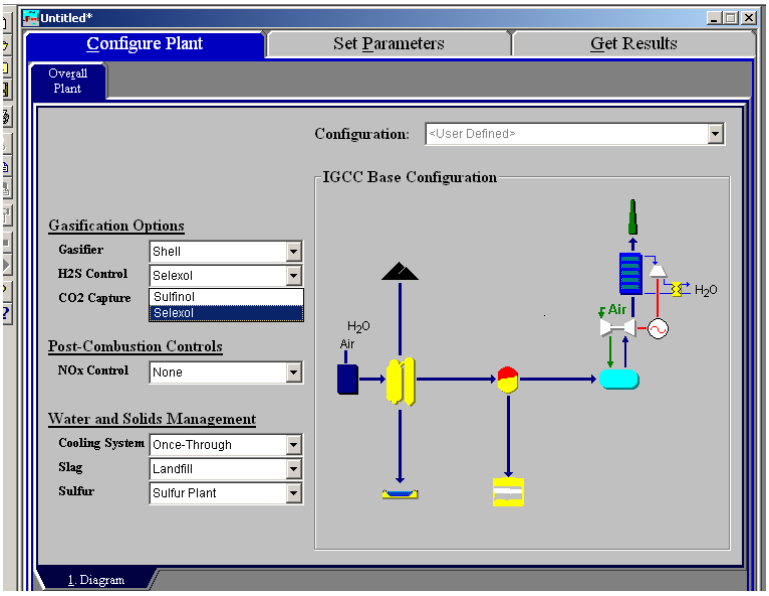

Figure 10-5. H2S control choices - Sulfinol and Selexol

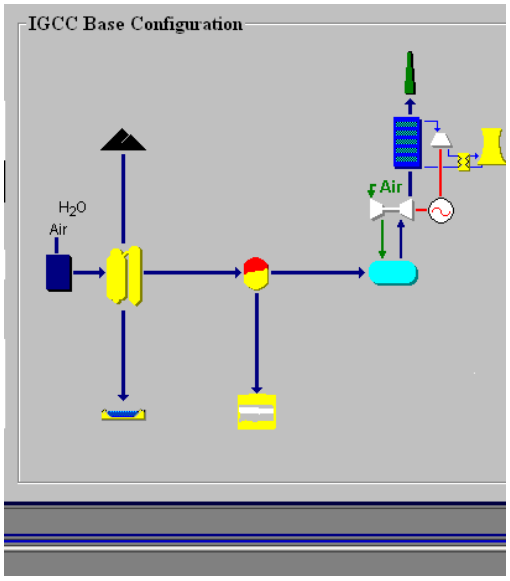

Figure 10-6. Diagram of IGCC base configuration without CO2 capture

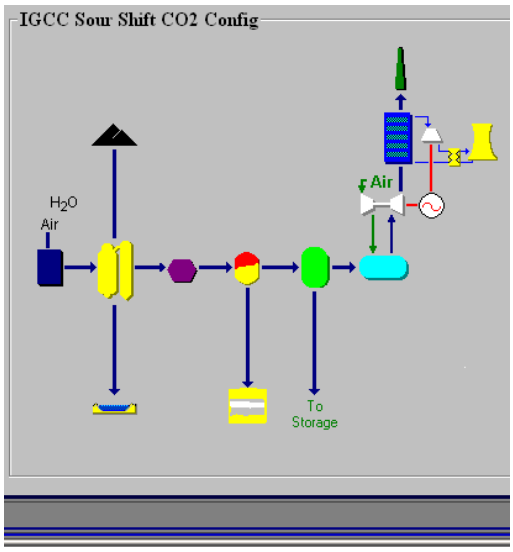

Figure 10-7. Diagram of IGCC plant with sour shift CO2 capture (this is activated only if Selexol is used for sulfur removal)

The range of H_2S removal efficiency has been modified to have a maximum value of 99.9% (line 4 in the Sulfur Removal tab). The sulfur removal block default parameters are shown in Figure 10-8.

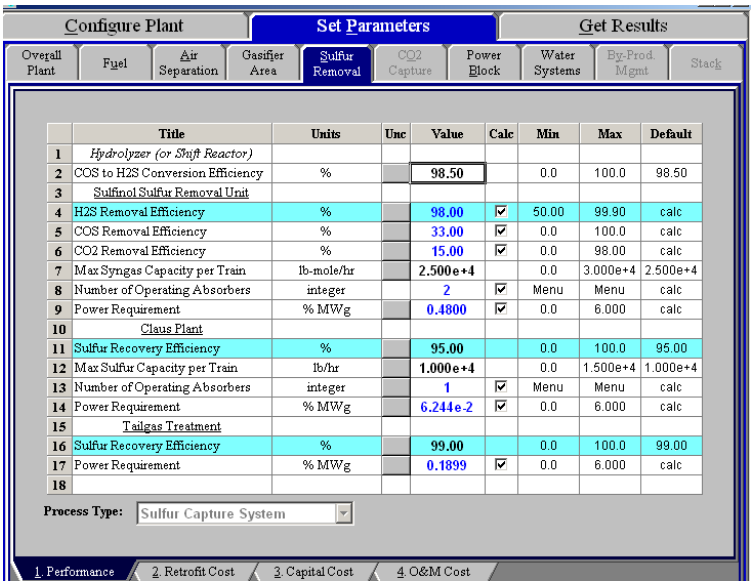

	Title	Units	Unc	Value	Calc	Min	Max	Default
1	*Hydrolyzer (or Shift Reactor)*							
2	COS to H2S Conversion Efficiency	%		98.50		0.0	100.0	98.50
3	Sulfinol Sulfur Removal Unit							
4	H2S Removal Efficiency	%		98.00	☑	50.00	99.90	calc
5	COS Removal Efficiency	%		33.00	☑	0.0	100.0	calc
6	CO2 Removal Efficiency	%		15.00	☑	0.0	98.00	calc
7	Max Syngas Capacity per Train	lb-mole/hr		2.500e+4		0.0	3.000e+4	2.500e+4
8	Number of Operating Absorbers	integer		2	☑	Menu	Menu	calc
9	Power Requirement	% MWg		0.4800	☑	0.0	6.000	calc
10	Claus Plant							
11	Sulfur Recovery Efficiency	%		95.00		0.0	100.0	95.00
12	Max Sulfur Capacity per Train	lb/hr		1.000e+4		0.0	1.500e+4	1.000e+4
13	Number of Operating Absorbers	integer		1	☑	Menu	Menu	calc
14	Power Requirement	% MWg		6.244e-2	☑	0.0	6.000	calc
15	Tailgas Treatment							
16	Sulfur Recovery Efficiency	%		99.00		0.0	100.0	99.00
17	Power Requirement	% MWg		0.1899	☑	0.0	6.000	calc
18								

Figure 10-8. Sulfur Removal block - range of removal efficiency modified to a maximum value of 99.9%

10.1.3 GE 7FB Gas Turbine

The updated IECM contains the option of GE 7FB gas turbine. The earlier version had only 7FA for a gas turbine. The user can select which turbine to use by clicking on the drop-down menu for gas turbine model (line 2 in the Power Block tab), as shown in Figure 10-9. The figure also shows default values for other parameters. The firing temperature of a 7FB turbine is 2500 ºF (line 6 in the Power Block tab) and the pressure ratio is 18.5 (line 12 in the Power Block tab) [12]. The defaults for adiabatic turbine efficiency (line 8 in the Power Block tab) and adiabatic compressor efficiency (line 13 in the Power Block tab) are chosen as 85.7 and 87.5 respectively. These values are arrived at by calibrating the model to match the simple cycle power output of 185 MW and net plant heat rate (LHV) of 9,469 kJ/kWh when the turbine is operated on natural gas as fuel [1].

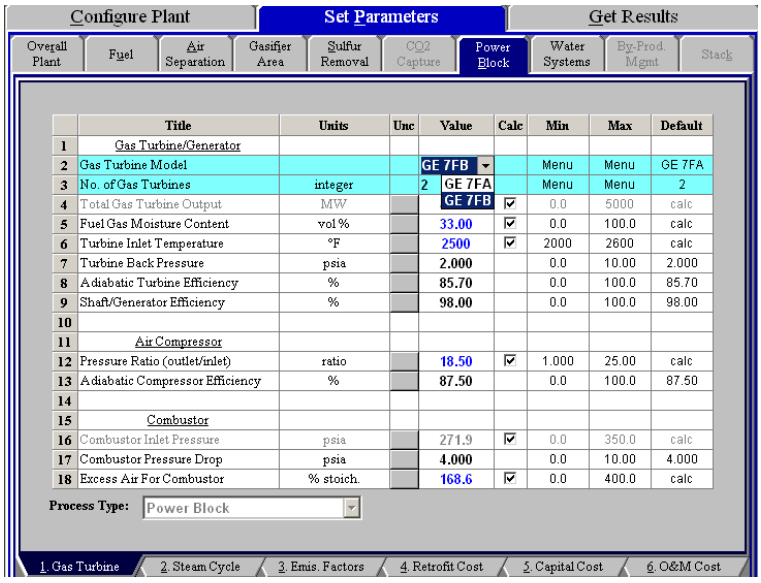

	Title	Units	Unc	Value	Calc	Min	Max	Default
1	Gas Turbine/Generator							
2	Gas Turbine Model			GE 7FB		Menu	Menu	GE 7FA
3	No. of Gas Turbines	integer		2 GE 7FA / GE 7FB		Menu	Menu	2
4	Total Gas Turbine Output	MW			☑	0.0	5000	calc
5	Fuel Gas Moisture Content	vol %		33.00	☑	0.0	100.0	calc
6	Turbine Inlet Temperature	°F		2500	☑	2000	2600	calc
7	Turbine Back Pressure	psia		2.000		0.0	10.00	2.000
8	Adiabatic Turbine Efficiency	%		85.70		0.0	100.0	85.70
9	Shaft/Generator Efficiency	%		98.00		0.0	100.0	98.00
10								
11	Air Compressor							
12	Pressure Ratio (outlet/inlet)	ratio		18.50	☑	1.000	25.00	calc
13	Adiabatic Compressor Efficiency	%		87.50		0.0	100.0	87.50
14								
15	Combustor							
16	Combustor Inlet Pressure	psia		271.9	☑	0.0	350.0	calc
17	Combustor Pressure Drop	psia		4.000		0.0	10.00	4.000
18	Excess Air For Combustor	% stoich.		168.6	☑	0.0	400.0	calc

Figure 10-9. Power Block - 7FB turbine added to IECM

The steam cycle also utilizes high pressure steam from the gas cooling section. To account for that, a heat rate factor was added to the code, for both capture and non-capture cases. The values for these factors were obtained by

calibrating this model with steam turbine output results in the NETL baseline report. Steam turbine output is calculated as follows:

$$MW_{Steam\,turbine} = \frac{\Delta H_{flue\,gas}}{HR_{steam\,cycle} \times factor \times (1 - \Delta T / T_{gasifier})}$$

where, $\Delta H_{flue\,gas}$ is the sensible heat recovered from flue gases in HRSG, $HR_{steamcycle}$ is the default steam cycle heat rate (9,000 BTU/kWh), and the factor in the denominator is the heat rate adjustment factor. The value of the factor is 0.6972 for non-capture cases, where a higher amount of steam is produced by radiant syngas cooling, compared to the quench cooling system in the capture case, where the factor has been estimated as 0.8756, when the gasification temperature is 2600 ^{o}F. The temperature term in the denominator adjusts the turbine output according to variation in gasification temperature. If the temperature is higher than 2600 ^{o}F, there will be more steam produced and hence more power output from the steam turbine and vice versa.

10.2 Modifications to IGCC Cost Models

New cost models were developed for new technologies and the existing cost models were updated using recent literature. This section lists the additions and modifications to IECM cost models for IGCC.

10.2.1 Shell Gasification System

Capital cost of Shell gasifiers is different from other gasifiers. New cost models had to be developed for IECM Shell gasifier cases. The exponential cost model is used here for gasifier cost equations.

$$C = C_{ref} \times \left(\frac{X}{X_{ref}} \right)^{m}$$

In doing cost estimation for slurry feed quench gasifiers, it was found that the cost varies with coal flow rate with an exponential factor of 0.943 [GE documentation IECM]. The same exponent (m = 0.943) is used in estimating the costs for Shell gasifiers.

NETL baseline report is used for reference cost cases. For non-CO_2 capture cases, a radiant syngas cooler is used with to cool raw gas from the gasifier, in the process generating high pressure steam. For cases with CO_2 capture, a quench cooling mechanism is used which helps in supplying a part of required water for the downstream water gas shift reactor. So, different cost models were developed for the non-capture and capture cases. Equation 1 shows the cost equation for the gasifier with radiant cooling section, used for non-capture cases. Equation 2 shows the cost equation for a gasifier with quench cooling, used to capture cases.

$$C_{gasifier,radiant} = 48{,}856 \times N_{T,G} \left(\frac{m_{coal}}{N_{O,G}} \right)^{0.943} (\$) \qquad (10\text{-}1)$$

$$C_{gasifier,radiant} = 37{,}334 \times N_{T,G} \left(\frac{m_{coal}}{N_{O,G}} \right)^{0.943} (\$) \qquad (10\text{-}2)$$

Where, N_T is the total number of trains, N_O is the number of operating trains and m_{coal} is the mass flow of as-received coal (tons per day).

10.2.2 7FB Gas Turbine

Cost models for gas turbine were also developed using NETL report as reference values. The determining variable is the number of turbines. Cost for one turbine is estimated as $47,431,000. For multiple turbines, this value is multiplied by the number of turbines.

10.2.3 Modifications to Existing Cost Equations

The cost models for other IGCC sections in the IECM were also updated to be in tune with recent values [2]. The same equations were used as in the earlier version but with an adjustment factor multiplied to the coefficient. The factors are shown in Table 10-1.

Table 10-1. Parameter Cost adjustment factors used to update the existing cost models to recent values

Process section	Cost adjustment factor
Air Separation Unit	1.471
Gasifier Area	
Coal Handling	4.337
Gasifier (non-capture)	1.096
Gasifier (capture)	0.946
Low Temperature Gas Cooling	0.591
Process Condensate Treatment	1.001
Activated Carbon Mercury Removal	0.002*gasification island cost
Sulfur Removal	
Sulfur Removal System-Hydrolyzer	7.539
Sulfur Removal System-Sulfinol	4.161
Sulfur Removal System-Selexol	1.25
Sulfur Removal System-Claus	3.026
CO2 Capture-Selexol	1.25
Power Block	
Gas Turbine	0.634
Heat Recovery Steam Generator	1.221
Steam Turbine	0.528
HRSG Feedwater System	3.584

10.3 Case Studies of IGCC Plants

The use of IECM is demonstrated by applying it to a few case studies. The first case is a replication of cases 5 and 6 of the NETL baseline study – Shell based IGCC without and with CO_2 capture, respectively. The other case studies show the ability of IECM in application to different input parameters and test the sensitivity of performance and cost behavior to those changes.

10.3.1 Case Study 1: NETL Baseline Report IGCC Cases

Case 5 of the NETL baseline report deals with an IGCC power plant using the Shell gasification system with radiant syngas cooling, without CO_2 capture. The plant uses Illinois#6 coal. Sulfinol process is used for H_2S removal. The net power output from the plant is 632 MW, produced using a GE 7FB combined cycle power plant. The plant uses dilution of syngas before entering the gas turbine combustor, to reduce its lower heating value to about 4.6 MJ/Nm^3.

Case 6 of the NETL baseline report utilizes the Shell gasification system with quench raw gas cooling. After shifting the syngas to convert almost all of the CO to CO2, co-capture of H2S and CO2 takes place in a dual stage Selexol process. Syngas entering the gas turbine combustor is diluted with both N2 from the ASU and humidification steam to reduce its heating value.

For this case study, performance and cost assumptions from the NETL cases 5 and 6 were given to IECM IGCC models, wherever possible. Efforts were made to match all the inputs but the possibility of missing out some parameters cannot be ruled out. The current IECM does not include N_2-integration capability. Lowering of heating value is achieved by increasing the moisture content of the syngas before entering the gas turbine combustor.

Owners' costs are not included in NETL cost estimations, whereas IECM defaults include owners' costs. Owners' costs were forced to be nearly zero by zeroing out certain factors.

The following are a few major changes that were made to the performance defaults in IECM, in order to replicate cases 5 and 6:

- Ambient Air Temperature (Avg.) (°F): 59.00 (default: 77.00)
- Auxiliary power requirements for different processes were changed to match the baseline values:
    - Total ASU Power Requirement (% MWg): 7.080
    - Gasifier Area Power Requirement (% MWg): 0.6400
    - Sulfur Removal COS to H2S Conversion Efficiency (%): 99.50 (default: 98.50)
    - H_2S Removal Efficiency (%): 99.00
    - H_2S Removal Power Requirement (% MWg): 0.12
    - Power Block Power Requirement (% MWg): 5.460
- Power Block Fuel Gas Moisture Content (vol %): 48.53 for non-capture and 50% for capture cases. NETL case assumed N_2-injection into the gas turbine combustor, which adds to the power generation capacity. Since N_2-injection is not used in IECM, the fuel gas moisture content value was modified to match the gas turbine output to 464 MW.

Important changes to the cost factors are:

- Capacity factor was changed to 80% (default: 75%)
- Discount Rate (Before Taxes) (fraction): 1.000e-4. Discount rate effectively set to zero as made near 0 because NETL report does not include owner's costs or interest during construction in the cost estimating methodology.
- Fixed Charge Factor (FCF) (fraction): 0.1750. NETL uses a fixed charge factor of 17.5%, considering IGCC as a high-risk technology.

Table 10-2 and Table 10-3 show the comparison of performance and cost results between IECM estimation and those reported in the baseline report for cases 5 and 6 respectively. It can be seen that most of the values match within +/- 2% of the reported values. The cost of electricity is slightly different because the NETL Baseline Study assumes small real escalation of coal prices, which is not modeled in the IECM.

Table 10-2. Comparison of results from IECM and NETL (case 5) for a Shell based IGCC plant without CO_2 capture

Parameter	IECM	NETL
Net power output (MW)	635.6	635.9
Net plant heat rate (BTU/kWh)	8,194	8,306
Net plant efficiency (%, HHV)	41.6	41.1
Total capital required (M$)	1,280	1,257
Total capital required ($/kW-net)	2,014	1,977
Cost of electricity ($/MWh)	80.61	80.5

Table 10-3. Comparison of results from IECM and NETL (case 6) for a Shell based IGCC plant with CO_2 capture

Parameter	IECM	NETL
Net power output (MW)	517.3	517.1
Net plant heat rate (BTU/kWh)	10,550	10,674
Net plant efficiency (%, HHV)	32.3	32.0
Total capital required (M$)	1,363	1,379
Total capital required ($/kW-net)	2,635	2,668
Cost of electricity ($/MWh)	106.8	110.4

Conclusion

This case study demonstrates the capability of IECM in obtaining similar results to the NETL study by varying the relevant inputs correspondingly.

10.3.2 Case Study 2: Effect of Plant Capacity on Capital Cost and Cost of Electricity

In this case study, the effect of changing plant size on the capital cost and cost of electricity is analyzed. In IECM, plant size can be changed by varying the number of gas turbines used in the plant. IGCC power plants with 1, 2 and 3 gas turbines are compared here. Performance and cost parameter assumptions are the same as in case study 1.

Figure 10-10 shows the results for capital cost as a function of net plant size, for both non-capture and CO_2-capture cases. Economy of scale for an IGCC power plant can be seen in this figure. As the net power output increases, the specific capital cost decreases. However, the rate of decrease is lower as the plant size increases. The economy of scale of capital cost can also be seen by its effect on the cost of electricity, as shown in Figure 10-11. The cost of electricity also decreases with increasing plant size.

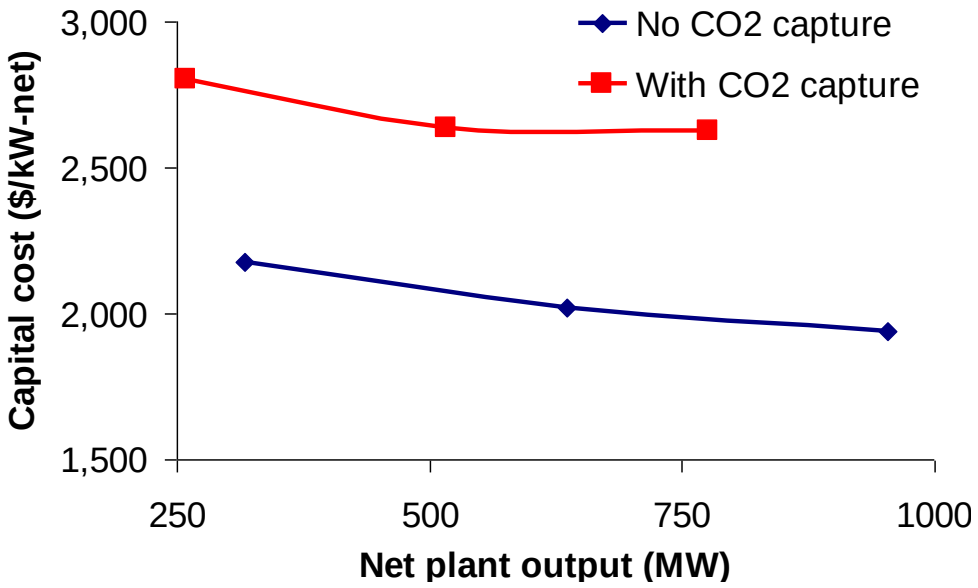

Figure 10-10. Sensitivity of capital cost to net plant output, with and without CO_2 capture. As the plant size increases, specific capital cost decreases. CO_2 capture increases the capital cost by more than 30%

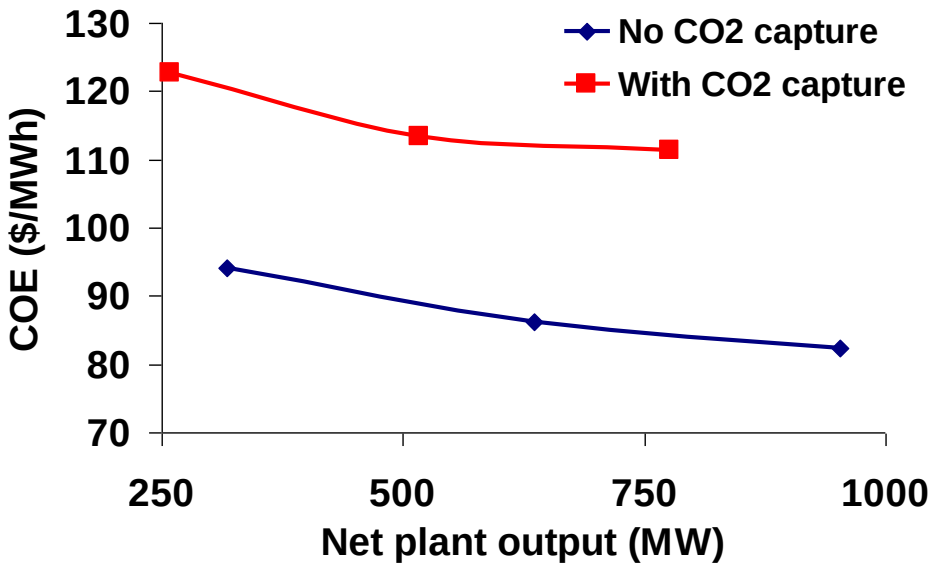

Figure 10-11. Sensitivity of cost of electricity to net plant output, with and without CO_2 capture. As the plant size increases, specific capital cost decreases. CO_2 capture increases the COE by about 30%

10.3.3. Case Study 3: Effect of Type of Coal on Performance and Cost

Different types of coals have different effects on the performance and cost of a power plant. Here, IECM is applied to IGCC power plants using three different types of coal

- Appalachian Medium Sulfur bituminous coal (also called as Pittsburgh#8)
- Illinois#6 bituminous coal
- Wyoming PRB sub-bituminous coal

The properties and cost of coals used in this analysis are shown in Table 10-4. The default performance and cost assumptions of IECM are used for this analysis. The ambient temperature is 77 ºF, and pressure is 14.7 psia. All the owners' costs are included. General facilities capital of 15%, engineering and home office fees of 10%, project contingency cost of 15%, and royalty fees of 0.5% of plant facilities cost was applied to all the process sections. The process contingency cost varies from process to process.

Table 10-4. Properties of coals used in this analysis

Coal	Appalachian medium sulfur	Illinois#6	Wyoming PRB
Rank	Bituminous	Bituminous	Sub-bituminous
Ash	7.24	11	5.32
C	73.81	61.2	48.18
H2	4.88	4.2	3.31
N2	1.42	1.16	0.7
Cl	6.00E-02	0.17	1.00E-02
S	2.13	3.25	0.37
O2	5.41	6.02	11.87
Moisture	5.05	13	30.24
HHV(BTU/lb)	13,260	11,670	8,340
Cost ($/ton)	45.24	42	8.75

Figure 10-12 shows the effect of coal type on the net plant efficiency, both for non-capture and CO_2 capture cases. The plant efficiency decreases with decreasing quality of coal and CO_2-capture has an efficiency penalty of roughly 9–10 percentage points. The CO_2 emission intensities of different kinds of coal are shown in Figure 10-13. CO_2 emissions per unit output increase with decreasing coal quality, either with or without CO_2 capture.

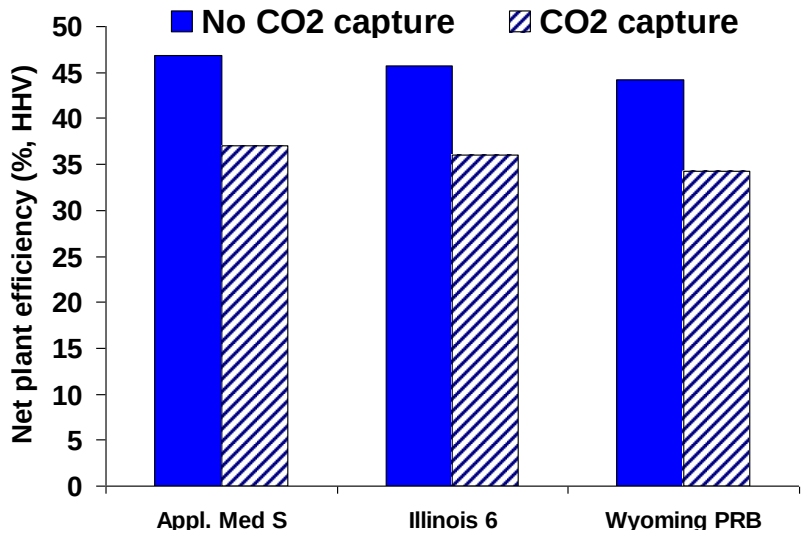

Figure 10-12. Effect of coal type on net plant efficiency of an IGCC power plant, with and without CO2 capture

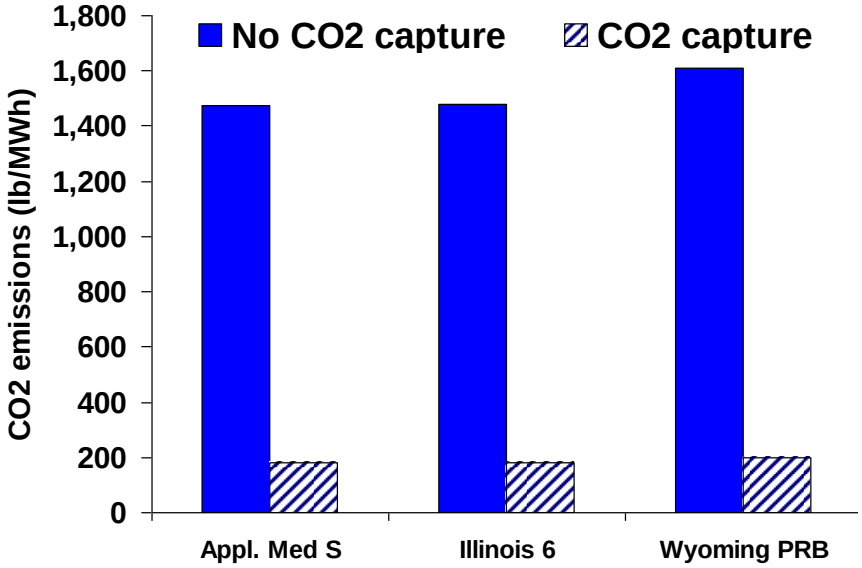

Figure 10-13. CO2 emission intensity of an IGCC power plant using different coal types

Figure 10-14 and Figure 10-15 show the effect of coal type on capital cost and cost of electricity, respectively. Capital cost of a plant using the lowest quality coal (Wyoming PRB) is about 12% higher than the one using the highest quality coal (Appalachian medium S). However, without CO_2-capture, cost of electricity of the plant using Wyoming PRB is the lowest of all three. This is because of the lower price of sub-bituminous coal than that of bituminous coals. CO_2-capture involves a capital cost increase of 20% for bituminous coals to 27% for sub-bituminous coals.

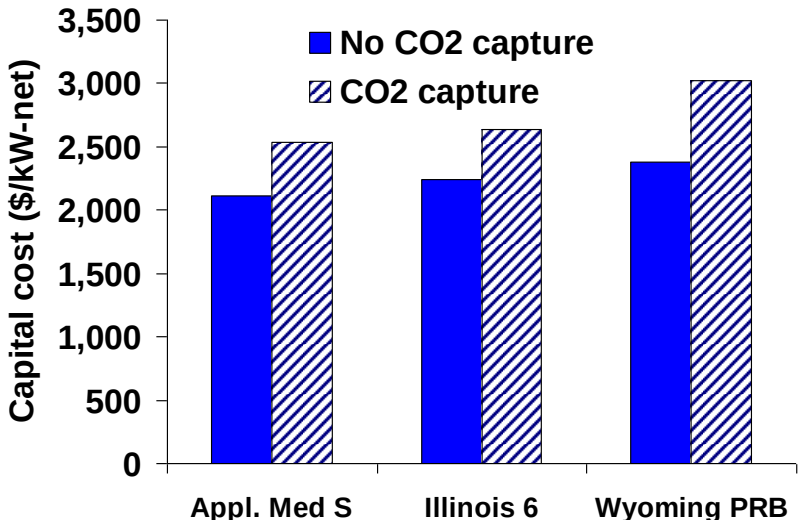

Figure 10-14. Effect of type of coal on capital cost of the plant, with and without CO2 capture

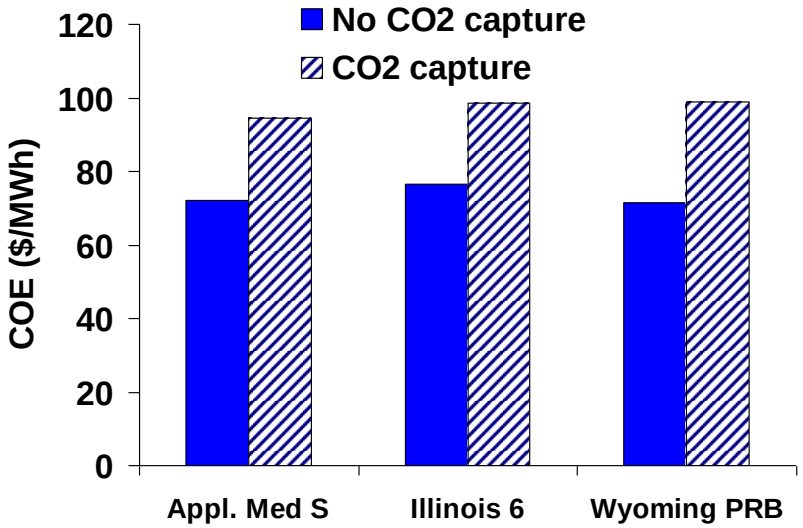

Figure 10-15. Effect of coal type on cost of electricity for an IGCC plant, with and without CO2 capture

10.4 Conclusion

Updates to the IGCC models of IECM user-interface were presented and the reasons and methodology of modifications were explained. Through the application of IECM to NETL case studies, the validity of IECM was demonstrated. The capability of IECM to do sensitivity analyses for various kinds of input parameters was also shown.

Appendix: Shell Gasification Model Development using Aspen Plus

Background and Objectives

In this report, results from a technical model of a Shell gasification process using 6 different types of coal are described. A process performance model was developed using Aspen Plus simulation software [6] that calculates the product gas compositions from a Shell gasifier operating on six different coals, including bituminous, sub-bituminous and lignite ranks. Gasification temperature and the amount of carbon lost in the slag were used as variables for sensitivity analysis. The results will eventually go into IECM software [8].

The objectives of this study are:

1. to build a process model for a Shell gasification process used for IGCC applications
2. to analyze the sensitivity of gas composition to variations in gasification temperature and carbon lost in slag

Introduction

Gasification of coal is essentially a reaction of carbon in coal with a source of hydrogen (usually steam) and/or oxygen to yield a gas containing predominantly carbon monoxide (CO), hydrogen (H2), carbon dioxide (CO_2) and methane (CH_4). Coal can be gasified to produce medium calorific value (10 – 16 MJ/m^3) synthesis gas (or syngas), consisting primarily of a mixture of CO and H_2. Synthetic natural gas whose main component is CH_4 can also be produced from coal. Since syngas is the reactant in FT reactions, only those gasifier technologies used to produce syngas are considered here.

Gasifiers that produce syngas generally involve reaction of coal with steam and oxygen in the presence of heat [2]. The main reactions occurring in these gasifiers are:

$C + H_2O \rightarrow CO + H_2$ $\quad \Delta H^o_{1000K}$ = 135 kJ/mol (A1)

$C + ½\ O_2 \rightarrow CO$ $\quad \Delta H^o_{1000K}$ = - 112 kJ/mol (A2)

$C + O_2 \rightarrow CO_2$ $\quad \Delta H^o_{1000K}$ = - 395 kJ/mol (A3)

A gasifier is fundamentally a chemical reactor. Based on the reactor type, gasifiers are classified as fixed/moving bed, fluidized bed or entrained flow gasifiers. Selection of gasifier depends on a number of factors including the coal characteristics, quality requirements of syngas, operating parameters, site-specific requirements and so on. Of the above-mentioned gasifier types, entrained flow design is the most widely used. These gasifiers operate at high temperatures and are characterized by very low residence time of coal (of the order of seconds). High temperatures limit the formation of methane. The advantage of entrained flow gasifiers is the flexibility of using any type of coal. Coal has to be pulverized to help in its rapid gasification. Within the entrained gasifier design, there is variability in the method in which coal is fed into the gasifier. Coal can be fed either dry or in the form of water slurry. GE/Texaco entrained flow gasifiers are the most commonly used design followed by Shell gasifiers.

Shell Gasification

A Shell gasifier is a dry-feed entrained flow pressurized gasifier [9] [11]. Unlike the slurry-feed gasifiers in which slurry is used as the medium of coal transport to the gasifier, Shell gasifier uses nitrogen gas (N_2) as the transport medium. Oxygen and a small amount of steam are also fed to the gasifier in which coal reacts with oxygen at temperatures in excess of 1370 ^{o}C and a pressure of 4.3 MPa. Gasification at such high temperatures maximizes the production of CO and H_2 and minimizes the production of CO_2 and hydrocarbon gases and liquids. Ash is removed at the bottom of the gasifier in the form of slag. The raw gas leaves the gasifier at 1600 ^{o}C and is cooled to about 900 ^{o}C by quenching with cooled recycle gas. Further cooling is achieved in a waste heat boiler which produces steam. The gas is then sent to gas-cleaning and scrubbing units.

For plants with CCS, NETL baseline report uses a water quench method to cool the raw syngas instead of a waste heat boiler. However, this does not affect the performance of the gasifier (Figure 10-16).

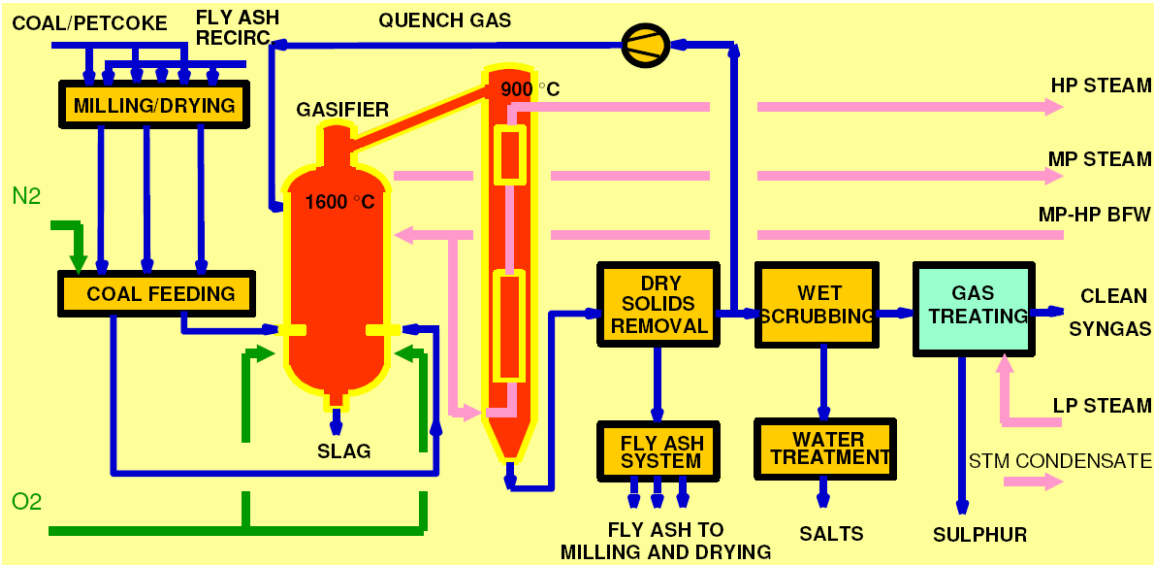

Figure 10-16. Effect Shell gasification process [10]

Performance Model in Aspen Plus

A mathematical model for gasification should duplicate the reactions between carbon and other components in coal with oxygen and steam fed into the gasifier. Different gasifiers inject steam in different ways. In slurry-based gasifiers such as GE and E-Gas, steam comes in the form of water in the slurry used to transport coal into the gasifier. There are non-slurry-based gasifiers (Shell) in which coal is transported into the gasifier using a nitrogen medium. Steam for such systems is fed directly into the gasifier. The other input is oxygen, which is fed into the gasifier from an Air Separation Unit (ASU). Thus, though the methods of injecting all the inputs into the gasifier may differ, gasification process is essentially a reaction of coal with water/steam and oxygen to produce syngas, as shown in Figure 10-17.

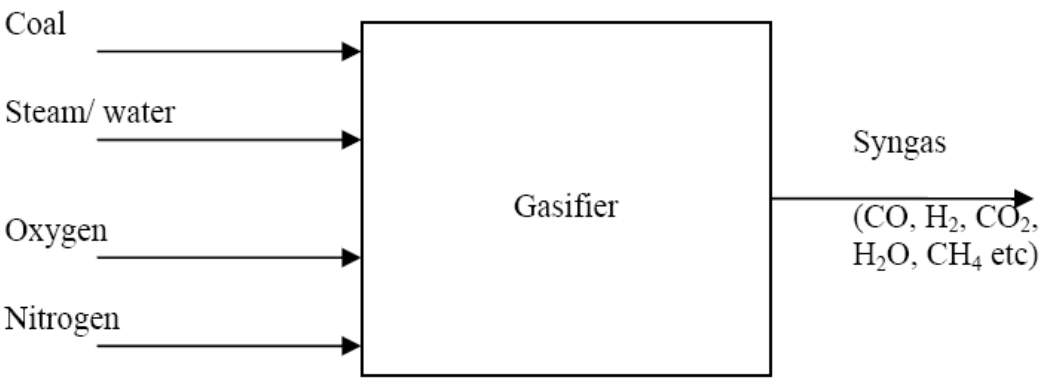

Figure 10-17. Block flow diagram of a gasifier

Coal Preparation

Six different types of coals are modeled here, whose ultimate analyses are given in Table 10-5. For the purpose of modeling using Aspen Plus, coal is a non-conventional solid, in the sense that it is composed of different component elements and cannot be represented as a single chemical species. This non-conventional material has

to be decomposed into conventional components which will then react in the gasifier. The elemental composition of coal is given by its ultimate analysis. The amount of moisture in coal is given by its proximate analysis.

This non-conventional material is then 'decomposed' into different conventional components using a RYIELD reactor, which calculates the composition of the products based on a given yield distribution. The distribution is input in the form of a calculator block which uses the data from ultimate and proximate analyses to calculate the mass fractions of carbon (C), hydrogen (H_2), nitrogen (N_2), chlorine (Cl_2), sulfur (S), water (H_2O), oxygen (O_2) and ash. The procedure for this calculation is shown below.

Mass fraction of every component is given by,

$$y_{component} = Component_{coal} \times (1 - Moisture_{coal})$$

The mass fraction of each component in coal, $Component_{coal}$, is obtained from the ultimate analysis and $Moisture_{coal}$ is obtained from the proximate analysis data.

Heat released in the decomposition process is fed into the gasifier block since this process is not separate from the gasification process for practical purposes. However, since temperature is specified as an input variable to the gasifier model, this heat input does not affect the product gas composition.

Table 10-5. Ultimate analyses of different coals

Coal	Appalachian low sulfur	Appalachian medium sulfur	Illinois#6	WPC Utah	Wyoming PRB	ND lignite
Rank	Bituminous	Bituminous	Bituminous	Bituminous	Sub-bituminous	Lignite
Ash	9.79	7.24	11	11.59	5.32	15.92
C	71.74	73.81	61.2	67.66	48.18	35.04
H2	4.62	4.88	4.2	4.85	3.31	2.68
N2	1.42	1.42	1.16	1.22	0.7	0.77
Cl	7.00E-02	6.00E-02	0.17	1.00E-02	1.00E-02	9.00E-02
S	0.64	2.13	3.25	0.61	0.37	1.16
O2	6.09	5.41	6.02	6.11	11.87	11.31
Moisture	5.63	5.05	13	7.95	30.24	33.03
HHV(MJ/kg)	30.36	30.78	25.30	26.09	19.36	13.97

Coal Drying, Slag Removal and Carbon-Loss

Since Shell gasification is a dry process, feed coal needs to be dried before injecting into the gasifier. For bituminous coals, coal is dried to 5% moisture by weight. For sub-bituminous and lignite, the moisture content in the dried coal is 6% and 12% by weight, respectively [11].

Though in the actual process, slag is removed at the bottom of the gasifier, for the ease of modeling, here the non-conventional component "ash" can be removed from the decomposed coal stream before the gasifier block.

Some amount of carbon in coal is lost in slag. For modeling purposes, this "carbon-loss" is accounted for before the gasifier block.

All the three processes discussed above – coal drying, slag removal and carbon loss – are modeled using a single separator block (SEP in Aspen Plus). The split fraction of water is specified using a design specification fortran block (DesignSpec) which fixes the weight fraction of water in the gasifier feed depending on the type of coal. Split fraction of carbon is specified using a sensitivity block which varies the carbon loss between 0 and 2% with an interval of 0.5%. Ash is also removed completely in this block.

Mass flow rate of dried coal (gasifier feed) as compared to the wet coal is given by the following equation:

$$\overset{g}{m}_{dried\ coal} = \overset{g}{m}_{wet\ coal} \times \frac{\left(1 - Moisture_{wet\ coal}\right)}{\left(1 - Moisture_{dried\ coal}\right)}$$

Oxygen and Steam Feeds

Most of the entrained flow gasifiers use oxygen as the oxidation agent. Oxygen is separated from air typically in a cryogenic air separation unit (ASU) and the 95% pure oxygen is fed into the gasifier. For this Aspen Plus model, ASU is not modeled explicitly. The gasifier is directly fed with 95% pure oxygen which is compressed from atmospheric pressure to the gasification pressure. The energy required for ASU and oxygen compression is modeled using equations developed for IECM.

The flow rate of oxygen is specified using DesignSpec such that the ratio of oxygen to carbon is 0.442 mol/mol, as calculated from the values in NETL baseline report. Some amount of steam is also injected as a separate stream directly into the gasifier block. The mass flow rate is of steam is specified as 9.65% of wet coal mass flow rate using DesignSpec [8]. These values are assumed to be the same for all coals.

Gasifier Block

In Aspen Plus, the reactor unit RGIBBS is used to model the gasification reactions. This can be used when the possible products are known but the exact reactions that take place to produce those components are not well-known. This reactor unit calculates the composition of the products based on the minimization of Gibbs' free energy. Apart from the material flow inputs to the reactor, the pressure at which reactions take place and either the reactor temperature or the heat duty has to be specified. It is assumed that all the reactions reach chemical equilibrium.

Considering the products in a typical gasifier product gas, apart from reactions 1 – 3 the following reactions are likely to take place in the gasifier [7]:

$C + 2\ H_2 \rightarrow CH_4$ (A4)
$CO + H_2O \rightarrow CO_2 + H_2$ (A5)
$2CO + O_2 \rightarrow 2CO_2$ (A6)
$CH_4 + H_2O \rightarrow CO + 3H_2$ (A7)
$S + H_2 \rightarrow H_2S$ (A8)

$N_2 + 3H_2 \rightarrow 2NH_3$ (A9)
$CO + H_2S \rightarrow COS + H_2$ (A10)

To see the effect of temperature on the products, gasification temperatures of 1371 ^oC (2500 ^oF), 1427 ^oC (2600 ^oF) and 1482 ^oC (2700 ^oF) are modeled.

Results

The syngas compositions obtained from Aspen Plus modeling are given in Table 10-6 through Table 10-23. Results are shown for all the coals at different gasification temperatures and carbon loss values. The following general observations can be made:

- as the carbon content in the fuel increases, the CO fraction in the product gas increases and CO_2 fraction decreases
- for a given carbon loss fraction, an increase in temperature increases the production of CO and decreases methane formation
- for a given temperature, CO formation decreases with increasing carbon loss

Table 10-6. Syngas composition for Illinois#6 bituminous coal at 1371 °C

Illinois # 6, dried to 5% moisture by weight, temperature 1371 °C					
Carbon in slag (%)	0	0.5	1	1.5	2
CO	0.574	0.571	0.569	0.567	0.565
H_2	0.302	0.301	0.300	0.299	0.298
CH_4	0.001	0.001	0.001	0.001	0.001
H_2S	0.008	0.008	0.008	0.008	0.008
COS	0.001	0.001	0.001	0.001	0.001
NH_3	0.000	0.000	0.000	0.000	0.000
CO_2	0.017	0.018	0.019	0.021	0.022
H_2O	0.029	0.031	0.033	0.034	0.036
N_2	0.058	0.059	0.059	0.059	0.059
O_2	0.000	0.000	0.000	0.000	0.000

Table 10-7. TabSyngas composition for Illinois#6 bituminous coal at 1427 °C

Illinois # 6, dried to 5% moisture by weight, temperature 1427 °C					
Carbon in slag (%)	0	0.5	1	1.5	2
CO	0.574	0.572	0.570	0.568	0.565
H_2	0.302	0.301	0.300	0.299	0.298
CH_4	0.000	0.000	0.000	0.000	0.000
H_2S	0.008	0.008	0.008	0.008	0.008
COS	0.001	0.001	0.001	0.001	0.001
NH_3	0.000	0.000	0.000	0.000	0.000
CO_2	0.016	0.017	0.019	0.020	0.021
H_2O	0.029	0.031	0.033	0.035	0.037
N_2	0.058	0.059	0.059	0.059	0.059
O_2	0.000	0.000	0.000	0.000	0.000

Table 10-8. Syngas composition for Illinois#6 bituminous coal at 1482 °C

Illinois # 6, dried to 5% moisture by weight, temperature 1482 °C					
Carbon in slag (%)	0	0.5	1	1.5	2
CO	0.575	0.573	0.571	0.568	0.566
H_2	0.302	0.301	0.300	0.299	0.298
CH_4	0.000	0.000	0.000	0.000	0.000
H_2S	0.008	0.008	0.008	0.008	0.008
COS	0.001	0.001	0.001	0.001	0.001
NH_3	0.000	0.000	0.000	0.000	0.000
CO_2	0.016	0.017	0.018	0.019	0.020
H_2O	0.030	0.032	0.034	0.036	0.038
N_2	0.058	0.059	0.059	0.059	0.059
O_2	0.000	0.000	0.000	0.000	0.000

Table 10-9. Syngas composition for Appalachian low sulfur bituminous coal at 1371 °C

Appalachian low sulfur, dried to 5% moisture by weight, temperature 1371 °C					
Carbon in slag (%)	0	0.5	1	1.5	2
CO	0.594	0.592	0.590	0.587	0.585
H_2	0.301	0.301	0.300	0.299	0.298
CH_4	0.001	0.001	0.001	0.001	0.001
H_2S	0.002	0.002	0.002	0.002	0.002
COS	0.000	0.000	0.000	0.000	0.000
NH_3	0.000	0.000	0.000	0.000	0.000
CO_2	0.014	0.015	0.016	0.017	0.019
H_2O	0.023	0.025	0.026	0.028	0.030
N_2	0.054	0.055	0.055	0.055	0.055
O_2	0.000	0.000	0.000	0.000	0.000

Table 10-10. Syngas composition for Appalachian low sulfur bituminous coal at 1427 °C

Appalachian low sulfur, dried to 5% moisture by weight, temperature 1427 °C					
Carbon in slag (%)	0	0.5	1	1.5	2
CO	0.595	0.593	0.590	0.588	0.586
H_2	0.302	0.301	0.300	0.299	0.298
CH_4	0.001	0.001	0.001	0.000	0.000
H_2S	0.002	0.002	0.002	0.002	0.002
COS	0.000	0.000	0.000	0.000	0.000
NH_3	0.000	0.000	0.000	0.000	0.000
CO_2	0.013	0.014	0.015	0.017	0.018
H_2O	0.023	0.025	0.027	0.029	0.031
N_2	0.054	0.055	0.055	0.055	0.055
O_2	0.000	0.000	0.000	0.000	0.000

Table 10-11. Syngas composition for Appalachian low sulfur bituminous coal at 1482 °C

Appalachian low sulfur, dried to 5% moisture by weight, temperature 1482 °C					
Carbon in slag (%)	0	0.5	1	1.5	2
CO	0.595	0.593	0.591	0.589	0.587
H_2	0.302	0.301	0.300	0.299	0.298
CH_4	0.000	0.000	0.000	0.000	0.000
H_2S	0.002	0.002	0.002	0.002	0.002
COS	0.000	0.000	0.000	0.000	0.000
NH_3	0.000	0.000	0.000	0.000	0.000
CO_2	0.013	0.014	0.015	0.016	0.017
H_2O	0.023	0.025	0.027	0.029	0.031
N_2	0.054	0.054	0.055	0.055	0.055
O_2	0.000	0.000	0.000	0.000	0.000

Table 10-12. Syngas composition for Appalachian medium sulfur bituminous coal at 1371 °C

Appalachian medium sulfur, dried to 5% moisture by weight, temperature 1371 °C					
Carbon in slag (%)	0	0.5	1	1.5	2
CO	0.594	0.592	0.589	0.587	0.585
H_2	0.305	0.304	0.303	0.302	0.301
CH_4	0.001	0.001	0.001	0.001	0.001
H_2S	0.006	0.006	0.006	0.006	0.006
COS	0.001	0.001	0.001	0.001	0.001
NH_3	0.000	0.000	0.000	0.000	0.000
CO_2	0.012	0.013	0.014	0.015	0.016
H_2O	0.019	0.021	0.023	0.025	0.026
N_2	0.053	0.053	0.053	0.053	0.053
O_2	0.000	0.000	0.000	0.000	0.000

Table 10-13. Syngas composition for Appalachian medium sulfur bituminous coal at 1427 °C

Appalachian medium sulfur, dried to 5% moisture by weight, temperature 1427 °C					
Carbon in slag (%)	0	0.5	1	1.5	2
CO	0.595	0.592	0.590	0.588	0.586
H_2	0.305	0.304	0.303	0.303	0.302
CH_4	0.001	0.001	0.001	0.001	0.001
H_2S	0.006	0.006	0.006	0.006	0.006
COS	0.001	0.001	0.001	0.001	0.001
NH_3	0.000	0.000	0.000	0.000	0.000
CO_2	0.011	0.012	0.013	0.014	0.015
H_2O	0.019	0.021	0.023	0.025	0.027
N_2	0.053	0.053	0.053	0.053	0.053
O_2	0.000	0.000	0.000	0.000	0.000

Table 10-14. Syngas composition for Appalachian medium sulfur bituminous coal at 1482 °C

Appalachian medium sulfur, dried to 5% moisture by weight, temperature 1482 °C					
Carbon in slag (%)	0	0.5	1	1.5	2
CO	0.595	0.593	0.591	0.588	0.586
H_2	0.305	0.304	0.303	0.302	0.301
CH_4	0.000	0.000	0.000	0.000	0.000
H_2S	0.006	0.006	0.006	0.006	0.006
COS	0.001	0.001	0.001	0.001	0.001
NH_3	0.000	0.000	0.000	0.000	0.000
CO_2	0.010	0.011	0.013	0.014	0.015
H_2O	0.019	0.021	0.023	0.025	0.027
N_2	0.053	0.053	0.053	0.053	0.053
O_2	0.000	0.000	0.000	0.000	0.000

Table 10-15. Syngas composition for WPC Utah bituminous coal at 1371 °C

WPC Utah, dried to 5% moisture by weight, temperature 1371 °C					
Carbon in slag (%)	0	0.5	1	1.5	2
CO	0.577	0.575	0.572	0.570	0.568
H_2	0.316	0.316	0.315	0.314	0.313
CH_4	0.001	0.001	0.001	0.001	0.001
H_2S	0.002	0.002	0.002	0.002	0.002
COS	0.000	0.000	0.000	0.000	0.000
NH_3	0.000	0.000	0.000	0.000	0.000
CO_2	0.014	0.015	0.016	0.017	0.018
H_2O	0.025	0.027	0.028	0.030	0.032
N_2	0.055	0.055	0.055	0.056	0.056
O_2	0.000	0.000	0.000	0.000	0.000

Table 10-16. Syngas composition for WPC Utah bituminous coal at 1427 °C

WPC Utah, dried to 5% moisture by weight, temperature 1427 °C					
Carbon in slag (%)	0	0.5	1	1.5	2
CO	0.578	0.575	0.573	0.571	0.569
H_2	0.317	0.316	0.315	0.314	0.313
CH_4	0.001	0.001	0.001	0.001	0.000
H_2S	0.002	0.002	0.002	0.002	0.002
COS	0.000	0.000	0.000	0.000	0.000
NH_3	0.000	0.000	0.000	0.000	0.000
CO_2	0.013	0.014	0.015	0.016	0.017
H_2O	0.025	0.027	0.029	0.031	0.033
N_2	0.055	0.055	0.055	0.056	0.056
O_2	0.000	0.000	0.000	0.000	0.000

Table 10-17. Syngas composition for WPC Utah bituminous coal at 1482 °C

WPC Utah, dried to 5% moisture by weight, temperature 1482 °C					
Carbon in slag (%)	0	0.5	1	1.5	2
CO	0.578	0.576	0.574	0.572	0.569
H_2	0.317	0.316	0.315	0.314	0.313
CH_4	0.000	0.000	0.000	0.000	0.000
H_2S	0.002	0.002	0.002	0.002	0.002
COS	0.000	0.000	0.000	0.000	0.000
NH_3	0.000	0.000	0.000	0.000	0.000
CO_2	0.013	0.014	0.015	0.016	0.017
H_2O	0.025	0.027	0.029	0.031	0.033
N_2	0.055	0.055	0.055	0.056	0.056
O_2	0.000	0.000	0.000	0.000	0.000

Table 10-18. Syngas composition for Wyoming PRB sub-bituminous coal at 1371 °C

Wyoming PRB, dried to 6% moisture by weight, temperature 1371 °C					
Carbon in slag (%)	0	0.5	1	1.5	2
CO	0.545	0.543	0.541	0.538	0.536
H_2	0.265	0.264	0.263	0.262	0.261
CH_4	0.000	0.000	0.000	0.000	0.000
H_2S	0.002	0.002	0.002	0.002	0.002
COS	0.000	0.000	0.000	0.000	0.000
NH_3	0.000	0.000	0.000	0.000	0.000
CO_2	0.042	0.043	0.044	0.045	0.047
H_2O	0.064	0.066	0.068	0.070	0.072
N_2	0.073	0.073	0.073	0.073	0.073
O_2	0.000	0.000	0.000	0.000	0.000

Table 10-19. Syngas composition for Wyoming PRB sub-bituminous coal at 1427 °C

Wyoming PRB, dried to 6% moisture by weight, temperature 1427 °C					
Carbon in slag (%)	0	0.5	1	1.5	2
CO	0.547	0.545	0.542	0.540	0.538
H_2	0.263	0.262	0.261	0.260	0.259
CH_4	0.000	0.000	0.000	0.000	0.000
H_2S	0.002	0.002	0.002	0.002	0.002
COS	0.000	0.000	0.000	0.000	0.000
NH_3	0.000	0.000	0.000	0.000	0.000
CO_2	0.040	0.041	0.042	0.044	0.045
H_2O	0.066	0.068	0.070	0.072	0.074
N_2	0.073	0.073	0.073	0.073	0.073
O_2	0.000	0.000	0.000	0.000	0.000

Table 10-20. Syngas composition for Wyoming PRB sub-bituminous coal at 1482 °C

Wyoming PRB, dried to 6% moisture by weight, temperature 1482 °C					
Carbon in slag (%)	0	0.5	1	1.5	2
CO	0.548	0.546	0.544	0.542	0.539
H_2	0.262	0.261	0.260	0.259	0.258
CH_4	0.000	0.000	0.000	0.000	0.000
H_2S	0.002	0.002	0.002	0.002	0.002
COS	0.000	0.000	0.000	0.000	0.000
NH_3	0.000	0.000	0.000	0.000	0.000
CO_2	0.039	0.040	0.041	0.042	0.043
H_2O	0.067	0.069	0.071	0.073	0.075
N_2	0.073	0.073	0.073	0.073	0.073
O_2	0.000	0.000	0.000	0.000	0.000

Table 10-21. Syngas composition for North Dakota lignite at 1371 °C

ND Lignite, dried to 12% moisture by weight, temperature 1371 °C					
Carbon in slag (%)	0	0.5	1	1.5	2
CO	0.496	0.494	0.492	0.490	0.487
H_2	0.253	0.252	0.251	0.250	0.249
CH_4	0.000	0.000	0.000	0.000	0.000
H_2S	0.006	0.006	0.006	0.006	0.006
COS	0.001	0.001	0.001	0.001	0.001
NH_3	0.000	0.000	0.000	0.000	0.000
CO_2	0.054	0.055	0.056	0.058	0.059
H_2O	0.088	0.089	0.091	0.093	0.095
N_2	0.093	0.093	0.093	0.094	0.094
O_2	0.000	0.000	0.000	0.000	0.000

Table 10-22. Syngas composition for North Dakota lignite at 1427 °C

ND Lignite, dried to 12% moisture by weight, temperature 1427 °C					
Carbon in slag (%)	0	0.5	1	1.5	2
CO	0.498	0.496	0.494	0.492	0.489
H_2	0.251	0.250	0.249	0.248	0.247
CH_4	0.000	0.000	0.000	0.000	0.000
H_2S	0.006	0.006	0.006	0.006	0.006
COS	0.001	0.001	0.001	0.001	0.001
NH_3	0.000	0.000	0.000	0.000	0.000
CO_2	0.052	0.053	0.054	0.055	0.057
H_2O	0.090	0.091	0.093	0.095	0.097
N_2	0.093	0.093	0.093	0.094	0.094
O_2	0.000	0.000	0.000	0.000	0.000

Table 10-23. Syngas composition for North Dakota lignite at 1482 °C

ND Lignite, dried to 12% moisture by weight, temperature 1482 °C					
Carbon in slag (%)	0	0.5	1	1.5	2
CO	0.500	0.498	0.496	0.493	0.491
H_2	0.249	0.248	0.247	0.246	0.245
CH_4	0.000	0.000	0.000	0.000	0.000
H_2S	0.006	0.006	0.006	0.006	0.006
COS	0.001	0.001	0.001	0.001	0.001
NH_3	0.000	0.000	0.000	0.000	0.000
CO_2	0.050	0.052	0.053	0.054	0.055
H_2O	0.091	0.093	0.095	0.097	0.099
N_2	0.093	0.093	0.093	0.094	0.094
O_2	0.000	0.000	0.000	0.000	0.000

Conclusions

This report explains the performance and cost updates to PC and IGGC models in the IECM. For the PC plants, updates were made to the Base Plant, Steam and the CO_2 Capture system. For the IGCC plants, Aspen Plus simulation software was used to predict the product syngas compositions obtained by gasifying six different types of coals using a Shell gasifier at different operating conditions.

References

1. EPRI, "Advanced Coal Power Systems with CO2 Capture: EPRI's CoalFleet for Tomorrow Vision" Report #1016877, Electric Power Research Institute, Palo Alto, CA, September 2008.
2. DOE/NETL, "Cost and Performance Baseline for Fossil Energy Plants. Volume 1: Bituminous Coal and Natural Gas to Electricity Final Report", August 2007.
3. C. A. Roberts, J. Gibbins, R. Panesar, G. Kelsall "Potential for Improvement in Power Generation with Post Combustion Capture of CO2" White Paper, http://uregina.ca/ghgt7/PDF/papers/peer/510.pdf.
4. DOE/NETL "Carbon Dioxide Capture from Existing Coal-Fired Power Plants" November 2007.
5. Steam, It's Generation and Use. Babcock and Wilcox. Barberton, Ohio. 2005
6. Aspen Technology, Inc., 2007, Ten Canal Park, Cambridge, MA 02141-2201.
7. Holt N.A.H and Alpert S.B, 2001, Integrated Gasification Combined-Cycle Power Plants, Encyclopedia of Physical Science and Technology, 897 – 924
8. IECM-cs, 2007, Integrated Env. Control Model Carbon Sequestration Edition, Carnegie Mellon Univ. Center for Energy and Env. Studies, http://www.iecm-online.com
9. Probstein R. F and Hicks R. E, 1985, Synthetic Fuels, Intl Student Edition, McGraw Hill, Singapore.
10. Steynberg A and Dry M., 2004, Fischer-Tropsch Technology, Studies in Surface Science and Catalysis, 152, Elsevier, Amsterdam.
11. Zuideveld P.L, 2005, Shell coal gasification using low-rank coals, Gasification Technologies Conference, San Francisco, Oct 9 -12.
12. Eldrid R, Kaufman L and Marks P., 2004, The 7FB: the next evolution of the F gas turbine, GE Power Systems, Schenectady, NY.